Sectional Analysis of Reinforced Concrete Members

By:
Evan C. Bentz

A thesis submitted in conformity with the requirements
for the degree of Doctor of Philosophy
Graduate Department of Civil Engineering
University of Toronto

Abstract

Title: Sectional Analysis of Reinforced Concrete Members

Degree: Doctor of Philosophy

Year: 2000

Department: Department of Civil Engineering, University of Toronto

Four easy to use programs have been written that allow for state of the art sectional analysis of reinforced concrete blocks, plates, beams, columns and shells. Unlike most sectional analysis programs, these programs include the effects of shear on behaviour. They are based on the assumption that plane sections remain plane, that there is no transverse clamping stress, and that the biaxial behaviour can be modelled well by the Modified Compression Field Theory (MCFT). Each of these assumptions is shown to be reasonable.

The programs are freely available on the World Wide Web at the listed addresses:

http://www.ecf.utoronto.ca/~bentz/m2k.htm Membrane-2000 for plates

http://www.ecf.utoronto.ca/~bentz/r2k.htm Response-2000 for beams and columns

http://www.ecf.utoronto.ca/~bentz/t2k.htm Triax-2000 for 3D blocks

http://www.ecf.utoronto.ca/~bentz/s2k.htm Shell-2000: shells with out-of-plane forces

This thesis describes the MCFT in detail as implemented in the programs as well as explaining new constitutive relations employed for the behaviour of concrete in tension. The strongest feature of the new programs is the employment of the longitudinal stiffness method, developed for this thesis, which calculates the shear stress profile for a beam or shell much faster and with more numerical stability than the previous state of the art.

The programs are verified against a set of experiments as well as against two new shear experiments performed for this thesis. They indicate the programs are good at predicting the behaviour of the elements. Response-2000 is compared to a database of 534 beams and shown to predict shear strengths with an average experimental over predicted shear strength ratio of 1.05 and with a coefficient of variation of 12%. This

compares favourably to the ACI code prediction ratios that have an average of 1.20 and a coefficient of variation of 32%.

It is suggested that the programs in this thesis represent a good first step in allowing rational, state of the art computer programs to be directly allowed in the code for elements subjected to shear.

Acknowledgements

It's been said that it does not really matter what you are doing in life so long as you are able to work and play with people that you like. For the five years that I have worked on this project, I have had the luxury of both liking what I am doing and liking the people that I have worked with. I can only hope that they have learned something from working with me as I have certainly learned a great deal from them.

My supervisor, M. P. Collins has done an outstanding job in showing what it means to be a professional engineer, an excellent professor and an excellent researcher. Whenever someone refers to an effective professor, I use him as the standard of measurement. I thank him for all that he has taught me.

I thank the government of Canada and my parents for financial assistance. Together they have made this a painless experience financially.

I wish to thank those that helped me in the laboratory part of this research: Pawan Gupta, Steve Cairns, Dino Angelakos, Julius Lenart, Gary McDonald, Vasile Radulescu, Paul Amikons, John McDonald and Peter Heliopoulos.

Finally I want to thank the many people that I have shared an office with over the past five years including: Dan Kuchma, Amr Helmy, Guillermo Gabrielli, Almila Uzel, Yoichi Yoshida, Young-Joon Kim, amongst others. I also want to thank the many friends I have made along the way including Terry Ramlochan, Andrea Boddy, Kyle Stanish, Nick Kosteski, Jason Muise, Gordon Lok, Rob Rose, Francesca Burke, and many others.

If this thesis can be as helpful to the engineering community as my friends and colleagues have been to me over the past 5 years, then this will be a very successful thesis indeed.

Table of Contents

List of Figures

List of Tables

Chapter 1: Introduction

1-1 Analysis of Structures

For over 2000 years, good engineers have had an understanding of the working of the materials they mould. They have understood that by carefully shaping geometry, it was possible to build larger and more impressive structures and avoid problems that might otherwise make a structure fall down. In the last centuries, science and mathematics have been introduced into structural engineering, augmenting the engineer's understanding with mathematical models that can be used to assist in design. Over the last 35 years there has been explosive growth in the power of these numerical models as a result of the use of computers. These new analytical models have allowed engineers to design and optimise engineering solutions that hitherto would have taken much longer to solve.

Some of these computer models have, unfortunately, removed the engineer from the design process in such a way that young engineers are potentially learning less from the design process than they used to, despite being able to work on larger problems. This removal has meant that some engineers are less able to identify errors in analyses and designs than their older colleagues who did not learn structural behaviour with the help of a computer.

For some design problems where geometry or intrinsic material behaviour is complex, computers are now a necessary part of the engineering process. With care, computer programs can be written so that they enhance the engineer's understanding of the problem rather than subtracting from it.

An example of a complex engineering design problem, which is the subject of this thesis, is the design of reinforced concrete beams, plates and shells to resist significant shear. The most common method of analysis, that of Ritter[1], explained in detail by Morsch[2], was defined a century ago. Despite this, shear has been and continues to be a problem. A set of historically important shear failures that appears to have strongly affected the 1963 ACI code shear provisions were the failures in 1955 and 1956 of a series of Air Force Warehouses, see Fig. 1-1. More recently, the 1991 failure of the

Sleipner offshore oil platform resulted in a loss of nearly 1 billion dollars. This failure was due to a number of problems including mistakes in computer analyses, as well as a code of practice that was unconservative for the particular shear dominant loading. In the 1995 Kobe earthquake, the large Hanshin expressway, see Fig. 1-2, failed in shear, again partly due to an unconservative code. More recently, in the summer of 1998, a parking garage collapsed in Toronto due to a shear failure.

Figure 1-1: Air force Warehouse

Figure 1-2: Hanshin Expressway Piers

During the last twenty five years, a considerable amount of research has been conducted world-wide with the aim of developing behavioural models for reinforced concrete in shear comparable to the rationality and generality of the plane-sections theory for flexure. This research is comprehensively reviewed in the Dec. 1998 state-of-the-art report by ACI-ASCE Committee 445 "Shear and Torsion"[3]. One group of rational models for shear, developed at the University of Toronto, is known as the "Modified Compression Field Theory" (MCFT)[4]. The programs in this thesis use this model.

The research described in this thesis was commenced in the belief that recent advances in both computational power and behavioural understanding make possible the development of a new generation of design models for reinforced concrete subjected to shear. To this end, a series of four programs have been written for the shear analysis and design of reinforced concrete elements. These programs incorporate a number of significant advances in the shear analysis of reinforced concrete. In the author's opinion,

the most important attribute of these programs is that they are designed to help the user understand the response of reinforced concrete elements loaded in shear.

These programs also are designed to provide only one answer for a given problem. Some engineering analysis programs provide the ability to "tune" results by changing one analysis parameter or another. While this flexibility is useful, it can be tempting to try to achieve unnaturally good agreement with experiments that have already been performed. It is felt that this does not serve the engineering community well. By calculating a single definitive shear strength, say, for a given set of basic material properties and sectional geometry, it is felt that a more stringent set of rules for judging quality is established.

Finally, these programs are designed to provide a numerical test-bed for large and complex problems. It is known, for example, that larger lightly reinforced structures tend to fail at lower shear stresses than smaller ones. Clearly, there is a limit to how large an experiment can be to test for this phenomenon. By making programs that are based on rational models, it is possible to make the best use of the few large concrete shear tests that do exist. With a demonstrated ability to predict trends that include these large tests, it becomes possible to predict, with reasonable confidence, shear response when experiments are not practical.

1-2 Sectional-Based Analysis of Concrete Structures

Engineering analysis can take many forms in a spectrum of complexity. At one end are hand and graphical methods of analysis that tend to be laborious, yet are good for developing an understanding of the solution technique to the problem at hand. At the other end of the spectrum are general-purpose, non-linear, finite element computer programs. These are far more powerful, yet they are sufficiently complex that it is generally necessary to take it on trust that they work properly. One generally does not do calculations to determine if moment equilibrium is maintained in a frame or if the calculated loads really can be carried by the cross section, for example. The input and output from these complex programs tend to be difficult to understand and verify.

In between these two extremes of analysis lies sectional analysis. This is a familiar topic to engineers as the idea is strongly embedded in codes of practice. The units of currency for a sectional analysis are the familiar concepts of axial load, moment and shear. The programs in this thesis fit into this category of analysis. This means that they do the analysis at one location in a beam or plate and calculate the strength and deformation in terms of moments, shears, curvatures, etc. Generally, the only assumption needed to make a sectional analysis is something akin to the familiar assumption "plane sections remain plane" of engineering beam theory.

In using the sectional analysis approach, the problem of determining the response of a reinforced concrete structure to applied loads is broken up into two interrelated tasks. First, the sectional forces at various locations in the structure caused by the applied loads are determined. This step is usually performed assuming that the structure remains linearly elastic. Then the response of a local section to the sectional forces is determined. In this second step, which is the sectional analysis, the non-linear characteristics of cracked reinforced concrete are taken into account. Two examples of calculating the sectional forces in reinforced concrete structures are shown in Fig. 1-3 and Fig 1-4. For the simple building frame shown in Fig. 1-3, the axial load, N, the moment, M, and the

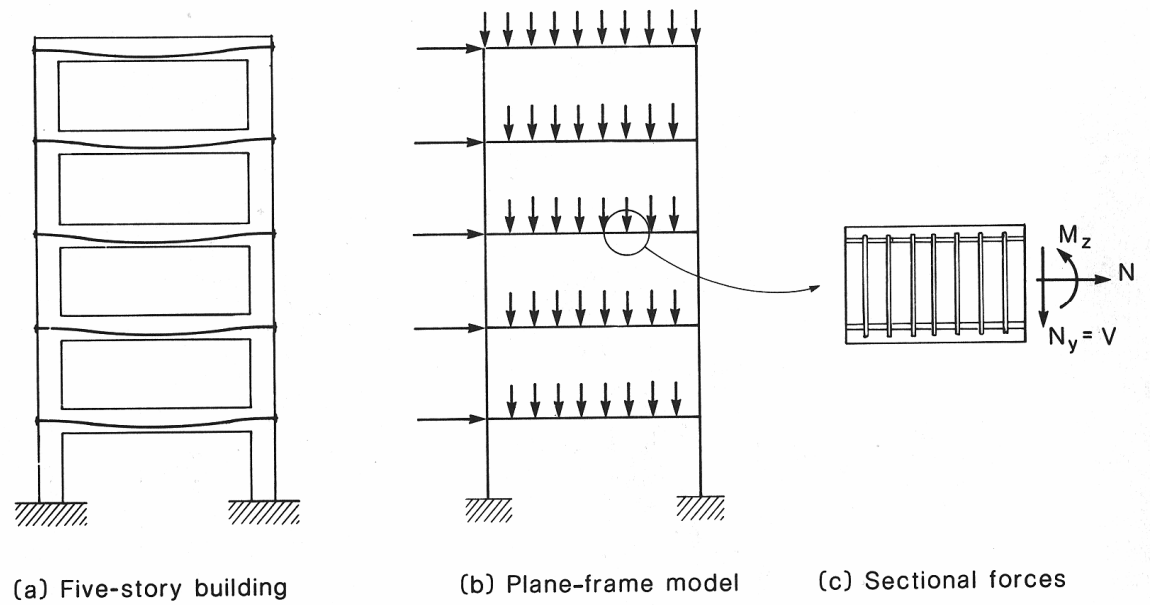

Figure 1-3 Determining sectional forces using plane frame analysis[5]

shear, V, at any particular location of the frame can be found using a plane-frame computer program. For the more complex concrete offshore platform, made up of plates and shells, the sectional forces at different locations can be found by integrating the stresses obtained from an elastic finite element analysis over the thickness of the element.

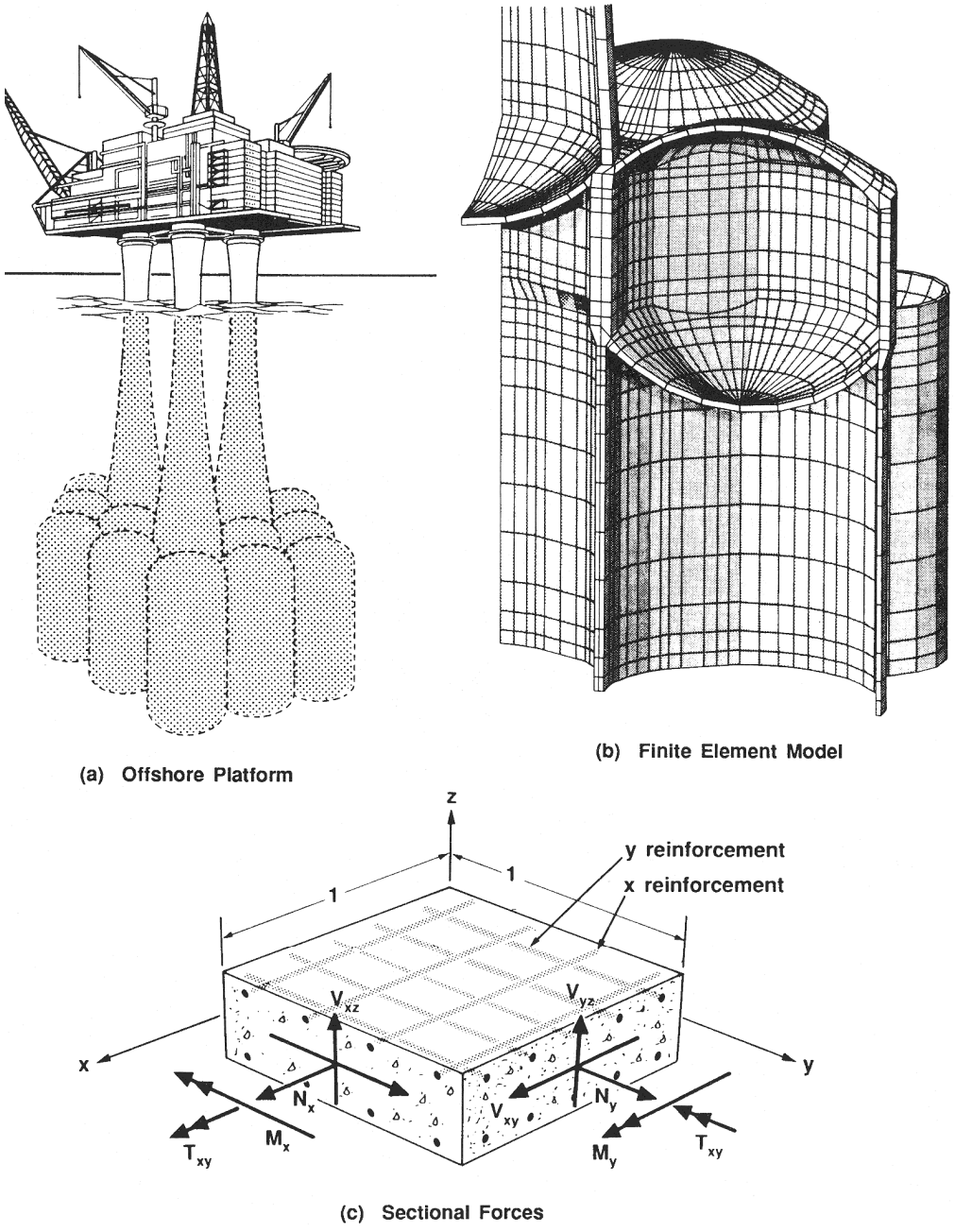

Figure 1-4 Determining sectional forces using finite element analysis[5]

The contribution of this thesis to the field is that it provides immediately useful programs that can be used by engineers and researchers to perform non-linear sectional analysis. These programs have been written so that they quickly allow checking of input and output data for errors. Additionally, in the process of viewing the results, the engineer using the program cannot help but learn about the behaviour of reinforced concrete. New analytical methods have been developed that improve the stability of the analysis while also increasing the speed many times over the previously existing state-of-the-art procedures.

While flexural sectional analysis (i.e. analysis without shear) of beams is generally considered to be a "solved problem," an equally rigorous and standard method for including shear does not exist in common practice yet. It is suggested that these programs can fill that gap and avoid some of the problems described above.

1-3 Brief Description of the Programs

The first program is Membrane-2000. This is a complete Microsoft Windows rewrite of the simple BASIC program "membrane" contained on the disk that came with the Prestressed Concrete Structures book by Collins and Mitchell[5]. This program will calculate the load-deformation relationship for membrane elements of reinforced concrete. That is, plates subjected to N_x, N_y, and V_{xy}. These are of the same type as the elements tested to derive the Modified Compression Field Theory.

The second program, Response-2000, is believed to be the most immediately useful of the four programs. It will calculate strengths and deformations for beams and columns subjected to axial load, moment and shear. The program, which is shown in this thesis to accurately model the behaviour of reinforced concrete, uses a new method for determining shear stress distribution. The program is thought of as being the successor of program Response[5, 38] and program Smal[6, 53]. In this respect, it is interesting to recall that

in the 1988 paper[6] which introduced the rigorous beam analysis procedure which lies at the heart of both SMAL and Response-2000, Vecchio and Collins stated:

> "Although too complex for regular use in the design of simple beams, the procedure has value in its ability to provide a rational method of analysis and design for members having unusual or complex geometry or loading, or whenever a more thorough analysis is warranted."

It is believed that the advances made in analysis techniques since that time and the advances made in computer power now mean that Response-2000 can in fact be used in day-to-day office practice.

The third program, Triax-2000, is of a more academic nature. It considers the behaviour of a general three-dimensional block of reinforced concrete.

The fourth program, Shell-2000 performs analyses for plates and shells subjected to all of the 8 force resultants shown in Fig 1-4 c. This new program performs a more rigorous analysis for out of plane shear than previously available. This program can be thought of as the next generation of program Shell474[7].

A user manual for these four programs is given in Appendix A of this thesis. More importantly, each of the four programs is freely available via the World Wide Web at the following addresses:

http://www.ecf.utoronto.ca/~bentz/m2k.htm for Membrane-2000
http://www.ecf.utoronto.ca/~bentz/r2k.htm for Response-2000
http://www.ecf.utoronto.ca/~bentz/s2k.htm for Shell-2000
http://www.ecf.utoronto.ca/~bentz/t2k.htm for Triax-2000

1-4 Types of Sectional Analyses.

Figure 1-5 summarises 6 different types of sectional analyses. The columns in the figure define the level of analysis. The model in the left column needs only a uniaxial stress-strain analysis to produce results, those in the middle column need biaxial stress-strain relations, and those in the right column need triaxial stress-strain relations. The rows indicate the level of numerical integration of the analysis. Models in the bottom row calculate behaviour at a point, those in the middle row integrate behaviour along a line and the model in the top row integrates behaviour over an area. The titles indicate what type of analysis could be performed if a series of such elements were strung together as finite elements. Figure 1-6 shows more information about each type of analysis along with where each of the programs in this thesis fits. Professor F.J. Vecchio has developed a number of finite element programs at the University of Toronto ([8, 9, 10, 11, 77]) and the location of these in the matrix is also shown. Finally, the loading is shown.

1-5 Assumptions in Sectional Analysis

For a sectional model to adequately model the behaviour of real elements, it is necessary for the structural element to be reasonably "long". For example, the shear span of a beam must be at least 2 times the depth of the beam in order for a shear analysis based on a sectional model to be accurate. Likewise, a shell element must have an area equal to 2 by 2 times the element thickness in a shear span sense. If the element is smaller than this, sectional analysis will typically be rather conservative.

The modelling assumptions in the implementation of sectional analysis including shear are first that engineering beam theory is valid. That is, a straight line drawn on the element before deformation will still be a straight line after deformation. The second assumption is that there is no significant net stress in the transverse direction. This means that the concrete and transverse steel forces must balance at each point through the depth of the element. Both these assumptions are good ones when the analysis is being performed a distance away from the support and the load point. Close to the load and to the reactions, however, there will be a transverse clamping stress from the application of

Figure 1-5
Sectional Analysis of
Reinforced Concrete

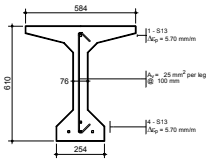

3D Frame

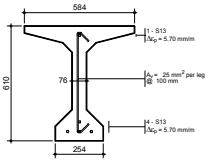

2D Frame

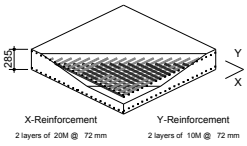

3D Shell

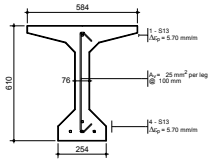

1D Frame

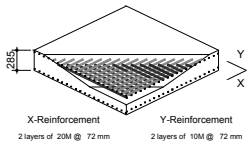

2D Shell

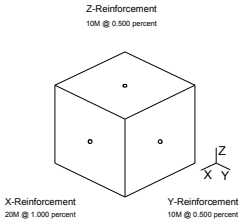

3D Block

Figure 1-6

Components of
Sectional Analysis Methods

3D Frame

Basis:
3D nodes in plane
Finite Element
None
Loading
M_X M_Y V_X V_Y T N

2D Frame

Basis:
2D nodes in a line
Finite Element
TEMPEST
Loading
N M V

Response-2000

3D Shell

Basis:
3D nodes in a line
Finite Element
RASP
Loading
N_X N_Y V_{XY} M_X M_Y M_{XY} V_{XZ} V_{YZ}

Shell-2000

1D Frame

Basis:
1D node at a point
Finite Element
None
Loading
N

2D Shell

Basis:
2D node at a point
Finite Element
TRIX
Loading
N_X N_Y V_{XY}

Membrane-2000

3D Block

Basis:
3D node at a point
Finite Element
SPARCS
Loading
N_X N_Y N_Z V_{XY} V_{YZ} V_{ZX}

Triax-2000

the load itself, which will tend to locally increase the strength. This is one reason that short beams are noticeably stronger in shear than long beams with the same cross section.

Figure 1-7 shows the results of two non-linear finite element analyses performed with program TRIX[8], which is a membrane element non-linear finite element analysis program based on the Modified Compression Field Theory. A 1.85 metre deep bulb-tee type section was loaded with a central point load on a 10 metre span. The analyses were performed to evaluate the appropriateness of the assumption of no clamping stresses in the transverse direction. For the first analysis, the strands in the beam were not prestressed, making the beam a reinforced concrete beam, while for the other, the strands were stressed to 1100 MPa (60% of ultimate stress). The plots show the transverse clamping stress at the top, middle and bottom of the web of the beams, all for a total applied load level of 3000 kN. The middle region of each shear span is highlighted in the diagram. It can be seen that in this middle region the effects of the transverse stresses near the support and point load have largely dissipated. Note that for the reinforced beam, there is little transverse stress in this middle region, but for the prestressed beam, there is a more pronounced clamping at mid-depth. This implies that a sectional model of this prestressed beam would be more conservative than for the reinforced concrete beam as the analysis would ignore the beneficial effect of this small compressive, clamping, stress. Based on analyses such as these summarised in Fig. 1-7, it can be concluded that the traditional assumption that the transverse stress is negligible is a very good one.

1-6 Contents of this Thesis

As is perhaps evident from the descriptions given above, the true products of this research project are the computer programs themselves. This thesis describes the analytical and experimental work upon which the programs are based.

Chapter 2 provides an introduction to each program with an example that highlights the use and type of analyses that can be performed with each program. The

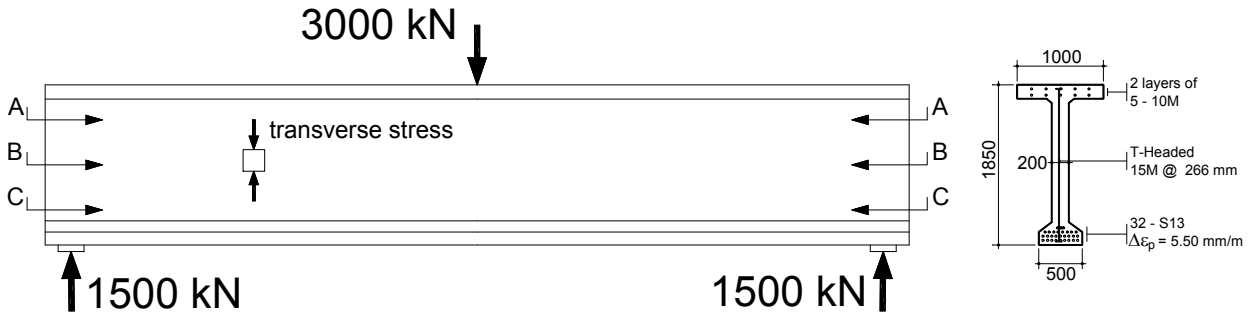

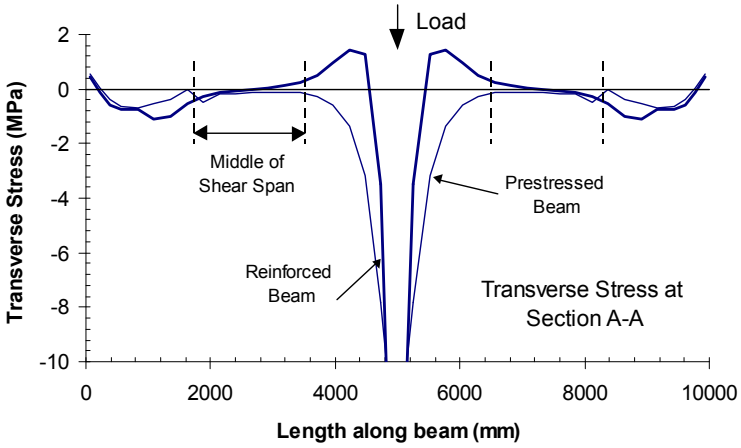

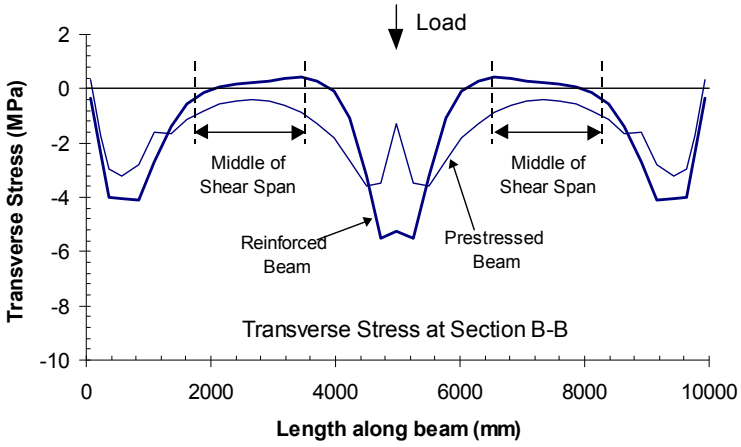

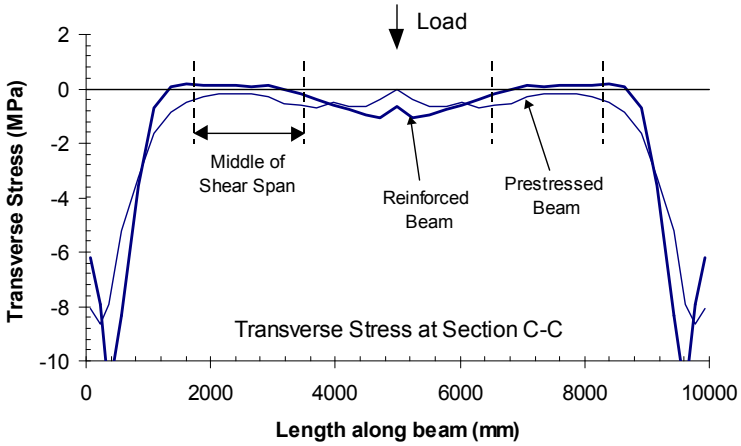

Figure 1-7: Example of Transverse stresses in web of 9250 mm clear span cracked reinforced and cracked prestressed concrete beams.

chapter is written in a “tutorial” style to allow the reader to follow along in trying the programs.

Chapter 3 explains the implementation of the MCFT in two dimensions and three dimensions. Chapter 4 extends that with an explicit discussion of the crack check. This crack check is a necessary part of the MCFT to ensure that equilibrium can be maintained at a crack.

Chapter 5 describes the concrete constitutive models used for the programs. New relations for the tension strength of concrete and tension stiffening are presented. These were found to be necessary to better capture observed behaviour of beams.

Chapter 6 describes the new method of calculating the shear stress profile in a beam or shell. This is one of the most important parts of this thesis as it has allowed a substantial increase in performance and stability over previous methods.

Chapter 7 provides brief descriptions of how each of the programs work. As the programs contain a total of about 150,000 lines of C++, the level of detail cannot be very high for this chapter.

Chapter 8 provides experimental corroboration for program Membrane-2000 from the literature. Chapter 9 explains the results from 2 new experimental tests performed for this thesis. Chapter 10 shows experimental corroboration for Response-2000 and Chapter 11 shows experimental corroboration for Shell-2000.

Chapter 12 provides more examples and advice on how to perform analysis of beams subjected to shear. Armed with this information, it is hoped that engineers will be capable of accurately predicting the response of reinforced concrete structures subjected to shear and that their understanding of the behaviour will be deepened.

Chapter 2: Examples of use of Programs

This chapter gives a short introduction to each program in terms of what can be done with them along with an example to show how to do it.

2-1 Program Installation

To install the programs from this thesis, simply copy them into a new directory and unzip the zip files. Consult your Microsoft Windows manual to find how to make a shortcut to the program or to add them to the start menu.

2-2 Quick Start: Membrane-2000

Membrane-2000 is the simplest of the four programs described in this thesis. It allows analysis of reinforced concrete shells subjected to in-plane forces (axial force in X and Y directions and in-plane shear). Internal reinforcement may be in orthogonal directions X and Y with an arbitrary number of bar layers and spacing allowed.

Membrane elements subjected to in-plane forces can be found in structural walls, the webs of beams, containment vessels, and cooling towers amongst many others. This is the type of element tested to develop the Modified Compression Field Theory. From a practical perspective, the edge forces used as inputs to Membrane-2000 could come from a linear elastic analysis of the entire structure. To demonstrate the program Vecchio's element PV20, tested in pure shear in 1981[11], will be examined.

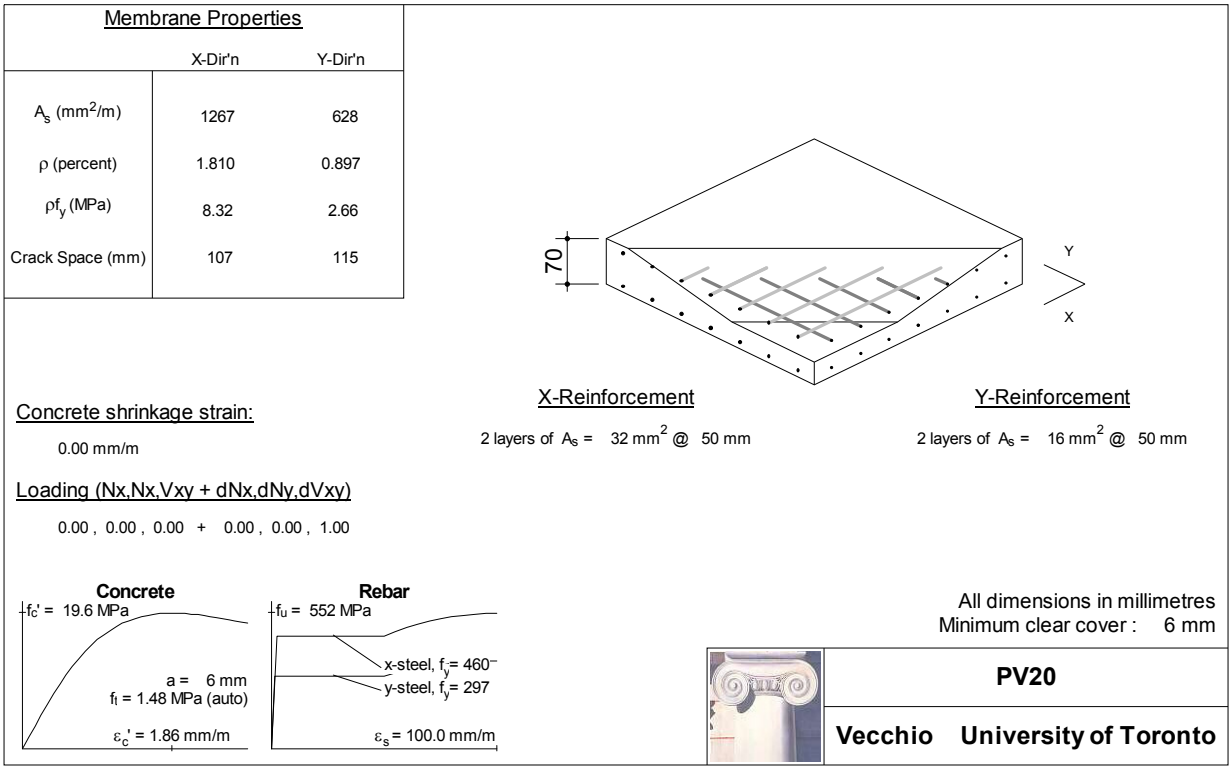

By default, membrane-2000 starts with PV20 loaded, so to see the element after starting the program, simply click on the cross section icon in the toolbar, which looks like a little membrane element or select the menu option “View | Cross Section”. The figure shown above is a direct print of the page that will appear.

The drawing attempts to document all the input parameters of the model to allow for easy error checking or quick documentation of a design. The properties shown on the page may be changed using the “define” menu. Additionally, double clicking on the drawing itself allows easy access to the define menu. For example, to change the stress-strain properties of the reinforcement in the X direction, it is possible to go to the “Define | Materials” menu option, or simply to double click on the drawing near the stress-strain line of the x-steel.

As this membrane element is already defined, an analysis may be performed immediately. Membrane-2000 allows 3 different analysis types to be performed. The simplest is a strain state analysis whereby the stress-resultants from a given strain state

(ε_x, ε_y, γ_{xy}) will be calculated. The second type of analysis solves for the strain state that corresponds to a selected load state (N_x, N_y, V_{xy}). The final analysis, "full response", is the most common. This will calculate the full load-deformation history for the element. Clicking on the "mcft" button in the toolbar will perform an analysis based on the Modified Compression Field Theory[4].

The screen will change to a 9-plot view as shown below. This is a standard view for the

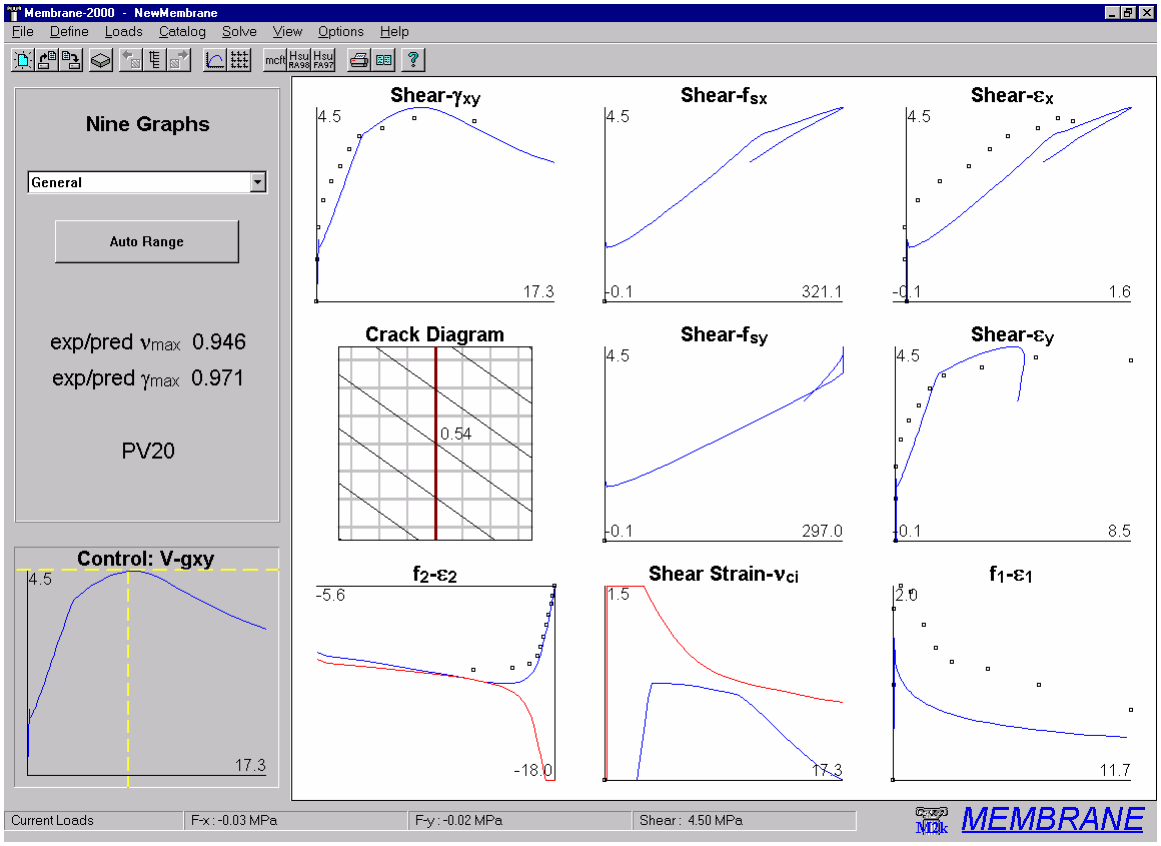

programs explained in this thesis. Each plot represents one variable of the solution for the panel PV20. For Membrane-2000, each plot is a full load-deformation plot. Some of the experimental data from the test[11] are included as well for comparison. Note that the while the experimental correlation is not especially good for some of the variables, the overall behaviour as represented by the Shear-γ_{xy} plot is quite reasonable.

Each of the programs in this thesis will work with either SI metric, US customary units, or kg/cm^2 units as used in, for example, Japan. By default, the programs start up in

SI metric (See Section 5-11 of the Appendix for information on how to change the default start units). The units may be changed in the "Options | Preferences" menu. For this example, stresses are in MPa, and strains are in parts per thousand (x 10^{-3} or mm/m).

On the left of the screen is a "control plot." It has crosshairs showing the currently selected load stage. This is the state that the crack diagram represents, with the crack width shown in mm. The red vertical line on the crack diagram indicates that the steel is yielding on average in the Y direction at this load level. Clicking with the mouse on the control plot, or using the Page-Up and Page-Down keys allow changing of the current load stage.

Also on the left, at the top, is a list-box that allows selection of which group of nine plots to examine. By default, the "General" page shows up. Another page shows Mohr's circles and a list of the full stress and strain state of the element.

To examine the data more closely from one of the plots, it is possible to right-click on the plot and select "view data." This allows the data to be copied to another application such as a spreadsheet to check the data or make other plots.

An analysis like this generally takes less than one tenth of a second. It becomes possible to quickly find the effects of different reinforcing levels, for example, this way. See the Appendix A for more information on Membrane-2000.

2-3 Quick Start: Response-2000

Response-2000 is perhaps the most immediately useful of the four programs explained in this thesis. It allows analysis of beams and columns subjected to arbitrary combinations of axial load, moment and shear. It also includes a method to integrate the sectional behaviour for simple prismatic beam-segments. The assumptions implicit in the program are that plane sections remain plane and that there is no transverse clamping stress across the depth of the beam. For sections of a beam or column a reasonable distance away from a support or point load, these are excellent assumptions. These are the same locations in beams that are usually the critical locations for brittle shear failures.

Unlike the other programs, Response-2000 does not have a default cross section entered into it. This is not a problem, however, as one can be made quickly. For this example, an 80 foot span prestressed concrete bridge girder and slab will be analysed.

First, as this example is presented with US customary units rather than the default SI metric, select it from the "Options | Preferences" dialog box. To select US units as a default each time the program begins, see section 5-11 of Appendix A.

Secondly, go to the "Define | Quick Define" dialog box. This is a "wizard" that allows a section to be created quite quickly, usually within 30 seconds. Each of the four programs in this thesis has such a wizard to make new files quickly.

The first page of the dialog box asks for a title and material properties. After entering a title, say, "Test Section" with the reader's initials for the "Analysis by" box, the material properties may be selected. For this example, the 5000 psi concrete, 60 ksi steel and 270 ksi strands are fine, so select the "Next" button.

The second page of the wizard asks for the concrete cross section. At the top of the list are simple sections such as rectangles and circles. In the middle of the list are more exotic shapes such as columns with interlocking hoops, and hollow columns. At the bottom are the "standard shapes" such as AASHTO girders. As this is what is needed here, scroll down near the bottom of the list and select "Standard Shapes AASHTO". Press tab (or click with the mouse) to the right side to select the type of section. Pressing any key will pop up a selection box to select a section from the currently defined listings. Select the AASHTO Type IV girder and press "ok". For the next input field, enter zero, as there will be no "haunch" on this section (i.e., no extra concrete between the top of the precast beam and the bottom of the slab.) Select a slab depth of 8 inches, and a slab width of 80 inches, and select "Next" to go to the next page of the wizard.

The third page allows selection of the longitudinal reinforcement for the section. The top half defines bars in the slab for this standard cross section case and the bottom defines non-prestressed steel in the bottom of the cross section. Leave the default of 20 #4 bars for the top, but remove the 3 #8 bars for the bottom by entering "0" for the number of bars in the bottom half of the screen. Press the "Next" button again to go to the last page of the quick menu.

The last page allows selection of the stirrups as well as the strands. Select "open stirrup" from the list of stirrup types. The default bar type of #4 is reasonable. Select a spacing of 16 inches. Switch the clear cover to 2 inches from the default value of "1.57", which is actually 40 mm converted to inches. Finally, enter 30 for the number of strands. The prestrain listed as 6.5 represents a jacking stress of 70% of ultimate, and is therefore reasonable. Select the "Finish" button to complete the definition of the section.

2-3-1 Automatic Cross Section

Response-2000 will automatically create the cross section as shown below similar to the one from Membrane-2000. As with the other programs, changing the geometry is achieved either through the use of the "define" menu or by double clicking on the drawing itself. For example, to change the stirrup spacing, double click on the text in the

drawing where it says "#4 @ 16.00 in." Like all the programs, this page is meant to include all the information needed to repeat the analysis or document it in the course of a design.

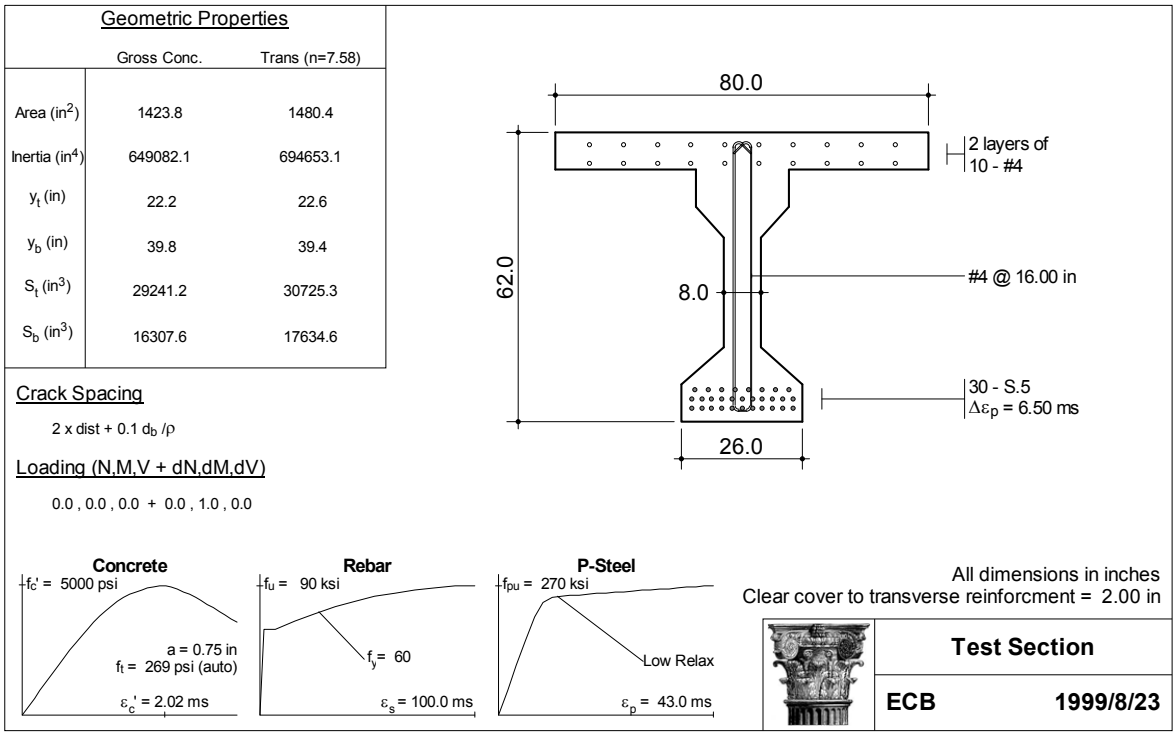

2-3-2 Analysis without shear

The default type of analysis for a new section is a simple flexural analysis with no axial load. To start it, select "Solve | Sectional Response" from the menu. The analysis should take perhaps 2 seconds to complete on an inexpensive 1999-vintage computer. The control plot will show up along with 9 plots as in Membrane-2000. In the case of Response-2000, the plots all represent the given variable plotted over the depth of the section for the load stage indicated by the control plot. Click on the "Auto Range" button on the top left of the screen below the menu to automate the scale of the plots, and click anywhere on the control plot. All the plots will automatically change depending on the new location on the control plot. Note that the loading is listed in the bottom bar of the program window. The crack diagram shows predicted crack widths in inches as well as an estimate of the pattern of cracking.

2-3-3 Analysis with Shear

A more involved analysis type, one that Response-2000 excels at, is the prediction of sectional behaviour including the effects of shear. For a beam like this, it may be decided to perform an analysis at a location 'd' from the end of the beam. At a uniformly applied load of 10 kips/ft, the moment and shear at this location are about 435 kip-ft and 109 kips respectively. These loads are entered into the Response-2000 "Loads | Loads" menu option. The column of entry fields on the left of this window is for initial loads and the column on the right is for any increment in load beyond that level. Leave the left values as zero and set the right side value for moment to 435 kip-ft and shear value to 109 kips. Note that the actual numbers here do not matter, only the ratios and signs. After clicking the "ok" button, select "Solve | Sectional Response" to start the analysis.

The analysis should take about 10 seconds to reach the peak load, and then about 20 more seconds to determine the post-peak ductility for the section. The following 9-plot screen will show up. These plots represent the state of the beam at failure, as shown by the location of the crosshairs on the control plots. Each plot is drawn with respect to the depth of the section. For example, the top centre plot shows the longitudinal strain versus depth for the section showing the basic assumption that plane sections remain plane.

The cross section in the top left is drawn darker in regions where it is predicted not to have cracked. In this case, only the web of the beam is predicted to be cracked at the shown failure load. The top right shows the variation in transverse strain over the depth, with a maximum of 7.3 parts per thousand near the top of the web. The crack diagram shows the predicted angle and width of cracks in inches. The shear stress plot shows that the shear is not uniformly distributed over the depth of the section, though it is fairly constant in the web at about 630 psi.

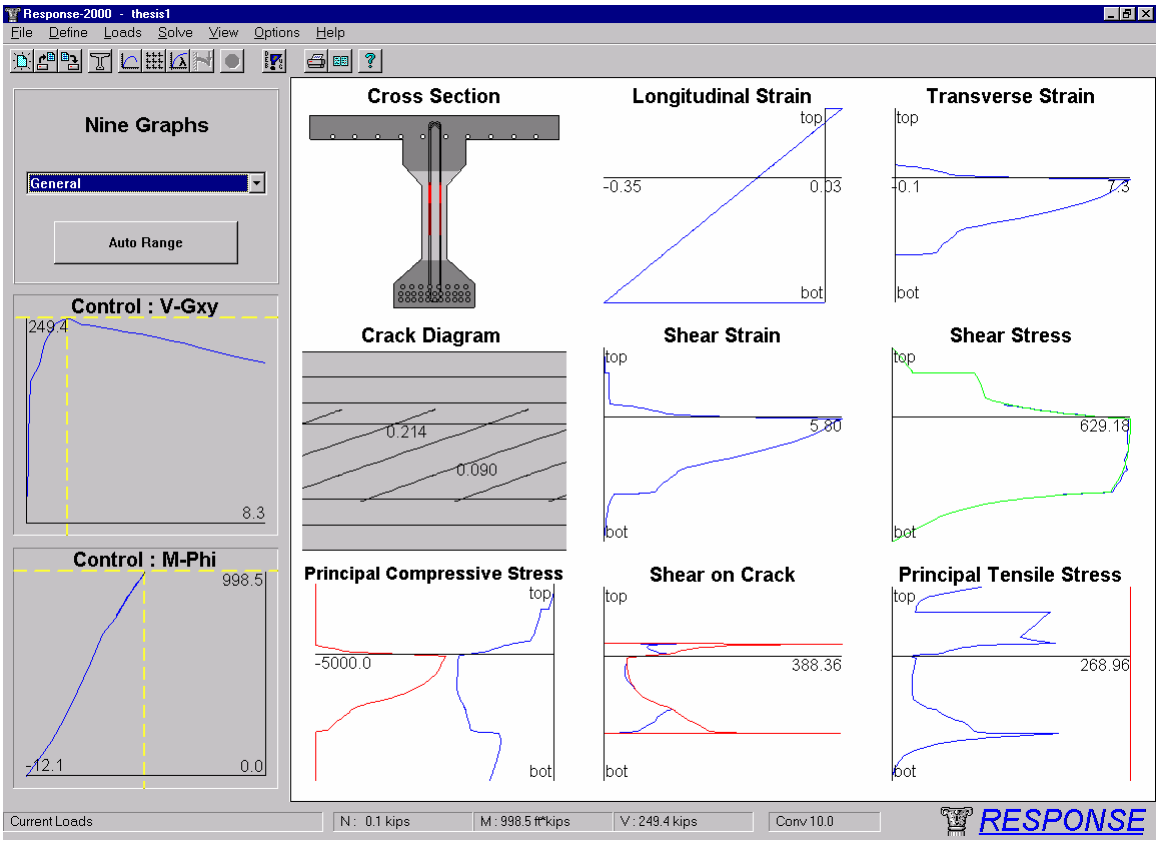

The bottom left plot of the 9 plots shows the principal compressive stress values. The red line at the left of the plot is the maximum allowed stress versus depth and the right blue line shows the applied stress. Note the shear has applied an additional diagonal compression in the web on top of the expected concrete stress profile from the prestressing force. The two lines on this plot are about to touch at the top of the web, indicating that this section is about to fail by crushing at the top of the web.

The two control charts show that the "V-Gxy" curve, that is, the shear force-shear strain plot, is descending with increasing shear strain, whereas the lower control chart, a moment curvature plot, is unloading along its loading curve. This indicates that the section is predicted to fail in shear. The maximum predicted shear capacity of the section is 249 kips. By scaling this from the loading, it is predicted that the beam would fail in shear at this location if the applied load were to increase to a level of 23 kips/foot.

2-3-4 Member Response

Response-2000 will calculate the full member behaviour for a prismatic section as well. To get a prediction of the behaviour of this 80-foot beam, such an analysis will be performed with the beam subjected to a uniformly distributed load. First select the "Load | Full Member Properties" menu option. Select the "length subjected to shear" at the top as 480 inches. (The analysis is done from one end to the mid-span of the beam.) Also, select in the top options a uniform distributed load rather than a constant shear analysis. This is the second option in the top list of three buttons. Click "ok" and select the "Solve | Member Response" option.

This analysis will calculate an entire Moment-Shear interaction diagram and determine the load-deflection properties and crack diagram for the entire 40 foot half span of the beam. The analysis on an inexpensive 400 MHz Pentium II takes about 60 seconds to complete. As the analysis continues, the growing M-V interaction diagram will be shown on the control plots. Periodically, the 9 plots will also update showing the sectional behaviour at the location of the crosshairs on the control plots. Note the transition from flexural failures under positive moment at the right of the interaction diagram to shear failures at the top of the interaction diagram and then back to flexural failures under negative moment at the left side. By clicking on the little squares on the plot, any of the integration points may be examined so see how the beam is behaving at that load combination.

When the analysis is complete, the screen will change to the deflection page as shown below. The top diagram is the predicted crack pattern at failure for the entire 40 foot half-span of the beam. The bearing support plate at the left bottom can be seen and the right side represents the midspan of the beam. Estimated crack widths are shown in inches. In the top control plot at the left is the M-V interaction diagram, which also shows the combinations of applied moments and shears along the length of the beam as a red line. For a uniformly distributed load, such as this, the majority of the loading line is a parabola, with the shear reduced to zero near the support due to non-sectional load resistance mechanisms in this region. The shape of this load diagram is explained in

Chapter 7. It can be seen from the interaction diagram that the loading envelope is touching the strength envelope almost simultaneously at the right side bottom (flexure in positive moment at midspan), as well as at the top (shear near support). Indeed, the midspan cracks are predicted to be almost 1 inch wide, and there is substantial shear cracking (0.147 inch cracks) near the support.

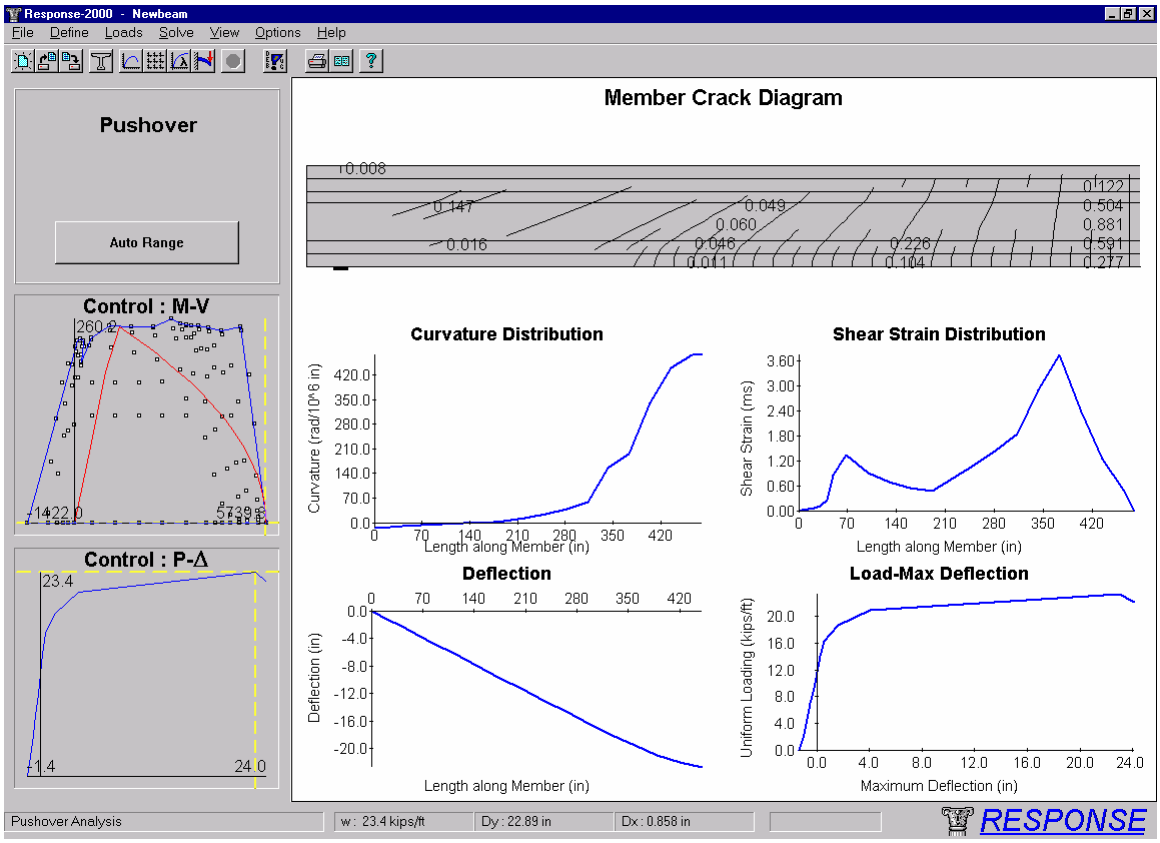

The bottom control plot shows the predicted load-deflection relationship for the beam (pushover analysis results for column analyses). The final behaviour is predicted to be fairly ductile, with a 22.9 inch deflection at a failure load of 23.4 kips/foot. Assuming that the load capacity is acceptable, this would seem to be a fairly efficient design in terms of shear versus flexural capacity; more stirrups would not be needed, as the beam would fail in flexure first. A lower amount of stirrups would subject the beam to a potentially brittle shear failure, however. In a design like this, it is wise to err on the conservative side of shear design and include somewhat more shear reinforcement than what has been provided. Of course Response-2000 allows any such option to be conveniently checked by changing the spacing of the stirrups, and rerunning the analysis.

2-4 Quick Start: Triax-2000

Triax-2000 is a program for the analysis of a 3 dimensional block of concrete. This program is analogous to Membrane-2000 in 3 dimensions. Such a block of concrete can be thought of as a 3D brick finite element. The relatively complex interactions of non-linear 3D stress-strain behaviour can be efficiently examined with Triax-2000. Additionally, the program may be considered as a model for well reinforced 3D locations, such as beam-column joints. It could fairly be argued that Triax-2000 is of less practical interest than the other three programs in this thesis

Loading for Triax-2000 consists of axial stresses in the directions X, Y and Z as well as shear stresses on the X-Y, Y-Z and X-Z planes.

The program has a default section built into it as shown below. As it is a 3D sectional analysis, the block has no physical dimensions, but is assumed to be of

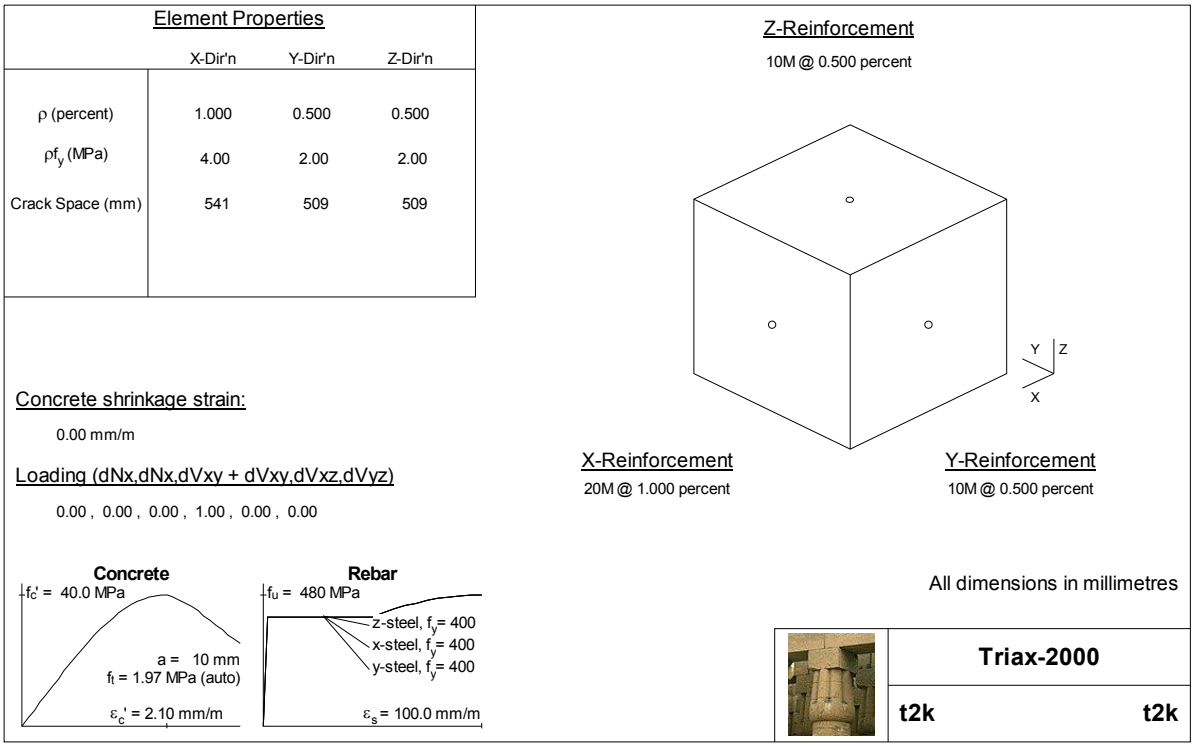

sufficient size in all three dimensions to cover a series of cracks.

Although it is a rather arbitrary loading, an analysis will be performed on the shown section with the following load ratios:

Load Direction	N_x	N_y	N_z	V_{xy}	V_{yz}	V_{xz}
Load Ratio	1.0	2.0	3.0	4.0	5.0	6.0

This loading represents triaxial tension on the element as well as increasing shear in all shear directions. These load ratios are entered into the program by selecting the "Loads | Loads" menu option. As in each of the programs explained in this thesis, there are two columns of numbers that may be entered. The left column is for the load level at which to start the analysis and the right column is for the loading ratios to be used for incrementing load after that point. Note that the actual values on the right column do not matter, only their relative values and signs are used in the program. Enter the above load levels into the right side column of the loads menu and close the loads dialog box by clicking the "ok" button.

On clicking the "solve" button on the toolbar, the now familiar nine plots show up with the results of the analysis as shown below. The control plot is automatically selected by the load ratios and in this case shows the load-factor vs. shear strain in the Y-Z direction.

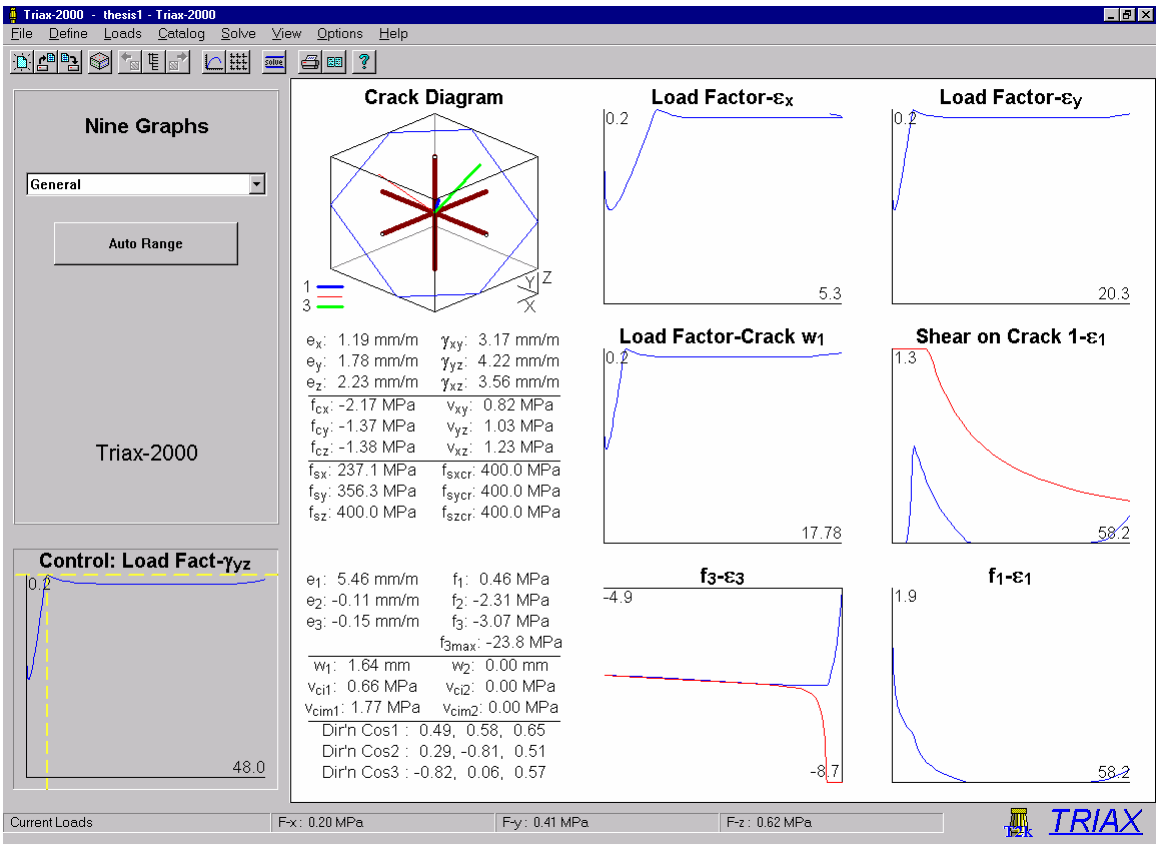

Triax-2000 shows a tabular list of all the strain and stress states for the element at the load marked by the crosshairs on the control plot. The crack diagram shows the principal directions as well as the intersection of the crack planes with the outside of the concrete volume. In general, 3D behaviour of this type requires some study to ensure that the results are indeed what is expected.

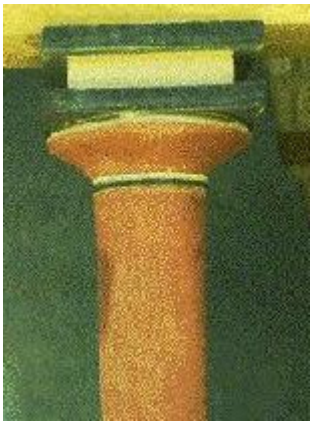

2-5 Quick Start: Shell-2000

The last of the four programs in this thesis is Shell-2000. It assembles a collection of Triax-2000 elements on top of each other to allow out-of-plane analyses of plates and shells. As such, it is a three dimensional analogue of Response-2000. It is a more general version of Membrane-2000 that will allow analyses that include out of plane forces. Such shell elements can be found in slabs and walls and, indeed, almost all structures made of plates or shells.

Loading for Shell-2000 consists of the following eight force resultants: Axial force in X and Y directions, moment about X and Y axes, out-of-plane shear about X-Z and Y-Z planes, twisting moment (M_{xy}) and in-plane shear. Shell-2000 is a superset of Membrane-2000 and can do all analyses that Membrane-2000 can do. Due to the inherent 3D nature of the implementation, however, it is slower than Membrane-2000.

The default element in Shell-2000, shown, is shell element SE4 tested by

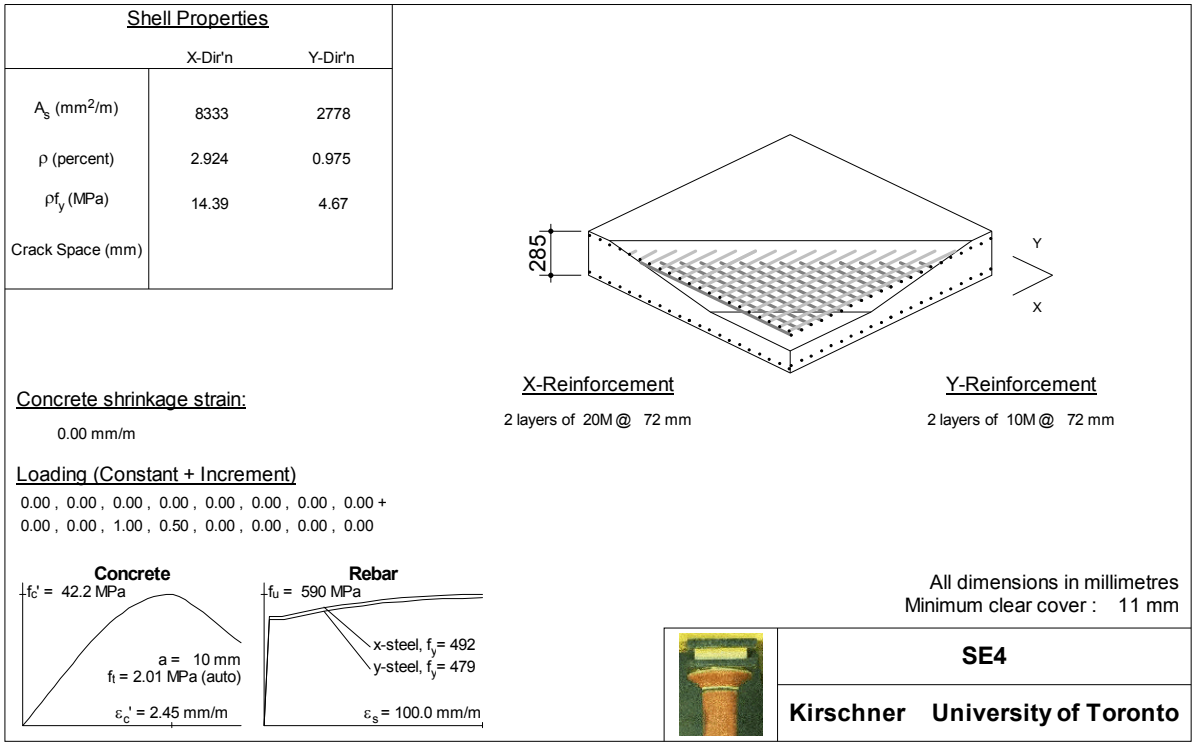

Kirschner and Khalifa from the original series of tests in the University of Toronto shell element tester conducted in 1984[12]. The loading is in-plane shear along with moment about the X-axis. Performing a "Solve | Full Response" will take less than 30 seconds and produce the following 9-plot picture of the element at failure.

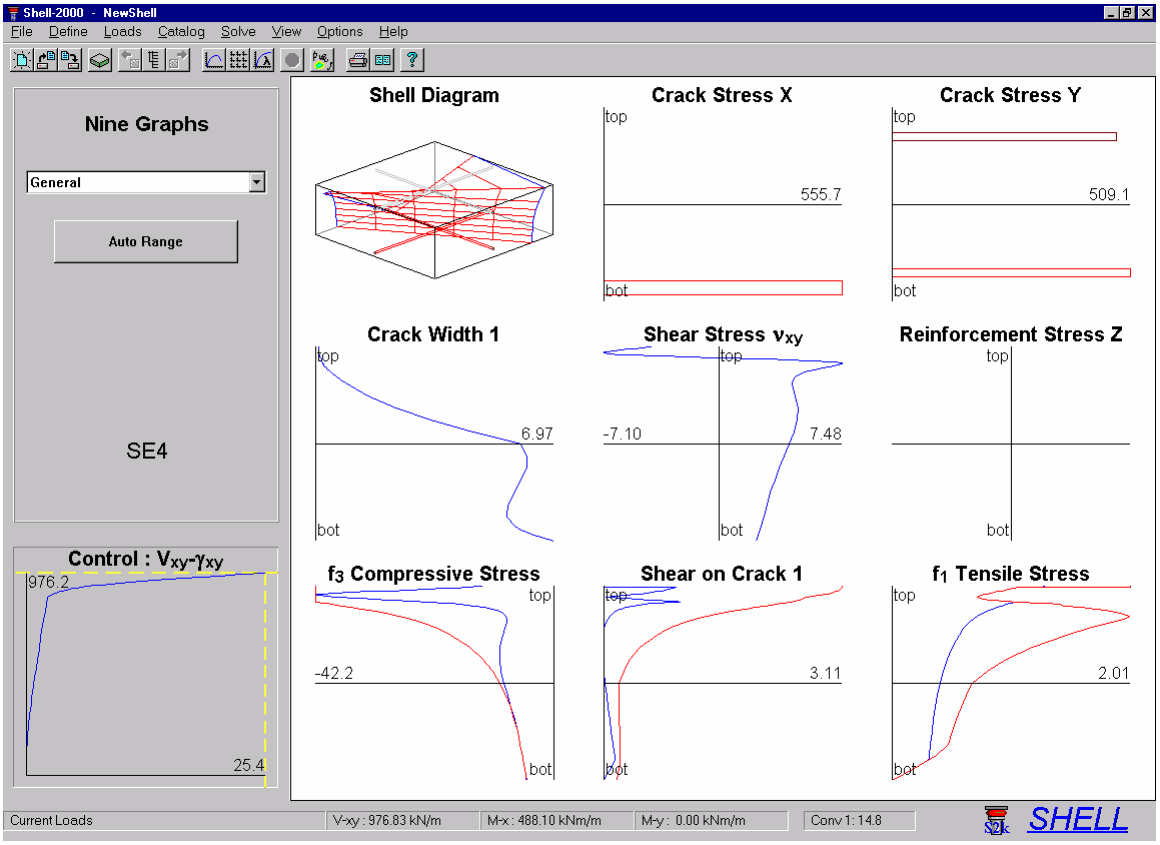

It can be seen from the control plot that failure is predicted to be fairly ductile. From the bottom line of the output window, the failure in-plane shear is predicted to be 976 kN/m. In the test, the element failed in a ductile fashion at an in-plane shear of 961 kN/m. The nine plots show the state of the element at failure. The steel is predicted to be yielding on the top and bottom of the shell in the Y direction as well as in the bottom side in the X direction. The crack plot shows that the element is predicted to have full-depth cracking, roughly in the X direction at the top (flexural compression side), and rotated through the depth as a result of the in-plane shear stress. From the principal compression plot, the concrete is predicted to be crushing (two lines touching) at the top due to the flexure as well as at the bottom due to the in-plane shear.

Chapter 3: The Modified Compression Field Theory and Related Numerical Techniques

3-1 General

Perhaps the most important differentiating element between different sectional models is the constitutive models that are employed. The programs in this thesis use the Modified Compression Field Theory (MCFT). This theory traces back through the Compression Field Theory of 1978[14] to the Diagonal Compression Field Theory of 1974[13]. Vecchio defined the original form of the MCFT in 1982[15] from the testing of 30 reinforced concrete panels subjected to uniform strain states in a specially built tester. The definitive description of the MCFT is in the 1986 American Concrete Institute paper "The Modified Compression Field Theory for Reinforced Concrete Elements Subjected to Shear"[4]. Since then, only two small changes have been made, both in 1987[16]. There have been other proposed changes to the theory, but at the University of Toronto, it is largely this 1987 version that is still used 13 years later. Since then, others have proposed similar models including Hsu and Zhang[17,18] and Kaufmann and Marti[19]. To allow comparison between some of these proposals, the methods of Hsu et al. have been explicitly included in Membrane-2000.

The MCFT is a general model for the load-deformation behaviour of two-dimensional cracked reinforced concrete subjected to shear. It models concrete considering concrete stresses in principal directions summed with reinforcing stresses assumed to be only axial. The concrete stress-strain behaviour in compression and tension was derived originally from Vecchio's tests and has since been confirmed with about 250 experiments performed on two large special purpose testing machines at the University of Toronto. Similar machines have been built in Japan and the United States, providing additional confirmation of the quality of the method's predictions.

The most important assumption in the model is that the cracked concrete in reinforced concrete can be treated as a new material with empirically defined stress-strain

behaviour. This behaviour can differ from the traditional stress-strain curve of a cylinder, for example. The strains used for these stress-strain relationships are average strains, that is, they lump together the combined effects of local strains at cracks, strains between cracks, bond-slip, and crack slip. The calculated stresses are also average stresses in that they implicitly include stresses between cracks, stresses at cracks, interface shear on cracks, and dowel action. For the use of these average stresses and strains to be a reasonable assumption, the distances used in determining the average behaviour must include a few cracks. Sectional models satisfy this by needing to be at least a couple of section depths long.

A penalty for using average stress-strain relationships is that an explicit check must be made to ensure that the average stresses are compatible with the actual cracked condition of the concrete. This so-called crack check is a critical part of the MCFT and the theories derived from it. The crack check involves limiting the average principal tensile stress in the concrete to a maximum allowable value determined by considering the steel stress at a crack and the ability of the crack surface to resist shear stresses.

As the overall stress response is based solely on average relationships, tempered with the crack-check, the method does not require an explicit calculation of dowel action force, shear stresses on crack, reinforcing stress at a crack, crack slip strains, and bond stresses. If required, the inferred values of some of these parameters may be calculated from equilibrium. The simplicity afforded by ignoring these more complex phenomena in cracked concrete is one of the strengths of the method.

Figure 3-1 summarises the Modified Compression Field Theory for the two dimensional case. The left panel shows the equilibrium equations which are in fact simply the equations of a Mohr's circle of stress. The middle panel shows the strain conditions, which also can be summarised by a Mohr's circle. Note the implicit assumption in the MCFT that the angle of principal concrete stress can be taken as equal to the angle of principal strain (θ). The final panel shows the stress-strain relationships for reinforcement, concrete in compression, and concrete in tension. The bottom of each

panel shows the components of the crack check to ensure that the average stresses can be transferred across the crack.

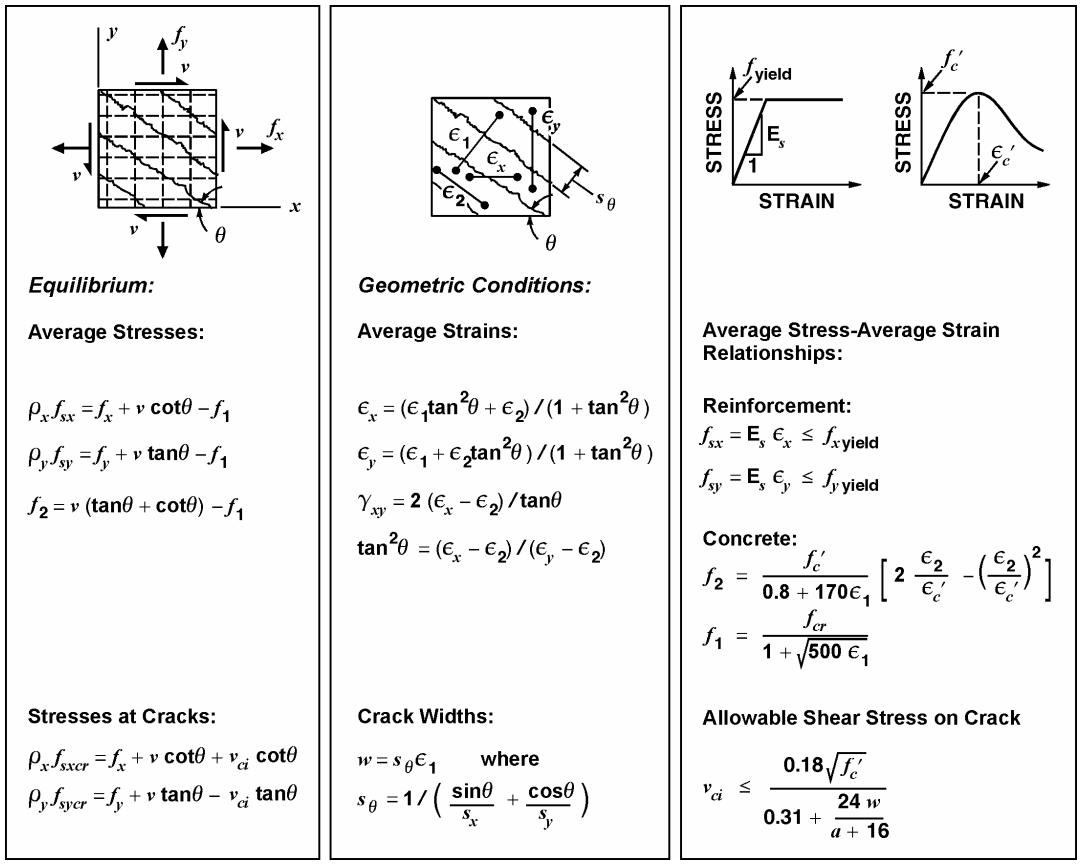

Figure 3 - 1 The Modified Compression Field Theory

3-2 Important Aspects of the MCFT

The following aspects of the MCFT are worth noting from within Figure 3-1.

3-2-1 Reinforcement average response (f_{sx}, f_{xy})

The MCFT assumes that the average behaviour of steel can be approximated by the bare-bar response. While this is an excellent assumption prior to yield at a crack, it is not obvious that it is appropriate after first yield of the reinforcement at a crack. Note that steel first yields at a crack due to any tensile stress in the uncracked concrete needing to be balanced by extra steel stress at a crack. Numerical simulations done by Porasz[20] in 1989 demonstrated that the error in assuming bare-bar behaviour for the average stress-

strain behaviour is relatively small. Much of the complexity in the models from the University of Houston[17,18] result from trying for more precision in the modelling of average steel stresses.

3-2-2 Concrete tensile stress response (f_1)

Concrete is assumed to be able to carry the full cracking strength prior to cracking. After cracking, tensile stresses in the uncracked concrete between the cracks will continue to stiffen the concrete, and in some cases will increase the strength. To model the high scatter behaviour of post-cracking, pre-reinforcement yielding tension stiffening, a simple equation for f_1 is shown in Fig. 3-1. The decrease in average stress after cracking represents bond degradation, formation of new cracks, and other damage mechanisms. In Vecchio's original formulation[15], the term shown in Fig. 3-1 as $\sqrt{500\varepsilon_1}$ was given as $\sqrt{200\varepsilon_1}$. The change of the coefficient from 200 to 500 was suggested by Collins and Mitchell in 1987[16] partly as a result of examining experimental results from larger elements than the 30 panels tested by Vecchio. Note that later in this thesis, the above tension stiffening model will be extended to more directly account for bond behaviour.

3-2-3 Concrete compressive stress response (f_2)

Uncracked concrete in compression is assumed to follow the cylinder stress-strain curve. The stress-strain curve shown in Fig 3-1 is a parabola, a function of the principal compressive strain (ε_2), as well as the principal tensile strain (ε_1). The tensile strain component models the decrease in apparent concrete compressive strength observed in tests when the concrete was transversely cracked. This often controls the strength of beams with stirrups.

3-2-4 Crack width (w)

When subjected to shear, new cracks may form, old cracks may close or become inactive. This complex load-history dominated behaviour is simplified to only a single set of parallel cracks forming at the average angle of principal compressive stress. The

spacing of the cracks (s_θ) is calculated with the shown equation that converts the calculated crack spacing in the two orthogonal directions to an estimated diagonal spacing. It is recommended that these crack spacings in the base X and Y directions be estimated as shown in Chapter 7, itself based on the method in Collins and Mitchell[5]. Crack widths are assumed to be simply the product of the principal tensile strain and the crack spacing (that is, elastic strains in the uncracked concrete between the cracks are ignored).

3-2-5 Shear on the crack (v_{ci})

It is assumed that there is a limiting interface shear stress on a crack that can be transmitted before the crack begins to "slip". The equation in the bottom right of Fig. 3-1 was derived from the experiments of Walraven[21]. This shear on the crack limit is higher for stronger concrete or larger aggregates (variable a). Increasing crack widths lower the maximum allowed shear on the crack. This limit is used in the crack check explained in Chapter 4.

Note that shear on the crack "interface", v_{ci}, is not an average stress, but a local one. Recall that the MCFT calculates the total element force state with average stresses at angle theta. The calculated shear on the crack is resisted by a crack also assumed to be at an angle of theta. This indicates that there must be a local deviation in angle of principal stress at a crack if there is to be any shear on the crack.

3-2-6 Local reinforcement stress at a crack (f_{sxcr}, f_{sycr})

Calculation of this term defines the crack check. Note that there are two equations, one for each direction of reinforcement, derived as a sum of forces in the X and Y directions locally at a crack. Clearly, the steel stress at a crack must be lower than some limit, usually the yield stress. See Chapter 4 for a full description of the crack check.

3-3 Modified Compression Field Theory in Three Dimensions.

The Modified Compression Field Theory was extended to three-dimensional behaviour by Kirschner[22] and again by Adebar[23] to include the crack check. Referring to Fig. 3-1, the same three aspects of equilibrium, compatibility and stress-strain relationships apply. Note that explicit equations are not directly presented, as they are available elsewhere in matrix format[24].

The three stresses in the 2D case (f_x, f_y, v_{xy}) extend to six (f_x, f_y, f_z, v_{xy}, v_{yz}, v_{zx}). The three strains in 2D (ε_x, ε_y, γ_{xy}) extend to six as well (ε_x, ε_y, ε_z, γ_{xy}, γ_{yz}, γ_{zx}).

The equilibrium equations are extended simply to include one additional equation for the Z direction. Note that the 2D tensor format (Mohr's circle) still applies as a 3D tensor. The angle theta in the 2D case extends to a set of 3 direction cosines for the 3D case (k_i, l_i, m_i). As in 2D, the 3D direction cosines of strain are assumed to be the same as the direction cosines of concrete stress.

The compatibility equations are similarly extended to represent a 3D tensor format.

The stress-strain relationships described above are implemented by allowing each principal direction to accept tension or compression. The softening of the compression equation is modified for cases with tension in the two transverse directions such that ε_1 is replaced by $\sqrt{\varepsilon_1 + \varepsilon_2}$ if ε_3 is the compression direction[12]. There have been no experiments yet performed on large blocks of reinforced concrete subjected to uniform three-dimensional states of strain and stress. As such, the technique here has not been directly verified, though it does work reasonably well for a series of 3D elements put together as shown by Selby[24] and Adebar[7], for example.

The crack spacing equation is directly extended to three dimensions as shown in equation 3-1.

$$s_{m\theta i} = \frac{1}{\frac{k_i}{s_{mx}} + \frac{l_i}{s_{my}} + \frac{m_i}{s_{mz}}} \tag{3-1}$$

The crack-check equations are described separately in Chapter 4.

3-4 Solving problems with the MCFT

Two classes of questions arise with general shear models such as the MCFT. The first is to find a stress state corresponding to a strain state, and the second it to calculate a strain state corresponding to a stress state. The second is much more difficult as it must be solved via numerical iteration. It has been found that using a secant based solution regime works very well in 2D and 3D for this second type of problem.

3-4-1 Calculate stress state from strain state:

The following series of steps solves this direct problem for the 3D case. The numerical example is for a 3D block of 40 MPa concrete (19 mm aggregate) with 1% of 400 MPa steel in the X direction, 0.5 % of 400 MPa steel in the Y and Z directions. Note that this is the default cross section that program Triax-2000 starts with, but shown here with parabolic concrete behaviour, and Collins-Mitchell 1987 tension stiffening to be consistent with the formulation given in Fig 3-1.

3-4-2 Solving for a 3D stress state from a 3D Strain state

The following steps and example values demonstrate calculation of a stress state from a strain state using the MCFT.

Steps	Numerical Example
Given: ε_x, ε_y, ε_z, γ_{xy}, γ_{yz}, γ_{zx}	1.03, 1.18, 1.65, 2.38, 3.00, 2.97 mm/m

a) calculate principal strains and directions
for 2D problems, use Mohr's circle
for 3D problems, use 3D Eigenvector routines

$\varepsilon_1, \varepsilon_2, \varepsilon_3$	4.08, -0.08, -0.15 mm/m

Direction Cosines:

k_1, l_1, m_1	0.52, 0.55, 0.65
k_2, l_2, m_2	0.51, -0.82, 0.27
k_3, l_3, m_3	-0.68, -0.19, 0.71

k_1, l_1, m_1 are the direction cosines of the first principal direction. The other terms are similarly defined for principal directions 2 and 3.

b) calculate principal stresses with equations from Figure 3-1

f_1, f_2, f_3	0.81, -2.06, -3.77 MPa

c) perform crack check to check limits on all tensile concrete stresses
See Chapter 4 for example on how to do this. In this case, it does not control.

d) rotate principal average concrete stresses back to rectangular directions

$f_{cx}, f_{cy}, f_{cz}, v_{xy}, v_{yz}, v_{zx}$	-2.06, -1.25, -1.70, 0.60, 1.26, 1.80 MPa

Note from this that the concrete stresses are generally compressive in the x, y and z directions when shear is applied as they will be balanced by the steel, itself in tension. Again, note that the rotation is provided with the same direction cosines used for the strain tensor. The directions of principal strain and concrete stress are assumed to coincide.

e) calculate average steel stresses (as in Figure 3-1)

f_{sx}, f_{xy}, f_{sz}	206, 236, 330 MPa

f) add average steel stresses to concrete stresses

fx, fy, fz	0.00, -0.07, -0.05 MPa

g) if desired, steel stresses at a crack and shear on crack components may be calculated as explained in Chapter 4.

3-4-3 Calculate strain state from stress state

It is common that a stress state is known and the strain state is the desired quantity. A very robust way to solve this is with the secant stiffness method. As described by Krpan[25]:

"The central idea of the procedure is the concept of secant modulus, see Fig. [3-2, 3-3]. Any stress-strain curve can be represented by the expression

$$\sigma = E_{secant}(\varepsilon) \times \varepsilon \qquad [3–2]$$

where the secant modulus, E_{secant} is a function of ε."

These secant moduli are shown for concrete and steel in Fig. 3-2 and 3-3.

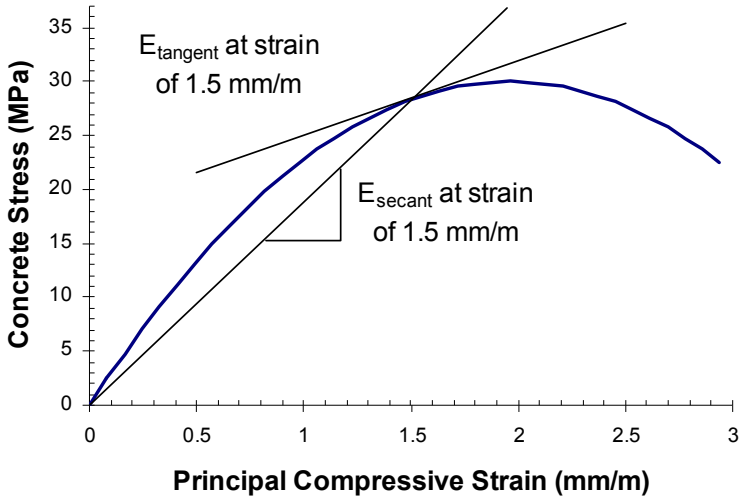

Figure 3 - 2: Secant and Tangent Modulus of Concrete

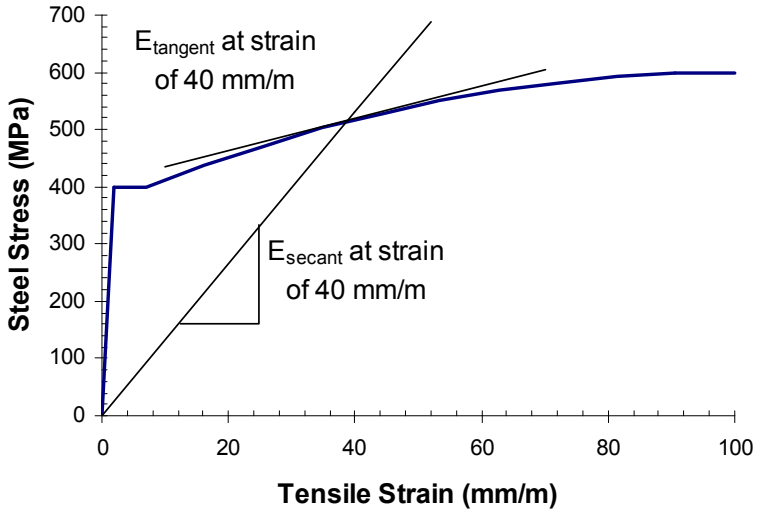

Figure 3 - 3: Secant and Tangent Modulus of Reinforcement

Using this scheme, the strain vector $\{\varepsilon\}$ is related to the stress vector $\{\sigma\}$ via the matrix [D] by the following:

$$[D]\{\varepsilon\} = \{\sigma\} \tag{3-3}$$

In two dimensions, $\{\varepsilon\} = \{\varepsilon_x, \varepsilon_y, \gamma_{xy}\}$

$\{\sigma\} = \{ f_x, f_y, v_{xy} \}$

In three dimensions, $\{\varepsilon\} = \{ \varepsilon_x, \varepsilon_y, \varepsilon_z, \gamma_{xy}, \gamma_{yz}, \gamma_{zx}\}$

$\{\sigma\} = \{ f_x, f_y, f_z, v_{xy}, v_{yz}, v_{zx} \}$

The secant stiffness matrix [D] is defined below.

Using this simple matrix equation, the solution for any unknown term can be found simply and with stability. The secant stiffness matrix is symmetric and fully populated.

An example is the calculation of the full-response solution of Triax-2000. An estimate is made of the strain state for a given desired load level. This is then checked with the above method for calculating stresses, and the secant stiffness is then calculated. A new estimated strain state is then calculated from the stiffness matrix. This procedure is repeated until the desired convergence on load is achieved.

3-5 Secant Stiffness in Two and Three Dimensions

The presentation of secant stiffness here will work for any biaxial or triaxial stress-strain relationship including linear and nonlinear ones. The presentation here is from the work of Selby[24]. The [D] matrix used above is calculated in the principal directions and rotated back to the rectangular directions afterwards. It is made up of both a concrete component $[D_c]$ and a steel component $[D_s]$ as follows:

$$[D] = [D_c] + \Sigma\, [D_s]_I \tag{3-4}$$

To determine the $[D_c]$ matrix, it is first necessary to calculate it in principal directions and then rotate it back to the X-Y-Z frame. This rotation is performed with the following relationship:

$$[D_c] = [T]^T[D_c]'[T] \tag{3-5}$$

The transformation matrix T is made up of the following terms.

$$[T] = \begin{vmatrix} k_1^2 & l_1^2 & m_1^2 & k_1l_1 & l_1m_1 & m_1k_1 \\ k_2^2 & l_2^2 & m_2^2 & k_2l_2 & l_2m_2 & m_2k_2 \\ k_3^2 & l_3^2 & m_3^2 & k_3l_3 & l_3m_3 & m_3k_3 \\ 2k_1k_2 & 2l_1l_2 & 2m_1m_2 & k_1l_2 + k_2l_1 & l_1m_2 + l_2m_1 & m_1k_2 + m_2k_1 \\ 2k_2k_3 & 2l_2l_3 & 2m_2m_3 & k_2l_3 + k_3l_2 & l_2m_3 + l_3m_2 & m_2k_3 + m_3k_2 \\ 2k_3k_1 & 2l_3l_1 & 2m_3m_1 & k_3l_1 + k_1l_3 & l_3m_1 + l_1m_3 & m_3k_1 + m_1k_3 \end{vmatrix}$$

k, l, and m are the direction cosines as noted above with the numerical example. Note that the matrix can conceptually be divided into 4 quarters, each a 3x3 matrix. The top left corner deals directly with effects in the axial directions to strains in the axial directions for example. The other quadrants include shear effects and so include at least two terms each as they will be affected by the two directions that make up that individual shear strain.

The matrix $[D_c]'$ is the stiffness of the concrete in principal directions defined as follows:

$$[D_c]' = \begin{vmatrix} E_{C1} & 0 & 0 & 0 & 0 & 0 \\ 0 & E_{C2} & 0 & 0 & 0 & 0 \\ 0 & 0 & E_{C3} & 0 & 0 & 0 \\ 0 & 0 & 0 & G_{C12} & 0 & 0 \\ 0 & 0 & 0 & 0 & G_{C23} & 0 \\ 0 & 0 & 0 & 0 & 0 & G_{C31} \end{vmatrix}$$

Where E_{C1}, E_{C2} and E_{C3} are principal secant stiffness values as follows:

$$\begin{aligned} E_{C1} &= f_1/\varepsilon_1 \\ E_{C2} &= f_2/\varepsilon_2 \\ E_{C3} &= f_3/\varepsilon_3 \end{aligned} \tag{3-6}$$

And G_{C12}, G_{c23} and G_{C31} are secant shear moduli as follows:

$$\begin{aligned} G_{C12} &= E_{C1}E_{C2}/(E_{C1}+E_{C2}) \\ G_{C23} &= E_{C2}E_{C3}/(E_{C2}+E_{C3}) \\ G_{C31} &= E_{C3}E_{C1}/(E_{C3}+E_{C1}) \end{aligned} \tag{3-7}$$

Because reinforcement is considered to only accept axial force, the matrices $[D_s]$ for the X Y and Z directions all have only one element. $[D_s]_x$ for example has a term in the top left corner equal to E_{sx}.rhox where

$$E_{sx}=f_{sx}/\varepsilon_x \tag{3-8}$$

The Y and Z directions are similar. Note that these are not tangent stiffnesses.

For 2D analyses, the $[D_c]$ matrix can also be written in terms of sines and cosines of the angle of principal stress/strain θ. For that case, use only columns and rows 1,2 and 4 in the above matrices, and make the following substitutions:

$$\begin{aligned} k_1 &= \cos(\pi-\theta) \\ k_2 &= -\sin(\pi-\theta) \\ l_1 &= \sin(\pi-\theta) \\ l_2 &= \cos(\pi-\theta) \end{aligned} \tag{3-9}$$

3-6 Tangent Stiffness in Two and Three Dimensions

In the longitudinal stiffness method described in Chapter 6, it is explained that the tangent stiffness of a biaxially loaded concrete element can be important in predicting behaviour. To calculate this, in concept, one need change the secant stiffness terms in the matrix $[D_c]$' from the secant values in Fig. 3-2 and Fig. 3-3 to the tangent values. All the methods used above to rotate from principal to X-Y directions still apply.

While in theory, this is a simple procedure, in practice it is more complex. The principal direction i tangent stiffness is defined as follows:

$$E_{ci} = \frac{df_i}{d\varepsilon_i} \tag{3-10}$$

Where f_i is the stress as defined in the equations in Fig. 3-1.

Clearly, if the concrete is in tension, the tension equation is used (which is only a function of the principal tensile strain) and if the concrete is in compression, the compression curve is used. Note that the compression curve is a function of two strains, the principal compressive strain (ε_2) for the location on the curve (f_2) and the principal tensile strain (ε_1) defining the height of the curve for the softening (f_{2max}). For each row of the final tangent stiffness matrix, say the first row, there will be a unique relationship between the change of ε_1 and the change of ε_2. In 2D and for the first row of the final matrix, any increase in ε_2 will also increase ε_1 by a factor of $\tan^2\theta$. This happens because the first row of the matrix is with respect to changes in the ε_x strain. Any change in ε_x will cause a change in both of the principal strains. For the second row, the rate of change of ε_1 with respect to ε_2 is $1/\tan^2\theta$, and for the third row, the rate is –1.0. This makes the derivatives more complex to calculate. If the principal compression equation in Fig. 3-1 is broken up as follows, the stiffness can be calculated:

$$\begin{aligned} f_2 &= f_{2\max} \cdot \text{Parabola} \\ E_{ci} &= \frac{d\text{Parabola}}{d\varepsilon_2} f_{2\max} + \frac{df_{2\max}}{d\varepsilon_1} \cdot \frac{d\varepsilon_1}{d\varepsilon_2} \text{Parabola} \end{aligned} \tag{3-11}$$

This means that the symmetry of the secant method above is broken. The tangent stiffness matrix is not symmetric. To calculate it, it is necessary to determine the derivative of ε_1 with respect to ε_2 for each row and calculate all the principal stiffness values. Then calculate the entire stiffness matrix and discard all of it except the needed row. Then repeat for the next row. For the 2D case, the matrix can be expanded algebraically, reducing the amount of unnecessary calculations. For the 3D case, the

simplest implementation is to numerically calculate the derivative and go through the matrix multiplication six times, once for each of the six rows.

Note that if the concrete principal tension is being affected by the crack check, as explained in chapter 4, it is necessary to include the stiffness of this crack check in the matrix as well. That is, the stiffness of the principal tension direction should be controlled by the crack check equations, if they govern, rather than by the base curve equation.

The shear stiffness terms in the i and j direction are calculated as follows:

$$G_{cij} = 0.5\ (f_i - f_j)/(\varepsilon_i - \varepsilon_j) \qquad (3\text{-}12)$$

Reinforcement stiffness is added in as above except that it must be the tangent stiffness of the bars rather than the secant stiffness, as shown in Fig. 3-3.

Were it not for the increased speed and stability of the longitudinal stiffness method over the traditional numerical methods, it would be difficult to justify this complexity. In fact, the increase in stability results in the programs running 5-15 times faster with the tangent stiffness matrix calculated this way over the older numerical methods of calculating tangent stiffness. It is suggested that this does indeed justify the complexity of the programming.

Chapter 4: The Crack Check

4-1 General

The crack-check in the Modified Compression Field Theory (MCFT) represents an explicit check to ensure that the average stress levels can be resisted locally at a crack. It has become apparent, in the past, that some researchers and engineers have implemented the MCFT without including the crack-check. This is unconservative and potentially unsafe. In a series of papers, for example, Hsu has shown that ignoring the crack-check can produce results that are very unconservative indeed[26, 27]. It is felt that the crack check is sufficiently important to warrant its own chapter, though it could be argued that it belongs in the previous chapter that introduced the Modified Compression Field Theory.

The need for the crack check is easy to demonstrate. Consider the concrete prism subjected to axial tension reinforced with 0.75% of 400 MPa steel as shown in Fig. 4-1. The total force on the element may be calculated as follows:

(4-1)

Figure 4 - 1: Prism in Tension

$$N = N_c + N_s \qquad (4\text{-}1)$$

Where N = total axial load
N_c = concrete component = $f_l \cdot A_c$
N_s = steel component = $f_{sx} \cdot A_s$ = $\rho \cdot f_{sx} \cdot A_c$

The stress-strain relations for average concrete and steel behaviour are defined by the usual MCFT equations as shown earlier in Fig. 3-1, and again here in Fig. 4-2 and 4-3 for concrete and steel respectively

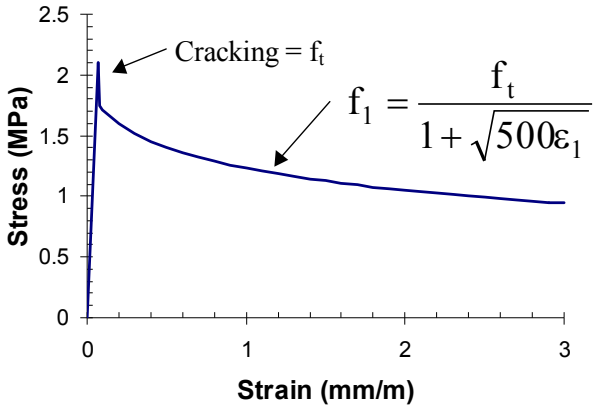

Figure 4 - 2: Average Tensile Stress f_1

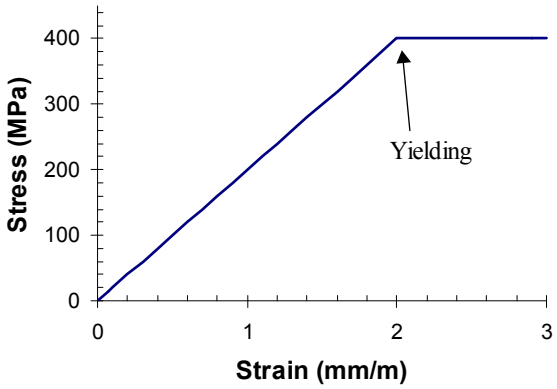

Figure 4 - 3: Average Steel Stress f_{sx}

A naïve analysis may produce the graph in Figure 4-4 for the total stress versus strain relationship. Note that the concrete and steel forces have been added together over the entire range of strain. This is not correct.

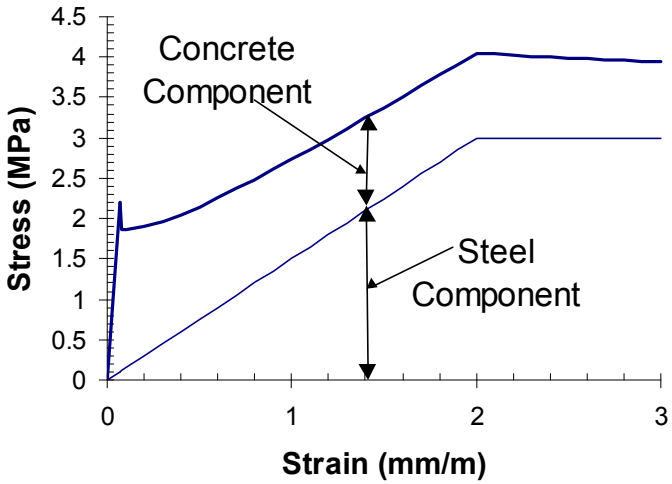

Figure 4 - 2: Total stress with no crack check

Consider the free body diagram shown in Figure 4-5 with the left half of the element drawn with average stresses as used in the MCFT and the right half with local stresses at crack where there will be no concrete tension.

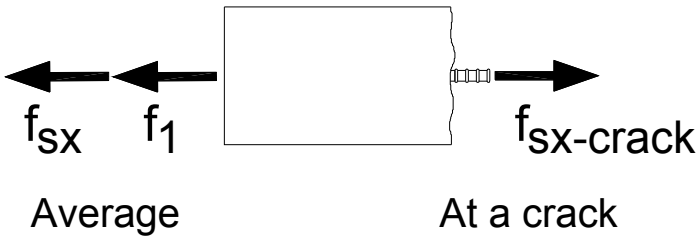

Figure 4 - 3: Free body diagram at a crack

Recalling that the MCFT, for simplicity, uses the same stress-strain curve for steel at a crack and on average, it is possible, indeed common, for both f_{sx} and f_{sx}-crack to equal f_y, the bare-bar yield stress. From the free body diagram, it is clear that the concrete tensile stress, f_1, must equal zero in this case. Ensuring that the local stresses at a crack not exceed the yield stress in this case is the job of the crack check. For reinforcement with, for example, a biaxial stress-strain response, it can be assumed that the stress at a crack will always be able to achieve at least the stress corresponding to the bare-bar stress at the given average strain.

Using this crack check results in the correct total stress plot prediction shown in Figure 4-6 for this element. This corrected answer includes the effect of the crack check to ensure that the steel stress never exceeds the yield stress of the bare bar at a crack.

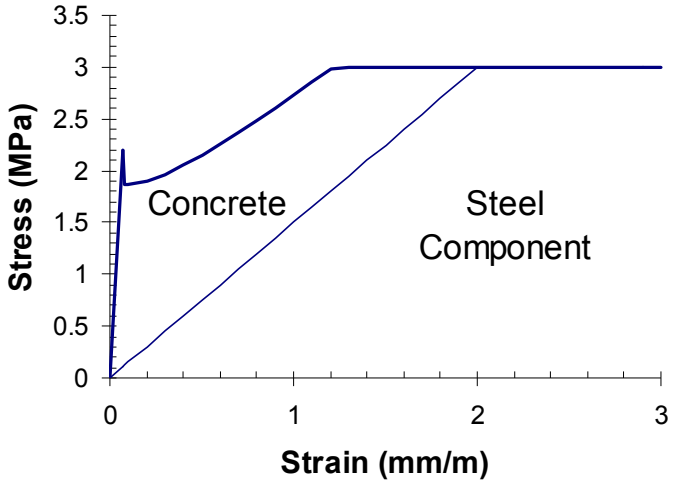

Figure 4 - 4: Total stress with crack-check

4-2 Crack Check in One Dimension

The above demonstration implicitly showed the crack check in one dimension. The equation that must be satisfied is simply a reorganisation of the above relationships, namely:

$$f_1 \leq (f_{sx\text{-}crack} - f_{sx})\,\rho \qquad (4\text{–}2)$$

4-3 Crack Check for Two Dimensional Node

When considering a biaxially loaded piece of reinforced concrete, as in, for example, the program Membrane-2000 or any traditional 2D MCFT analysis, the crack check becomes slightly more complex than the above equation.

Firstly, a uniaxial check must be made in each direction of reinforcement similar to the above equation for 1D but, also, there is the additional inclusion of the possibility of a shear on the crack surface itself. It is assumed that the crack cannot transmit any direct concrete axial tension across it. As stated in Chapter 3, it is assumed that the directions of principal stresses are able to rotate locally at a crack and thus allow shear on the crack to occur if equilibrium demands it. Implicitly it is assumed that the concrete is trying to maintain as high an average tensile stress as it can, with the maximum equalling the base constitutive equation for tension stiffening.

Consider the free body diagram, shown below in Fig. 4-7, of a two dimensional piece of reinforced concrete drawn at a crack on the top right and on average at the bottom left. Note that the cut is at an angle theta, the same angle as the cracks, principal strains and concrete stresses in the MCFT. Note that the force arrows for the reinforcement are only drawn once, rather than once per bar, to maintain simplicity.

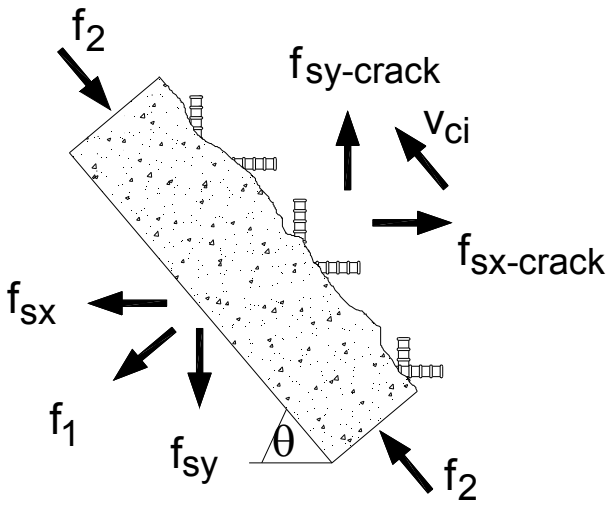

Figure 4 - 5: Two dimensional crack check

Immediately, the principal compressive stress (f_2) can be seen as irrelevant as it is self-equilibrating. The stresses of importance at a crack are the two steel stresses locally at a crack ($f_{sy\text{-}crack}$, $f_{sx\text{-}crack}$), as well as the potential shear on the crack (v_{ci}). Note that there are three stress resultants at the crack, but only two equations of equilibrium (ΣF_x, ΣF_y). This indicates that there is more than one solution satisfying equilibrium for the behaviour at a crack. The traditional approach used in the MCFT is to assume that the steel load-resisting mechanism is stiffer than the shear on the crack mechanism, and so the shear on the crack is minimised. The importance of this assumption was found to be small in comparison to an alternate assumption that the angle of average principal strain is maintained locally at a crack. Recall that the angle of principal stresses, in contrast, will generally rotate locally at a crack as compared to the average direction due to the nonlinear behavior of the steel.

This assumption of minimising shear on the crack has the effect of "using up" all the steel capacity in the weak direction before any shear on the crack is required. As this behaviour is only happening locally at a crack, it will have no effect on the overall stress-strain state unless it requires the lowering of the princpal tensile stress.

Summing forces in the X and Y direction on the above diagram results in a series of equations that define the crack check. These equations have been summarised in Table 4-1, which includes all the steps needed to satisfy the crack check in two dimensions. Following these steps will ensure that the stress at a crack is not in excess of yield in either the X or Y directions and that the shear on the crack is less than the limit based on crack width. The average concrete tensile stress thus calculated (f_1), can be used with the rest of the MCFT equations as presented in Chapter 2.

Table 4-1: Explicit Steps for 2D-MCFT Crack Check

Calculate following properties from equations in MCFT in Figure 3-1

Base equation of tensile stress (f_{1a})

Base equation of maximum shear on Crack ($v_{cimax} = v_{ci1}$)

Average steel stresses (f_{sx},f_{sy})

Perform crack check to limit principal tension to satisfy equilibrium

1) Calculate reserve capacity in X and Y direction steel (f_{1cx} f_{1cy})

$f_{1cx} = \rho_x (f_{yx} - f_{sx})$	This is the extra average stress required in the
$f_{1cy} = \rho_y (f_{yy} - f_{sy})$	X or Y direction to yield the longitudinal steel.

2) Biaxial yield without shear on crack (f_{1b})

$f_{1b} = f_{1cx} \sin^2\theta + f_{1cy} \cos^2\theta$	Ensures that load required to cause biaxial yield of reinforcement at a crack is not exceeded.

3) Max shear on crack for biaxial yield (v_{ci2})

$v_{ci2} = \lvert f_{1cx} - f_{1cy} \rvert \sin\theta \cos\theta$	Calculate the shear on the crack required to Achieve biaxial yield of the reinforcement

4) Calculate maximum allowed tensile stress from X and Y direction equilibrium

$f_{1c} = f_{1cx} + \min(v_{ci1} , v_{ci2}) \cot\theta$	Calculate maximum tension from equilibrium
$f_{1d} = f_{1cy} + \min(v_{ci1} , v_{ci2}) \tan\theta$	f_{1c} is for X dir'n, f_{1d} for Y dir'n equilbrium

5) Take minimum of all calculated values for final value of principal tension

$f_1 = \min(f_{1a} , f_{1b} , f_{1c} , f_{1d})$	Select Minimum Value

To calculate the actual equilibrium-based steel stresses at a crack and the value of the shear on the crack (v_{ci}), use the following steps, using the notation in Table 4-1. This cannot be made into a simple equation because, as noted above, there are more unknowns

than equations. By using these steps, the shear on the crack (v_{ci}) will be defined, allowing the steel stress at a crack to be calculated from the equations in Fig. 3-1.

Condition	Meaning	Shear on crack equation
$f_{1cx} = 0$ and $f_{1cy} = 0$	Average Biaxial Yield	$v_{ci} = 0$
$f_{1cx} > f_{1cy}$ and $f_{1cy} < f_1$	Y direction dominant Y yield at crack	$v_{ci} = (f_1 - f_{1cy}) \cot\theta$
$f_{1cx} > f_{1cy}$ and $f_{1cy} > f_1$	Y direction dominant No yield at crack	$v_{ci} = 0$
$f_{1cx} < f_{1cy}$ and $f_{1cx} < f_1$	X direction dominant X yield at crack	$v_{ci} = (f_{1cx} - f_1) \tan\theta$
$f_{1cx} < f_{1cy}$ and $f_{1cx} > f_1$	X direction dominant No yield at crack	$v_{ci} = 0$

Finally, the following equations will calculate the reinforcement stresses at a crack using the calculated shear on the crack.

$$f_{sx\text{-}crack} = (f_1 + v_{ci} \cot\theta)/\rho_x + f_{sx} \qquad (4\text{-}3)$$

$$f_{sy\text{-}crack} = (f_1 - v_{ci} \tan\theta)/\rho_y + f_{sy}$$

4-4 Crack Check for Three Dimensional Node

Just as the 2D crack-check is more complex than the 1D crack-check, the 3D crack-check is more complex than the 2D case. Table 4-2 describes the crack check in three dimensions. This derivation is based on that of Adebar[23], modified to be consistent with the steps presented above. Following these steps will satisfy the requirement that the steel stress in each direction is not in excess of yield, and that the shear on the crack is less than the maximum allowed for the given crack width.

Table 4-2: Explicit Steps for 3D MCFT Crack Check

Calculate following properties from Equations of MCFT

Given strain state and direction cosine (k_i, l_i, m_i) of direction "i"

Calculate base equation of tensile stress (f_{1a})

Calculate base equation of maximum shear on crack ($v_{cimax} = v_{ci1}$)

Calculate average steel stresses (f_{sx}, f_{sy}, f_{sz})

Perform Crack Check to limit principal tension to satisfy equilibrium

1) Calculate reserve capacity in X Y and Z direction steel (f_{1cx} f_{1cy} f_{1cy})

$f_{1cx} = \rho_x (f_{yx} - f_{sx})$

$f_{1cy} = \rho_y (f_{yy} - f_{sy})$

$f_{1cz} = \rho_z (f_{yz} - f_{sz})$

This is the extra average stress required in X, Y or Z direction to yield the longitudinal steel

2) Triaxial yield without shear on crack (f_{1b})

$f_{1b} = f_{1cx} k_i^2 + f_{1cy} l_i^2 + f_{1cz} m_i^2$

Ensures that load required to cause triaxial yield of the reinforcement at a crack is not exceeded

3) Max shear on crack for biaxial or triaxial Yield (V_{ci2})

$v_{ciXYm} = | f_{1cx} - f_{1cy} | k_I l_I$

$v_{ciYZm} = | f_{1cy} - f_{1cz} | l_I m_I$

$v_{ciZXm} = | f_{1cz} - f_{1cx} | k_i m_I$

Calculate the shear on the crack required to achieve biaxial yield of the reinforcement

$v_{ci2}^2 = v_{ciXYm}^2 + v_{ciYZm}^2 + v_{ciZXm}^2$

This is the maximum shear on the crack

4) Limit shear on crack to maximum

if $v_{ci2} > v_{cimax}$, then pro-rate v_{ciXY}, v_{ciYZ}, v_{ciXZ}

4) Calculate Maximum allowed tensile stress from XY, YZ, XZ plane equilibrium

$f_{1c} = f_{1cx} + (| v_{ciXYm} l_i | + | v_{ciZXm} m_i |) / k_I$

$f_{1d} = f_{1cy} + (| v_{ciXYm} k_I | + | v_{ciYXm} m_i |) / l_I$

$f_{1e} = f_{1cz} + (| v_{ciXZm} k_I | + | v_{ciYZm} l_i |) / m_I$

Calculate maximum tension from equilibrium of inducing biaxial yield in each plane

5) Take minimum of all calculated values for final value of principal tension

$f_1 = \min(f_{1a} , f_{1b} , f_{1c} , f_{1d}, f_{1e})$

Select minimum value

Unlike the 2D case, calculating the shear on the crack and steel stresses at a crack for any given load level is complex. Recall that in two dimensions, there were 2 equations and 3 unknowns required to calculate the behaviour at a crack. In three dimensions, there are 3 equations and 5 unknowns. The equations are the sum of forces in the X, Y and Z directions. The 5 unknowns are the reinforcement stresses at a crack in

the X Y and Z directions along with two components of the shear on the crack. Shear on the crack in three dimensions is a 3D vector, but it is known that the shear on the crack must be in the plane of the crack, removing an unknown.

A simple algorithmic method as used above will not suffice for this case. An elegant way to solve the problem is to realise that the calculation of the answer is in fact a nonlinear optimisation problem of quadratic programming. Once the shear on the crack components have been found, the steel stresses may be calculated simply with equations, similar to the 2D case above. While there are only two components to the shear on the crack as the vector must be in the plane of the crack, it is simpler to leave the solution in terms of three components. The requirement that the vector remain in the plane of the crack will be maintained with the form of the equations used. As such, the problem is to find the 3 components of the shear on the crack subject to the constraint that the steel not exceed yield in any direction and that the shear on the crack be a minimum.

Using the assumption that the goal is to minimise the shear on the crack, and the notation in Table 4-2, the following quadratic programming problem arises:

$$\text{Minimise} \quad v_{ci}^2 = v_{ciXY}^2 + v_{ciYZ}^2 + v_{ciXZ}^2 \tag{4-4}$$

$$\begin{aligned}
\text{Subject to:} \quad & v_{ciXY} \le v_{ciXYm} \\
& v_{ciYZ} \le v_{ciYZm} \\
& v_{ciXZ} \le v_{ciXZm} \\
& v_{ciXY} \ge -v_{ciXYm} \\
& v_{ciYZ} \ge -v_{ciYZm} \\
& v_{ciXZ} \ge -v_{ciXZm} \\
& -l_i v_{ciXY} - m_i v_{ciXZ} < (f_{1cx} - f1)\, k_I \\
& k_i v_{ciXY} - m_i v_{ciYZ} < (f_{1cy} - f1)\, l_i \\
& k_i v_{ciXZ} + l_i v_{ciXZ} < (f_{1cz} - f1)\, m_i
\end{aligned} \tag{4-5}$$

Each of these constraint equations is one of the biaxial yield equations from Table 4-2. With only three degrees of freedom and nine constraints, this problem can easily be implemented using the brute force approach of checking each constraint individually and then by checking the intersection of different constraint planes. Note that the traditional simplex method of linear programming may not be used, as this is a nonlinear problem.

Once the shear on the crack components are calculated, the steel stresses at a crack can be calculated with the following equations using the notation in Table 4-2:

$$\rho_y(f_{syCRACK} - f_{sy}) = f_l + \frac{v_{ciXY}k_i - v_{ciYZ}m_i}{l_i}$$

$$\rho_x(f_{sxCRACK} - f_{sx}) = f_l + \frac{-v_{ciXY}l_i - v_{ciZX}m_i}{k_i} \qquad (4\text{-}6)$$

$$\rho_z(f_{szCRACK} - f_{sz}) = f_l + \frac{v_{ciXZ}k_i + v_{ciYZ}l_i}{m_i}$$

4-5 Crack Check against Flexural Yield for Cross Section

In calculating the allowable concrete tensile stress for sections subjected to flexure, as in Response-2000 and Shell-2000, a method is needed to limit concrete tension when controlled by flexural yield to ensure that the concrete on both sides of the entire crack surface is in equilibrium.

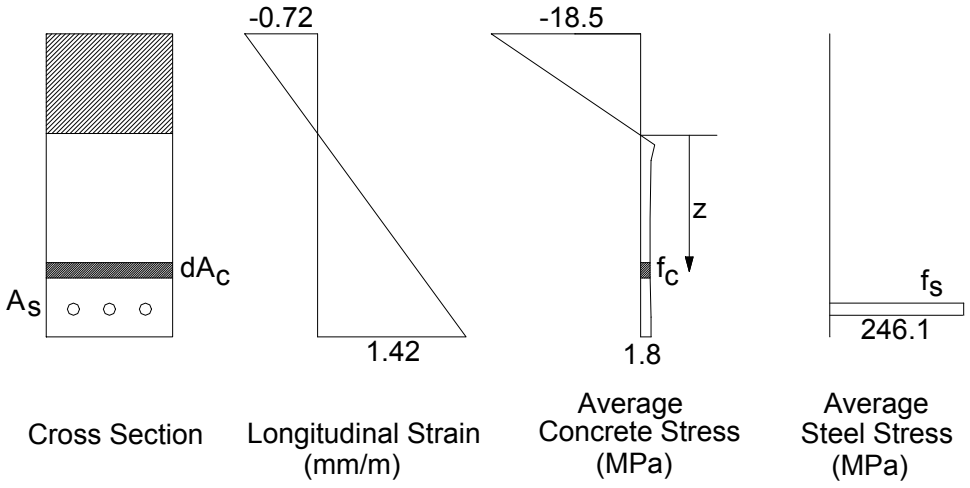

Figure 4 - 6: Beam in Flexure

Figure 4-8 shows a rectangular beam in simple flexure. Assuming that there is no direct concrete tensile stress transferred across a crack, moment equilibrium about the neutral axis produces the following equation:

$$\int f_c \cdot z \cdot dA_c = \sum A_s (f_{s-crack} - f_{s-average}) z_s \qquad (4\text{-}7)$$

That is, the moment about the neutral axis caused by the average concrete tension must equal the moment caused by the difference between the steel force on average and the steel force at a crack.

Specifying a maximum allowable stress at a crack, say the reinforcement yield stress, the equation may also be used to calculate the maximum allowable average concrete tensile stress that still maintains equilibrium. For Response-2000, this method is used to directly calculate the f_{1cx} term from Table 4-1. For Shell-2000, it is used to directly calculate the terms f_{1cx} and f_{1cy} in Table 4-2. That is, the method calculates the maximum horizontal component of the average concrete tension and shear on the crack that can be tolerated.

In the programs, the equation above is made an inequation in order to act as a crack check equation. As such the right hand side of the above equation is first used to calculate the maximum allowable concrete moment, a capacity moment. The maximum allowed reinforcement stress at a crack is the larger of the yield stress and the bare-bar stress corresponding to the average strain multiplied by a strain concentration factor. This strain concentration factor is taken as 2.0 for regular reinforcement and 1.25 for 7-wire strand prestressing reinforcement that has poorer bond characteristics. This technique of an explicit strain concentration factor contrasts with the technique of a bond stress based approach as recommended by Kaufmann, Marti and Alvarez[19, 50].

The left side of the equation above is calculated in two steps. Figure 4-9 describes the terms used in the calculation. The goal is to determine the largest average concrete stress component that can be tolerated without yielding the longitudinal reinforcement. A moment (M_1) is first calculated assuming a concrete stress of twice the cracking stress (f_t) at the neutral axis and zero at the bottom of the cross section. This variation in concrete tensile stress is integrated by taking moments about the neutral axis.

A second Moment (M_2) is then determined as the remainder of the capacity moment after M_1 is subtracted. A maximum value of average concrete tensile stress at the bottom of the cross section is calculated that would cause this moment. If the concrete exactly achieved the stress profile from 2 f_t at the neutral axis and f_{1max} at the bottom of the beam, the longitudinal steel would just yield at a crack.

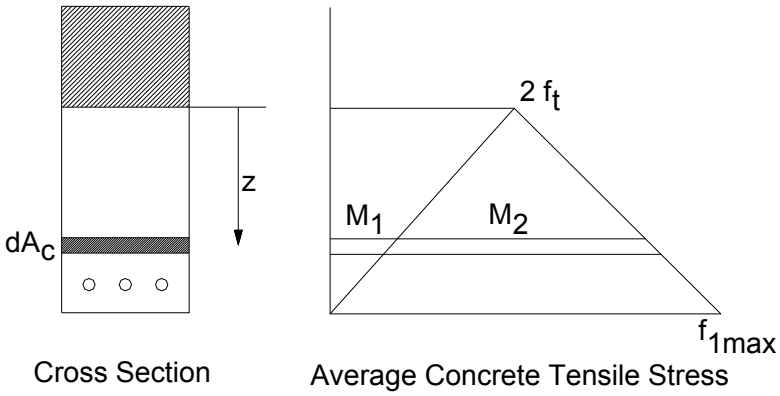

Figure 4 - 7: Concrete Moment

The reason for using twice the concrete cracking stress as an allowable stress near the neutral axis is that for cross sections without transverse reinforcement, the longitudinal tensile demand immediately below the flexural cracking front can exceed the cracking stress. That is, the horizontal component of the principal tensile stress added to the horizontal component of any shear on the crack sums to more than the cracking stress. Though this demand is high, the reinforcing steel below the crack front will, in general, have sufficient capacity to equilibrate this. If it does not, then this technique will lower the allowable tension to ensure it satisfies equilibrium. The use of two components to the flexural crack check is necessary as a single component was found to be numerically less stable. The two components more smoothly transition from a case with plenty of extra capacity at a crack and no capacity at a crack.

As this process does not require the results of biaxial or triaxial stresses, the flexural yield crack-check performed in this way is non-iterative.

There are some restrictions implicit in this method.

1) The concrete compression block is totally ignored in the analysis.
2) The assumption that a bar is always able to have a strain concentration factor of 1.25 or 2.0 at a crack means that bars that are linearly elastic up to failure are predicted to rupture at a strain well below the real rupture strain and stress. Further research is needed to develop more appropriate methods for such materials.
3) If there are no bars crossing the cracked zone, equilibrium requires that there be no average concrete stress. This was found to badly affect convergence at first cracking, however. As such, if there are no bars crossing the crack face, the concrete stress is not reduced. This is done for computational stability despite flagrantly violating equilibrium. The programs in this thesis are, therefore, not appropriate for calculating the flexural behaviour of plain concrete specimens. A case where this is more common is in the response of a singly reinforced section subjected to negative bending.
4) It is possible that in attempting to yield the top bar in a flexurally cracked zone, the bottom bar will rupture before the top can yield. This means that the calculated capacity concrete tension moment cannot be achieved. This is not dealt with explicitly, but shows up in an inability to calculate stresses at a crack. This generally has only a small effect on practical cross sections.

To calculate stresses at a crack on completion of the biaxial/triaxial solution for each node, the steps are basically reversed to calculate the stress in each bar. The moment caused by the combined principal tension and shear on the crack is computed about the crack face. An increase in curvature is then calculated about the crack front to induce the same moment.

Due to the possibility that some of the bars may become nonlinear during this calculation, it must be iterative. To save time, the stress at a crack is only calculated once per load stage, just before showing it to the user.

Chapter 5: Concrete Constitutive Relations

The Modified Compression Field Theory (MCFT) treats cracked concrete as a new material, so it is necessary to define the stress-strain characteristics of this new material. As the MCFT is based on principal stress-principal strain relationships with a special check for shear on the crack, the relations may be divided into the categories of behaviour in compression, behaviour in tension and behaviour in interfacial shear.

5-1 Behaviour in Compression

The compression response is divided into two components, the base curve and the compression softening relationship. The base curve represents the behaviour of a uniform block of concrete subjected to uniform compressive stress. While a standard concrete cylinder is transversely restrained by the loading platens and therefore is not really uniform, it is assumed that the stress-strain curve of a cylinder represents the base curve. Also, while a standard cylinder must be tested at 28 days to be called f_c', the idea that the cylinder strength on the day of testing can also be called f_c' will be used here.

There are a series of base curves available in the programs for modelling concrete. These are explained in Section 2 of the program's User Manual in Appendix A. The recommended base curve, the Popovics curve, is shown in Figure 5-1 for a series of different strength concrete cylinders. This base curve was defined by Popovics[51] and partially calibrated by Porasz[20] is shown in the following equations (in MPa units):

$$f_2 = f_c' \frac{n(\varepsilon_2 / \varepsilon_c')}{n - 1 + (\varepsilon_2 / \varepsilon_c')^{nk}}$$
$$n = 0.8 + \frac{f_c'}{17} \qquad (5\text{-}1)$$
$$k = 0.67 + \frac{f_c'}{62}$$

Where: f_c' = peak stress from cylinder test
ε_c' = strain at peak cylinder stress
n = curve fit parameter
k = factor for loss in post peak ductility for high strength concrete

if $\varepsilon_2/\varepsilon_c' < 1.0$, k = 1.0.
if $\varepsilon_2/\varepsilon_c' > 1.0$, k = equation above

The parabolic base curve, is shown below in Fig. 5-2. The Popovics method is recommended over the parabolic as it better models initial stiffness and, more importantly, post-peak behaviour.

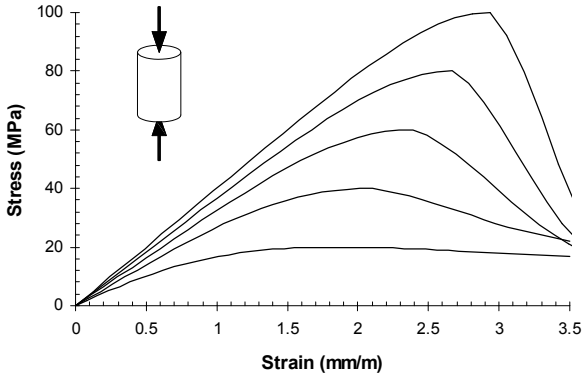

Figure 5 - 1: Popovics Concrete Base Curve

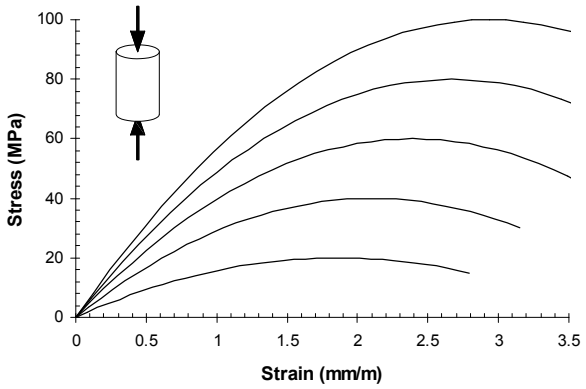

Figure 5 - 2: Parabolic Concrete Base Curve

For both of these curves, the strain at peak stress (ε_c') is needed to complete the definition. This is a function of the shape of the base curve as well as the initial tangent stiffness of the concrete (E_c), itself a function of the stiffness of the aggregate. If the initial tangent stiffness of the concrete is known, or a stress-strain curve from a cylinder test is available, an estimate of the strain at peak stress may be made. If neither are available, then the following method is suggested[5] (in MPa units)

$$E_c = 3320\sqrt{f_c'} + 6900$$
$$\varepsilon_c' = \frac{f_c'}{E_c}\frac{n}{n-1} \qquad (5\text{-}2)$$

where the parameter n is defined above

Figure 5-3 shows this relationship compared to a selection of data representing the peak stress and strain at peak stress for test cylinders associated with shear tests from the

University of Toronto[15, 28] and the University of Houston[29, 30, 31]. The data from the Toronto tests give higher than predicted ε_c' values as Toronto's crushed limestone aggregate tends to produce lower stiffness concrete than that predicted by the equation above.

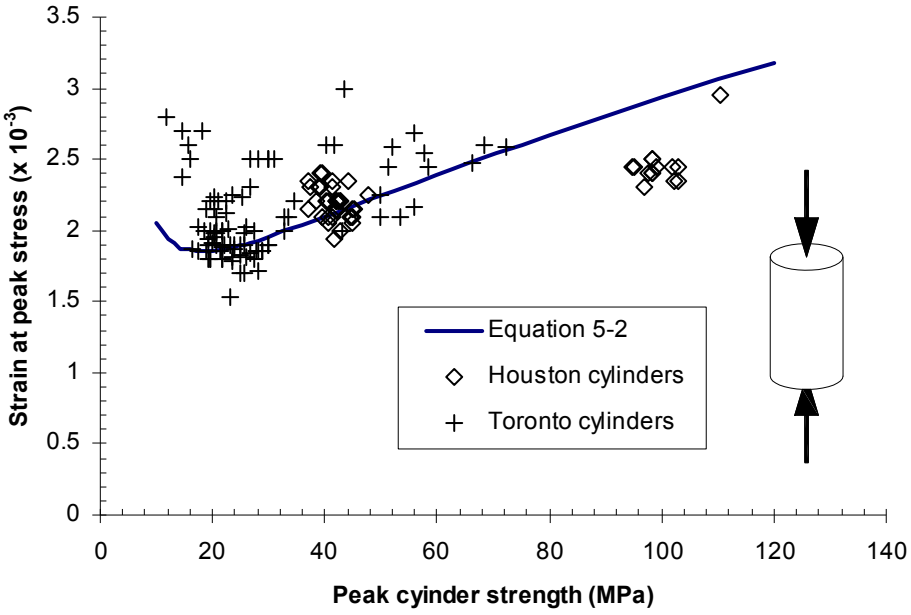

Figure 5 - 1: Strain at peak stress

The second part of the compressive response of concrete is compression softening, which represents the tendency for concrete to reduce in strength and stiffness as a result of transverse cracks caused by tensile straining at 90° to the compression. While initially the equations were based on the diameter of the Mohr's circle of strain[14], it has since been recast as a function of the principal tensile strain of the concrete[11].

For compression softening of normal strength concrete, it is suggested that the equation in Figure 3-1 be used. This equation is shown in Fig. 5-4 along with experimental data from a series of tests performed at the University of Houston by Pang[30] (triangles) and Belarbi[29] (diamonds). This equation was suggested in 1984 based largely on the results of tests on concrete specimens 20 to 30 MPa in strength[52]. The relationship can be seen to model the data from these more recent Houston concrete specimens well.

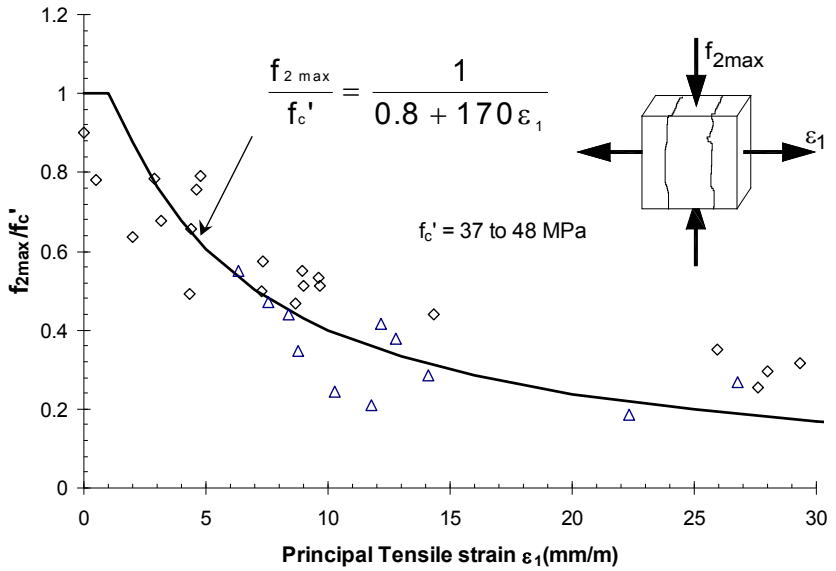

Figure 5 - 2: Compression Softening: Normal strength concrete

For very strong concrete, say more than 90 MPa (13 ksi), it is recommended that the equation proposed by Porasz in 1989 be used[20]. This equation lowers the maximum compressive stress as a function of base concrete stress as well as principal tensile strain. Figure 5-5 shows a series of 100 MPa concrete experimental data points from the University of Houston tested by Zhang in 1998[17], compared with this equation.

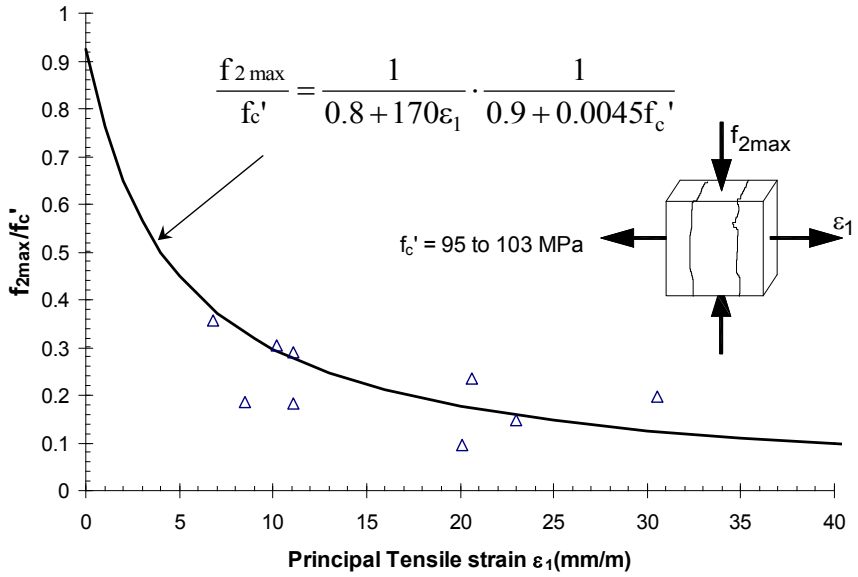

Figure 5 - 3: Compression softening: High strength concrete

5-2 Behaviour in Tension: Uncracked Concrete

Concrete in tension is assumed to act linearly until first cracking with a stiffness equal to the initial compression tangent stiffness. Cracking is clearly an important phenomenon in concrete. Traditionally, the use of the ACI shear cracking stress of $4\sqrt{f'_c}$ (psi), $0.33\sqrt{f'_c}$ (MPa) has been suggested for use in the MCFT. However, it has been found that this prediction of cracking strength is not particularly good for high strength concrete. Figure 5-6 shows the cracking strength versus concrete compressive strength for a series of large reinforced concrete elements[11, 29, 30, 31, 32, 33] along with the ACI relationship.

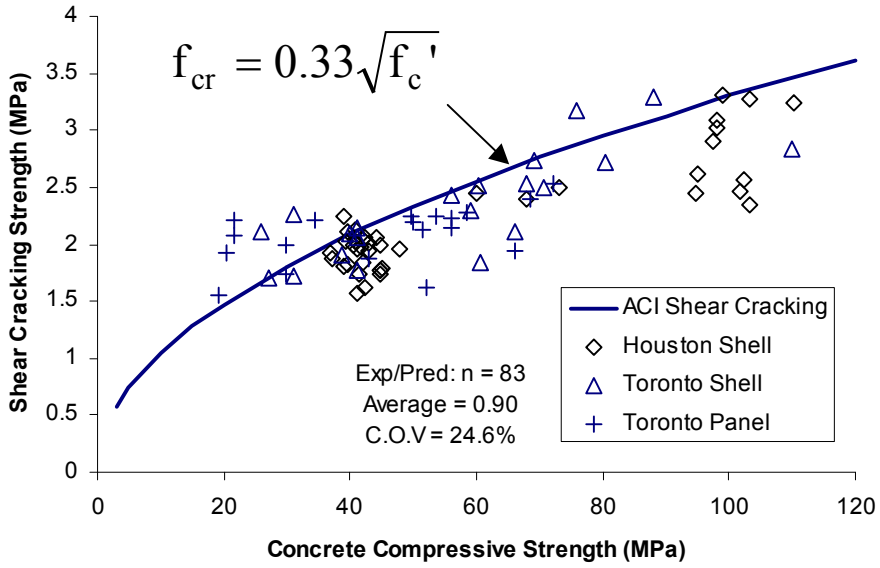

Figure 5 - 4: ACI Shear cracking strength of concrete

The fit to the higher strength data is not especially good. Instead, the programs in this thesis all use the following relationship for the cracking strength of a large volume of concrete (MPa units):

$$f_t = 0.45(f_c')^{0.4} \tag{5-3}$$

Figure 5-7 compares this equation to the same data set used above.

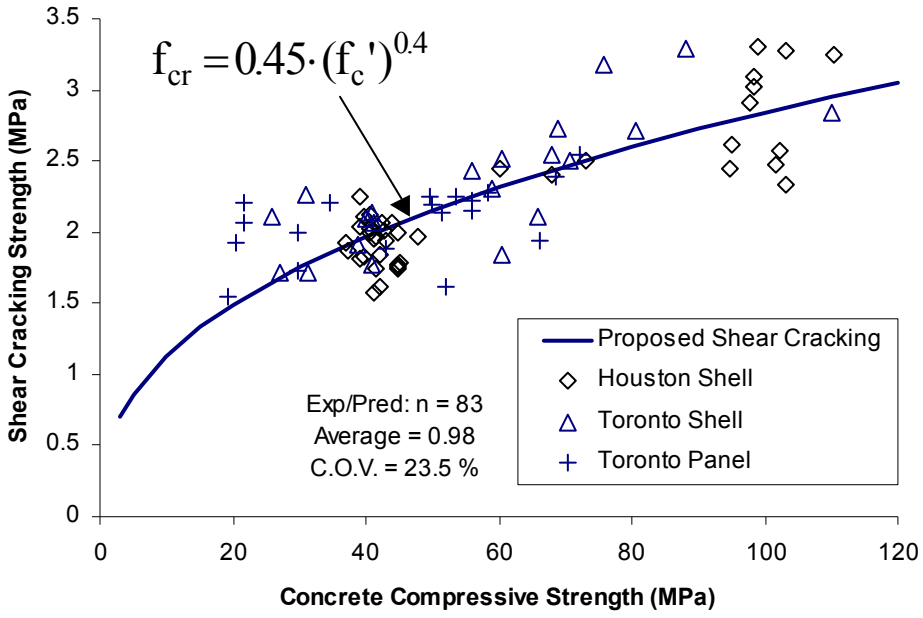

Figure 5 - 5: Proposed shear cracking strength of concrete

Figure 5-8 compares the proposed cracking strength equation to the traditional ACI equation. It can be seen that for concrete strengths less than, say, 40 MPa, there is only a small change in the predicted cracking strength. For 120 MPa concrete, however, the predicted cracking strength drops by 18% below the ACI value. This is important in predicting the behaviour of high strength concrete beams without stirrups.

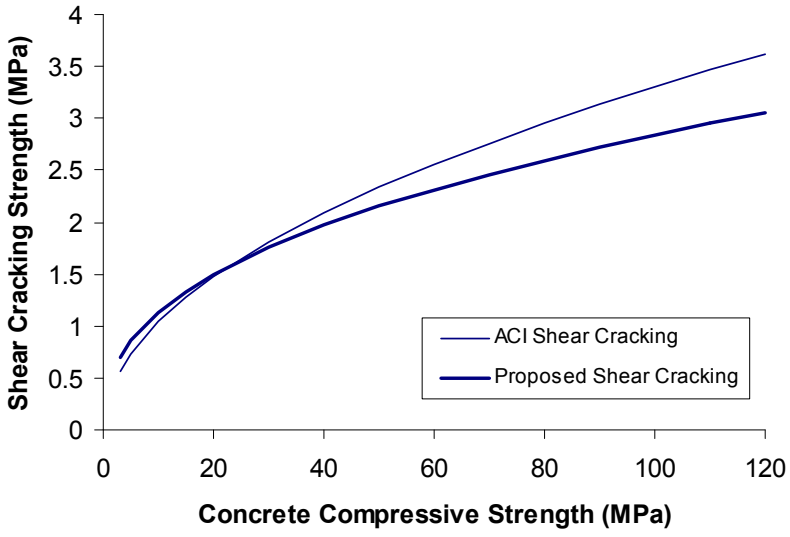

Figure 5 - 6: Comparison of shear cracking strengths

Note that the relation proposed is appropriate for structural analysis of a large volume of concrete. The data points used to derive it are from uniformly loaded elements containing up to 1 m^3 of concrete volume. Tests involving small volumes of concrete or with high strain gradients through the depth can be expected to show higher strengths. For example, the modulus of rupture test on a 150 x 150 mm cross section only exposes one one-thousandth as large a volume of concrete to high tensile stresses as the large element tests do. The chance of the weakest, and hence controlling, piece of concrete being in this small volume is remote, meaning that strengths from the modulus of rupture tests are generally higher than the above equation would predict. It is recommended that even if such results as modulus of rupture or split cylinder strengths are available for a given concrete, the above equation be used.

5-3 Behaviour in Tension: Well Reinforced Cracked Concrete

After cracking, reinforced concrete elements can still carry tension between the cracks through the action of bond. The concrete tension between cracks results effectively in a more substantial cross section than that of a bare bar and, as such, this phenomenon has become known as tension stiffening. Many different equations for the average tensile stress in the concrete after cracking have been proposed over the years. The models available in the programs are listed in Section 2 of Appendix A. Three of the equations are described below and plotted in Figure 5-9:

The first equation is that proposed by Vecchio[15], based on his original 30 panel elements.

$$f_1 = \frac{f_t}{1 + \sqrt{200\varepsilon_1}} \tag{5-4}$$

The second equation was proposed by Collins and Mitchell[16], based partly on the results of the large shell element tests.

$$f_1 = \frac{f_t}{1 + \sqrt{500\varepsilon_1}} \tag{5-5}$$

The third equation presented here is the Tamai[34] equation as used by Hsu and his colleagues at the University of Houston.

$$f_1 = \frac{f_t}{\left(\frac{\varepsilon_1}{0.00008}\right)^{0.4}} \tag{5-6}$$

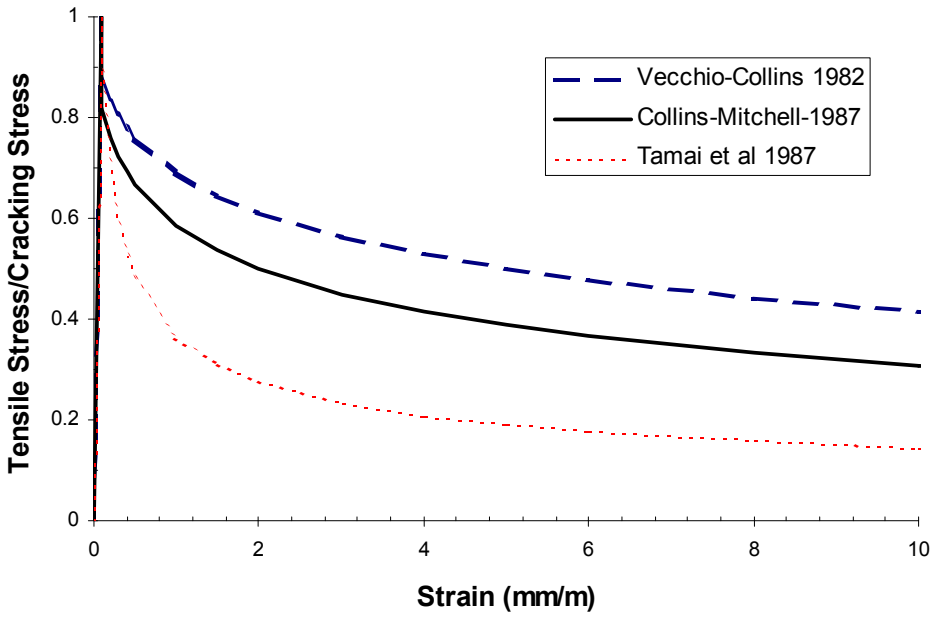

Figure 5 - 7: Comparison of tension stiffening relationships

Note that there is a substantial variation between these predictions. Generally, the 1982 equation fits well to tests in the small University of Toronto panel tester, the 1987 relation fits well to data from the larger University of Toronto shell element tester, and the Tamai relation has done a reasonable job with the data from the University of Houston. If an equation of the same form of the MCFT is fitted to the Houston data originally used to justify the use of the Tamai equation, a coefficient of 1500 is produced, rather than the 200 and 500 in the other equations. It has been something of a mystery why these differ as much as they do, though various explanations such as overall size have been used.

Consider that tension stiffening is largely a bond phenomenon. That is, it is the bond between the reinforcing bar and the concrete that causes any tension to develop in the concrete between the cracks. Collins and Mitchell[5], for example, recommended that tension stiffening be reduced by a factor of 0.7 for plain bars or strands which will have poorer bond properties than deformed bars. It is proposed that concrete tension stiffening should be made a more specific function of bond characteristics of the reinforcement. Thus, at locations where the concrete is reinforced with a closely spaced array of small diameter bars, the average tensile stress in the cracked concrete can be expected to be higher than at locations reinforced with a widely spaced array of large diameter bars. The typical cross-sections tested in the three research program mentioned above are shown in Fig 5-10. Note that the bond characteristics of each will be different.

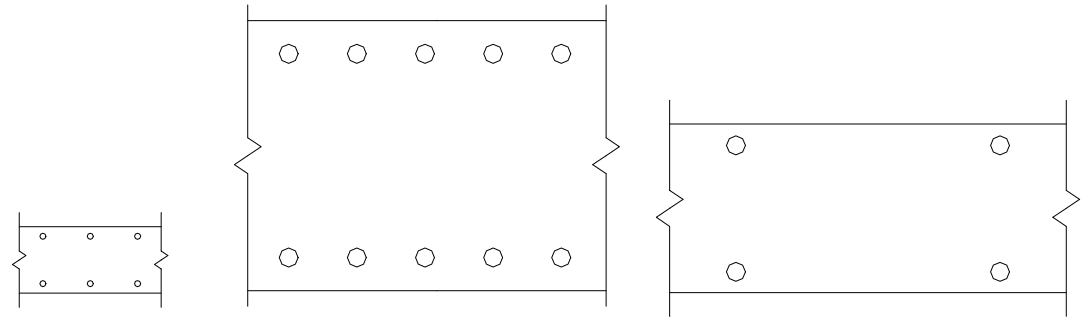

Figure 5 - 8: Scale of element tests

An appropriate parameter to indicate the bond characteristics of different arrays of reinforcement is to divide the area of concrete in tension by the perimeter of all the reinforcing bars bonded to the area. Thus,

$$m = \frac{A_c}{\sum d_b \pi} \tag{5-7}$$

For the typical elements shown in Fig. 5-10, this bond parameter works out to be 62 mm for the University of Toronto panel tests, 163 mm for the University of Toronto shell element tests, and 421 mm for the University of Houston shell element tests.

If the coefficient of the MCFT style tension stiffening equation is plotted with respect to this bond term, the plot shown in Fig. 5-11 is produced.

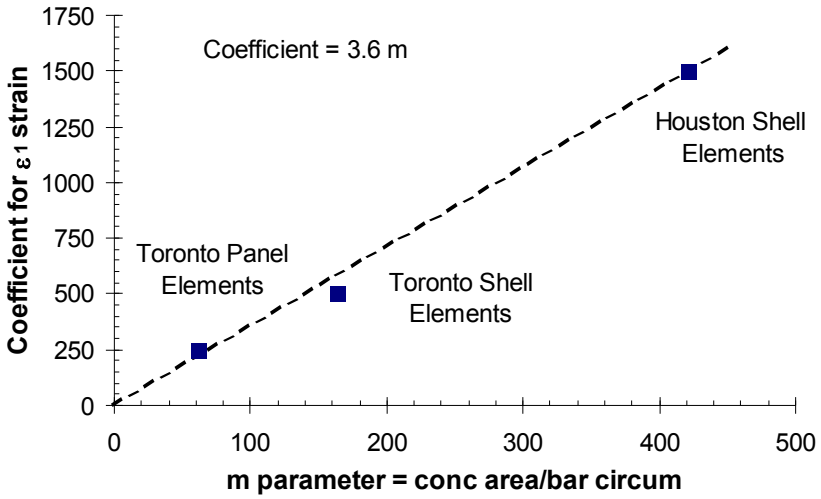

Figure 5 - 9: Tension stiffening vs. m parameter

There is a clear relationship suggesting that for elements with poorer bond properties, i.e. larger m values, the tension stiffening should be lower.

The above relation is based on tension stiffening equations that were averaged from a number of elements in each series. By plotting the trend with individual

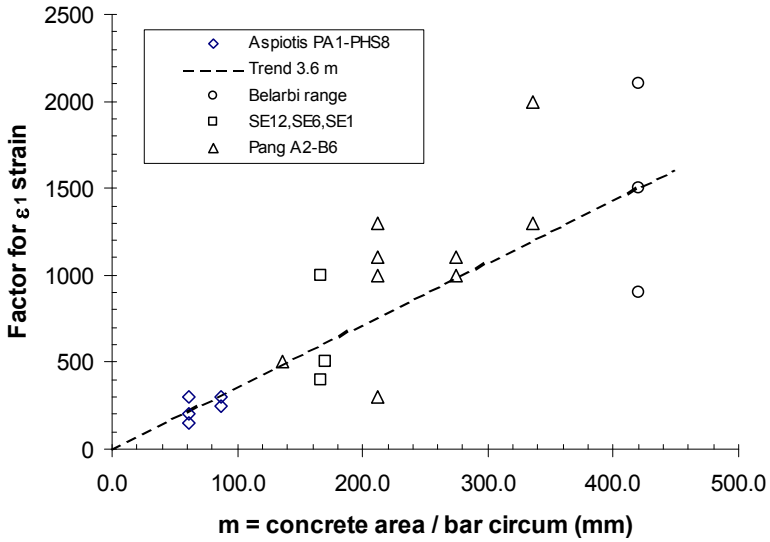

Figure 5 - 10: Tension stiffening vs. m for individual elements

shear experiments[32, 29, 30, 12], Fig. 5-12 is obtained. It can be seen that while the data for individual elements involves much greater scatter, there is a clear trend supporting the relationship suggested above.

Based on this, it is proposed that for uniformly reinforced concrete, the coefficient in the denominator of the MCFT tension stiffening equation normally shown as 500 be replaced by the term 3.6m as follows:

$$f_1 = \frac{f_t}{1 + \sqrt{3.6m \cdot \varepsilon_1}} \qquad (5\text{-}8)$$

$$m = \frac{A_c}{\sum d_b \pi}$$

where m is the bond parameter in millimetres

A_c is the area of concrete effectively bonded to the bar

d_b is diameter of bar in concrete stiffened area

This will improve the scatter of the predictions of uniform elements subjected to shear, as shown in Chapter 8. Note that this equation will only affect the behaviour between first cracking and when the crack-check begins to control the behaviour. The fact that this parameter has units indicates that it will be dependent on the absolute size of the specimen tested. It is suggested that this term partly explains the size effect in shear as shown in Chapter 10.

For biaxially or triaxially loaded elements, there will often be different values of the m parameter in the different reinforcement directions. It is recommended for these cases that the selected value of the m parameter be the lowest value for each of the orthogonal reinforcement directions. This means that the tension stiffening will be controlled by the direction that has the best bond properties. This was found to reasonably model the experimental behaviour.

5-4 Behaviour in Tension: Poorly Reinforced Cracked Concrete

The equation proposed above is appropriate for regions of reinforced concrete that are relatively close to reinforcement, such as in the membrane element experiments described. Further away from reinforcing steel, however, the proposed equation is not appropriate to use. Figure 5-13, based on Collins & Mitchell[5], shows the CEB-FIP suggestions for the effective concrete embedment zone. Concrete in this zone, within 7.5 d_b of longitudinal steel, can be assumed to have a significant average tensile stress between the cracks. Outside this region, it is assumed that there is not any significant average concrete tensile stress after cracking. That is, it would be appropriate to use the tension stiffening relation proposed above in the embedment zone, but not outside of this region. This simplification is appropriate for analyses without shear, but less so when shear is considered. In beams without transverse reinforcement, for example, it is the average concrete tensile stress that must balance the diagonal compression in the web. Selecting a tension stiffening equal to zero would then imply that there is no shear carrying capacity in a beam where the web extends more than 7.5 bar diameters from the reinforcement. Taylor, amongst others, demonstrated that the webs of such beams can carry in the order of half of the applied total shear force by aggregate interlock[35]. As such, a method is needed to calculate an appropriate level of tension stiffening for regions that are a fair distance away from reinforcement.

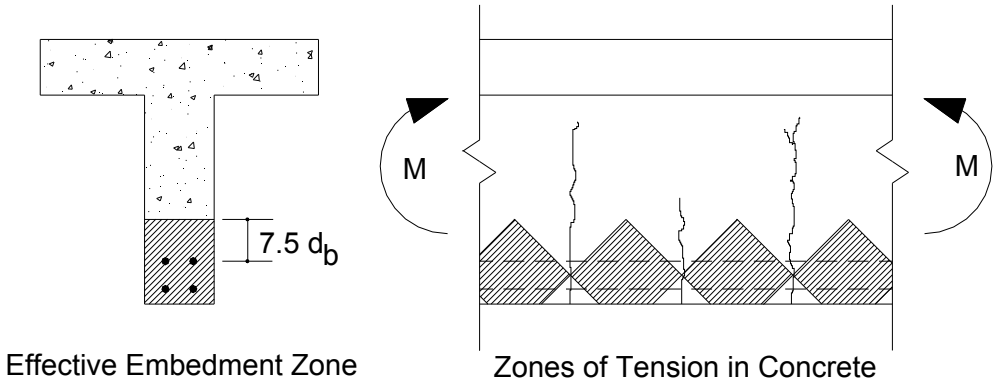

Figure 5 - 11: Tensile stress in cracked concrete

To model such conditions, consider the "tooth" of concrete between cracks shown in Fig 5-14. It is reinforced with a single bar and loaded in axial tension via the bar. Tension stiffening in this example will be an average concrete tensile stress in the direction of the bar above and below the bar. A linear elastic finite element analysis was performed for such an element assuming that the concrete stress at the elevation of the bar was constant and just below the cracking strength.

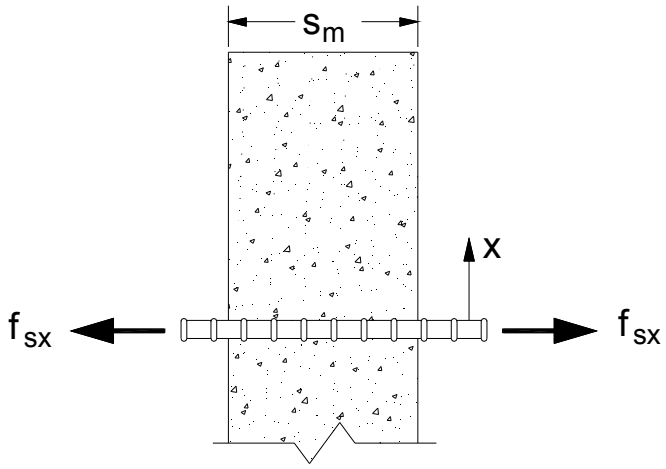

Figure 5 - 12: Concrete between cracks

Figure 5-15 plots the average concrete tensile stress versus the x-axis in Fig 5-14.

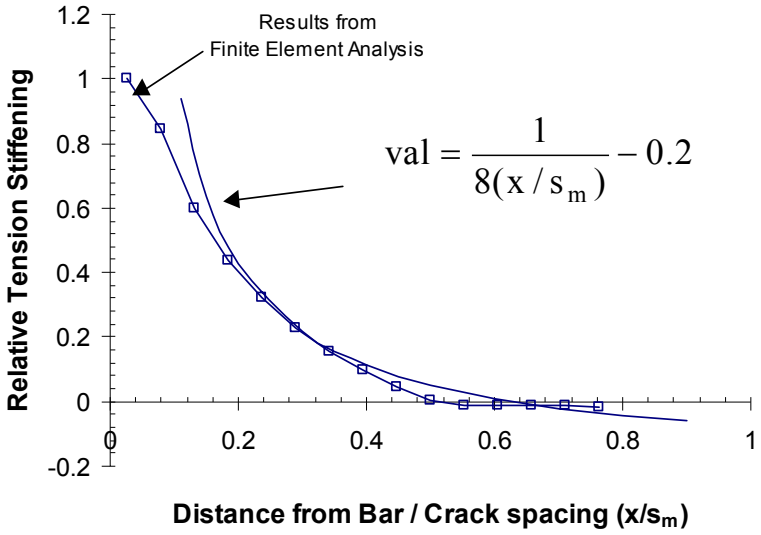

Figure 5 - 13: Tension stiffening vs distance from bar

The stress values have been normalised with respect to the maximum values found just above the bar. Also shown is a simple curve fit equation.

The analysis predicts that the average tension in the concrete will reduce to zero as the distance away from the bar reaches about half the crack spacing. This is expected from St. Venant's principal as the "stress bulb" will be symmetrical about each half of the tooth's width. Beyond half the crack spacing away from the bar, the predicted average concrete stress is in fact slightly compressive.

To spot check this analysis, consider the typical concrete elements drawn in Fig. 5-10. The geometry of these is such that no point in the concrete is further from a reinforcing bar than about 0.25 to 0.3 times the predicted crack spacing. Based on the average value of tensile stress in Fig. 5-15 over that range, it might be expected that the total tension stiffening would be about 0.6 times the maximum value. The base MCFT tension stiffening equation predicts that level of tension stiffening for a strain of about 1 mm/m which is about half of the yield strain. This suggests that the calculated values from the finite element analysis are reasonable.

To attempt to directly use the results from Fig 5-15 in sectional analysis, a few difficulties arise. The biggest is that the real crack spacing over the depth of a beam is discretely changing. The predicted crack spacing, explained in Chapter 7, smoothly increases approximately as 2 times the distance from a bar plus a value at the bar. As such, as the distance away from the bar increases, the crack spacing also increases. To deal with such issues, some empirical curve fitting was necessary to make the above finite element analysis directly connect with the programs. This fitting was performed with Response-2000 on a series of 83 elements without shear reinforcement.

Figure 5-16 shows a portion of the bottom of a concrete beam. The tension stiffening (f_1) at depth z in the figure is calculated as follows.

$$f_1 = \frac{f_t}{1 + \sqrt{M \cdot \varepsilon_1}} \tag{5-9}$$

Where $M = 3.6 \cdot 2 \cdot (A_c / \Sigma \pi d_b)$ $s_{mz} < 2s_{mbase}$

$M = 3.6 \cdot 2 \cdot (A_c / \Sigma \pi d_b) / \sqrt{(1/(8 \cdot z_d / s_{mz}) - 0.2)}$ $s_{mz} > 2s_{mbase}$

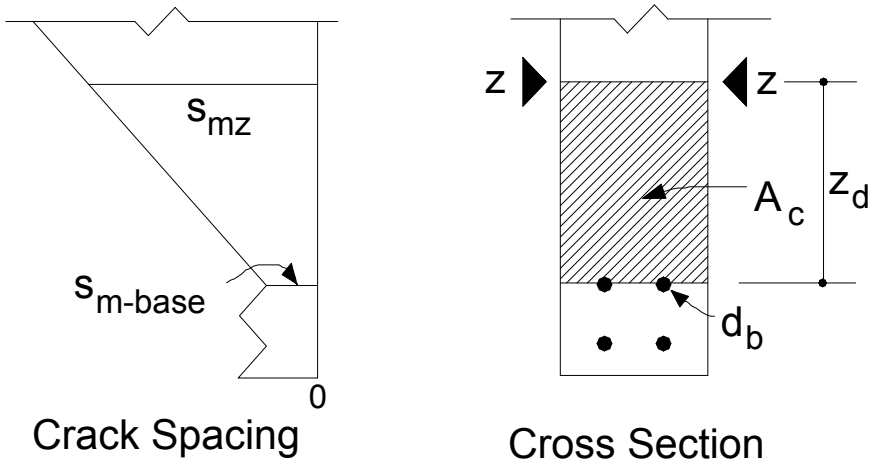

Figure 5 - 14: Tension stiffening parameters

Note that the curve fit equation in Figure 5-15 only comes into effect if the location of interest in the concrete is a sufficient distance from the nearest steel. This distance is assumed to equal twice the crack spacing at the bar for simplicity. Nearer to the bar than this, the equation is similar to the equation presented above for the average value over a membrane element.

Note equation 5-9 represents the incremental value of tension stiffening. The earlier equation in Fig. 5-11 models the average tension stiffening for all of the area of concrete in Fig. 5-16, whereas this new equation is the value to apply at the location z alone. To simply model this difference from the average and the incremental value, a factor of 2.0 is applied to the equation. It was found that the results are not sensitive to this factor.

Table 5-1 shows the use of the proposed tension stiffening equations for a given strain state for a beam. The beam is 1 metre deep, with 4-30M bars 100 mm up from the bottom face of the beam. For the given strain state, the tension stiffening parameters are calculated showing the distribution of average concrete tension over the depth of the element. Chapter 10 compares the effect of these proposed tension stiffening equations on the quality of predictions of Response-2000.

Table 5-1 Tension Stiffening Equations Demonstration

fc' 30 MPa 1000 x 300 mm cross section
Ft 1.75 MPa 4 – 30M bars 100 mm up = 2800 mm^2

				Near Bar	Far from Bar						
Depth (mm)	strain (mm/m)	s_{mz} (mm)	Ac (mm^2) x 10^3	M term Eq. 5-8	z_d (mm)	dist/s_{mz}	Best fit Equation Fig 5-15	M term Eq. 5-9	s_{mz} $s_{m\text{-}base}$	Select M	Stress (MPa) Eq. 5-9
1000	-1.01	1000	270	5156	900	0.90	-0.06				
900	-0.70	1000	240	4584	800	0.80	-0.04	Uncracked			
700	-0.07	1000	180	3438	600	0.60	0.01				
650	0.09	1000	165	3151	550	0.55	0.03	19081	2.71	19081	0.77
600	0.24	1000	150	2865	500	0.50	0.05	12811	2.46	12811	0.63
510	0.52	910	123	2349	410	0.45	0.08	8441	2.02	8441	0.56
400	0.87	715	90	1719	300	0.42	0.10	5493	1.48	1719	0.79
300	1.18	520	60	1146	200	0.38	0.13	3241	0.99	1146	0.81
200	1.49	325	30	573	100	0.31	0.21	1262	0.49	573	0.91
100	1.80	203	18	344	0	0.00	1.00	344	0.00	344	0.98
0	2.12	325	30	573	100	0.31	0.21	1262	0.49	573	0.83

Notes: As listed in Chapter 7, Crack spacing cannot exceed member depth for beams in flexure
Ac term cannot be less than the width multiplied by twice the bar diameter
The controlling type of tension stiffening is shaded.

5-5 Concrete in Interfacial Shear

The shear on the crack relationship used in the programs is the base equation proposed over 12 years ago for the MCFT. The only difference is that the effective aggregate size is reduced from the real value down to zero over concrete strengths between 60 and 80 MPa. This has been done as high strength tests are observed to fail with cracks cutting through the aggregate, rather than around the aggregate as with

normal strength concrete. This same argument also applies to lightweight concrete. The effect of making a lower effective aggregate size is to lower the maximum shear on the crack for stronger concretes. The methods proposed by Gupta[80] should be examined to determine if they allow for better modelling of behaviour of interfacial shear.

5-6 Time Dependent Effects

Vecchio[11] noted that concrete tested at a young age tends to have a higher cracking strength relative to its compressive strength than older concrete. As some of the results in the experimental verification database are of experiments done on very young concrete, sometimes three days after casting, a simple way to account for this early age effect is presented here.

Vecchio's panels were generally tested at an age of about seven days, with three days of curing. An examination of the cracking strength and the tension stiffening shows that there is indeed a correlation between the time between the completion of curing and the test and a strength increase. Figure 5-17 shows the data for elements tested in pure shear for the cracking strength, showing a trend towards higher strength for early age.

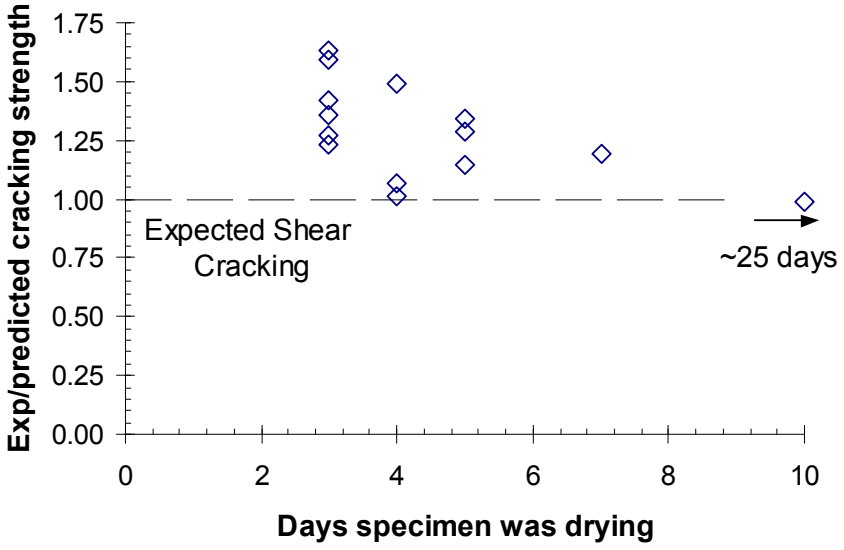

Figure 5 - 15: Cracking strength vs. drying time

Figure 5-18 shows the same pattern for tension stiffening. In this case, the base MCFT tension stiffening relationship was compared to the observed tension stiffening. A factor was calculated for the reported data points that indicated the relative value of the observed tension stiffening with respect to the expected value. For example, if a test showed results identically the same as what the base equation predicts, then it would have a value of 1.0, while another test having an average tension stiffening twice what was expected would have a value of 2.0. Plotting these factors versus the days between the completion of curing and testing produces the following trend:

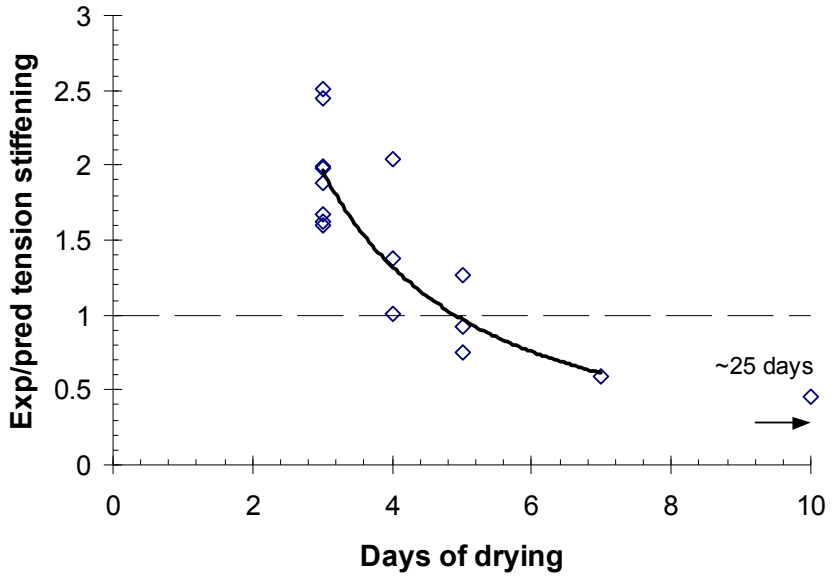

Figure 5 - 16: Tension stiffening vs. drying time

There is a clear trend for higher tension stiffening for early age concrete. This will be a function of a number of things including shrinkage and surface drying. Vecchio's specimens were 70 mm thick and some were of relatively low concrete strength, suggesting that the patterns seen here for 5 days may be applicable to older specimens that are larger.

The following is suggested for analyses of young concrete structures. For concrete that is younger than 7 days, it is recommended that the automatically calculated tensile strength of concrete be increased by 25%. This corresponds to Vecchio's original

observation that the younger concrete tended to crack at $5\sqrt{f'_c}$ (psi) rather than $4\sqrt{f'_c}$ (psi) as expected. It is suggested that beams tested at 14 days of age not have the cracking strength modified. Ages between these two limits may be linearly interpolated.

Chapter 6: The Longitudinal Stiffness Method

While most sectional analysis programs do not include the effects of shear stresses that vary through the depth of the element, Response-2000 includes the effects of beam shear stresses, and Shell-2000 includes the effects of out-of-plane shear stresses, which both vary through the depth of the element. The challenge is to determine the distribution of shear stress with depth. It will be affected by the width of the section, the material properties of the concrete, and the location and amount of reinforcement. The technique used is based on equilibrium of longitudinal stresses as derived by Jourawski in 1856[36].

The new method presented here is an extension of the methods used by earlier nonlinear sectional analysis programs[37, 6, 53] extended to increase performance and computational stability. The method is used in Reponse-2000 and Shell-2000 to calculate a new estimate of the shear stress profile for a given load level. The programs assume an initial profile and then use this procedure to calculate a new profile and iterate until the assumed and calculated profiles are in agreement.

6-1 Traditional Shear Stress Calculation

Consider the prismatic beam on simple supports shown in Fig 6-1. The right side of the figure is a free body diagram of the part of the beam between sections A and B.

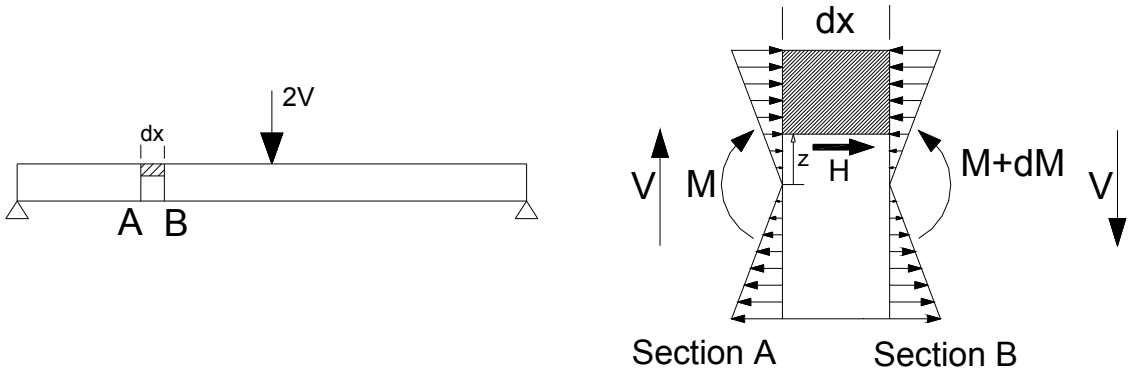

Figure 6 - 1 : Shear stress calculation

This section of beam is dx units long, and subjected to constant shear V and no axial load. The moment at section A is taken as M, and, due to the shear, the moment at section B will be higher, M + dM = M + V·dx. The assumed linear longitudinal strain gradient from the moment will cause a longitudinal stress profile with compression on the top and tension on the bottom of the cross section. Consider the shaded section at the top right of Fig 6-1 as a free body diagram of the top of the beam, from elevation z up to the top of the beam. It is subjected to a force on the left from the moment, but a higher force on the right from the slightly higher moment. This requires a balancing force on the cut plane of the beam, shown as H. Due to the summation of moments about a point equalling zero, the shear stress in a horizontal plane at a point must equal the vertical shear stress. As such, the force H divided by the beam width and dx results in the vertical shear stress on the beam at depth z. This is the same derivation used to produce Jourawski's familiar relationship:

$$v = \frac{V \cdot Q}{I \cdot b} \tag{6-1}$$

An implicit assumption in this theory is that plane sections remain plane it was used to calculate the longitudinal stresses. Though the shear strains associated with the calculated shear stress will warp the section, violating plane sections, the warping does not affect the longitudinal stress gradient for regions of constant shear[78].

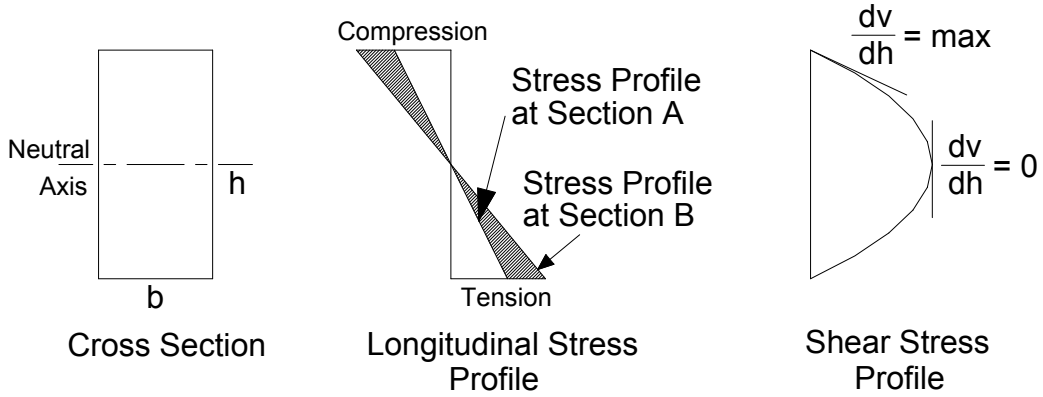

Figure 6 - 2: Internals of shear stress calculation

It is useful to examine in more detail what is happening in the description above. Figure 6-2 shows the simple case of a linear elastic rectangular cross section subjected to shear. The stress profile that will occur at Section A and B, as in Fig 6-1, are drawn together on the same axis for comparison. As section A has a smaller moment, it will have a smaller stress profile than at section B where the moment is larger. The shaded region represents the difference in stress profiles between the two sections. It is this difference that defines the shear stress profile. Also shown is the shear stress distribution, which for this case is a parabola. Note that the slope of the shear stress plot with respect to depth is zero at mid-depth, and maximum at the top and bottom of the section. These slopes are directly proportional to the difference in the longitudinal stresses at sections A and B. That is, the shaded area on the middle plot at any given depth is proportional to the derivative of the shear stress plot with respect to the beam depth.

In this case, the difference in longitudinal stresses between sections A and B is linear, so the shear stress profile is parabolic. For general nonlinear materials, however, the difference in longitudinal stress profiles will not necessarily be linear. The difference in strains between sections A and B, on the other hand, will always be linearly distributed over the depth when the assumption of plane sections remaining plane is used. If this change in longitudinal strain profile is known along with the longitudinal stiffness (i.e. rate of change of longitudinal stress with longitudinal strain) over the height of the beam, the shear stress profile can be generated. This is the basis of the method described in this chapter.

6-2 Previous state-of-the-art

To use Jourawski's theory for shear stress distribution for the analysis of reinforced concrete beams, the nonlinear behaviour of concrete must be included. The nonlinearity means that the problem generally must be solved numerically rather than analytically. The previous state-of-the-art for sectional analysis of concrete beams including shear is represented by Program SMAL[6], which divides a beam into a fixed number of layers and assumes that the stress-strain state is constant for that layer. Each

layer may have a different width. The shear stress is then calculated at the interface of each of these layers. A full load-state/strain-state analysis is done at sections A and B in Fig 6-1, separated by the distance dx, suggested by Vecchio and Collins as d/6. The "dual section analysis" procedure then numerically integrates the stresses above each layer interface in the section and calculates the resulting shear stress profile down the depth.

6-3 Development of method and problems with previous methods

The work in this thesis started, partly, as an amalgamation of Programs Response[38] (that was available in the Collins & Mitchell textbook[5]) and program SMAL[6]. Response-2000 is a total rewrite of the older Response, now called Response-90, but benefited from the experience gained in its writing 10 years ago. It was found in the development of Response-90 that a good way to improve the numerical stability of the analysis was to automatically subdivide layers that were poorly interpolated. For example, if flexural cracking happens to occur in the middle of a layer, it is wise to divide that layer in half to improve numerical stability. As an earlier step in developing Response-2000, this dynamic layering routine was added to the dual section analysis methods as implemented in SMAL.

While program SMAL is relatively stable, there remain situations where the program will stop in the middle of operation and no longer converge. With small adjustments in the input conditions, it can often be made to converge. It was thought that the use of the dynamic layering would reduce the incidences of this instability. On the contrary, it was found that the Response-2000 became less stable than SMAL when dynamic layering was implemented. Over a period of about a year, a series of issues were discovered that indicated that the numerical methods used by SMAL were inherently unstable in certain circumstances. These problems only became visible with the precision that comes out of a dynamic layering routine. For example, issues relating to the exact depth of cracking will only be important in SMAL if the manually assigned

layer divisions happen to coincide with the calculated crack front. In cases where this did happen, however, it is likely that SMAL would be unable to converge to a solution.

Primarily, the problems arise due to numerical instabilities in calculating a small difference of two large numbers. The shaded area in Fig. 6-2, used to calculate the shear stress profile, for example, is calculated as the difference of the stresses at sections A and B. If the distance between sections A and B, dx, is reduced, the answer is a smaller difference between large numbers. This might suggest that increasing the dx term should increase stability. It was found, however, that smaller values of dx generally led to more stable solutions. If it was made too small, however, numerical noise would creep in and make the programs iterate unnecessarily. The balance point was not obvious.

Three major problems were discovered with the previous state-of-the-art methods for shear stress profile evaluation. They will be demonstrated with the 1 metre deep Tee-Beam shown. It has 1.2% of 400 MPa longitudinal steel and 0.8 MPa of stirrups. The concrete strength was selected as 100 MPa to highlight the effects. The applied loads are a moment of 1.5 kNm for every 1 kN of shear force. SMAL96 predicts the shear capacity as 456 kN for this section with the analysis taking 24 seconds. Response-2000 predicts a shear capacity of 480 kN, controlled by longitudinal yield with a solution time of 5 seconds. The predicted shear stress profile from Response-2000 at a shear force of 456 kN, is shown to the right as well.

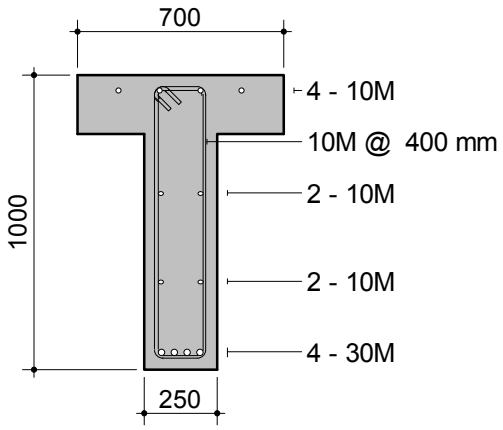

Figure 6 - 3: Sample section

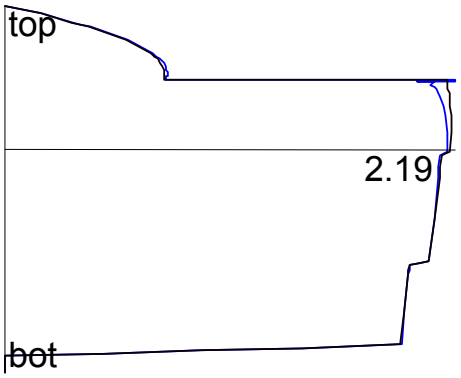

Figure 6 - 4: Shear stress profile

The first problem encountered resulted from the necessity to numerically solve for a desired value of axial load, moment and shear at both sections A and B in Fig. 6-1. Numerical convergence always includes some error, but the shear, and axial load, must be essentially identical between section A and B. Figure 6-3 shows a shear stress profile generated with an earlier version of Response-2000 that used the older shear stress profile methods as used by SMAL at a shear of 456 kN. It can be seen that the shear stress profile does not "close" at the top, that is, the shear stress is not calculated as zero at the top and bottom face of the beam as required. This was caused by a difference in axial load between sections A and B of only 2.2 kN. This corresponds to an average stress on the gross concrete area of 0.0065 MPa. The error in longitudinal strain that this axial load represents is 0.1 micro strain. This means that methods like that in SMAL must either solve to axial strains to a precision of 1 part in 10,000, or "smear" the error if the shear profile does not close.

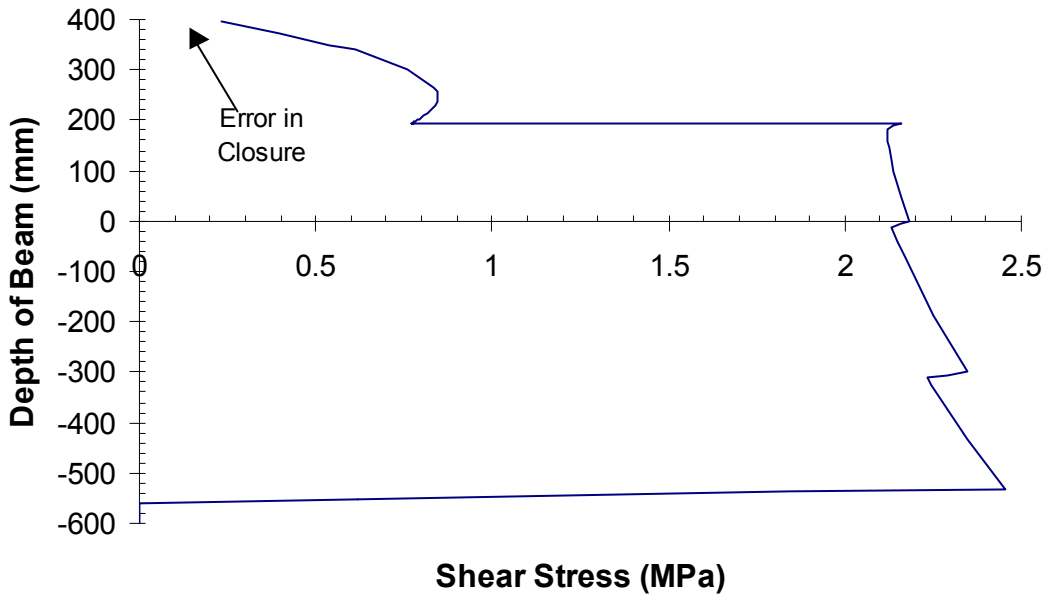

Figure 6 - 3: Error in axial load convergence

A second problem is that the depth of cracking for section A will be different from the depth of cracking at Section B, due to the different moments at each section. The effect of this is that a large jump in the shear stress profile is predicted in the region between the cracking depths. Figure 6-4 shows the effect for the example beam with a shear of 180 kN. This spike does not appear to have any real physical significance. More importantly, it is strongly dependent on the distance dx between sections A and B. For some cross sections, this spike can make the predicted shear stress negative in the middle of the web for positive shear, for example, which also suggests that it is a non-physical artefact of the calculation.

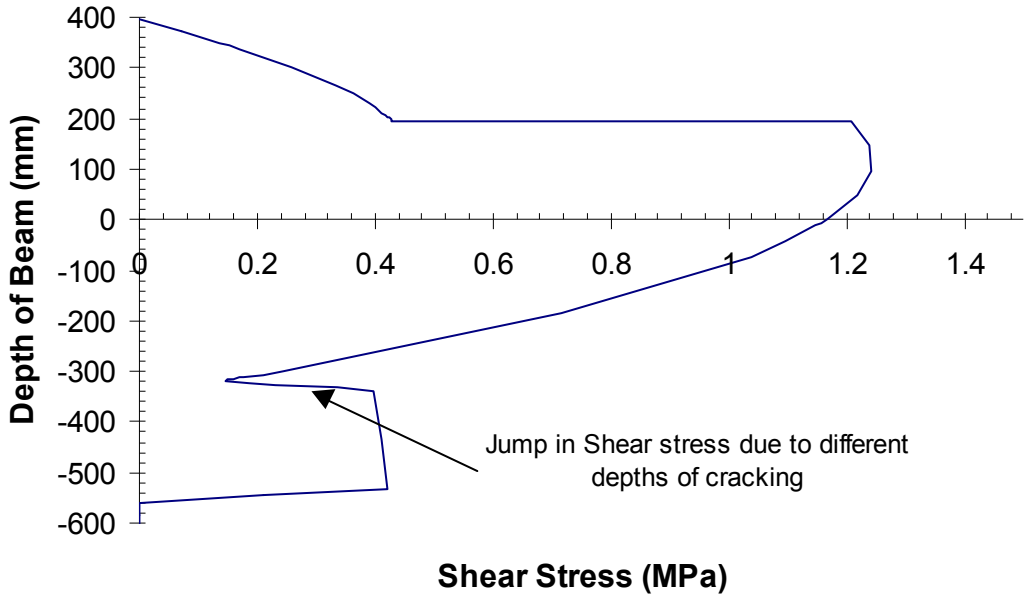

Figure 6 - 4: Error in crack depth

A third issue is that the distance between the sections A and B in Fig 6-1 turns out to be important in predicting the shear stress profile. SMAL suggests a value of d/6 for this parameter, Response-2000 had used a value of about 10 mm for all beams, and now effectively uses zero mm as a result of the new methodology in this chapter. Figure 6-7 compares the shear stress profile predicted by SMAL, the old version of Response-2000 and the new version of Response-2000 for a shear of 456 kN. Clearly this parameter has a large effect on the predictions. SMAL predicts the largest shear stress near the bottom

of the section whereas the new method predicts it near the top of the web. The predictions of Response-2000 tend to have smaller scatter than that of SMAL, suggesting that the Response-2000 profiles are better than the SMAL profiles.

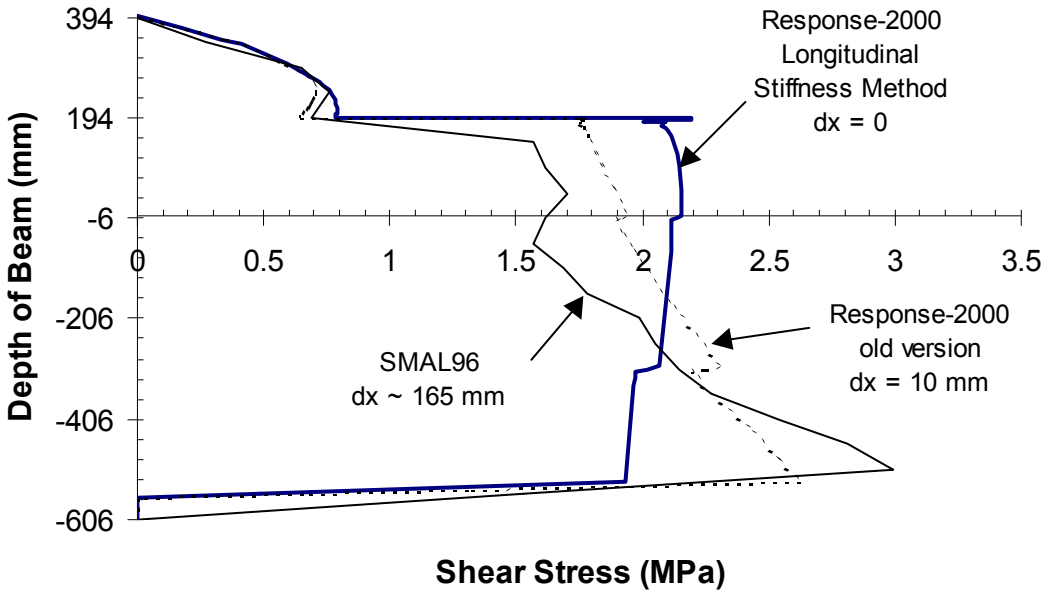

Figure 6 - 5: Effect of distance dx

Each of these three issues resulted in analyses with old Response-2000 taking longer than they should have as a result of extra iteration, and, in some cases, preventing a solution completely. While the increasing performance of computers has made the efficiency issue less important, it does not help for cases when a solution is not possible at all due to numerical instability.

A series of techniques were implemented in Response-2000 to work around the three problems. While they generally worked, they did not represent an elegant solution. The longitudinal stiffness method was then developed to deal directly with these problems and provide faster, more stable solutions.

6-4 The Longitudinal Stiffness Method

This new method works by taking the limit as the distance dx between sections A and B in Fig. 6-1 goes to zero. The numerical problems vanish and the method is virtually guaranteed to be able to find a shear stress distribution for all cases, interestingly, with small modifications, even for cases with no shear applied.

It remains a numerically implemented method, but it no longer requires the calculation of behaviour at both sections A and B. Recall that the old method took the difference between the longitudinal stresses at sections A and B and divided by the distance between them, in the process of calculating the shear stress. This step is replaced by calculating the derivative of longitudinal stress with respect to longitudinal strain at each point in the depth of the cross section.

The use of derivatives mean that the solution for only one location need be obtained rather than the two needed for the earlier method. As there is only one section, the axial forces and shears are guaranteed to match on each "side" of the analysis. Also, there is only one depth of cracking to consider. Implementing this method has allowed Response-2000 to run 5-15 *times* faster than it did using the older dual section analysis style techniques, largely from a reduction in amount of iteration. Much of this iteration was, in fact, partially induced by the dynamic layering routines that made it more stable in solving to individual load levels. Program SMAL, which does not use the dynamic layering is comparable in wall-clock speed to the new Response-2000 when it is able to obtain a solution. As a result of the dynamic layering, however, Response-2000 calculates much more data for each load level. A typical SMAL analysis may have 20 layers in it, whereas a Response-2000 analysis may have 50 layers. The method presented here scales directly to 3D as implemented in Shell-2000.

6-5 Details of the Method

What follows is a description of the method in two dimensions. The 3D method is not presented, as it is a direct extension and would be redundant.

The analysis begins with a load-deformation state for the cross section. An initial assumption of a shear-strain profile is needed. For a first load step, this initial guess can be reasonably taken as the simple linear elastic solution derived by Jourawski. For later load steps, the previous shear strain distribution can be used as the initial estimate.

The load-deformation state throughout the depth of the element will consist of a series of biaxial MCFT nodes. The first step in calculating the shear stress distribution is to calculate the tangent stiffness in the X-Y-Gamma directions for each node as explained in Chapter 3. Each node will result in a 3x3 matrix of stiffness, K_i:

$$\begin{bmatrix} \frac{dN_x}{d\varepsilon_x} & \frac{dN_x}{d\varepsilon_y} & \frac{dN_x}{d\gamma_{xy}} \\ \frac{dN_y}{d\varepsilon_x} & \frac{dN_y}{d\varepsilon_y} & \frac{dN_y}{d\gamma_{xy}} \\ \frac{dv_{xy}}{d\varepsilon_x} & \frac{dv_{xy}}{d\varepsilon_y} & \frac{dv_{xy}}{d\gamma_{xy}} \end{bmatrix} = K_i = \begin{bmatrix} a & b & c \\ d & e & f \\ g & h & i \end{bmatrix} \tag{6-2}$$

Recall the basic assumption with sectional analysis methods that there is to be no total stress in the transverse direction. As such, it is necessary to modify the stiffness matrix to account for this before using it in the longitudinal stiffness method. Specifically, since:

$$K_i \begin{pmatrix} d\varepsilon_x \\ d\varepsilon_y \\ d\gamma_{xy} \end{pmatrix} = \begin{pmatrix} dN_x \\ dN_y \\ dv_{xy} \end{pmatrix} \tag{6-3}$$

and dN_y must equal zero, simple algebraic rearrangement shows that the modified nodal tangent stiffness matrix can be represented as:

$$K'_i = \begin{bmatrix} a - \frac{b \cdot d}{e} & c - \frac{b \cdot f}{e} \\ g - \frac{h \cdot d}{e} & i - \frac{h \cdot f}{e} \end{bmatrix} = \begin{bmatrix} j & k \\ m & n \end{bmatrix} \tag{6-4}$$

So that

$$K'_i \begin{pmatrix} d\varepsilon_x \\ d\gamma_{xy} \end{pmatrix} = \begin{pmatrix} dN_x \\ dv_{xy} \end{pmatrix} \tag{6-5}$$

This nodal stiffness now models the stiffness of longitudinal stress and shear stress to longitudinal strain and shear strains while maintaining no change in stress in the transverse direction. Note that as the basic tangent stiffness matrix (K_i) is non-symmetric, the reduced stiffness matrix (K_i') will also be non-symmetric.

These local nodal stiffness matrices may now be integrated to produce the global sectional forces tangent stiffness matrix J:

$$\begin{bmatrix} \frac{dN}{d\varepsilon_{x0}} & \frac{dN}{d\phi} & \frac{dN}{d\gamma_{xy0}} \\ \frac{dM}{d\varepsilon_{x0}} & \frac{dM}{d\phi} & \frac{dM}{d\gamma_{xy0}} \\ \frac{dV}{d\varepsilon_{x0}} & \frac{dV}{d\phi} & \frac{dV}{d\gamma_{xy0}} \end{bmatrix} = J \tag{6-6}$$

So that:

$$J \begin{pmatrix} d\varepsilon_{x0} \\ d\phi \\ d\gamma_{xy0} \end{pmatrix} = \begin{pmatrix} dN \\ dM \\ dV \end{pmatrix} \tag{6-7}$$

Where $d\varepsilon_{x0}$ change in longitudinal strain at the geometric centroid of the gross concrete area
$d\phi$ change in curvature
$d\gamma_{xy0}$ change in average shear strain for section
dN change in global axial force
dM change in global moment
dV change in global shear force

These nodal stiffness terms are integrated over all the layers in the depth of the beam. In the programs, this integration is done quadratically as the dynamic layering routines automatically check for accuracy using that assumption. Using C++ notation

where J[0][0] is the top left matrix element, and the notation in Fig. 6-6, the summation over all layers may be done as follows:

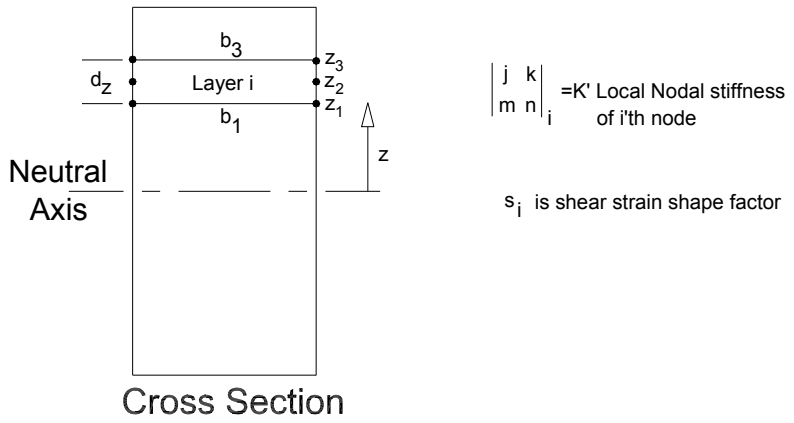

Figure 6 - 6: Parameters for global stiffness matrix calculation

Global Axial Force Stiffness

$J[0][0] \mathrel{+}= (j_1 \cdot b_1 + 4 \cdot j_2 \cdot b_2 + j_3 \cdot b_3) \cdot dz/6$
$J[0][1] \mathrel{+}= (j_1 \cdot b_1 \cdot z_1 + 4 \cdot j_2 \cdot b_2 \cdot z_2 + j_3 \cdot b_3 \cdot z_3) \cdot dz/6$ z included for curvature
$J[0][2] \mathrel{+}= (k_1 \cdot b_1 \cdot s_1 + 4 \cdot k_2 \cdot b_2 \cdot s_2 + k_3 \cdot b_3 \cdot s_3) \cdot dz/6$ s included for shear strain

1st order parts of Moment Stiffness
$J[1][0] \mathrel{+}= (j_1 \cdot b_1 \cdot z_1 + 4 \cdot j_2 \cdot b_2 \cdot z_2 + j_3 \cdot b_3 \cdot z_3) \cdot dz/6$ z for moment
$J[1][1] \mathrel{+}= (j_1 \cdot b_1 \cdot z_1 \cdot z_1 + 4 \cdot j_2 \cdot b_2 \cdot z_2 \cdot z_2 + j_3 \cdot b_3 \cdot z_3 \cdot z_3) \cdot dz/6$ z for moment & curvature
$J[1][2] \mathrel{+}= (k_1 \cdot b_1 \cdot z_1 \cdot s_1 + 4 \cdot k_2 \cdot b_2 \cdot z_2 \cdot s_2 + k_3 \cdot b_3 \cdot z_3 \cdot s_3) \cdot dz/6$ z for moment

2nd order parts of moment stiffness
$J[1][0] \mathrel{+}= dz \cdot dz/60 \cdot (b_3 - b_1)(j_1 - 2 \cdot j_2 + j_3)$
$J[1][1] \mathrel{+}= dz \cdot dz/60 \cdot (b_3 - b_1)(j_1 \cdot z_1 - 2 \cdot j_2 \cdot z_2 + j_3 \cdot z_3)$
$J[1][2] \mathrel{+}= dz \cdot dz/60 \cdot (b_3 - b_1)(j_1 \cdot s_1 - 2 \cdot j_2 \cdot s_2 + j_3 \cdot s_3)$

Global Shear Stiffness

$J[2][0] \mathrel{+}= (m_1 \cdot b_1 + 4 \cdot m_2 \cdot b_2 + m_3 \cdot b_3) \cdot dz/6$
$J[2][1] \mathrel{+}= (m_1 \cdot b_1 \cdot z_1 + 4 \cdot m_2 \cdot b_2 \cdot z_2 + m_3 \cdot b_3 \cdot z_3) \cdot dz/6$ z included for curvature
$J[2][2] \mathrel{+}= (n_1 \cdot b_1 \cdot s_1 + 4 \cdot n_2 \cdot b_2 \cdot s_2 + n_3 \cdot b_3 \cdot s3) \cdot dz/6$ s included for shear strain

Where: b_1,b_2,b_3 are the top middle and bottom widths of the section for the layer
z_1,z_2,z_3 are the depths in the section corresponding to the widths b_1,b_2,b_3
dz is total layer depth $= z_3-z_1$
s_1,s_2,s_3 are the multipliers of the average shear strain for the given depth. Note that the shear strain is defined as an average value (the global shear strain) as well as with a shape profile that varies over the

depth with an average of 1.0. These terms define the shape of the shear strain profile.

j,k,l,m are the stiffness terms from K' as defined above for nodes 1,2,3

This global tangent stiffness matrix calculated from the biaxial tangent stiffness of the nodes serves two purposes. Firstly it can be used to solve for the next load stage for an analysis. That is, it can be used to solve for the next global strain state estimate to use to minimise the error in the force state. Secondly, and more importantly for this chapter, it can be used to calculate the shear stress distribution.

6-6 Calculating shear stress profiles.

With a load-deformation state at a given "in-situ strain" of ε_{x0}, ϕ, and γ_{xy0}, a tangent stiffness matrix is calculated as described directly above. Unlike the case of solving for global forces, however, the individual stiffness terms over the depth are retained. This can represent a significant amount of storage as, for example, Shell-2000 can require up to 1750 independent stiffness terms from the nodal matrices.

Using the global stiffness matrix, the following matrix calculation is performed to solve for a tangent "virtual strain".

$$J\begin{pmatrix} d\varepsilon_x \\ d\phi \\ d\gamma_{xy} \end{pmatrix} = \begin{pmatrix} 0 \\ V \\ 0 \end{pmatrix} \tag{6-8}$$

If this virtual strain is added to the in-situ strain in the beam, a new force state is predicted that would have the same axial load, the same shear, but a moment that differs by exactly V·1 metre. This virtual strain profile, when multiplied by the longitudinal stiffness terms over the depth, will produce the equivalent of the shaded area on Fig. 6-2. This then directly leads to the shear stress as before. By selecting a moment increment of V·1 metre, it is as though the distance between sections A and B has been selected as 1 metre. In fact, due to the use of derivatives for the stiffness, it is effectively zero metres.

The next step is to calculate through the depth of the beam the equivalent of the shaded area in Fig. 6-2. Whereas previously it was necessary to calculate the difference of the longitudinal stress at section A and section B of the free body in Fig. 6-1, this value is now directly calculated as the virtual strain times the appropriate stiffness. The value calculated by this multiplication is the rate of change of shear flow with respect to depth in the beam. At any given depth, the rate of change of shear flow with respect to depth would be calculated as:

$$\Delta q = j \cdot (d\varepsilon_x + z \cdot d\phi) + k \cdot d\gamma_{xy} \tag{6-9}$$

Where Δq is the slope of the shear flow diagram with respect to depth
j and k are the top two terms from the K' matrix at depth z
z is the depth at this location
$d\varepsilon_x$, $d\phi$, and $d\gamma_{xy}$ are the global virtual strains from above

This change in shear flow is then integrated over the depth of the section and divided by the local element widths to find the shear stress profile. Note that the tangent stiffness of the longitudinal steel must also be included using the same virtual strain concept with the tangent stiffness of the steel.

When implemented properly, the only way that this method can fail to find a solution is if the determinant of the J matrix is zero. If it is zero because there is no stiffness against moment, then no solution can be found. It has been found that this is very rare, but can happen in the case of beams subjected to high shear with full-depth cracking and all longitudinal and transverse steel yielding.

Chapter 7: How the programs work

The previous chapters have provided background into the analytical methods used in the programs. This chapter provides details of how the programs work internally so that others may implement similar programs.

7-1 Membrane-2000/ Triax-2000

Membrane-2000 is closely related to Triax-2000 in that Membrane-2000 considers a single biaxial stress-strain node, and Triax-2000 considers a single triaxial stress-strain node of reinforced concrete. Both programs work in a similar manner internally.

Both programs are based exclusively on the secant stiffness method in two and three dimensions as explained in Chapter 3. For full load-deformation analyses, a variable is automatically selected as being the most critical, usually a shear strain, and then that value is incremented in small steps. The other strains are then iteratively determined with the secant stiffness matrix until the load ratios match the desired values. It has been found that the secant stiffness method is surprisingly stable and can solve for most solutions quite efficiently. For single load solutions, the same technique is used, but the load vector is fully defined with the full strain state then determined iteratively.

7-2 Response-2000/Shell-2000

Most of this discussion is written directly towards Response-2000. Shell-2000 is directly analogous in internal structure. Response-2000 is based on a series of biaxial nodes integrated along a line through the cross section. The global strain state is made up of the longitudinal strain at the centroid of the gross concrete cross section (ε_{x0}), the curvature (ϕ), and the average shear strain (γ_{xy0}). As the shear stress profile, and hence shear strain, varies over the depth of the cross section, a numerical profile is used that modifies the average strain (γ_{xy0}) to produce the desired shape of shear strain through the

depth. This profile has an average value of 1.0 and is zero at the top and bottom of the cross sections. For uncracked concrete on rectangular sections, the profile is a parabola with a maximum value of 1.5.

Each biaxial node in Response-2000 is defined by the longitudinal strain ε_x (from ε_{x0} and ϕ and depth) and the shear strain (from γ_{xy0} and the shear strain profile). The third strain required for biaxial stress-strain state, say the transverse strain, must be calculated from equilibrium based on the assumption that there is no total transverse clamping stress.

To solve for any arbitrary load stage or an interaction diagram requires a fair amount of nested iteration. Figure 7-1 shows the general steps in the iteration procedures used in Response-2000.

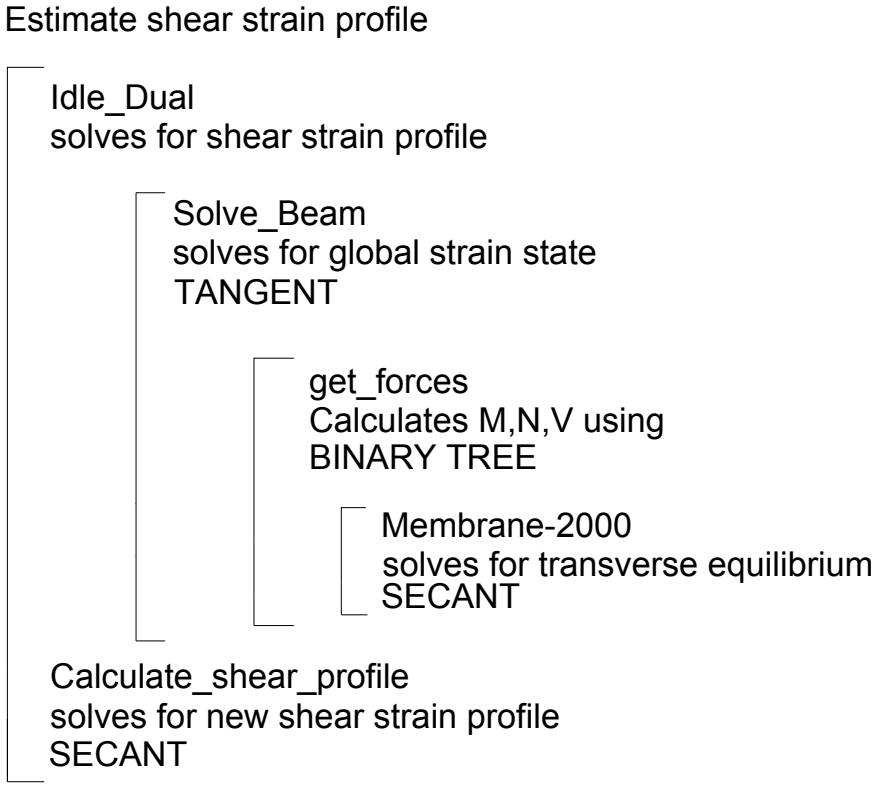

Figure 7 - 1: Response-2000 loops

Response-2000 has 4 major nested loops. Note that the one furthest in is effectively the same as Membrane-2000. This inner loop calculates the transverse strain needed to ensure that there is no overall transverse stress on the nodes consistent with the basic assumption of the sectional model.

The loop outside that, the get_forces loop, calculates the sectional forces (N, M, V) on a cross section for a given global strain state. This is iterative as the cross section is automatically divided up ("dynamic layering") in a binary tree fashion similar to Reference 38 to ensure that the stress levels are interpolated well throughout the height of the beam.

The loop outside that layer, the solve_beam loop, calculates the global strain state needed to achieve the desired global load ratios (N, M, V).

The final outer loop, idle_dual, iterates on the shear strain profile until the assumed profile matches the one calculated with the longitudinal stiffness method from Chapter 6.

7-3 Each component in more detail: Response-2000

Each analysis must begin with an estimate of the shear strain profile. Initially, the linear elastic strain profile from "VQ/Ib" is appropriate, and for later load stages, the profile from the previous load stage is used. Each analysis must also start with an estimate of the global strain state, that is, initial values for ε_{x0}, ϕ, and γ_{xy0}. Normally, at the start of an analysis, these are assumed to be zero though in the event of shrinkage or strain discontinuity, they are taken as a linear fit to those profiles. For later load stages, the strain state from the previous load level can be used to estimate new global strain states.

The Idle_Dual function has the "idle" prefix as it is called during idle processing. This allows the program to support multitasking on co-operative multitasking operating

systems. The first step in this function is to create a new load stage. With the initial strains from above, one variable (generally curvature) is selected to be constant to implement strain controlled behaviour. A call is made to the solve_beam function to solve for the other 2 global strains that correspond to the correct moment: shear: axial force ratios. The shear strain profile is then recalculated based on the longitudinal stiffness method. If the newly calculated profile is close to the assumed profile, the load stage is completed. If the new profile is not close enough to the old one, then another iteration is required. The longitudinal stiffness method calculates a shear stress profile, which is converted to a strain profile using a secant stiffness method for non-zero initial stress levels and tangent method for zero initial shear stress levels.

The solve_beam function solves for the global sectional strain state that causes the desired load ratios. It first calls for the global tangent stiffness matrix as explained in chapter 6, and then uses that to iteratively reduce the error in the sectional forces with a tangent technique. The get_forces function is the most important function called as it updates the current sectional force state from a given sectional strain state.

The get_forces function will calculate the overall forces on a section based on the given global strain state. For each node, a longitudinal strain is known as well as is the shear strain. The transverse strain is calculated for each node to ensure that the node is in equilibrium in the transverse direction. This is performed with the secant stiffness method from Membrane-2000. The get_forces function first assumes that 8 layers throughout the thickness are sufficient and these are calculated. The stresses are then calculated at the quarter points of each layer and compared to the quadratic interpolation from the existing nodes of the layer. If the quadratic interpolation matches the check point, then the analysis will accept that layer. If the interpolation is poor, then the layer is automatically divided in two.

These series of nested loops may sound intimidating, but in fact they mesh together well and produce a fast solution for the problems.

7-4 Long Term Equations

Response-2000 includes a routine to allow automatic consideration of the effects of shrinkage, creep and relaxation. These procedures are based on the AASHTO-94[39] provisions and similar to the methods in Collins & Mitchell[5]. The reason to explicitly include them is that the usually suggested method of dealing with creep, increasing the strain at which concrete cylinders reach peak stress, can cause problems in an analysis for shear. Using the method built into Response-2000 will avoid these problems.

Shrinkage is calculated in Response-2000 with the following equation

$$\text{Shrink} = -0.00051\, k_s\, k_h\, (t/(t+35)) \tag{7-1}$$

Where: t is time in days the concrete has been exposed to drying
k_h is factor to account for humidity. Response-2000 assumes k_h=1.0
k_s is a factor for geometry:

$$k_s = \frac{\sqrt{\frac{t}{26e^{14.2\cdot VOS}+t}}}{\sqrt{\frac{t}{t+45}}} \cdot \frac{(1064 - 3700\cdot VOS)}{923} \tag{7-2}$$

Where: VOS is volume to surface area ratio in metres

Creep is estimated from the traditional creep factor as follows:

$$\Phi = k_c k_f\, 0.80 \frac{(t-7)^{0.6}}{10+(t-7)^{0.6}} \tag{7-3}$$

$$k_f = \frac{62}{42+f_c'}$$

$$k_c = 3.5 \frac{\sqrt{\frac{t}{26e^{14.2\cdot VOS}+t}}}{\sqrt{\frac{t}{t+45}}} \cdot \frac{(1.80 - 1.77\cdot e^{-21.3\cdot VOS})}{2.587} \tag{7-4}$$

The strand relaxation factor is estimated by the following equation.

$$\text{R-fact} = 1 - \log(24\, t) / 40\, (f_{pi}/f_{py} - 0.55) \tag{7-5}$$

A single load analysis is carried out by Response-2000, first ignoring all these parameters, and at a load equal to the long-term moment value entered by the user.

While shear is ignored to speed the calculation, axial load is considered. This analysis will result in a short-term longitudinal strain profile.

A new analysis is then calculated with the shrinkage applied, the prestressing strands relaxed, and the concrete having a strain at peak stress modified by the creep factor above. This will produce a second longitudinal strain profile corresponding to the long term behaviour of the beam at the sustained moment.

The difference between these two strain profiles is calculated and added to the user defined shrinkage profile. This will then implicitly include creep and shrinkage in the calculations. An analysis performed after this will represent short-term loading (i.e. in a manner of hours to days) on a structure that has been loaded for a long term (i.e. many years).

Note that the increase in concrete strength that long term hydration will cause is ignored as this is too dependent on individual mix properties.

7-5 Automatic Crack Spacing

It is suggested that crack spacings always be automatically calculated. Specific values may be selected, but these will be prone to errors and potentially miss important effects in the shear response of concrete, such as the size effect.

The crack spacing is based on the CEB suggested crack spacing relationship[5]:

$$\text{Crack spacing} = 2\,c + 0.1\,d_b/\rho \qquad (7\text{–}6)$$

where c is the diagonal distance to the nearest reinforcement in the section
d_b is the diameter of the nearest bar
ρ is the percentage of steel

This model is treated slightly different by the different programs.

For Membrane-2000 and Triax-2000, the distance c is taken as the largest diagonal distance between a bar and any point in the concrete. Note that this does not attempt to model the average crack spacing, but the largest, and therefore most critical crack spacing.

Response-2000 and Shell-2000 calculate crack spacing over the depth of the section, as it will change over the depth. For these calculations, the term c is taken as the largest diagonal distance from the current depth to a reinforcing bar. The ρ term is taken as the percentage of steel within a concrete area 7.5 d_b above and below the bar. When between different layers of reinforcement, the $0.1d_b/\rho$ term is linearly interpolated between the calculated values at the bars. If a section is subjected to bending, the crack spacing is not allowed to exceed the section depth.

For cases with no reinforcement, the crack spacing is selected as five times the depth of the section.

7-6 Hoop Reinforcement

Special treatment is given to transverse reinforcement that is in the form of hoops. Figure 7-2 shows a column with hoops. It is assumed that there are no strains perpendicular to the direction of shear loading. This means that the part of the hoop that is pointing that way will not experience any straining due to the shear. Confinement would induce strain at this location, but this is not currently implemented in Response-2000.

To account for this, the hoop strains ε_h are calculated from the transverse strains ε_t based on a Mohr's circle:

$$\varepsilon_h = \varepsilon_t \sin^2(\alpha) \tag{7-7}$$

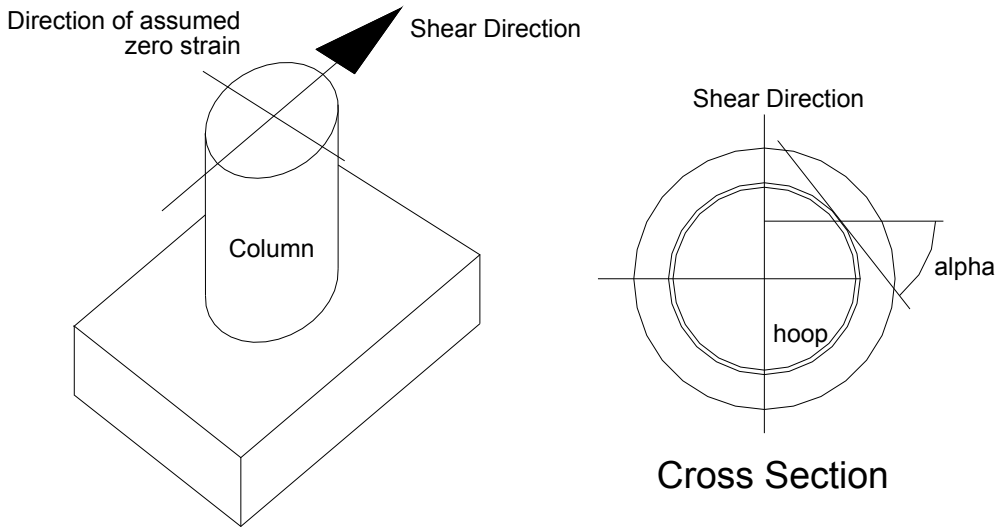

Figure 7 - 2: Treatment of hoops in Response-2000

Additionally, only the component of the force in the hoop in the transverse direction may influence the shear response, that is, the hoop force must be multiplied by the sine of angle alpha.

7-7 Member Response Analysis

Response-2000 can calculate a load-deflection curve for a prismatic beam subjected to point loads or a uniform loading as shown in Chapter 2. As Response-2000 is a sectional analysis program, it is necessary to calculate the stress and strain state for a series of individual cross sections to allow this. To be as general as possible, Response-2000 calculates the full moment-shear interaction diagram in order to calculate beam deflections.

Response-2000 divides up the beam into 20 short segments. For each segment, the axial load, moment, and shear force are determined from the applied loads. The curvature and shear strain associated with this load level is then interpolated from the interaction diagram. This is integrated with the moment-area method to calculate the load deflection relationship for the beam segment.

Shown in Fig. 7-3 is a Moment-Shear interaction diagram of a beam without stirrups. The horizontal axis represents moment and the vertical axis represents shear. The outer line enclosing all the points represents the failure envelope. Any force combination that touches this line will result in failure of the cross section. At the far right hand side, the failure will be in positive flexure, at the left it will be in negative flexure, and the sloping top represents shear failures.

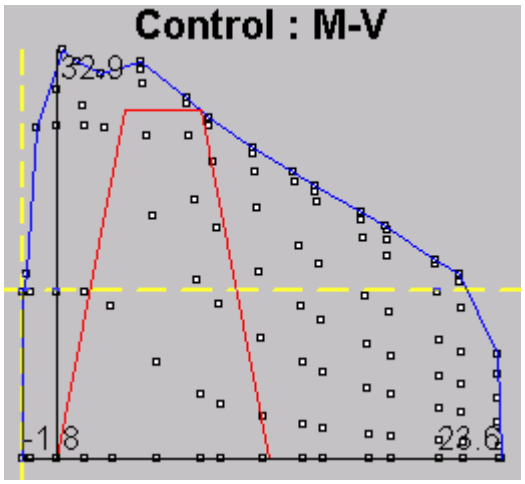

Figure 7 - 3: Moment-shear interaction diagram

Each of the squares within the interaction diagram represents a solved combination of moment, shear and axial load. This means that the curvature, shear strain and longitudinal strain can be interpolated throughout the interaction diagram using the values at the squares. The interpolation is performed with finite element shape functions.

If a line representing the shear and moment along the length of the beam is traced on the interaction diagram, as shown, the curvature and shear strain can be calculated for each point along the line and integrated together to predict the member load-deflection curve.

A difficulty arises when using this method with shear, however. It is known that due to diagonal cracks requiring horizontal projection, amongst other reasons, that it is not appropriate to do an analysis with the full shear and moment directly below the point load or over the support. It is generally assumed, however, that it is appropriate to do analyses with full shear a distance d or d_v away from the point loads or supports. To model this, the following rule was defined as shown in Figure 7-4 to define what parts of the sectional loading is "active" for the deflection analysis.

It is proposed that within a distance of d from a point load and d from a support, there are other support mechanisms that mean the entire load is not supported in a sectional mode. These other modes include direct strut action from the load as well as clamping from the load itself and from the support. Recall that Response-2000 assumes that there is no overall stress in the transverse direction. Clearly that is not true directly under the load nor directly over the support.

Based on this assumption of other mechanisms supporting the shear, the active shear force diagram has been "clipped" over a distance d as shown in Fig 7-4.

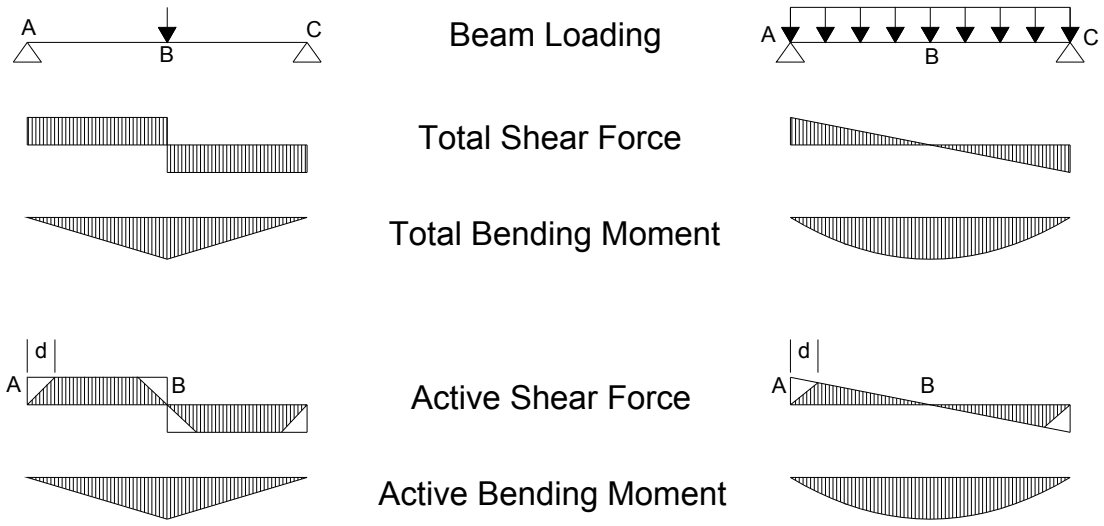

Figure 7 - 4: Active shear zones for deflection calculation

Note that this is only safe if the "other mechanisms of support" are indeed able to resist the load. For simple beams with point loads or uniform loads, this is a good assumption. It is consistent with the method used to calculate the experimental verification for Response-2000 in Chapter 10, for example. In the event, however, the load is supported in a peculiar way, say with the beam hanging from the top flange rather than sitting on a supports, this may not be a safe assumption.

Referring to Fig. 7-4, Response-2000 does the analysis for half of the beam, from A to B. For both the point load and the uniform loading, the familiar shear diagrams are trimmed for a distance d from the ends.

In the event that it is desired not to trim the active shear diagrams, Response-2000 can be told to do so. Selecting the left side support (location A) as a "hanging support" results in the piece not being clipped from the diagram on the left. If the right side support (location B) is changed to be a "hanging load", the right side will not be clipped.

In the event that the regions where the shear is clipped interfere with each other, that is, that the beam is less than 2 d long, Response-2000 assumes that the sectional force demand is equal to the lower region that is still shaded. As this region does not reach up to the top of the shear diagram, it is predicted that beams shorter than 2 d will have increasing strengths. This is shown in an example in Chapter 10.

7-8 Column Ends

For analyses of columns, an additional effect is supported, that of yield penetration into the loading block at the bottom of the column. This can increase the measured deflection of a column and be important in cases such as evaluation of seismic performance by means of a push-over analysis.

To directly support yield penetration, Response-2000 allows selection of a column end for the specimen being analysed with the additional calculation of this yield penetration. It is included by superimposing an additional curvature for a length near the end of the beam or column. The length of this flexural element, $D\phi$, is calculated as:

$$D\phi = 0.022 \cdot \sigma_m \cdot d_b \qquad (7\text{-}8)$$

Where: 0.022 is user adjustable

σ_m =maximum steel stress in cross section

d_b = bar size associated with that maximum stress case

The additional curvature for this extra element is calculated as follows:

$$\phi = \varepsilon/\text{dist} \qquad (7\text{-}9)$$

Where: ε = strain in highest loaded bar
dist = distance from highest stressed bar to compression face of column.

Chapter 8: Experimental Verification of Membrane-2000

Membrane-2000 is a program for the analysis of reinforced concrete membranes subjected to in-plane shear forces and axial loads. As the Modified Compression Field Theory (MCFT) is based directly on experiments such as these, demonstrating that the program predicts experiments well will also demonstrate that the MCFT works. Given that all four programs in this thesis are based on the MCFT, this is a useful thing to note.

8-1 Tests Compared to 1987 MCFT

The MCFT was fully defined in its current form in 1987. The experiments selected to corroborate both the MCFT and the program Membrane-2000 will all be tests performed after 1987. As such, they will be as close to "predictions" as one can get in that the theory used to make the calculations is older than the tests themselves. The tests will be selected from tests performed at the University of Houston over the past 10 years. For comparison, the two theories from the University of Houston empirically derived from these tests will also be shown.

In the comparison graphs, the thick solid line represents the MCFT, the thin solid line represents the Rotating Angle-Softened Truss model[17], and the thin dashed line represents the Fixed angle-Softened Truss Model[18]. If only one thin line is visible, then the fixed and rotating angle models predict the same result. All calculations were performed with Membrane-2000.

Membrane-2000 was set in the 1987 base-MCFT mode as shown in Fig. 3-1 in Chapter 3. This means that the parabolic stress-strain curve was used for concrete along with the base MCFT tension stiffening equation.

For each graph, the horizontal axis is shear strain in parts per thousand, and the vertical axis is shear stress in MPa.

8-1-1 Tests of Pang and Hsu[30]

These tests involved normal strength concrete subjected to pure shear. The A-series contained equal reinforcing levels in X and Y directions and the B series contained different levels in X and Y. Specimen A1 is not included due to an edge failure.

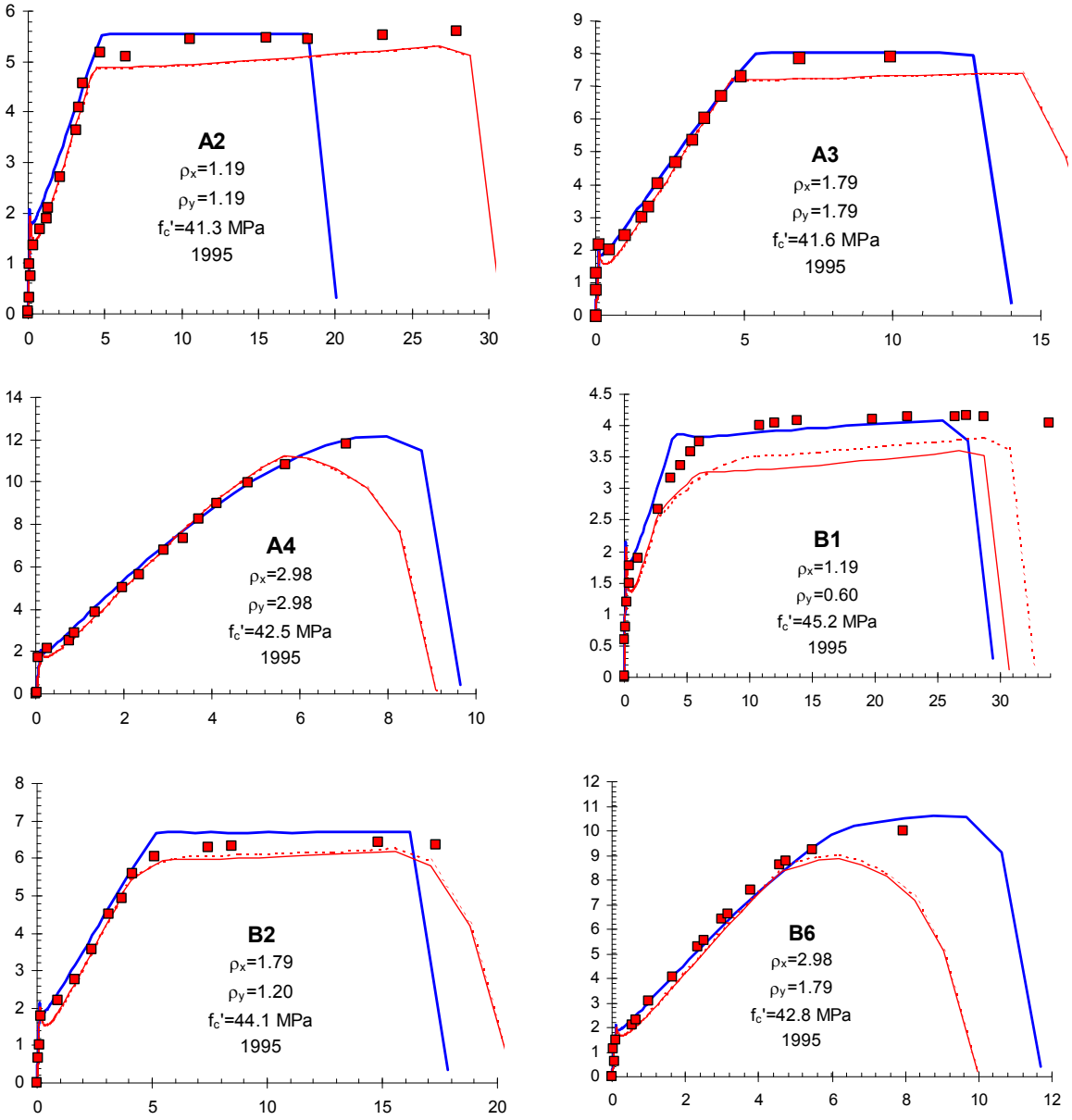

Figure 8-1 (a to f): Comparison of predictions of shear panels

X-Axis: Shear strain (x 10^{-3}) Y-Axis: Shear stress (MPa)

Thick line: MCFT-1987 predictions

Thin solid line: RA-STM 1998 predictions, thin dashed line: FA-STM 1997

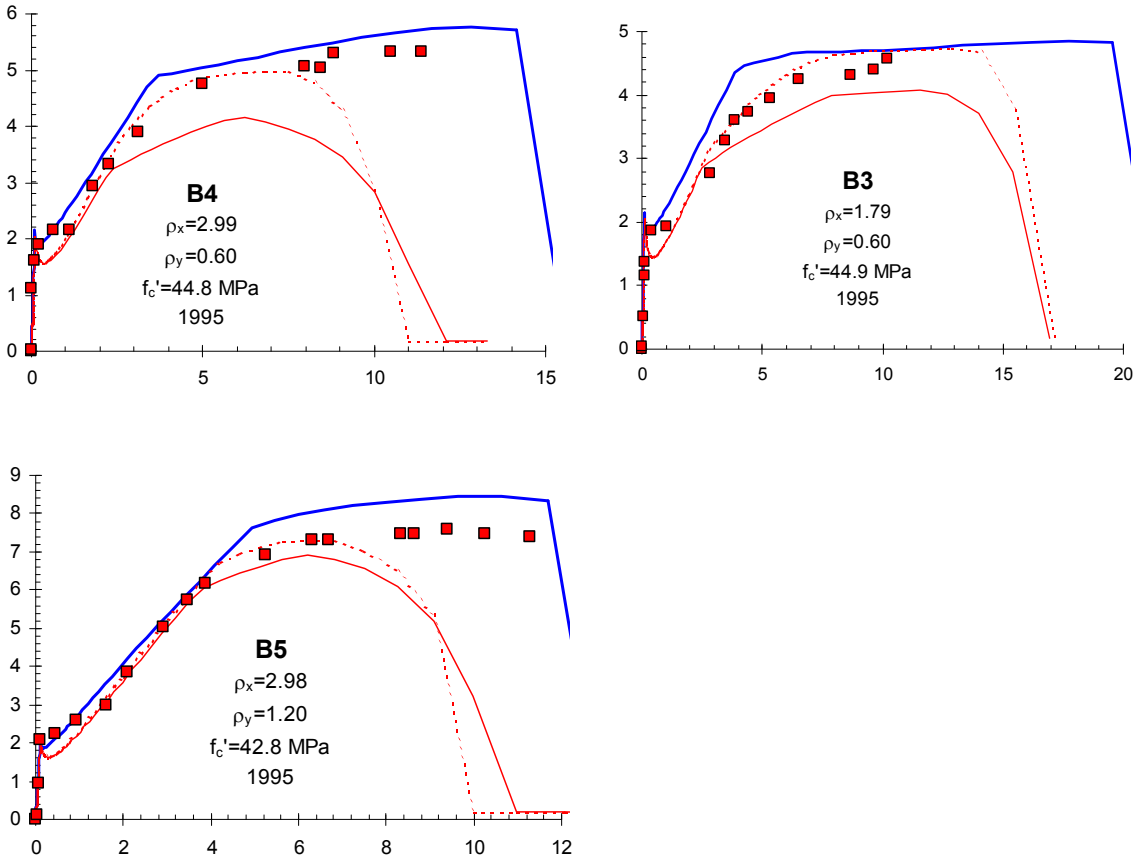

Figure 8-1 (continued, g-i) Comparison of predictions of shear panels

X-Axis: Shear strain (x 10^{-3}) Y-Axis: Shear stress (MPa)

Thick line: MCFT-1987 predictions

Thin solid line: RA-STM 1998 predictions, thin dashed line: FA-STM 1997

8-1-2 Tests of Zhang and Hsu[31]

These tests were similar to the tests above but used 100 MPa concrete.

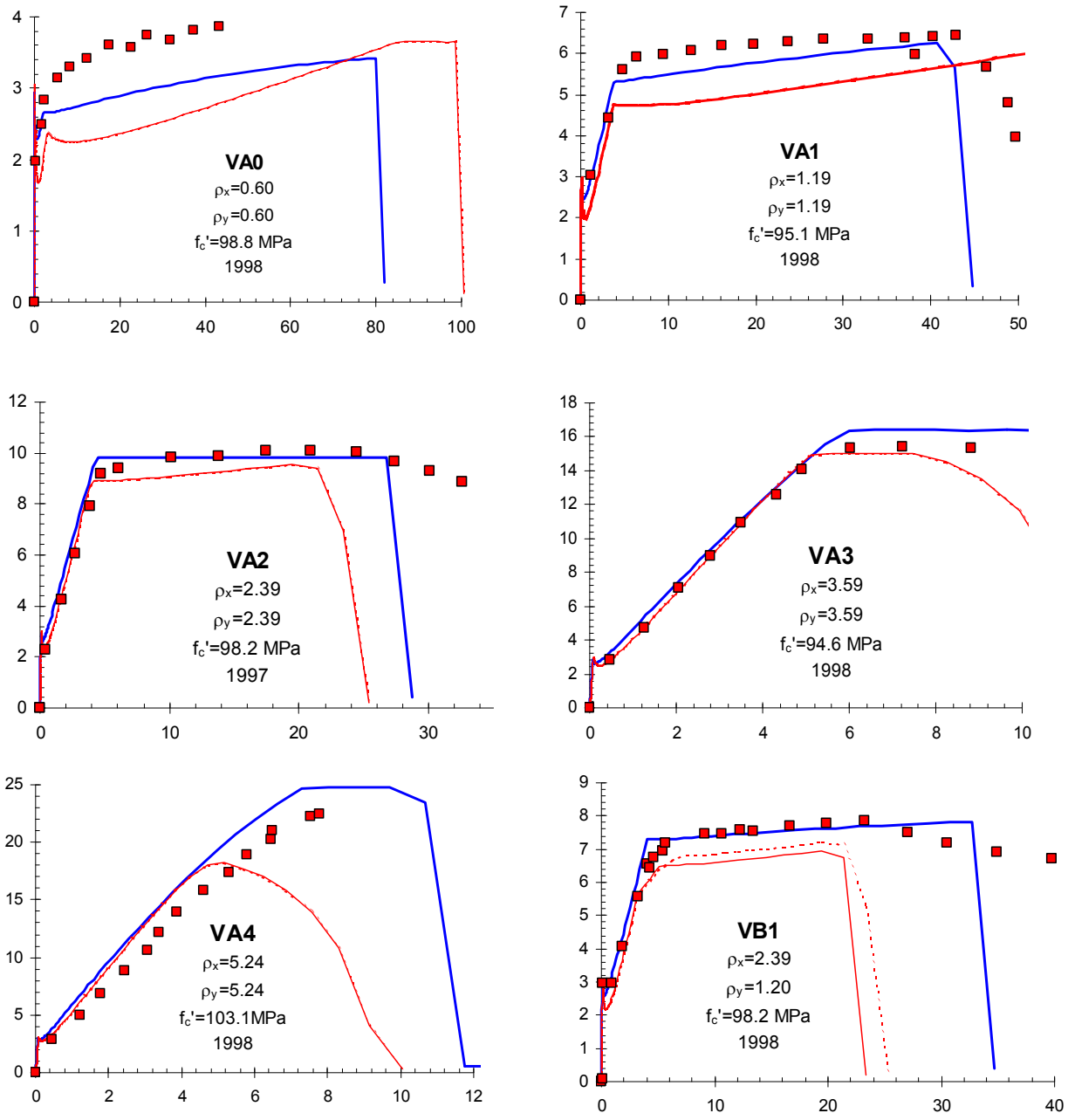

Figure 8-2 (a to f): Comparison of predictions of shear panels

X-Axis: Shear strain (x 10^{-3}) Y-Axis: Shear stress (MPa)

Thick line: MCFT-1987 predictions

Thin solid line: RA-STM 1998 predictions, thin dashed line: FA-STM 1997

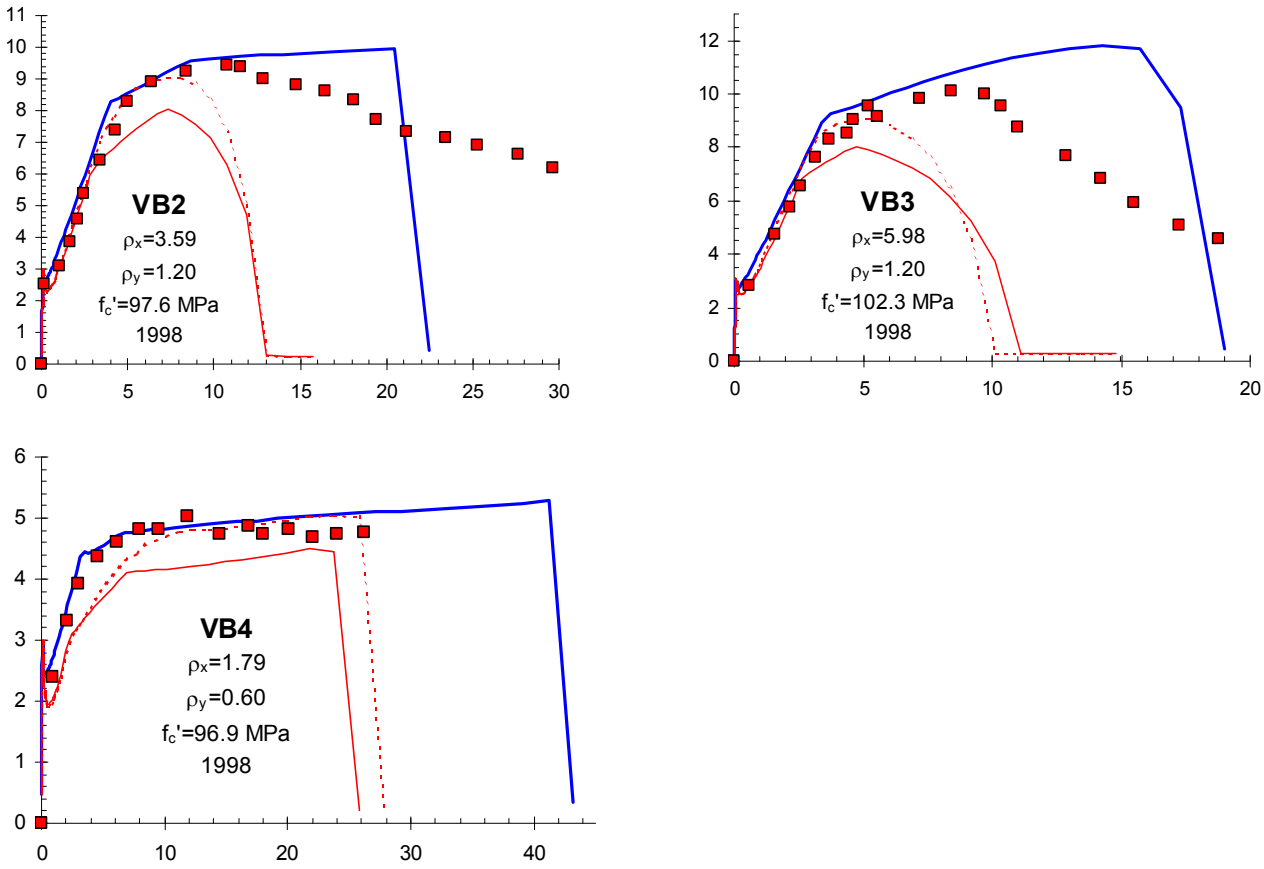

Figure 8-2 (continued h to i): Comparison of predictions of shear panels

X-Axis: Shear strain (x 10^{-3}) Y-Axis: Shear stress (MPa)

Thick line: MCFT-1987 predictions

Thin solid line: RA-STM 1998 predictions, thin dashed line: FA-STM 1997

Note the tendency for the very high strength concrete elements to be slightly over-predicted by the MCFT. This is due to the compression softening relationship and is the source of the suggestion to use the Porasz[20] relationship for high strength concrete as listed in Chapter 5.

In general, all three methods do a good job in predicting the behaviour of reinforced concrete subjected to in-plane shear. It is, perhaps, surprising that the two Houston models do not do better, given that they were derived based on this data set. It is satisfying that the MCFT does a good job predicting behaviour of experiments conducted at another University, tested by different researchers on a different testing frame.

8-2 Tests Compared to Proposed Constitutive Models

Membrane-2000 operates by default using the constitutive relations suggested in Chapter 5. The following plots compare how the same elements as above compare to the constitutive relation changes proposed in Chapter 5. By comparing the graphs for the 1987 MCFT to the new changes, it can be seen that the changes to the predictions are small for membrane elements. The only real differences are that the new predictions have a better fit to the tension stiffening part of the curve and a better estimate of post-peak ductility for the high strength concrete specimens.

8-2-1 Tests of Pang and Hsu[30]

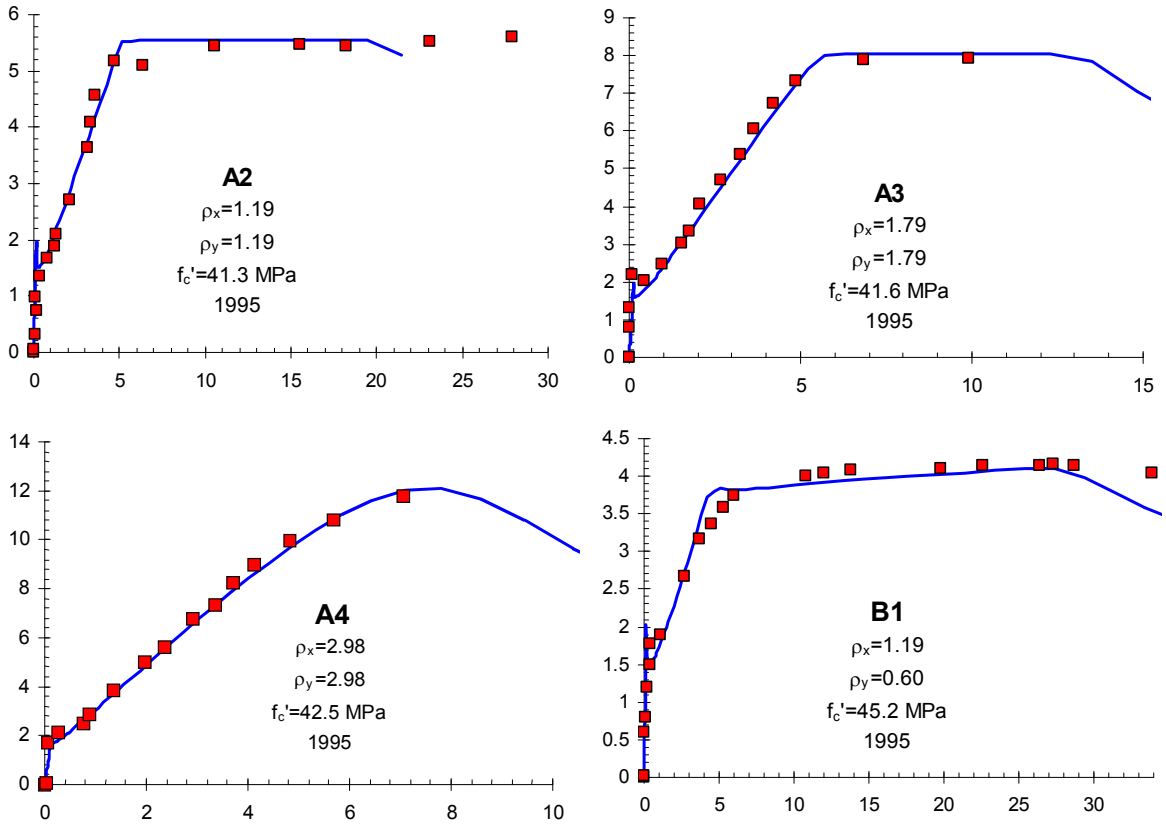

Figure 8-3 (a to d): Comparison of predictions of shear panels

X-Axis: Shear strain (x 10^{-3}) Y-Axis: Shear stress (MPa)

Thick line: MCFT-1987 predictions

Thin solid line: RA-STM 1998 predictions, thin dashed line: FA-STM 1997

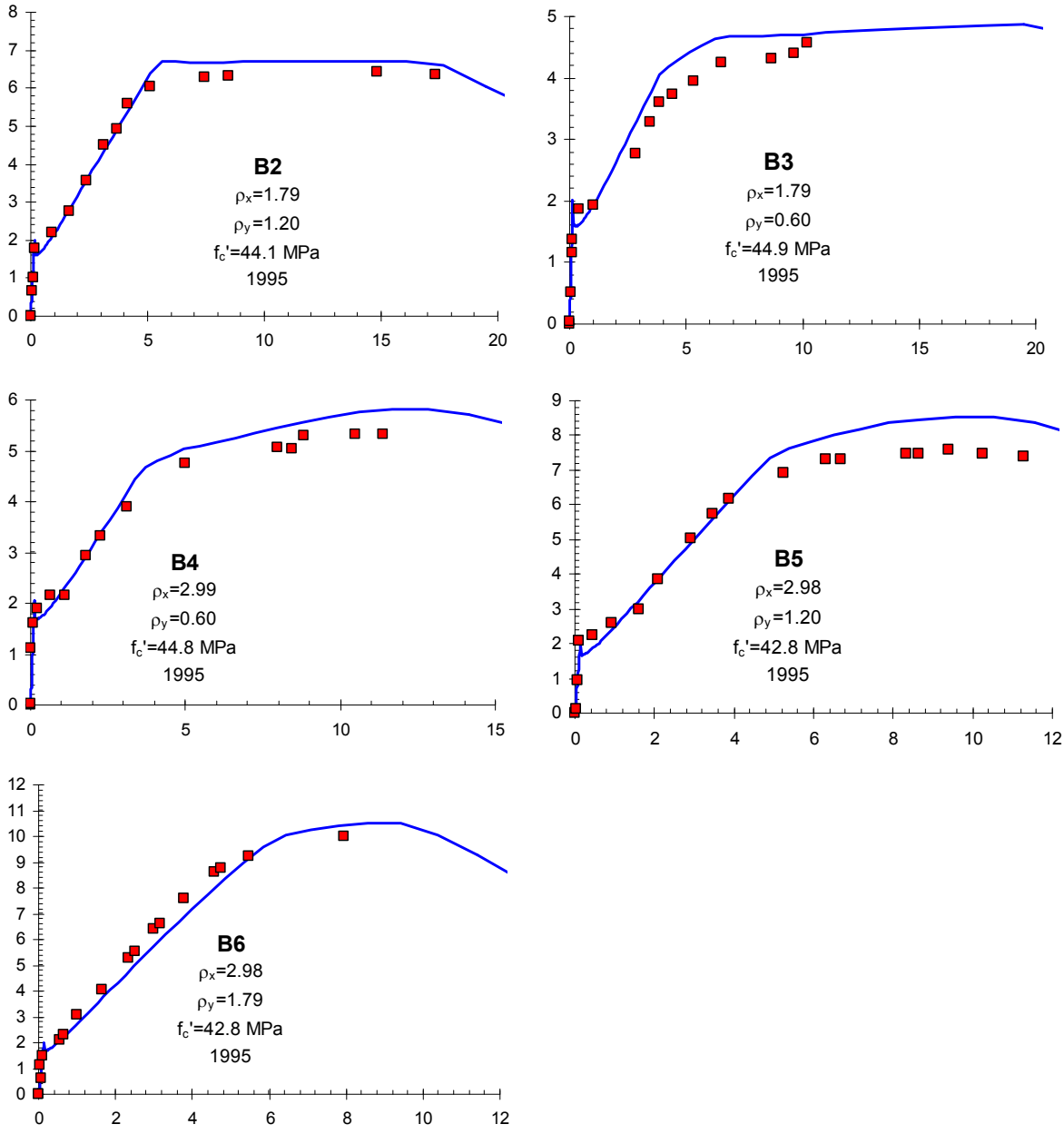

Figure 8-3 (e to i): Comparison of predictions of shear panels

X-Axis: Shear strain (x 10^{-3}) Y-Axis: Shear stress (MPa)

Thick line: MCFT-1987 predictions

Thin solid line: RA-STM 1998 predictions, thin dashed line: FA-STM 1997

8-2-2 Tests of Zhang and Hsu[31]

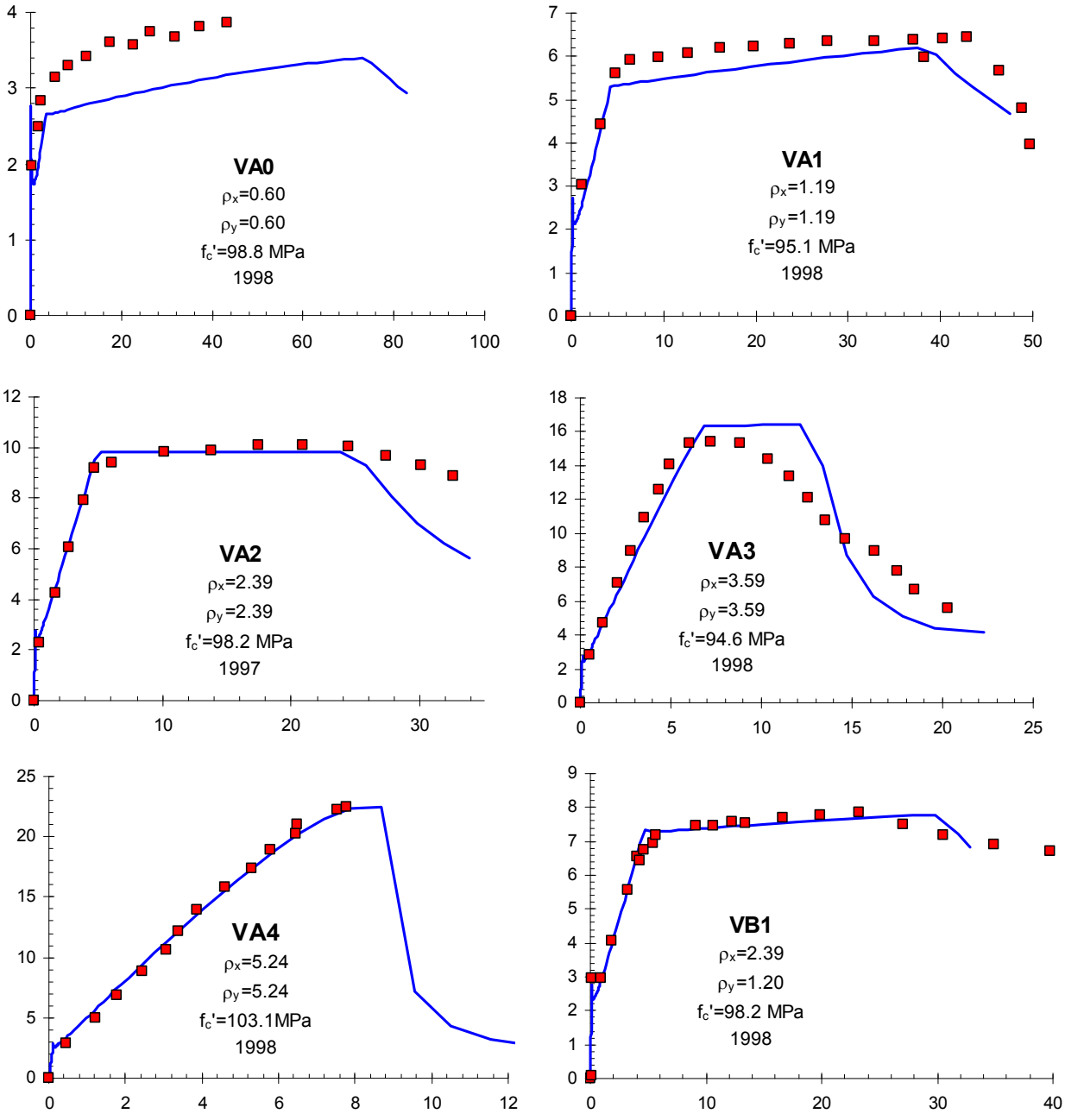

Figure 8-4 (a to f): Comparison of predictions of shear panels

X-Axis: Shear strain (x 10^{-3}) Y-Axis: Shear stress (MPa)

Thick line: MCFT-1987 predictions

Thin solid line: RA-STM 1998 predictions, thin dashed line: FA-STM 1997

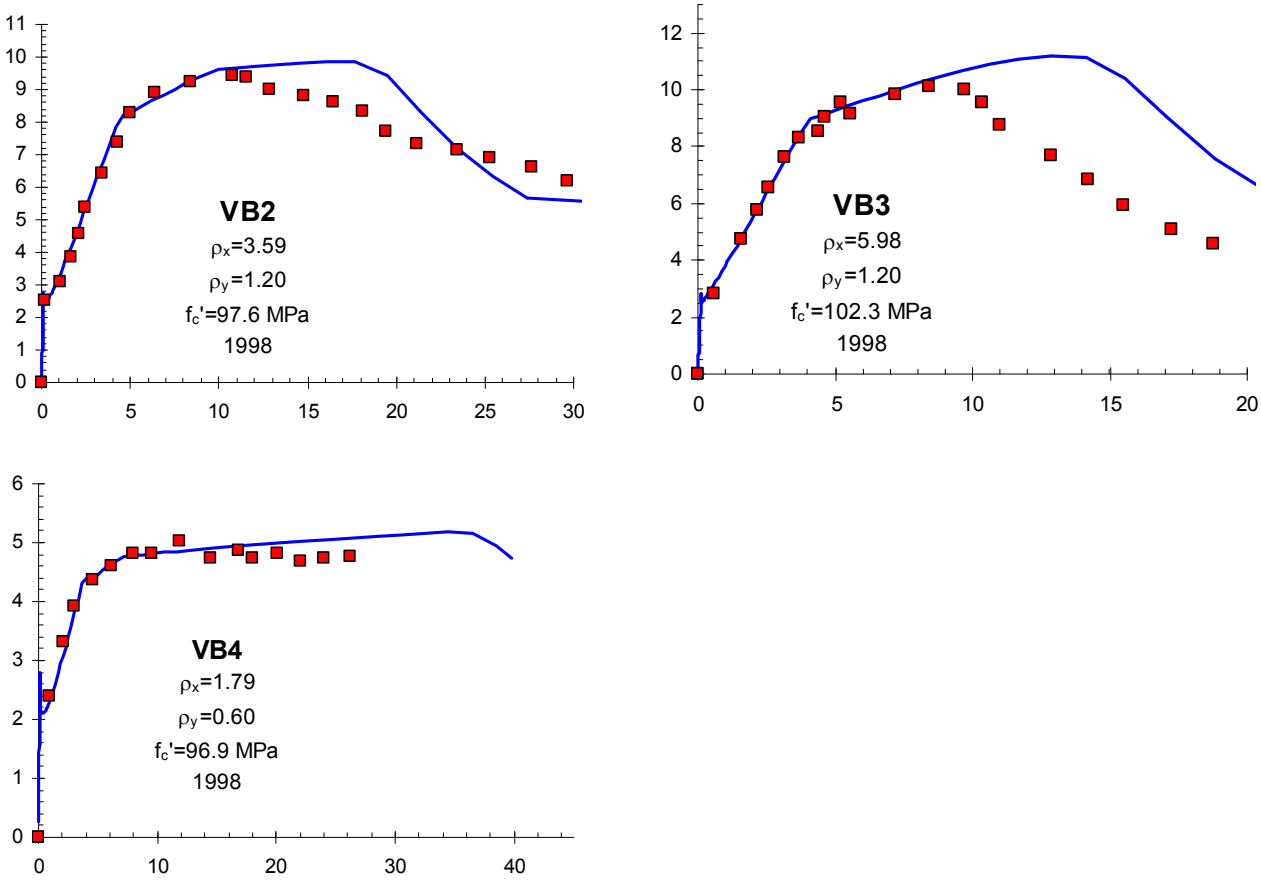

Figure 8-4 (g to i): Comparison of predictions of shear panels

X-Axis: Shear strain (x 10^{-3}) Y-Axis: Shear stress (MPa)

Thick line: MCFT-1987 predictions

Thin solid line: RA-STM 1998 predictions, thin dashed line: FA-STM 1997

Chapter 9: Experimental Program

9-1 General

As the work for this thesis was commencing, a number of shear tests on large lightly reinforced concrete beams were being performed. They were suggesting that the use of very high strength concrete (>90 MPa) was not attaining the expected strength increase over normal strength concrete, but instead, was providing a strength decrease [54, 40]. The crack faces were observed to be relatively smooth with cracks going straight through aggregate rather than around the aggregate as with weaker concretes. This apparent reduction in aggregate interlock called into question some of the assumptions that had been made regularly in the analysis of high strength concrete. A small test program using the shell element tester was developed for this thesis to answer some of these questions. Another series of tests were also commenced to attempt to find what range of concrete strengths had this effect[40].

The Modified Compression Field Theory assumes that the majority of the tensile straining in the concrete will effectively happen at a series of parallel cracks at an angle theta. Compression is transferred parallel to this in the uncracked concrete between the cracks. In elements reinforced with different amounts of reinforcement in the X and Y directions, the angle of cracks is found to rotate during the test as the weaker direction of steel strains at a different rate than the strong direction. This means that the concrete strut carrying the compression parallel to the current crack direction may in fact have cracks in it from previous loading. These earlier cracks would be at an angle to the compression and would be subjected to shear stresses on the crack face that would be resisted by aggregate interlock. Traditionally it was assumed that these earlier cracks would be relatively small, and thus able to resist the applied compression. The question was whether very high strength concrete specimens were able to achieve enough resistance to carry sufficient compression. Earlier tests by Bhide[28] on lightweight concrete, which also tends to crack through the aggregate, found that the assumptions about aggregate interlock were reasonable, but those tests had only about 1-2 MPa of

compression. Higher levels of compression would presumably be more critical and potentially shed light on the unexpected beam test results.

To answer this question, two full-scale shell elements were designed and constructed. Both were geometrically identical, but the first used normal strength (34 MPa) concrete, and the second used very high strength (110 MPa) concrete. Differences between the behaviour of these two elements would provide information about the effects of using very high strength concrete.

The goal was to make the elements as sensitive as possible to the effects that were causing concern. As a result, the element thickness was large and contained reinforcement with relatively poor crack control characteristics. Previous shell elements had a cover of 10 mm, while these elements had 70 mm clear cover. The in-plane spacing of the bars was kept at a reasonable spacing to ensure that the elements would act in a uniform way across the test region. The reinforcement levels were selected as 1.758% in the strong direction and 0.400% in the weak direction. This level of reinforcement was selected to ensure that if the element achieved biaxial yield of both directions of reinforcement, as expected, it would be subjected to significant compression. Loading was applied in tension horizontally with the strong direction of reinforcement angled at 32 degrees to this direction. This combination was selected to achieve the brittle loading in the test region of biaxial tension and shear. The loading and the reinforcement direction were predicted to induce large rotation of crack angles during the test, yet still maintain large principal compression. The normal strength element was tested at an age of four months, but the high strength concrete specimen was tested at an age of almost three years. This delayed testing had the desirable result of maximising any shrinkage and drying effects.

Overall, these two elements were unusual in that they were amongst the largest elements tested in the shell element tester, with the highest strength, largest cover, largest age, and were the first elements tested with reinforcement at this angle.

The details of the specimen geometry are shown in Table 9-1. Table 9-2 shows the material properties. Figure 9-2 shows the stress-strain characteristics of the reinforcement. Figure 9-3 shows the reinforcing grid on the North side of the element, looking north (i.e. looking through the element). Table 9-3 defines the instrumentation and loading of the element. Appendix B contains detailed Zurich surface strains and photographs of the elements.

9-2 Testing Apparatus

The tests were performed in the University of Toronto shell element tester[22]. This facility, completed in 1984, has seen over 100 tests of large reinforced concrete specimens tested in in-plane shear, out-of-plane shear, punching shear, and flexure amongst others. Figure 9-1 shows the Shell Element tester with a square concrete specimen in the middle.

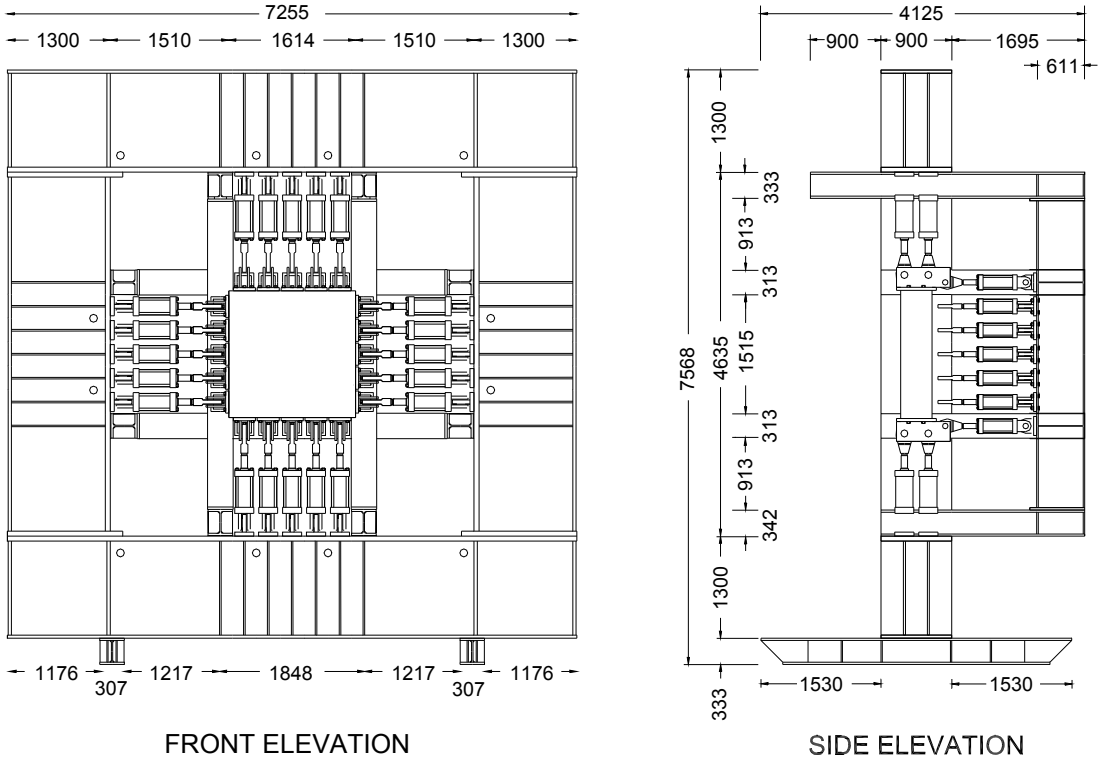

Figure 9 - 1:The University of Toronto Shell Element Tester

Table 9-1 Specimen Geometry

Geometry:	Square shell element	1626x1626 mm.	
	Thickness:	398 mm	
	Clear concrete cover:	65 mm at connector blocks	
		70-80 mm at centre of specimen (due to tying of bars)	

Reinforcement skewed 32.2 degrees from the horizontal. X direction closer to Horizontal, Y direction closer to vertical

X-Direction steel	
No. 20M @ 86 mm both sides	1.758 %
Y-Direction steel	
No. 10M @ 126 mm both sides	0.400 %
Z-Direction steel	
4 - 6 mm ϕ bars for instrumentation	~0.00 %

10M bars placed on outer side of specimen both sides for bad crack control
6 mm ϕ bars hooked around 20M bars for good bond

Table 9-2 Material Properties

Concrete HS1:	cast:	May 19, 1996	tested:	Sept 12-13, 1996
	f_c'	34.2 MPa (116 days)	ε_c'	2.00 mm/m
Concrete HS2:	cast:	July 5, 1996	tested	June 23-24, 1999
	f_c'	110 MPa (>1000 days)	ε_c'	mm/m

Steel See Figure 9-2 below

20M:	This steel had a well-defined yield plateau up to a strain of 7.5 mm/m		
f_y	473 MPa	E	196,000 MPa
f_u	667 MPa		

10M:	This steel has a roughly bi-linear behaviour		
f_y	458 MPa (@ 0.2 % offset)		
E	198,000 MPa	E_{post}	5,500 MPa (ε<40 mm/m)
f_u	692 MPa	ε_u	200 mm/m

6 mm ϕ bars: Ignored for analysis purposes as it could add only the equivalent of 0.02 MPa stress to the concrete section.

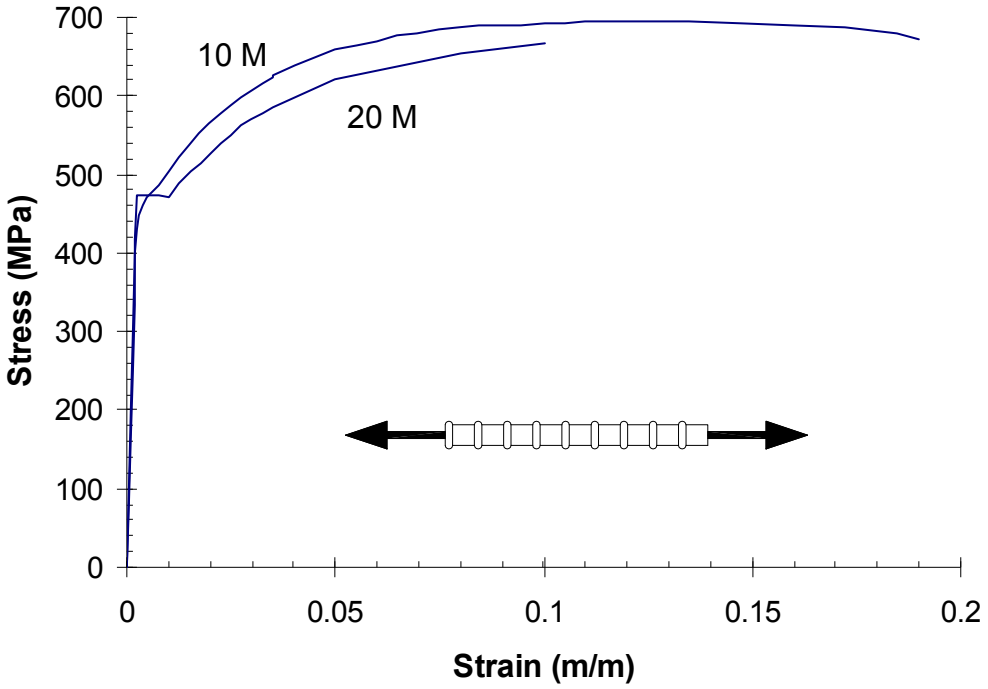

Figure 9 - 2: Stress-strain properties of reinforcement

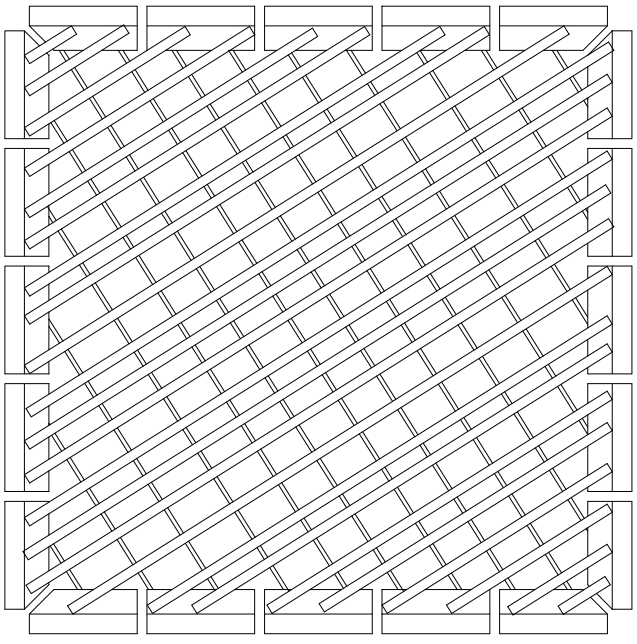

BAR LIST
No. 20M

LENGTH (mm)	NUMBER
1750	12
1620	4
1375	4
1240	4
1010	4
850	4
660	4
460	4
275	4
110	4

BAR LIST
No. 10M

LENGTH (mm)	NUMBER
1750	8
1610	4
1305	4
965	4
650	4
305	4

Figure 9 - 3: North layer of reinforcement

Table 9-3 Instrumentation and Loading

Instrumentation: 24 strain gauges:		4 on 20M bars each side 4 on 10M bars each side 8 on 6 mm ϕ bars total
	12 LVDT's	2 vertical, 2 horizontal and 2 diagonal, each side
	Zurich Targets	300 x 300 mm grid each side
	Hydraulic Pressure	2 lines on input pressure, and return pressure

Loading:

Specimen was connected to loading yokes on all 4 sides, though top and bottom yokes not connected to jacks. 6 Rigid Links used, 3 in-plane (2 at bottom, 1 at East side), and 3 out of plane (2 at top, 1 bottom centre). Loading in axial tension in horizontal direction.

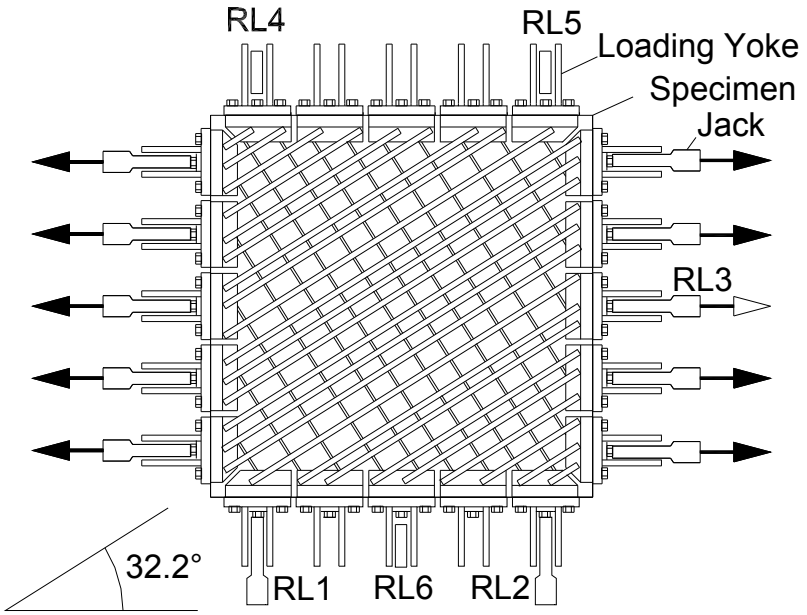

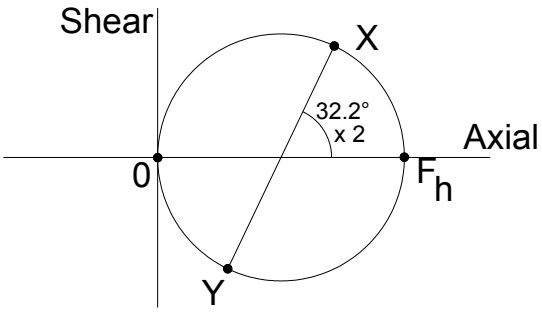

$F_x = 0.716\ F_h$

$F_y = 0.284\ F_h$

$v = 0.450\ F_h$

Mohr's circle of (constant) loading ratios

9-3 General Observations: HS1

The two elements acted very similarly. Each set of new cracks that formed was at an angle different than the previous set of cracks. Figure 9-4 shows HS1 at an early phase in loading as well as at the last load stage when concrete was spalling off the surface. Initial cracking in the top photo is seen as about vertical in response to the horizontally applied load. Later cracks formed at an increasingly rotated angle, with the failure cracks forming 25-35 degrees away from vertical. The cracks rotated towards the strong direction of reinforcement. Final crack widths were 5-15 mm with substantial slip along their lengths although this was not measured with this element. Looking closely, the original vertical cracks, later re-marked with a dashed line, can be seen on the second photo. These early cracks do not appear to have controlled the failure of the element.

For this element, the failure was relatively ductile with ultimate failure being controlled by rupture of a number of the 10M bars and spalling of the cover. Table 9-4 describes individual test observations during the test, and Figure 9-5 shows the horizontal deflection versus horizontal stress for the element. Table 9-5 summarises the measurements made during the test.

Figure 9 - 4: Element HS1 soon after cracking and just before failure

Table 9-4: Observations During Testing of HS1

Loading:	Initially loaded up to 1 MPa tension, unloaded and then reloaded to "work out" initial strains
Load Stage 1:	1 Crack on South side, 0.15 mm wide. No cracks on North side.
Loading:	2 audible sounds as specimen cracks over height, take a load stage
Load Stage 2:	3 cracks on N side, 3 cracks on S side. Mark cracks in Black, miss one on Bottom South East corner.
Loading:	Another audible crack, with large deflection. Take load stage immediately
Load Stage 3:	Mark new cracks in black. Re-mark original cracks with red dotted line. Many new cracks at a rotated angle. Large region uncracked on east side
Loading:	Pause during testing to observe cracks, then continue (LS 3B)
Load Stage 4:	Many new cracks, lower angle than before, some in order of 30-35 degrees from vertical. Stop for the day, take load down to 0.2 MPa Mark new cracks in green.
Overnight:	Load is lost overnight. Upon reloading, there is no sign of trouble
Loading:	Smooth increase in load. Reduced stiffness. Noises again, load stage. LVDT's SD1 and ND1 saturate. Must partly estimate strains from here.
Load Stage 5:	Last load stage: Zurich Gauge cannot be used as cracks too big. Mark cracks in blue, measure large ones with tape measure. Specimen making quiet crackling sounds. It was creeping extensively ~ 15 mm horizontally *during* load stage. Reset LVDT's to allow more measure of deflection. During crack marking, 10M bar ruptures from top east side of specimen. More load taken off for safety.
Loading:	Cannot recover the load, specimen deforms highly at lower load. 3 more bars rupture. Load removed due to concerns about jack travel
After:	Specimen still in one piece. Surface delaminated over majority of surface

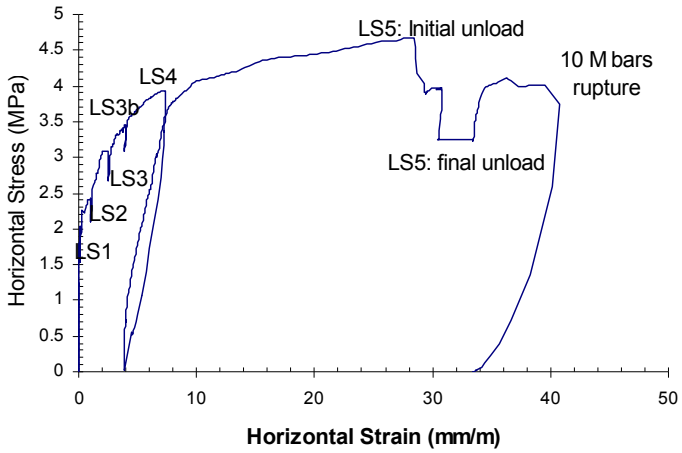

Figure 9 - 5: Loading of HS1

Table 9-5 is the excel spreadsheet.

9-4 General Observations: HS2

Element HS2 acted similarly to HS1. Figure 9-6 shows photos of the element soon after cracking and near failure. Due to the higher strength concrete, the stress at first cracking was higher. The initial cracks in HS1 were 0.15 mm in width. For HS2, the initial cracks were 0.35 mm wide. The extent of cracking at failure was similar. Crack slips were measured for this element and found to be about the same as the width of the cracks. That is, a 7 mm crack was found to have slipped about 7 mm in the direction of the crack. Table 9-6 lists observations made during the testing, and Table 9-7 summarises the measurements made during the test.

Table 9-6: Observations During Testing of HS2

Loading:	Initially load up to 1 MPa to work out system then unload
	Reload until first cracking
Load Stage 1	Mark cracks with thin black lines
	Initial cracks up to 0.35 mm wide
	2 cracks south side, 1 crack north side
	150 mm triangles in each corner delaminated both sides
	Cracks primarily outside LVDT's, so not totally picked up
Loading:	New cracks form
Load Stage 2	many new wide cracks. Element cracks again during Zurich Readings
	Delamination same as load stage 1.
	New cracks have some slip, about 0.4 mm slip on a 0.4 mm wide crack
	Cracks marked in thin green
Loading:	New cracks form
Load Stage 3	Some new cracks. Some follow angle of reinforcement
	No change in delamination
Unloading:	unload element overnight
	Pressure slowly lost overnight, but element not damaged
Loading:	reload to load level of previous night
Load Stage 4	New Zurich Load stage after restoring load to previous night level
	No new cracks, so no photos taken
Loading:	3 new cracks on south face
Load Stage 5	New cracks marked in black
	Old green cracks slipping roughly as much as they are wide
	Black cracks slipping too.
	Delamination mostly around sides, but small location in centre too, S side.

Loading: Load Stage 6	existing cracks extend lots of slip on cracks. Generally 2/3 of crack width. Black cracks 2.5 mm wide with 2.0 mm slip Majority of cover now delaminated
Loading: Load Stage 7	New cracks form mark new cracks Black cracks 7 mm wide with 5 mm slip.
Loading:	Element unable to restore load. Three pauses to reset the LVDT's to prevent saturation. Bars begin to rupture. Over 5 ruptured. Test terminated due to bars rupturing.
After:	Specimen still in one piece. Surface delaminated over majority of surface, though no spalling.

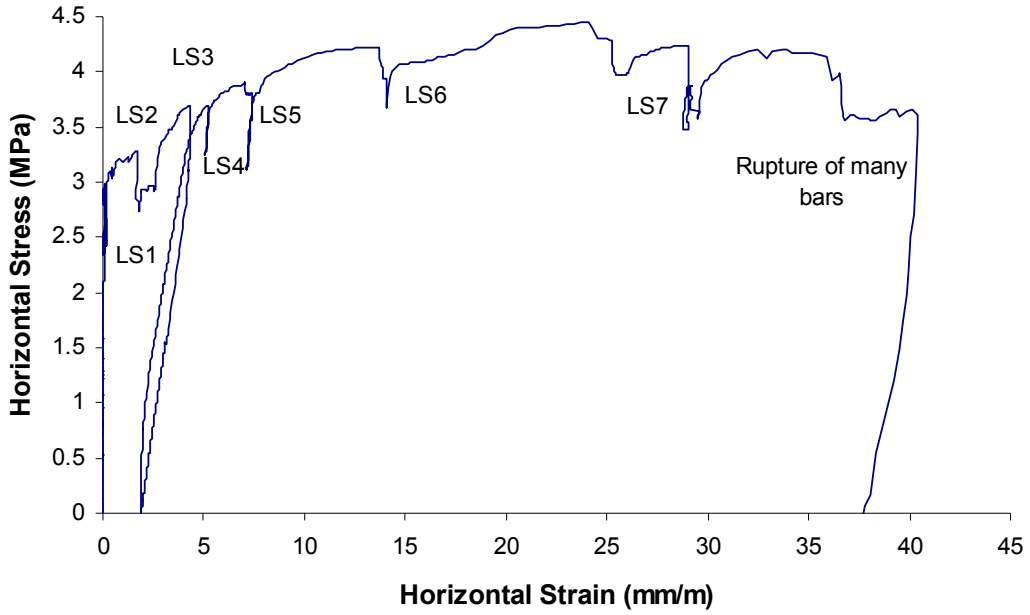

Figure 9 - 6: Loading of HS2

Figure 9 - 7: Element HS2 soon after cracking and just before failure

Table 9-7 is excel spreadshhet

9-5 Comparison of behaviour and predictions: HS1

The following plots show the behaviour of the element. Figure 9-8 shows the shear-shear strain plot for the element. Also plotted is the prediction from the MCFT and the Rotating Angle Softened Truss model. It can be seen in this figure and the three that follow that the MCFT prediction for this normal strength concrete is good, though it overestimates the stress levels over a large part of the test. The failure load was well predicted. The RA-STM prediction is relatively poor in comparison for both strength and ductility.

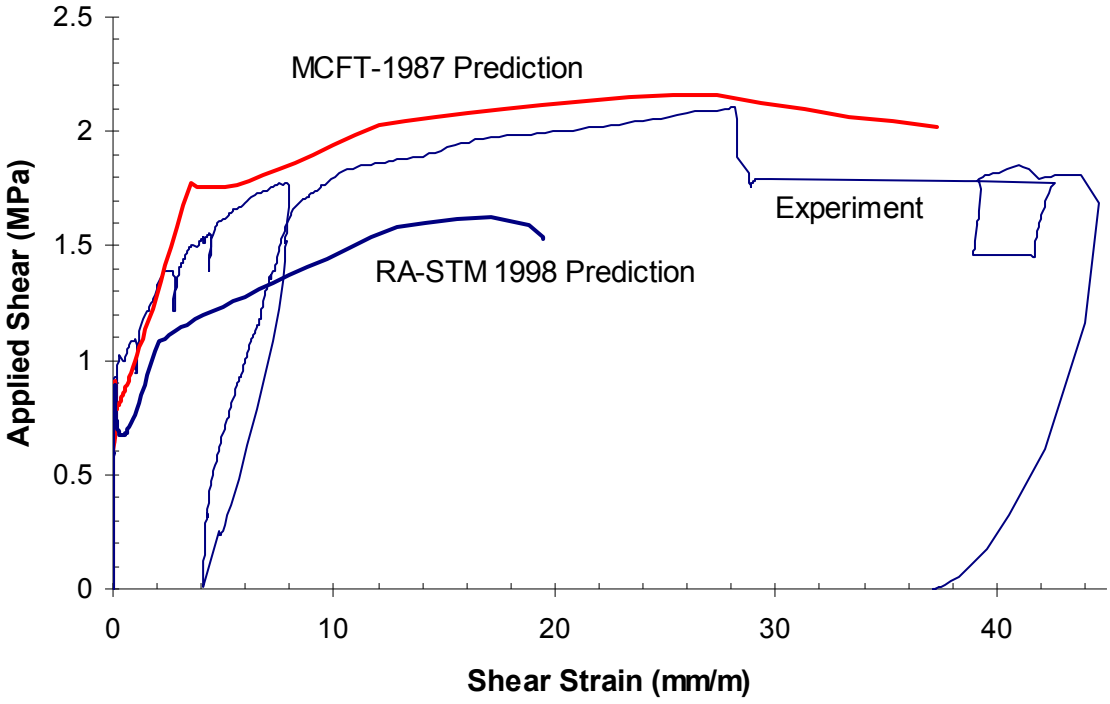

Figure 9 - 8: HS1 Shear stress - shear strain

Figure 9-9 shows the principal stress and strain angle along with the predicted angle theta from the MCFT. Note that the angle of stress and strain are not equal, though assumed so by the MCFT. The calculated angle is a reasonable approximation of both, however.

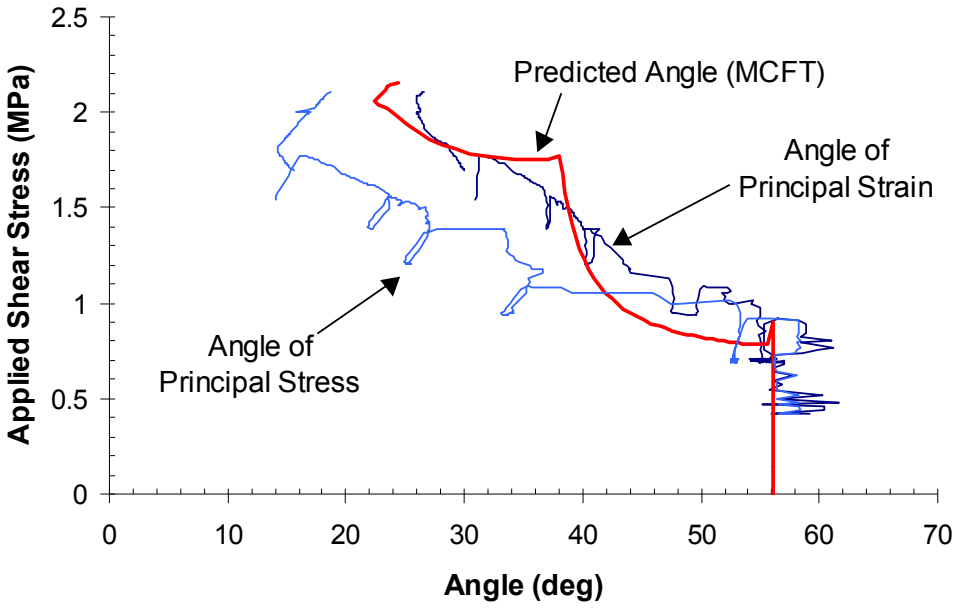

Figure 9 - 9: HS1 Angles

Figure 9-10 shows the principal tensile stress-strain relationship observed with the predicted relationship. The fit is quite good considering that tension measurements are

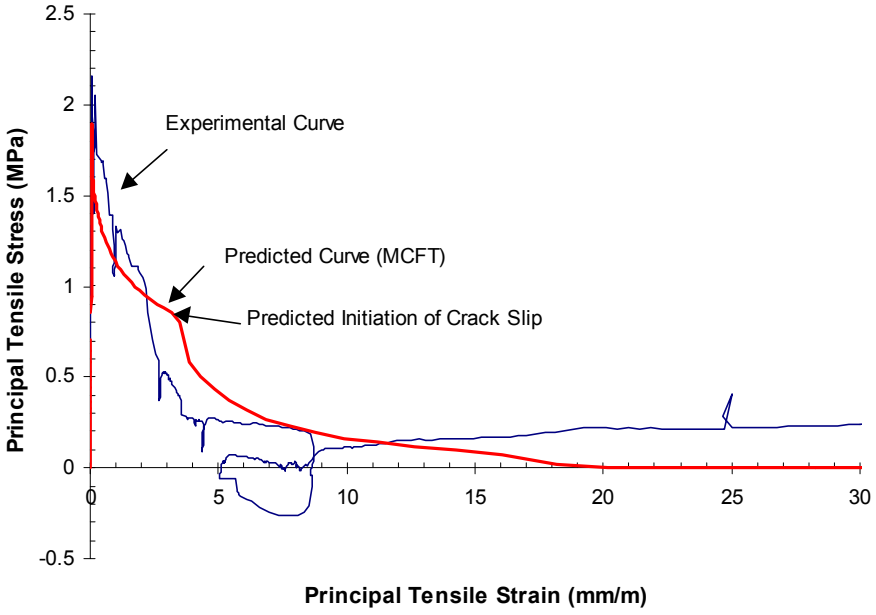

Figure 9 - 10: HS1 Tension stiffening

small differences between large numbers and hence tend to have high scatter. The measured values do not extend down to zero with higher strain suggesting that some other mechanism was strengthening the panel, such as kinking of the reinforcement at a crack. The loop where the curve goes negative was during the overnight unloading of the panel.

Figure 9-11 shows the measured compressive stress-strain relationship and the predicted values. The results, again, are good. Note that the observed stresses and strains were dramatically lower than the shown cylinder curve. The concrete failed at a stress of only 20 % of the cylinder strength. The maximum compressive strain observed was about twice the strain at peak stress for the cylinder.

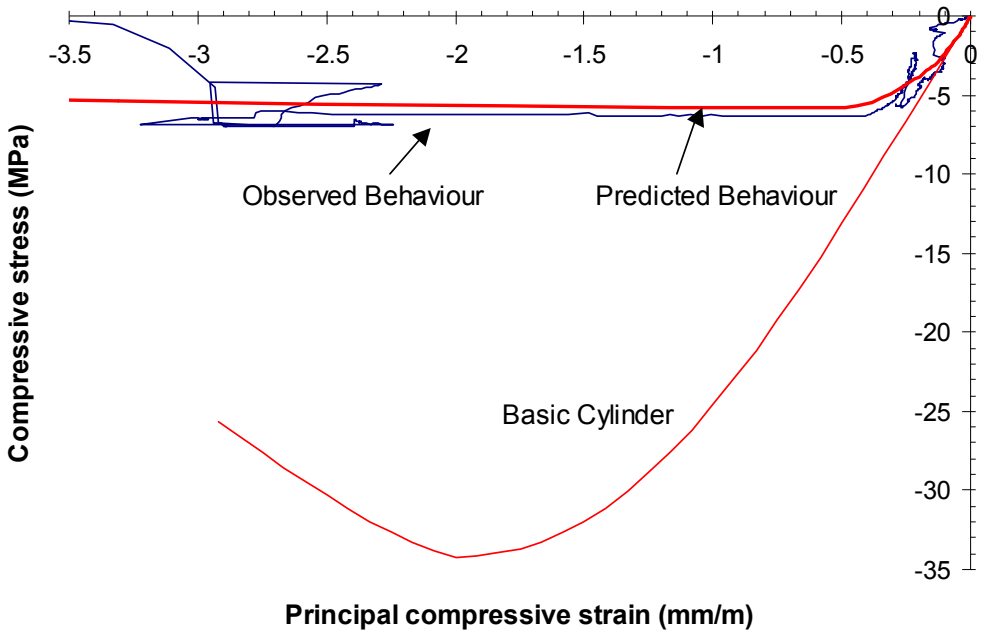

Figure 9 - 11: HS1 Compressive response

9-6 Comparison of behaviour and Predictions: HS2

Figure 9-12 shows the shear stress-shear strain plot for the element. Also plotted is the prediction from the MCFT and the Rotating Angle Softened Truss model. Recall that this element was made of very high strength concrete and was tested partly to determine if the MCFT is unconservative for such elements. It is seen that the basic predictions are indeed unconservative for this element. The strength is substantially overpredicted, as is the ductility. The prediction here was made with the Porasz/Collins concrete model, as recommended for very high strength concrete in chapter 5, yet was still unconservative. Note that despite being calibrated partly on large high strength elements, the RA-STM also does a poor job and is almost equally unconservative as the MCFT for this element.

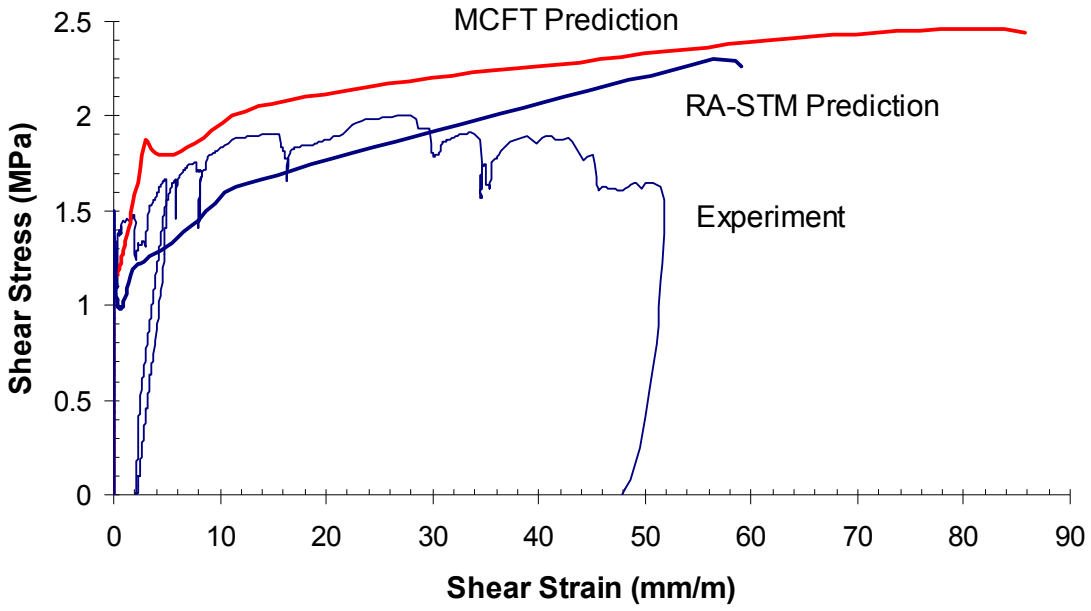

Figure 9 - 12: HS2 Shear stress-shear strain

Figure 9-13 shows the principal angles. The MCFT prediction of the angle is not as good as it was for HS1. The angles of principal stress and strain are similar in the tests, as before, but the predicted angle is 10-20 degrees away from that.

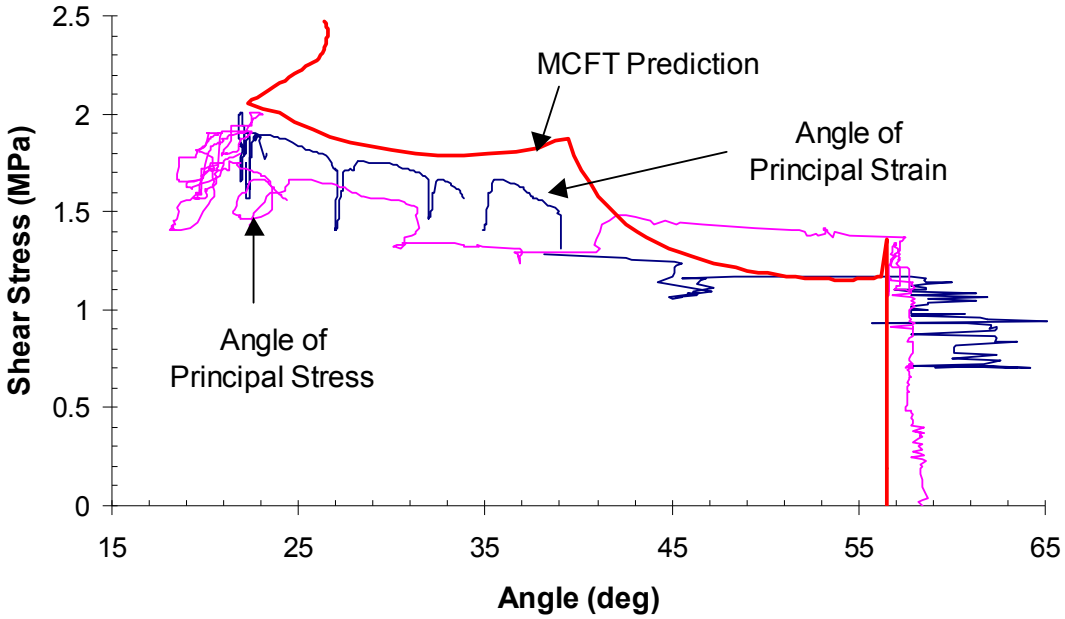

Figure 9 - 13: HS2 Angles

Figure 9-14 shows the observed tensile stress-strain response from the test. As with HS1, the prediction is quite good. Note that the MCFT assumption of zero tension stiffening after yield of the steel is well supported by the data.

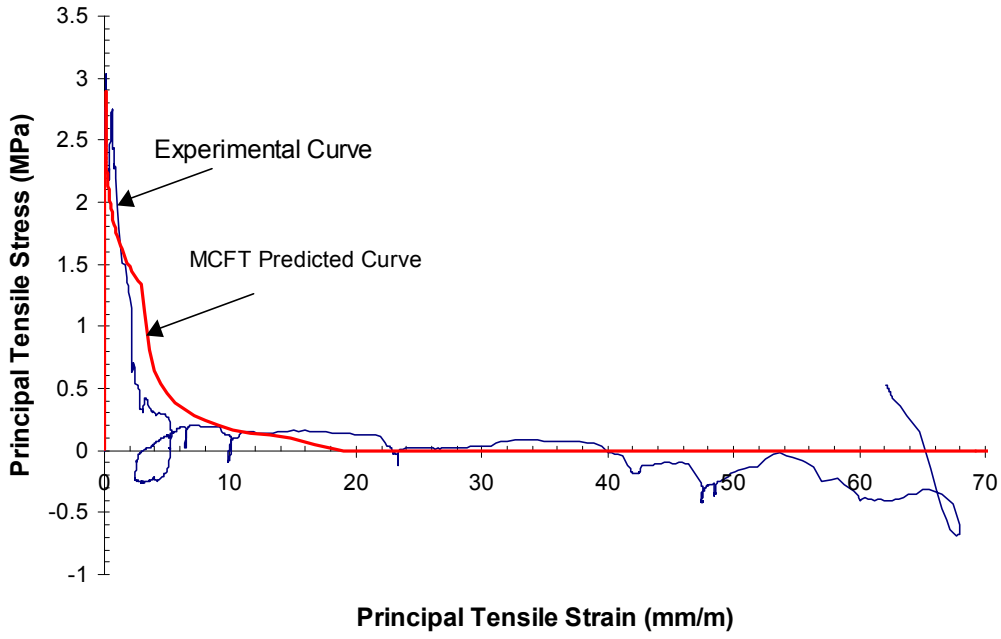

Figure 9 - 14: HS2 Tension stiffening

Figure 9-15 shows the observed compressive stress-strain curve for test HS2. The data shows virtually no strain development on loading as a number of major cracks intersected only some of the LVDTs used to calculate the strains. The maximum stress observed is basically the same as for the much weaker concrete of HS1. Note that more stress was observed in the concrete than predicted, but the result was still unconservative as the angles were poorly modelled.

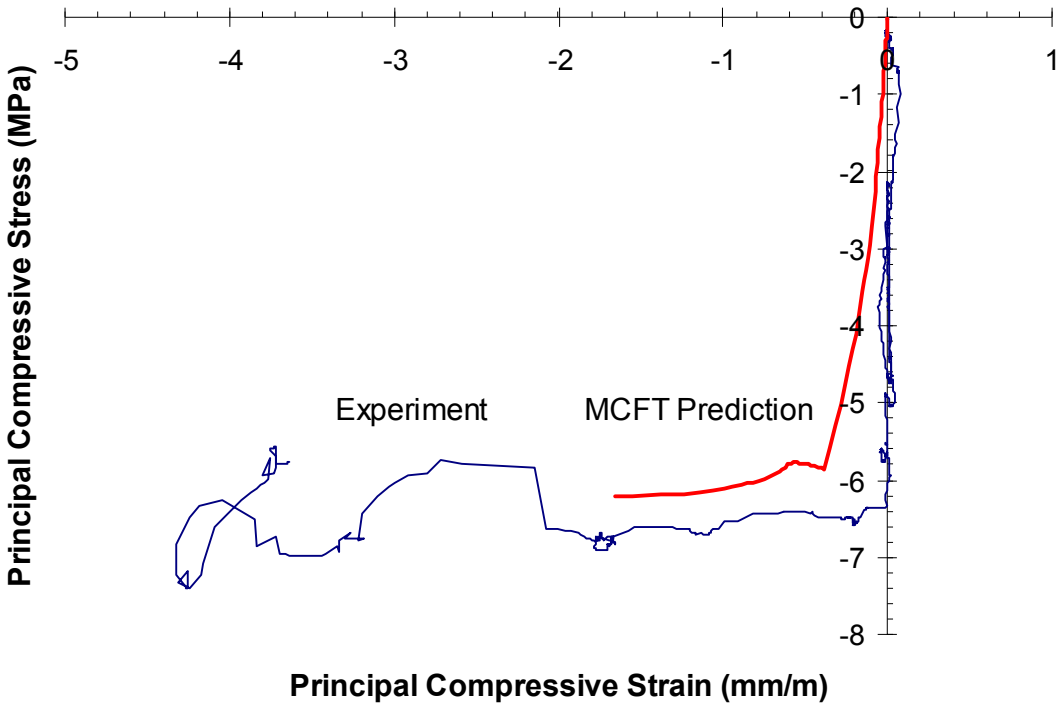

Figure 9 - 15: HS2 Compressive response

9-7 Comparison of HS1 and HS2

Figure 9-16 compares the experimental behaviour of the two elements. Despite HS2 having about three times the concrete strength, it was actually slightly weaker than HS1. The ductility and stiffness characteristics were very similar between the two elements. The only significant difference was that the higher strength panel cracked at a higher stress.

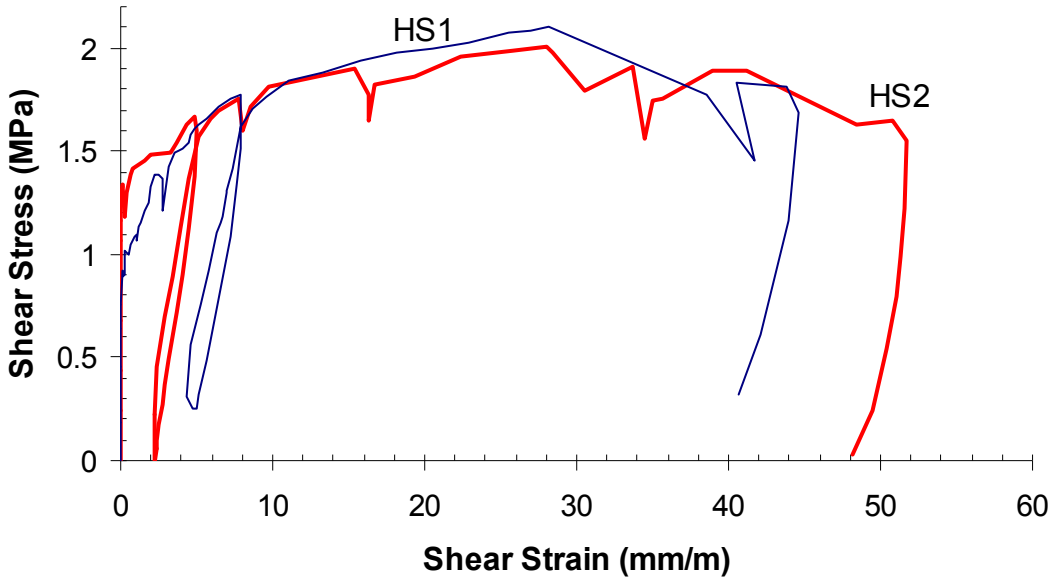

Figure 9 - 16: HS1 and HS2 shear-shear strain

On examination of the predictions, with Membrane-2000, it appeared that the unconservative predictions of HS2 were strongly influenced by the assumption that the reinforcing bars could strain harden on average. While they certainly did strain harden at a crack, based on the strain, the analysis also assumed that the bars would strain harden in the concrete between the cracks. Figure 9-17 shows the experimental data for HS2 compared to the prediction above as well as a prediction if the bars are assumed to be unable to achieve a stress in excess of the yield stress. It can be seen that the prediction is no longer unconservative. As no strain hardening is the usual assumption for design purposes, the results of this experiment apparently do not bring into question the safety of structures designed with the MCFT. On the other hand, stress-strain curve for the 10M

bars in the specimen did not have a yield plateau, so assuming a constant stress of yield seems poor. Further research is needed to quantify the effects of strain hardening branch of the reinforcement on element predictions.

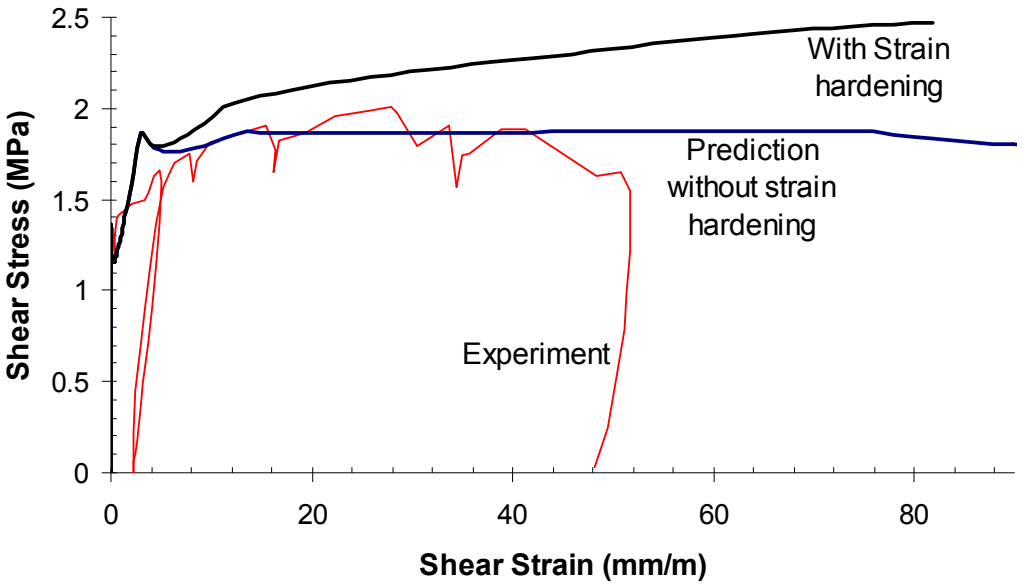

Figure 9 - 17: HS2 Predictions without strain hardening

Chapter 10: Experimental Verification of Response-2000

As a beam/column sectional analysis program that includes shear, Response-2000 will be illustrated using selected experimental results for beams and columns tested in shear over the past 40 years. Chapter 12 provides additional information on how to perform such shear analyses with Response-2000.

The first part of this chapter demonstrates the value of the proposed changes in tension stiffening relationships as explained in Chapter 5.

The second section shows Response-2000 compared to individual test series. These series were selected to demonstrate that Response-2000 can successfully predict a number of important behavioural trends associated with the shear behaviour of reinforced concrete. Where appropriate, the predictions of code methods are shown as well.

The third part of this chapter shows Response-2000 compared to a large database of 534 beams. There have been over 10,000 shear tests reported in the literature over the past 100 years. When databases that aggregate all this data, as are currently being prepared, are available, the program can be compared to more tests. Tests were originally selected for this data set simply in terms of what was available at hand. None of these tests were discarded if the program predicted them poorly. Later, a more systematic procedure was chosen to select additional elements by examining what regions of input parameters were missing from the existing database. There is a strong bias in the selected data towards larger members. Before about 1965, beams tested in shear were generally about 12 inches deep and 10 feet long. This was based on storage restrictions, loading restrictions and tradition. Since that time, it has been found that larger beams tend to fail at a lower shear stress than geometrically similar smaller beams. As these larger beams tend to be less conservatively predicted, they were preferentially selected. The average beam depth in the database is only 500 mm, however, as there are a number of important tests that were included from the older database.

Appendix C gives some details of the 534 beams in the database.

10-1 Effects of tension stiffening changes

Changes to the tension stiffening relationships used in the Modified Compression Field Theory for use in the programs in this thesis were proposed in Chapter 5. This short section demonstrates the effect of these changes on a series of 64 beams. The selected beams are a subset of the full database in Appendix C and are identified there. They were selected because they include a wide range in depth and were generally lightly reinforced longitudinally. They all have no transverse reinforcement and are constructed with normal strength concrete. By selecting a subset of the database, the remaining experiments could then be used to verify that any calibration was appropriate.

Figure 10-1 shows the experimental over predicted shear strength for these beams if the traditional tension stiffening relationship of the MCFT, as shown in the figure, is used. The horizontal axis has been selected as overall beam depth because this was found

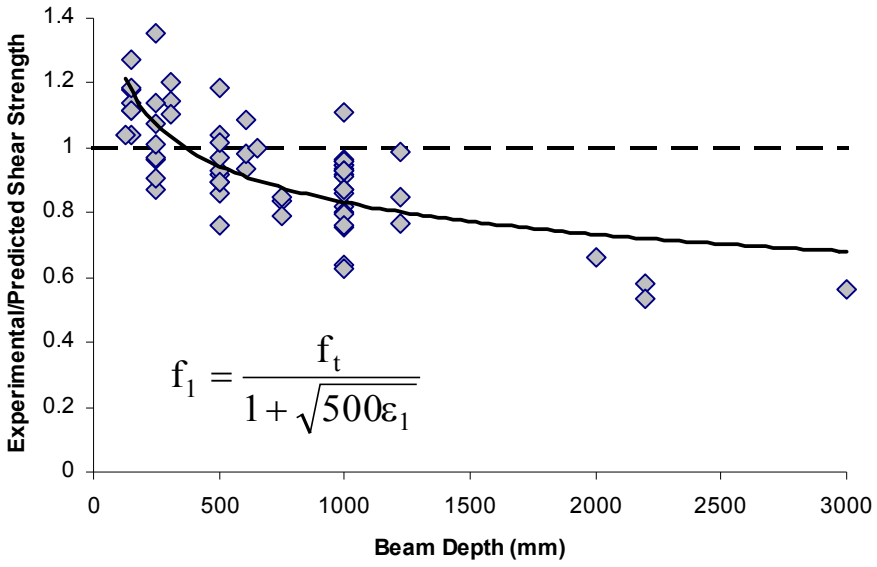

Figure 10 - 1: Experimental/Predicted, Base MCFT

to have the strongest correlation with the data. It can be seen that there is a strong correlation with larger members being predicted poorly.

Figure 10-2 shows the same set of data as predicted by Response-2000 using the tension stiffening relationships from Chapter 5. It can be seen that the prediction is much better.

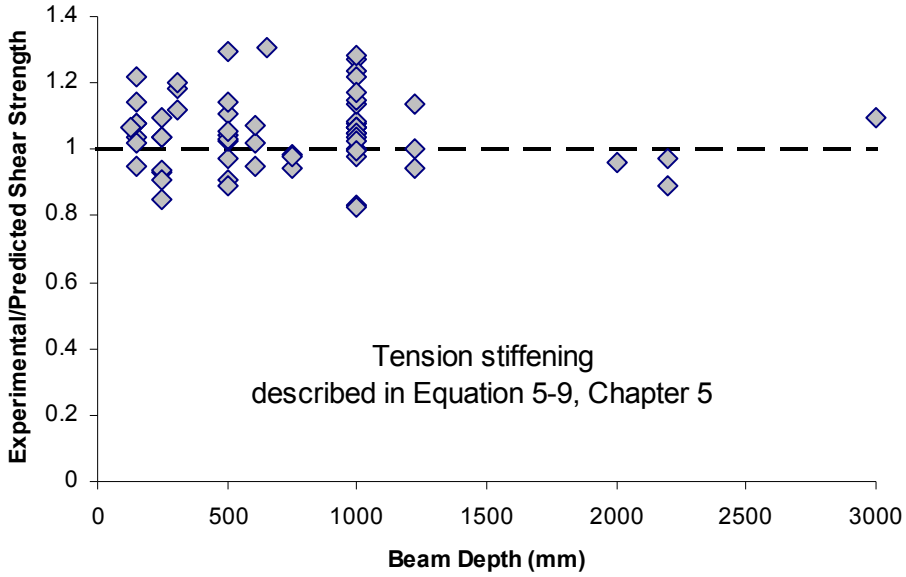

Figure 10 - 2: Experimental/Predicted, Response-2000

The remainder of this chapter shows the predictions of Response-2000 with the newer tension stiffening relations as proposed in Chapter 5.

10-2 Arbesman and Conti: Prediction of sectional response

Perhaps the most important beam test in the development of the Compression Field Theory was Beam CF1 (Compression Field 1) tested by Arbesman and Conte[71,5] in

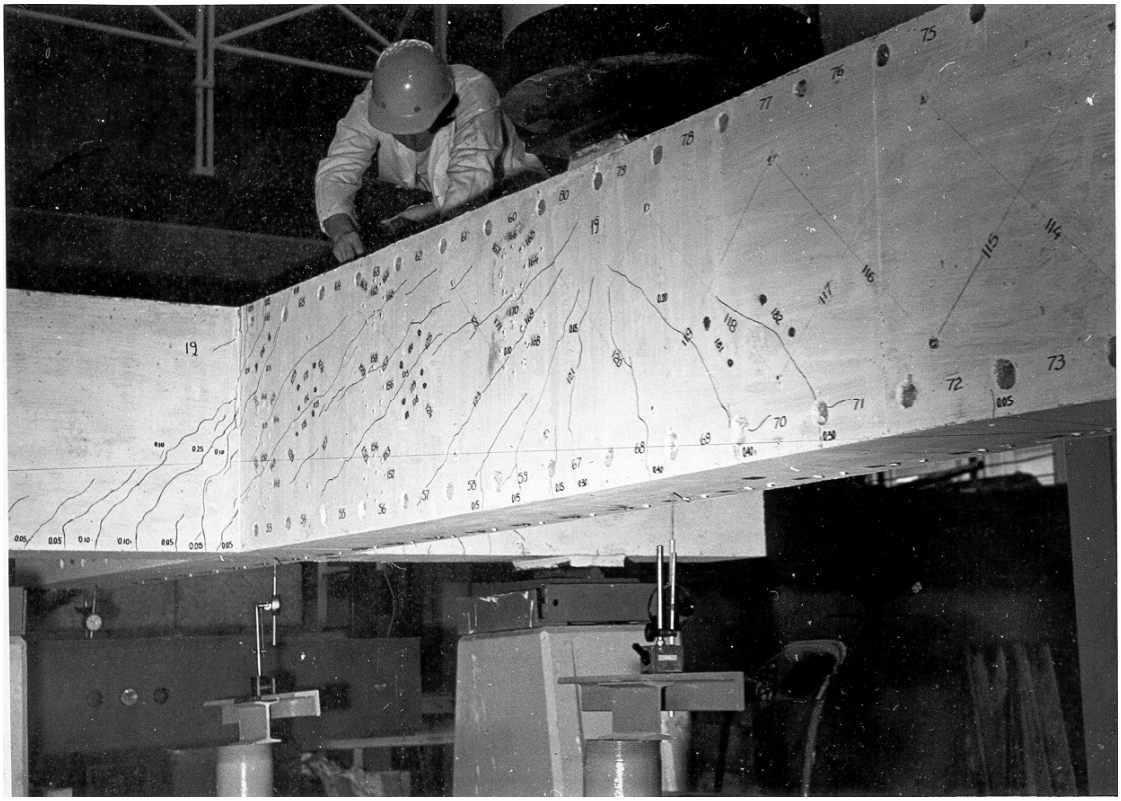

1973. The photograph shows the beam during the test. This beam was a prestressed hollow box girder beam, heavily instrumented. It was loaded in such a way that the test region was subjected to negative moment near the person in the photograph and positive moment just to the right by the dial gauge. There was a point of zero moment in the middle of the test region. Failure of the beam was by flexural yielding at the positive moment location and crushing of the web of the box girder (shear failure) near the location of zero moment.

The beam was entered into Response-2000 as an I-beam section. Figure 10-3 shows the predicted and experimental moment-curvature results at a location below the point load. The experimental curvature was determined from measured longitudinal strains of the top and bottom steel. The analysis was performed without shear (i.e. a flexural analysis.) The results obtained are remarkably good. Unfortunately, this

extremely high level of precision is only occasionally attained with Response-2000, or with any other analysis procedure for reinforced concrete.

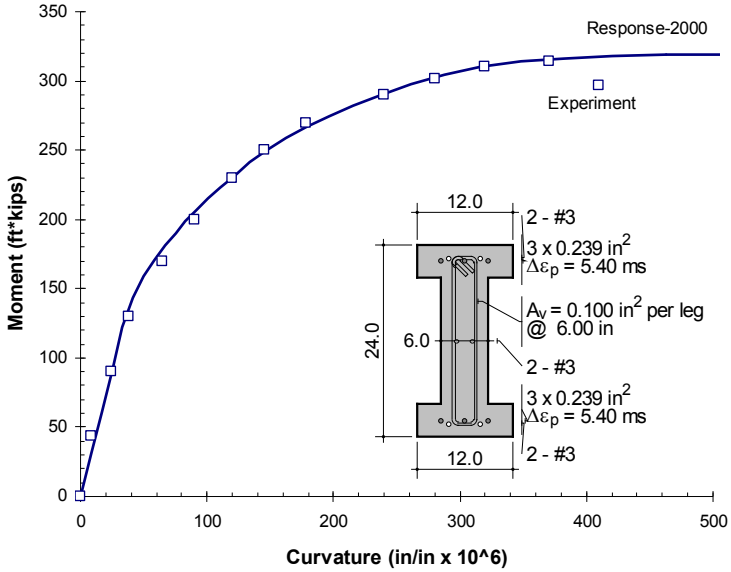

Figure 10 - 3: Moment-curvature of CF1

Figure 10-4 shows the shear force versus shear strain for CF1 in the middle of the test region where the moment was equal to zero. The shear strain was measured by taking the difference in strains of two diagonals at 45° to the horizontal. The very good

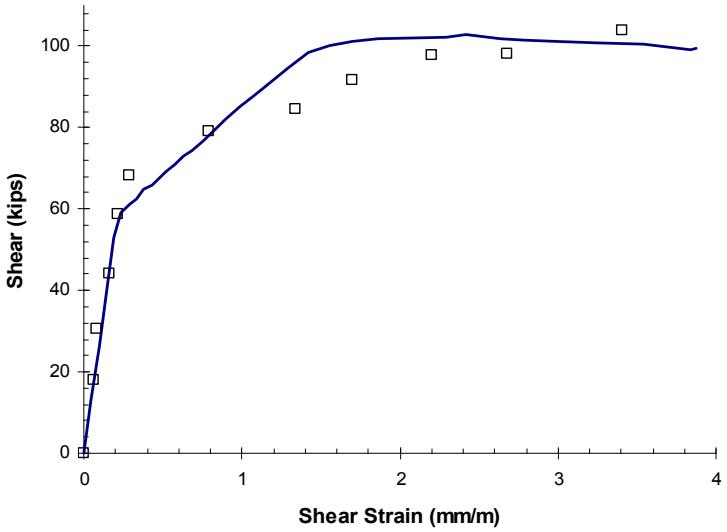

Figure 10 - 4: Shear-shear strain CF1

agreement between theory and experiment shown in the figure is more representative of what can be expected for Response-2000.

While Response-2000 always calculates the full load-deformation relationship for a section, sometimes it is the strength that is of primary interest. The following examples show the influence of a series of input variables on the predictions of strength from Response-2000.

10-3 Taylor: Effect of aggregate size

Taylor[41] played an important role in the investigation of the mechanisms of shear response. One of his series of tests examined size effect and the influence of aggregate size. Fifteen beams were tested varying in depth from 150 mm to 1 metre and constructed with 22 to 34 MPa concrete. Figure 10-5 demonstrates that the equation used for the maximum shear on the crack, which controls failure for beams like these without stirrups, models the effects of aggregate size appropriately.

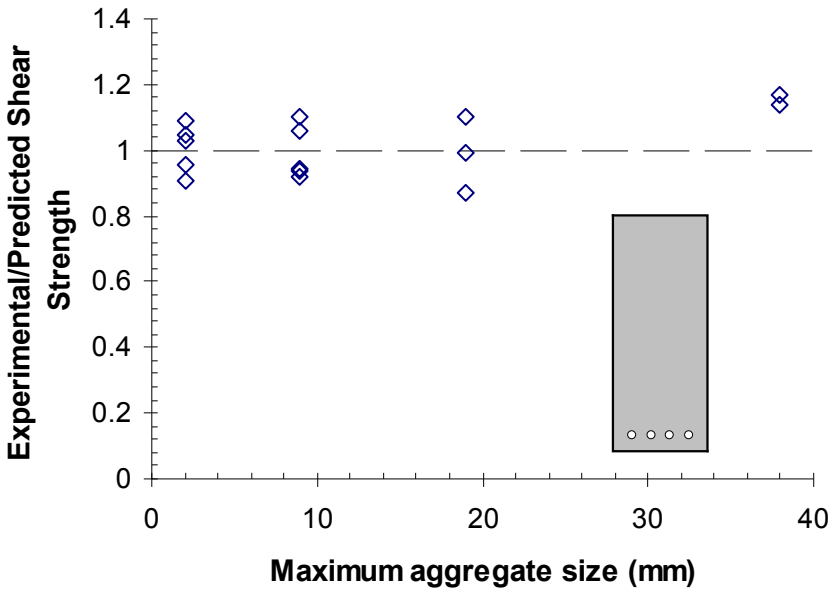

Figure 10 - 3: Effect of aggregate size

10-4 Shioya et al: Size effect in shear

In what is surely the most impressive series of shear tests yet performed, a large-scale test program in Japan[42,43] tested beams that varied in depth from 100 mm (4 inches) up to 3000 mm (10 feet). The largest of these beams was 36 m (120 feet) long, weighed almost 400 tonnes and contained 1000 times the volume of concrete of a standard beam shear test. The testing of the largest of these beams is shown below.

This largest beam was tested upside-down against a specially built prestressed concrete support beam. Loading was uniformly applied on the bottom of the beam by the filling of a water bag, lifting the beam against its own self weight and the restraints at the end of the beam. The beam contained 0.4% of longitudinal reinforcement which, though a small percentage, still represented 6000 kg of reinforcing in the one beam. There was no transverse reinforcement in any of the beams in the series.

These tests model a foundation style structure. Such structures generally have light amounts of longitudinal reinforcement and no transverse reinforcement. It might be

felt that a structure 3 metres deep is unrepresentative of real construction practice. This is not the case however. Many multi-storey buildings contain beams that are more than 1 metre deep, often transfer girders above the first floor of a building. A typical industrial building near Toronto contains 2 metre deep girders supporting process equipment weighing thousands of kilonewtons. In portions of the Toronto subway system tunnels, one-way slabs are 3 metres thick without transverse reinforcement. Similar 3 metre deep tunnel-roof slabs exist in Japan over sub-surface highways, where the prevalence of earthquakes adds a level of concern. The Petronas Towers in Kuala Lumpur Malaysia, currently the tallest buildings in the world, are built on 2-way slabs that are 4.5 metres deep of solid concrete. Finally, in Japan there are 100 m diameter underground liquid natural gas storage facilities that contain slabs at their base designed against groundwater pressure. These base slabs are up to 8 metres (25 feet) thick of solid concrete without transverse reinforcement. Each of these examples is already built in the field, sometimes using design codes that do not deal with the size effect in shear.

Figure 10-6 shows the predictions of Response-2000 to the test series that

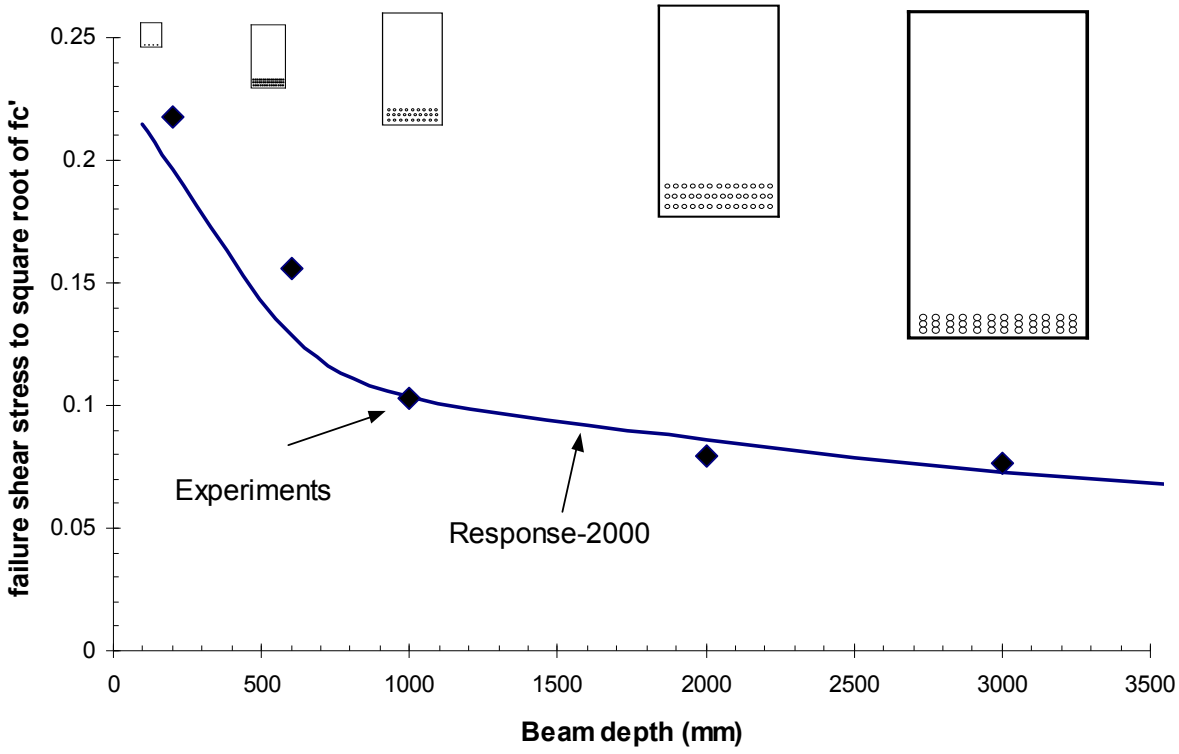

Figure 10 - 4: Shioya et al size effect

included the 3 metre deep beam above. The trend is remarkably well predicted by the program.

The ACI code assumes that members without stirrups can resist a stress of $0.167\sqrt{f'_c}$ (MPa units, $2\sqrt{f'_c}$ psi units) prior to failure. This was based upon laboratory testing which primarily used beams about 300 mm deep. Note that the value of 0.167 is reasonable value for elements of that depth based on the graph above. On the other hand, the largest of the beams failed at about 45 % of this value. This is an unsafe situation.

Response-2000 is also able to predict the total load deflection response for prismatic beams. The calculated response for the largest of the Japanese beams is shown compared to the measured response in Fig 10-7. It can be seen that excellent agreement was obtained.

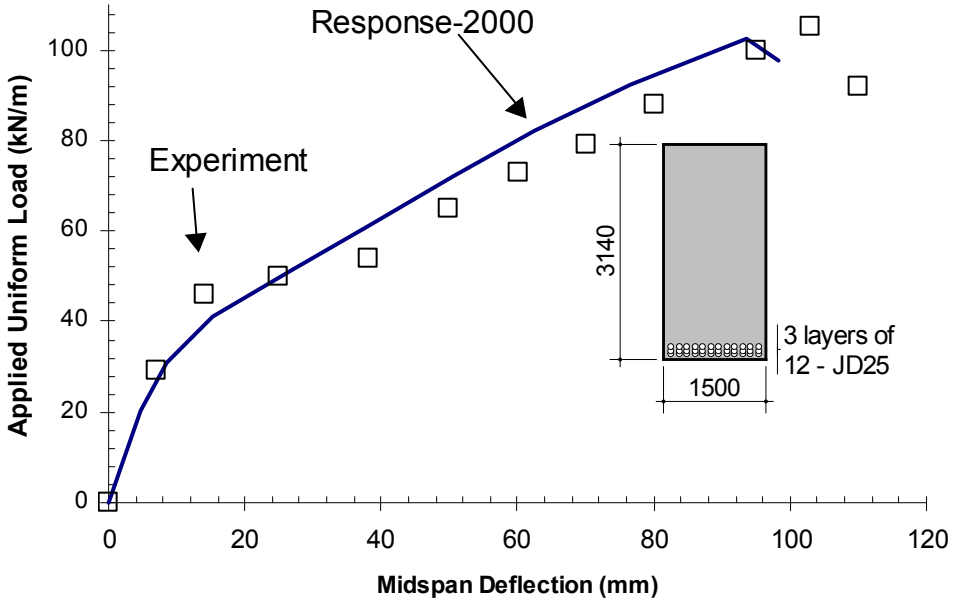

Figure 10 - 5: Load deflection, 3000 mm deep beam

The following figure shows the observed crack pattern observed by the Japanese researchers as well as the deflection prediction page from Response-2000. The predicted crack pattern is shown for half the beam and is reasonably accurate. The distribution of

curvature and shear strains shows the strong interaction which occurs in this beam between shear and moment. For example, it might be expected that the highest shear strain would occur at the end of the beam where the shear is highest but this is not the case. Rather, it occurs in a region from about 1/6th of the span to 1/3rd of the span where both the shear and moment have high values.

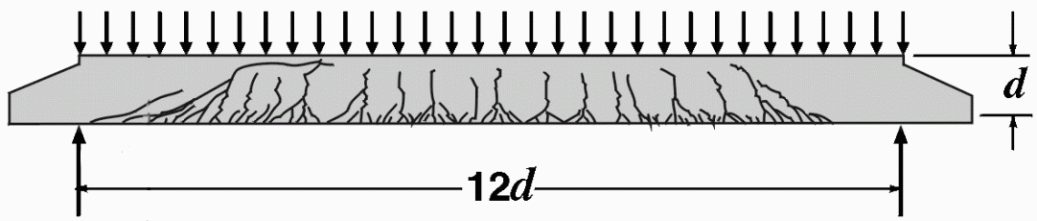

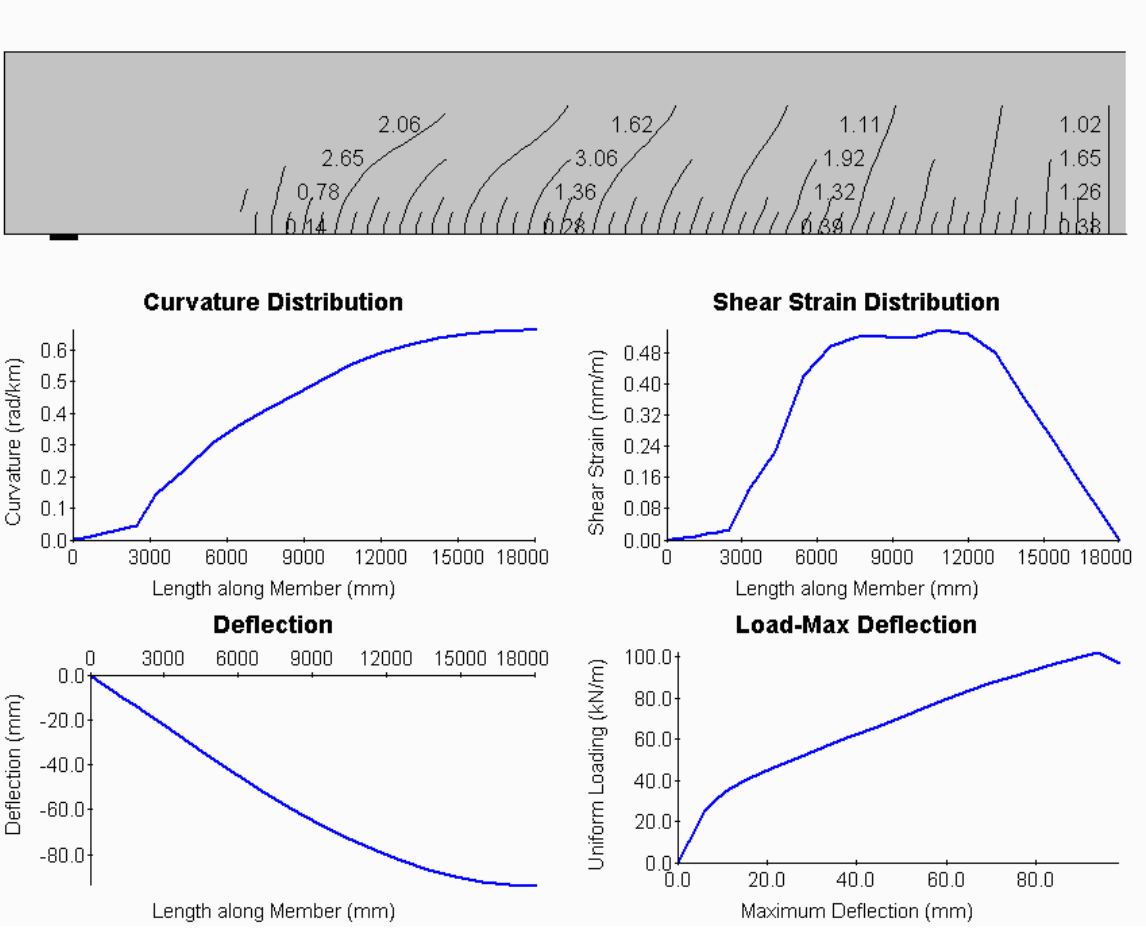

10-5 Kani: Effect of a/d ratio

Kani[44,45] started shear research at the University of Toronto in the late 1950's. Over a period of 10 years, he tested approximately 800 beams in shear in an attempt to solve "the riddle of the shear failure."

Out of this extensive selection of data, a single series is shown here. These tests show the effect of shear span to depth ratio (a/d ratio) on the shear strength of 610 mm deep beams with 2.8 % longitudinal reinforcement and normal strength concrete. Response-2000 predicts the data very well for beams with an a/d ratio greater than 2.5. Beams shorter than that are affected by direct strut action supporting the load. The dashed line shows the results of calculations done with a simple moment to shear ratio style calculation as for the tests with an a/d greater than 2.5. This is seen to be very conservative for these short beams. The method proposed in Chapter 7, shown by the thicker line, does a much better job at predicting the shear capacity. This technique calculates the strength, and deflection, from the moment-shear interaction diagram.

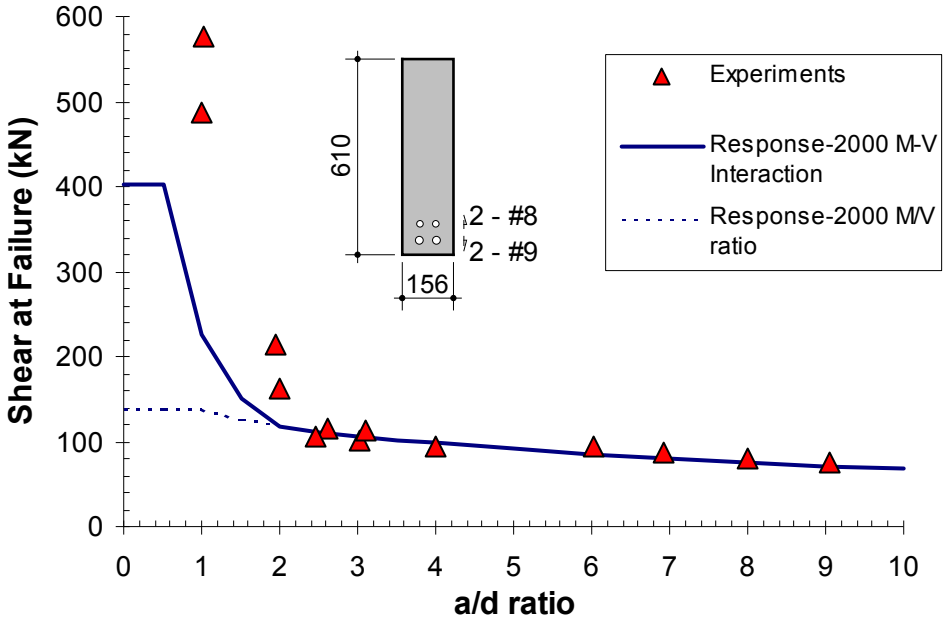

Figure 10 - 6: Effect of a/d ratio

10-6 Moody, Viest, Elstner, Hognestad: Concrete strength: small beams

In an important series of tests used to calibrate the benchmark 1963 ACI code, research[46] was carried out on beams without transverse reinforcement but with a large amount of flexural reinforcement against different concrete strengths. Data like this was the basis of the code expression of $2\sqrt{f'_c}$ (psi units) for the V_c term in the code as mentioned above. The graph shows that Response-2000 is able to predict this type of behaviour well.

For simplicity, the authors of the ACI code chose to select a lower limit on the then existing test data and use this to specify a safe level of loading for a structure. In the figure, the ACI code is seen to be conservative for these tests.

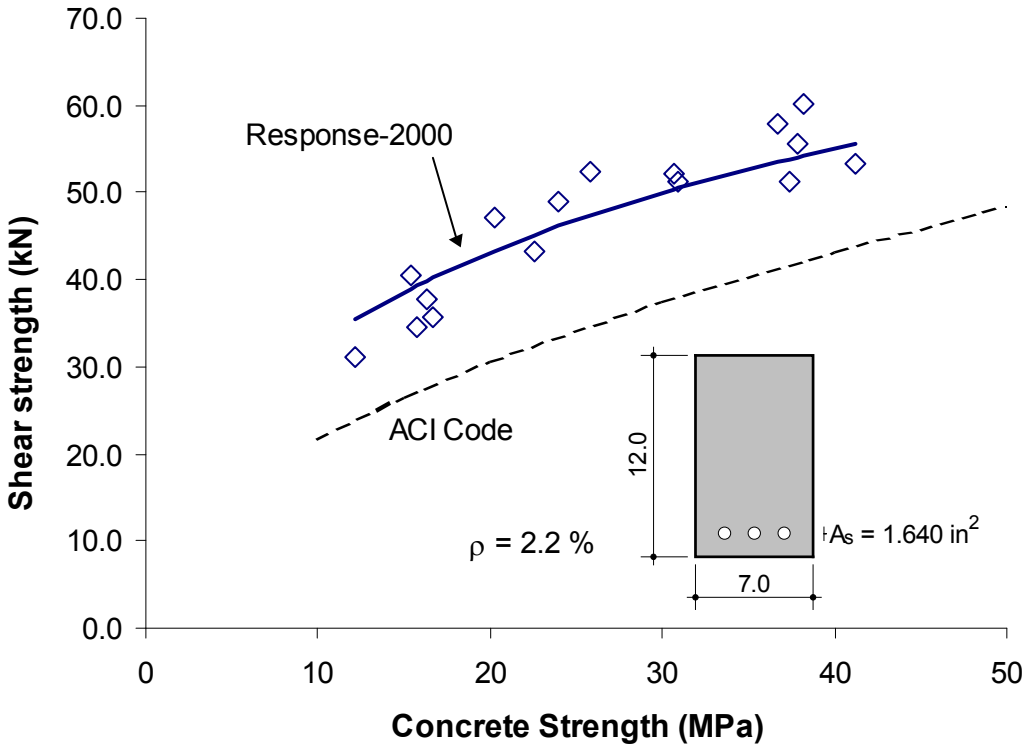

Figure 10 - 7: Effect of concrete strength on small heavily reinforced beams

10-7 Angelakos: Concrete strength: large lightly reinforced beams

Angelakos[40] recently completed an experimental project at the University of Toronto that studied the variation in shear strengths of large lightly reinforced concrete beams made with different strengths of concrete. Like the small, heavily reinforced beams in Fig. 10-9, these beams had no transverse reinforcement. The small beam tests would suggest that the ACI code shear strength equation should be conservative for the beams up to at least 50 MPa.

The test results for the large lightly reinforced beams are shown in Fig.10-10. It was found that the ACI code for these members is unconservative over the entire range of concrete strengths. The beam with the highest concrete strength failed at a shear less than half the predicted capacity of the ACI code. Response-2000 can be seen to do a better job of predicting these strengths, though it too becomes rather unconservative for the higher concrete strengths. Further research is required to explain this discrepancy, with work of Gupta[80] looking promising.

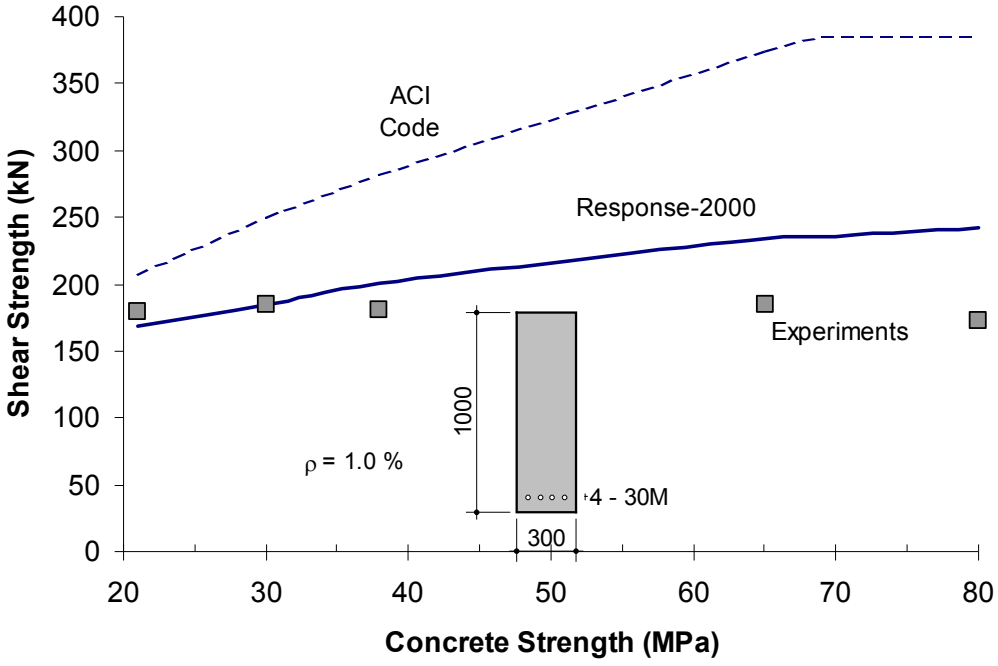

Figure 10 - 8: Effect of concrete strength on large beams without stirrups

10-8 Adebar & Collins: Effect of axial tension

For members without stirrups, the ACI code suggests that the shear strength is very sensitive to axial tension, reducing to zero for an axial tensile stress of 500 psi. Figure 9-10 compares the ACI and Response-2000 predictions with the experimental results reported by Adebar and Collins[56]. It can be seen that the ACI predictions are very conservative for members with high tensions.

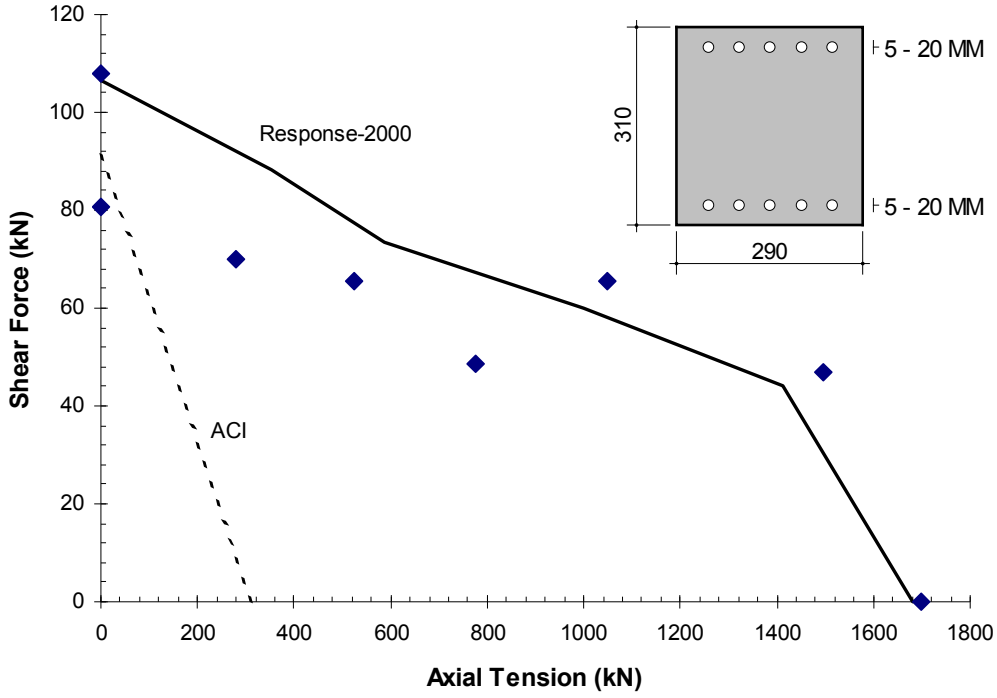

Figure 10 - 9: Effect of axial tension

10-9 Khalifa: Transverse Reinforcement on round columns

The examples presented so far were from rectangular beams or box beams. Khalifa[47] tested round columns with a small axial compression in a specially designed testing frame. The primary variable of the study was the level of transverse reinforcement. It can be seen that the increase in shear strength from increasing transverse reinforcement is predicted accurately.

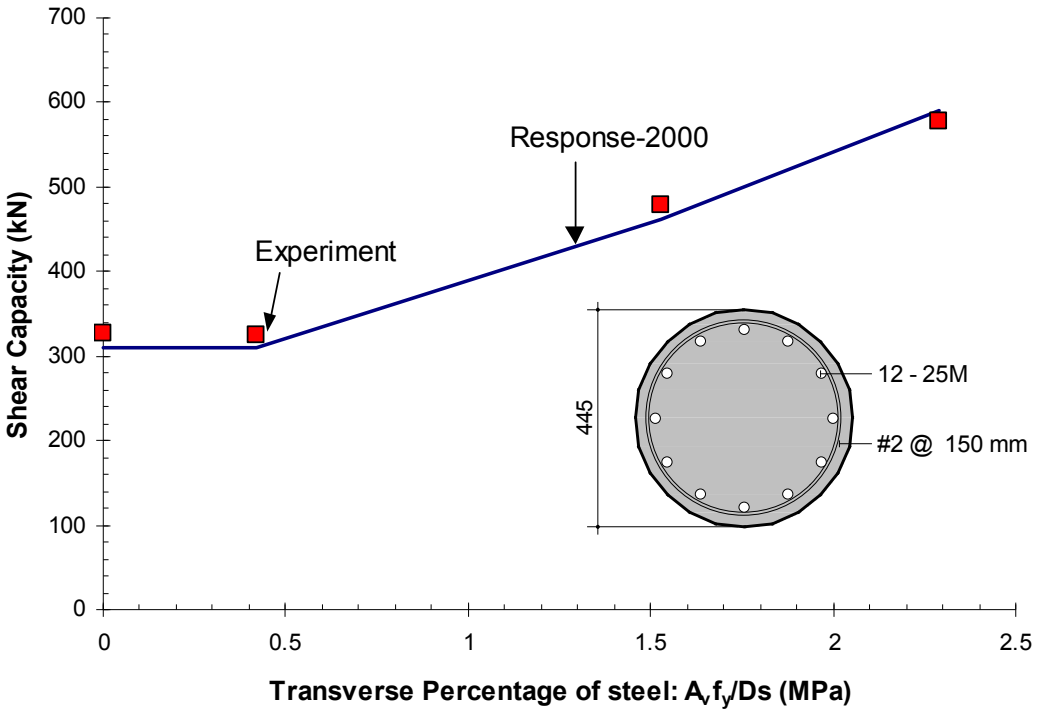

Figure 10 - 10: Effect of transverse reinforcement

10-10 MacGregor: Draped reinforcement in prestressed beams

MacGregor's[48] doctoral work reported the testing of 87 prestressed beams with about half failing in flexure, and half in shear. These beams are important as they formed the basis of the web-shear cracking/flexure shear cracking provisions currently in the ACI code for the shear strength of prestressed concrete beams. In 22 of these beams, the prestressing strands were angled or draped for the outer third of the beam length on each end. Figure 10-13 shows the predictions of Response-2000 compared to the angle of drape. It can be seen that the program is successful in dealing with draped strands in prestressed I-Beams. The results for these small beams show a fair scatter, however.

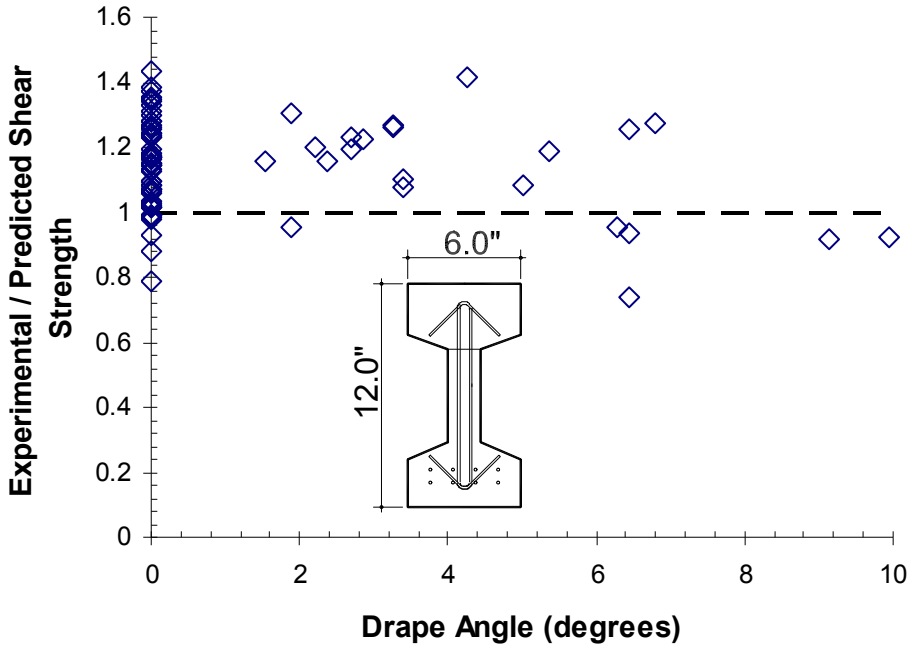

Figure 10 - 11: MacGregor - Drape of Reinforcement

Figure 10-14 shows the quality of the predictions of Response-2000 versus the percentage of transverse reinforcement for the tests reported by MacGregor. It can be seen that the predictions are good, but for low levels of transverse steel, Response-2000 becomes more conservative. Recall that in Chapter 1 it was shown that prestressed concrete beams may be more conservative than reinforced concrete beams due to the

presence of transverse compression in the web of the beams. This is a possible explanation for the somewhat conservative nature of the predictions made for these tests.

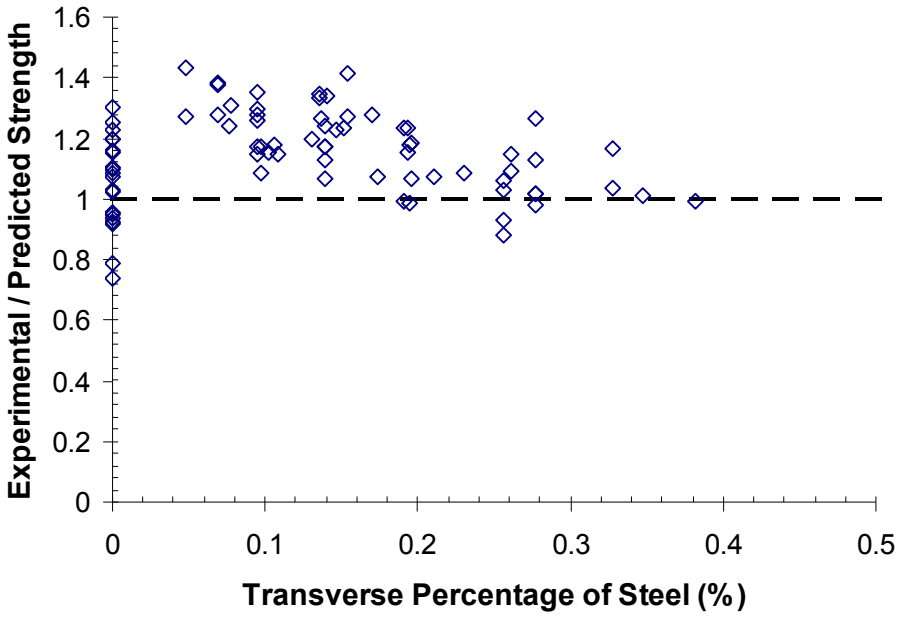

Figure 10 - 12: Macgregor, effect of transverse reinforcement

10-11 Benzoni, Priestley and Seible: Interlocking spiral column

A relatively new type of bridge pier used in California involves the use of two interlocking spiral hoops as shown below. This reinforcement configuration provides efficient confinement for a column with a "rectangular" section. However, calculating the shear strength of such a column from, say, the ACI shear equations is not a straightforward task. To answer some of the questions about the shear behaviour of these columns, Benzoni, Priestley and Seible conducted tests in 1995 at the University of California, San Diego[49]. The results from one of these tests, Inter-4, are shown here.

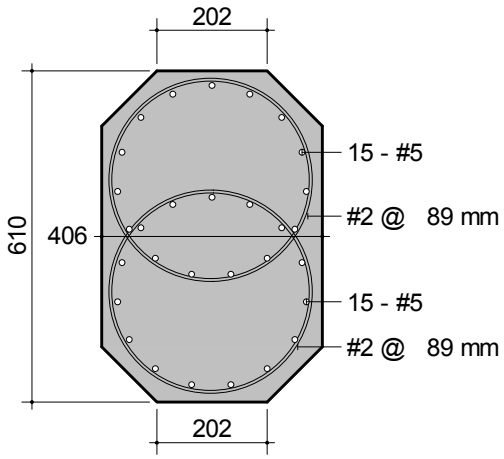

The cyclic loading for this column was as shown below left. Note that the axial load in the column was different for the push and

Loading Configuration

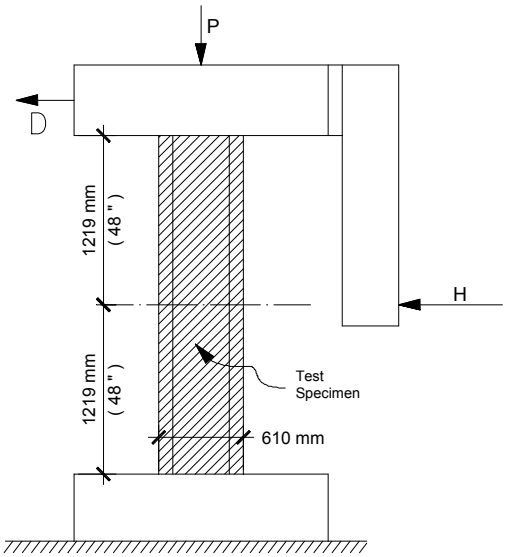

Vertical Load P:
P= 994 + 2.45 H (kN) when H pushes
P= 994 - 4.33 H (kN) when H pulls

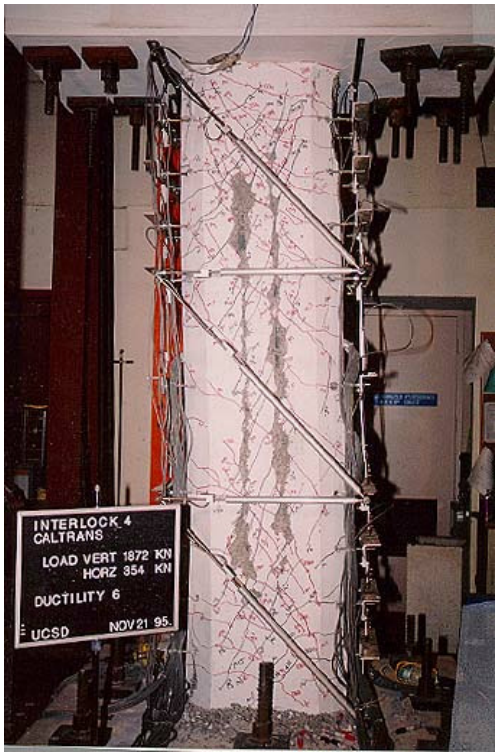

pull cycle in the loading. A photo of the beam at failure is also shown above. It can be seen that the failure involved longitudinal crushing bands with no evidence of flexural failure.

An analysis was carried out a distance d_v from the bottom of the column with Response-2000 including the effect of shear. The results of this are shown here:

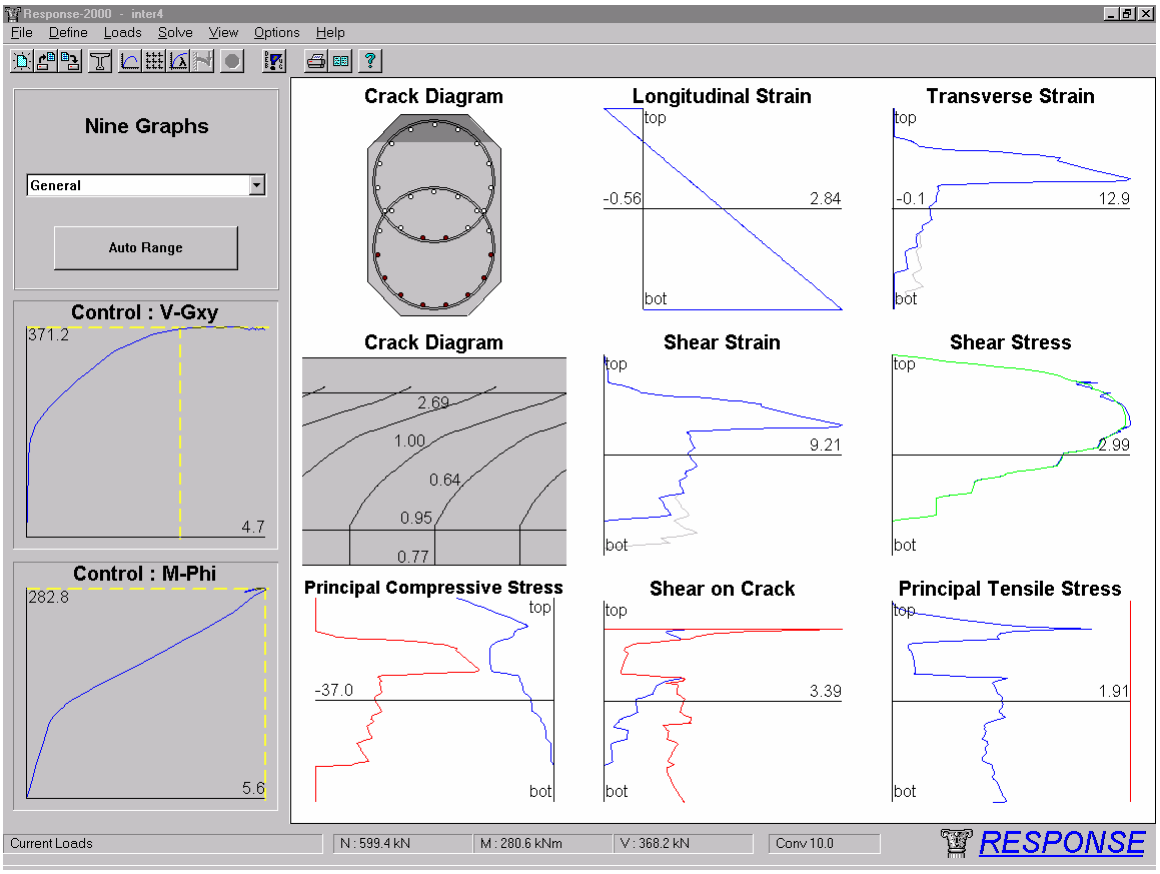

Observe the predicted cause of failure from the Response-2000 analysis: local crushing of the web and high shear strains and high transverse strains just above the location where the lower hoop ends. That is, about 75 mm up from the mid-height of the section. In the bottom left of the 9 plots, the maximum allowable compression is approaching the applied stress. At higher deformations, the concrete crushes and the load reduces. While there is longitudinal yielding, there is still plenty of flexural capacity in the non-yielding bars. This local crushing of the web is symptomatic of a longitudinal shear failure. It can be seen in the photo of the failed specimen that the concrete failed by

crushing at about the same place as predicted by the analysis, over a substantial height of the column.

The failure shear from the analysis is predicted to be 371 kN for the case of the horizontal load, H, pulling. An analysis for flexure indicates that flexural failure at the ends is less critical than a shear failure at a distance of d_v from the ends. As such, the column is predicted to fail in shear at a load of 371 kN vs. the observed failure of 379 kN.

If a Response-2000 full member response is performed, the crack pattern on the right is produced at the predicted failure. Figure 10-15 shows the predicted load deflection plot superimposed on the experimental hysteresis loops. The variable axial load meant that the capacity of the column in the "push" direction was stronger than in the "pull"direction. Despite the complex geometry and unusual loading, Response-2000 was able to provide a reasonable estimate of strength, displacements and failure mode.

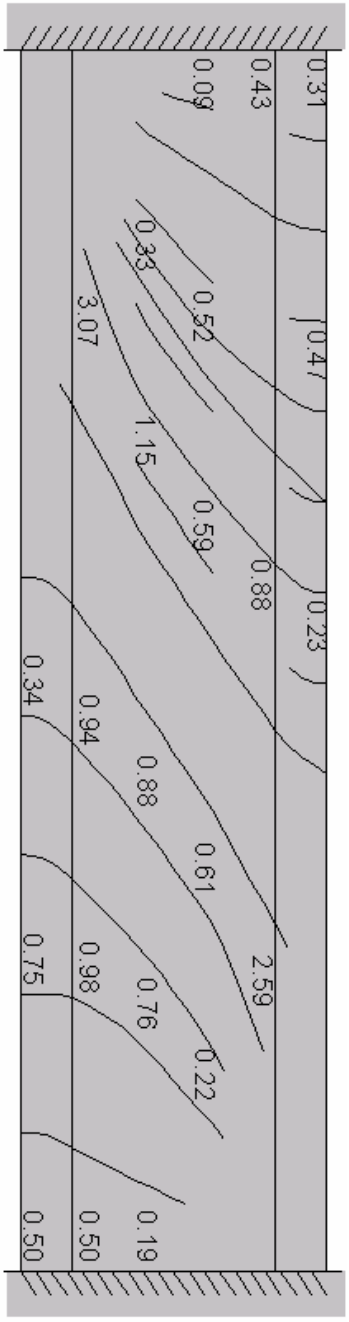

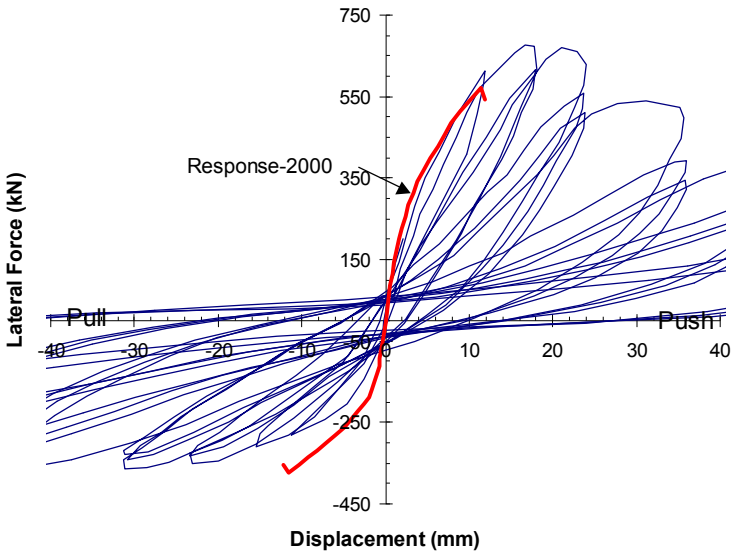

Figure 10 - 13: Inter4 predicted load deflection

10-12 Comparison to 534 Beams

The previous pages demonstrated the quality of predictions of Response-2000 against individual test series. The following pages demonstrate the quality of the predictions against a database of 534 beams. This database includes rectangular beams and columns, round columns, prestressed sections and I beams. Table 10-1 summarises the tests and Appendix C lists all the data. The performance of Response-2000 is shown below compared to different variables from this database.

10-12-1 Shear span to depth ratio (a/d ratio)

This ratio is a commonly used indicator of potential shear problems with Kani warning that the "valley of shear failure" typically occurs for a/d values between about 2 and 5. The data in the verification database had a/d ratios falling between 2 and 8. The larger values had higher longitudinal percentages of steel to ensure shear failures. Results for beams with an a/d less than 2.0 (i.e. deep beams) will generally be very conservative due to direct strut action from the load point to the support. They have not been included in the database.

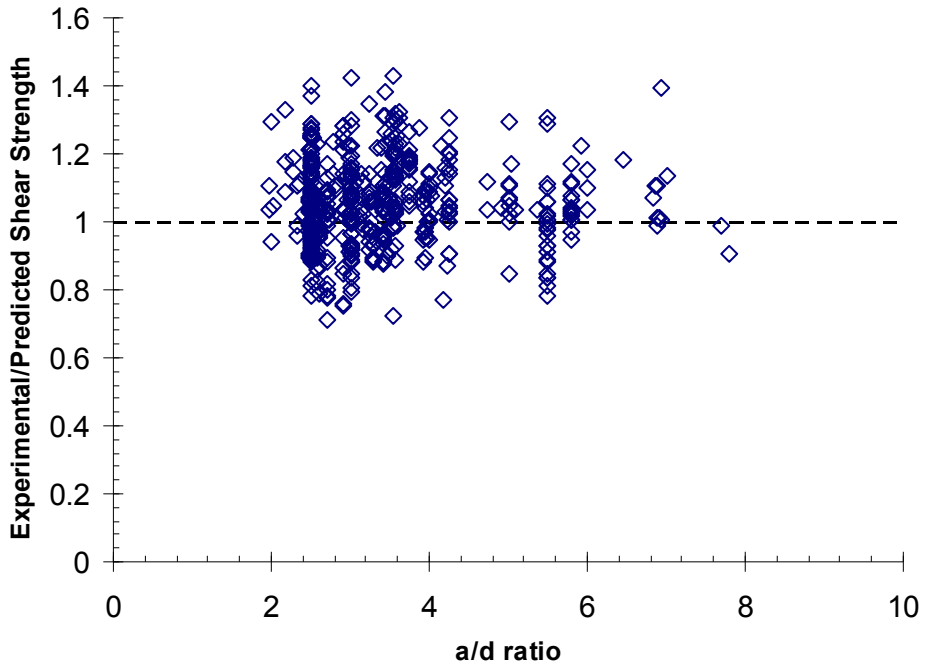

Figure 10 - 14: a/d ratio

10-12-2 Beam depth

Figure 10-17 shows the results compared to the depth of the beam. It can be seen that the size effect in shear is successfully accounted for.

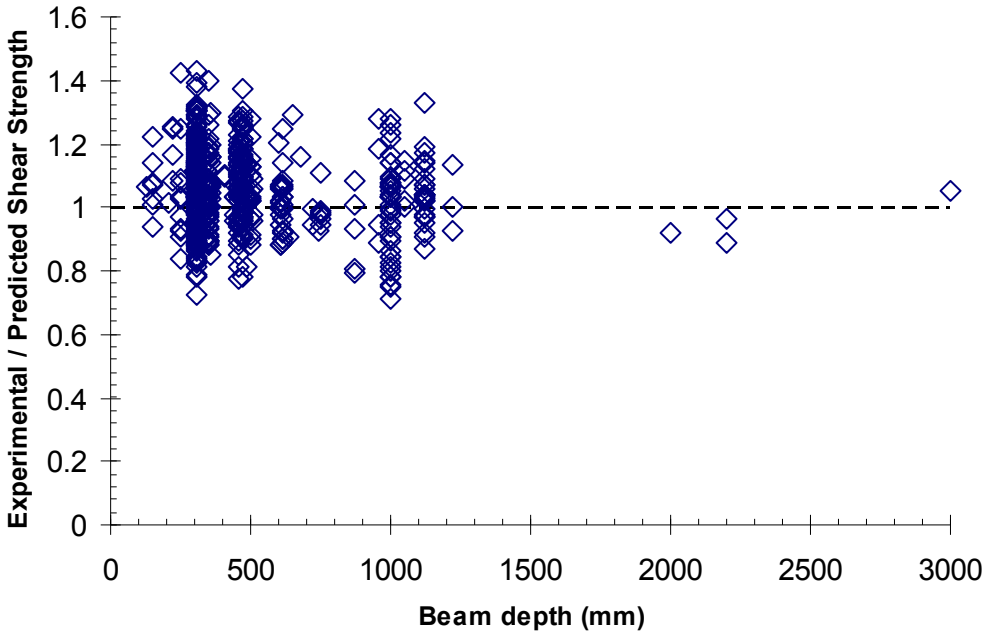

Figure 10 - 15: Beam depth

Page to put the table from excel on!

10-12-3 Concrete strength

Concern has been expressed about the accuracy of code equations for the shear strength of members made from very high strength concrete. Figure 10-18 shows that Response-2000 is able to account for concrete strengths well.

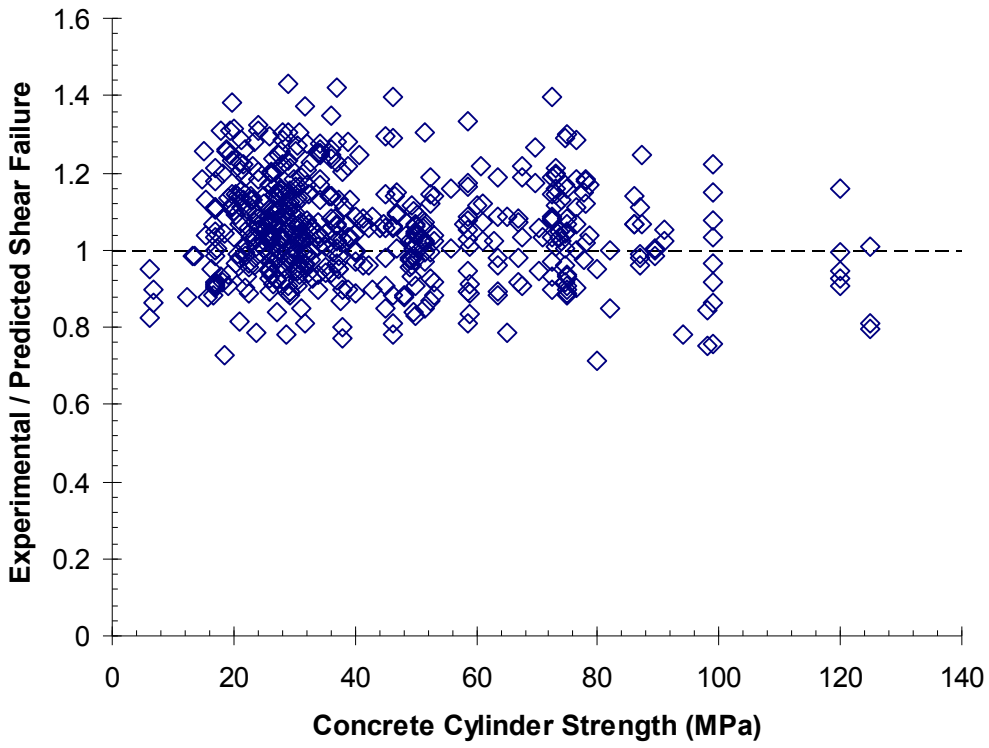

Figure 10 - 16: Concrete strength

10-12-4 Longitudinal percentage of reinforcement

Beams with a lower percentage of longitudinal reinforcement have been observed to fail at lower shear strengths. Figure 10-19 shows that Response-2000 is able to predict such behaviour well.

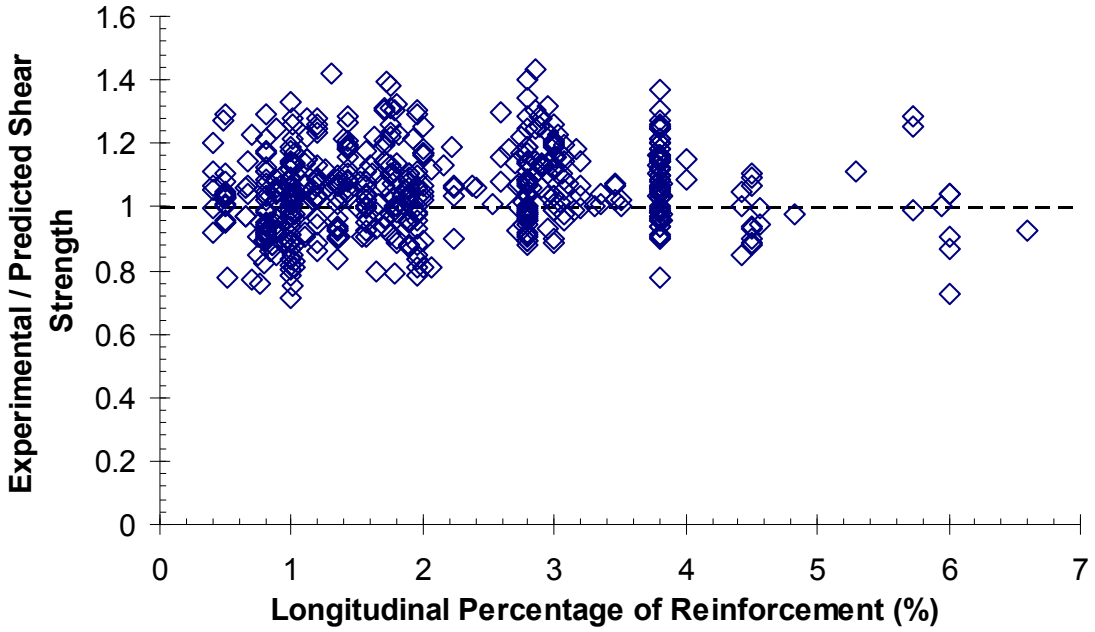

Figure 10 - 17: Longitudinal Percentage of Reinforcement

10-12-5 Transverse percentage of reinforcement

Figure 10-20 shows the ability of Response-2000 to predict shear failures as a function of how much transverse steel is provided.

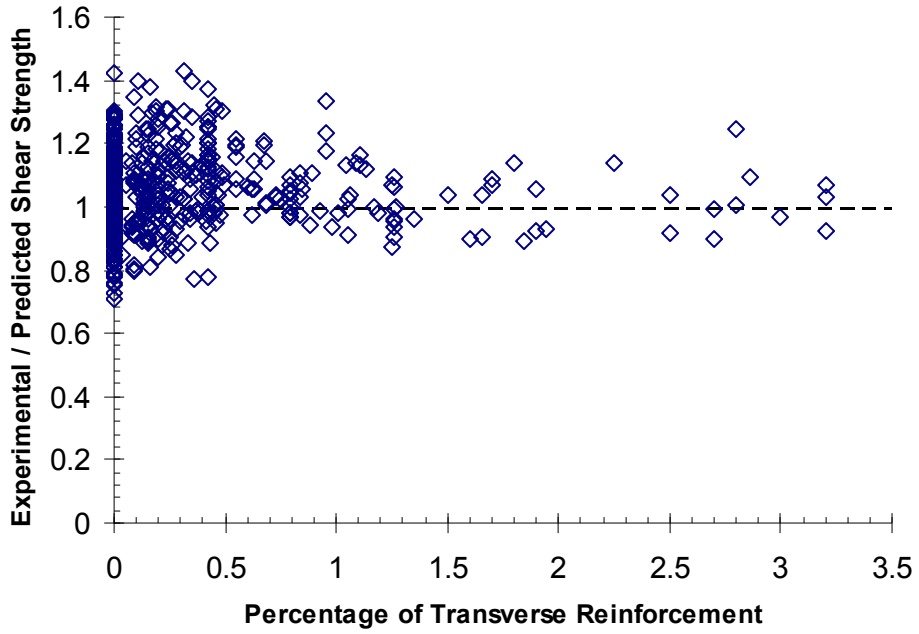

Figure 10 - 18: Transverse percentage of reinforcement

10-12-6 Shear strength

Figure 10-21 shows that Response-2000 is not biased towards stronger or weaker specimens. Note that the horizontal axis in this case is logarithmic.

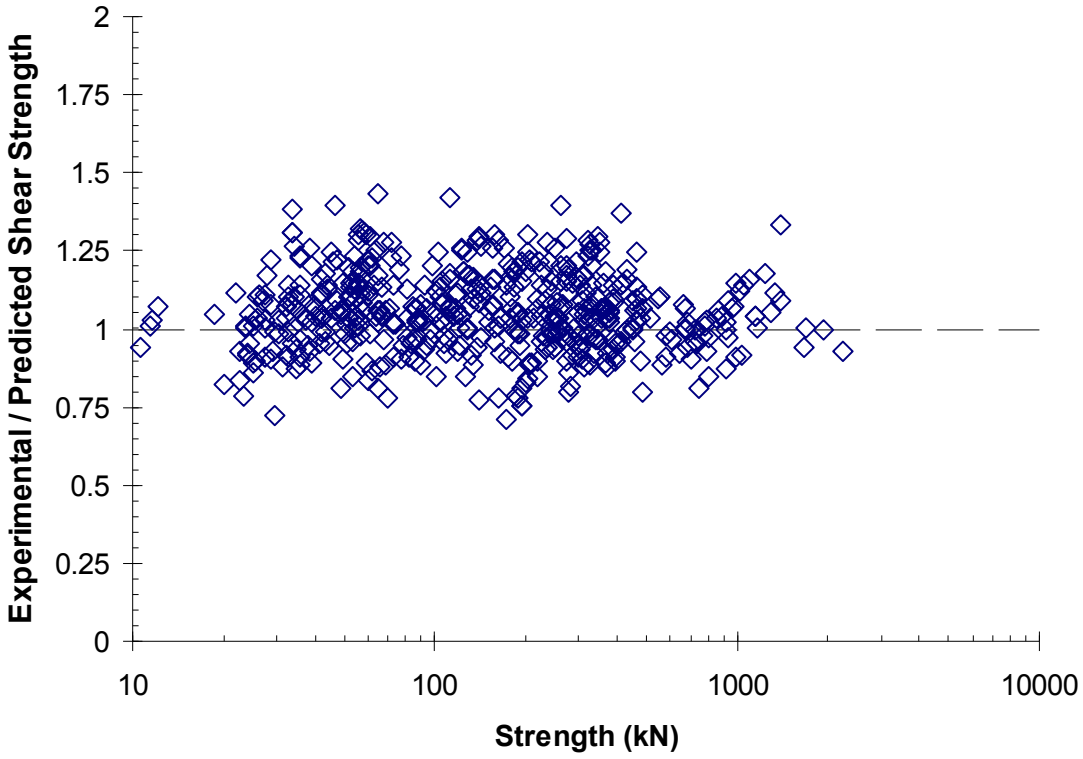

Figure 10 - 19: Shear strength

10-12-7 Overall Predictions

Figure 10-22 shows the entire dataset compared as experimental shear vs. predicted shear capacities. The average experimental over predicted shear strength for the data set is 1.05 with a coefficient of variation of 12.0%. Figure 10-23 shows the predictions of the ACI code in a similar format. The ACI code equations yield an average of 1.20 with a coefficient of variation of 32.1%. Note that while there is a significant scatter to the ACI predictions, the predictions are all conservative for failure shears less than 70 kN (15 kips). This is the general range of failure shear strengths for small tests such as those shown in Fig. 10-9. It would appear that the extrapolation of these results to larger, and hence stronger beams, is not well modelled by the code.

While Response-2000 compares very well to the code provisions for predicting strength, it is important to realise that the results from Reponse-2000 have an important difference over most code methods. The ACI provisions, for example, were based on a curve fit to a large data set. As such, it should be expected that such a method would do well at predicting shear strengths. For Response-2000, on the other hand, the majority of the constitutive methods are based on a totally different kind of experiment, the shear panel experiment. While it may be assumed that these panel tests would be directly applicable to beams, indeed that is why the shear tests were done in the first place, it is satisfying to see that they are.

Figure 10-24 shows a histogram of the predictions of Response-2000, with Figure 10-25 showing the similar figure for the ACI code.

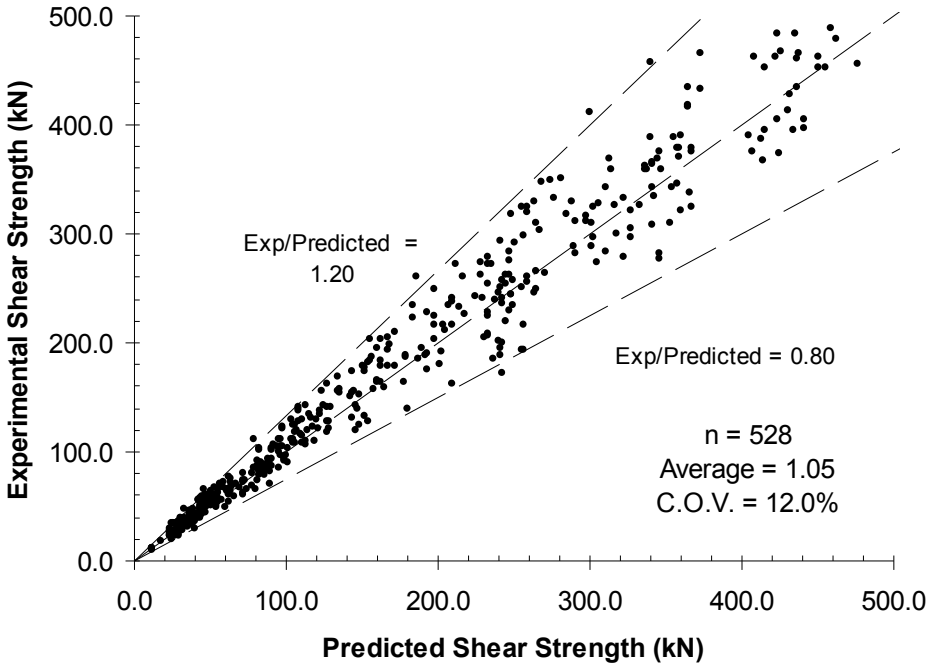

Figure 10 - 22: Response-2000 experimental and predicted shear strength

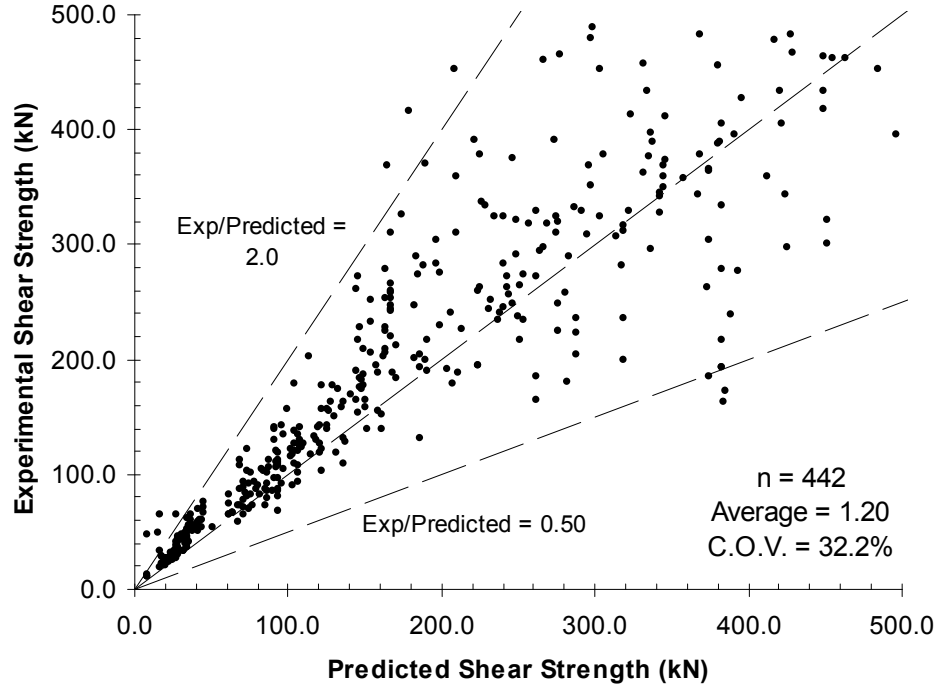

Figure 10 - 23: ACI experimental and predicted shear strength

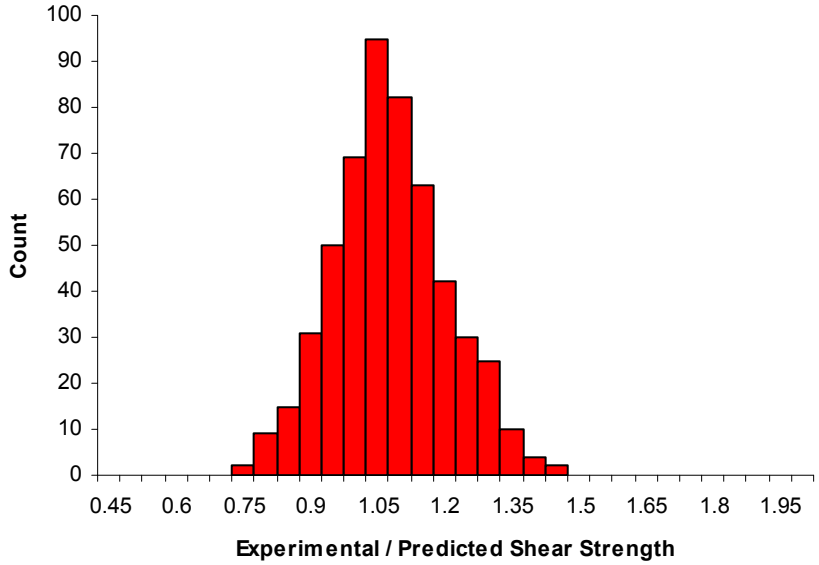

Figure 10 - 20: Response-2000 experimental/predicted ratio

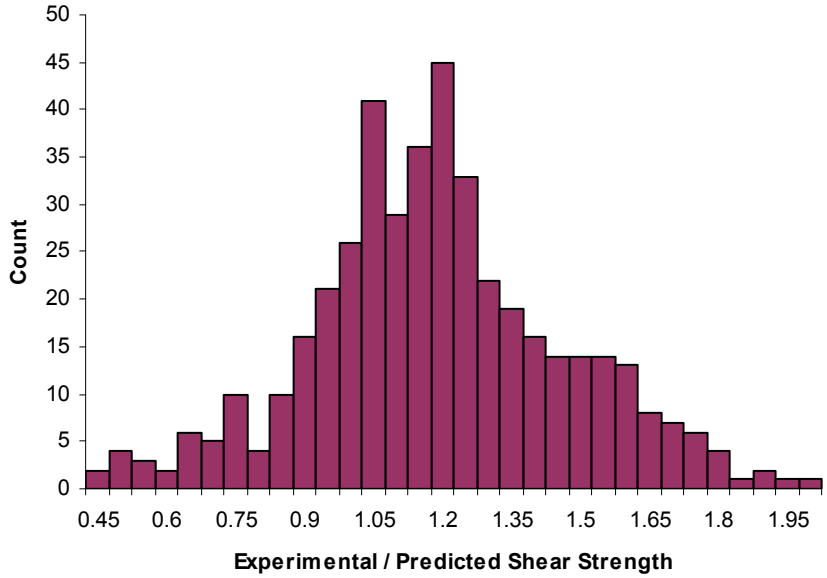

Figure 10 - 21: ACI experimental/predicted shear strength

Chapter 11: Experimental Verification of Shell-2000

Shell-2000 will calculate load-deformation relationships and strengths for plates and shells. In a sense it is a superset of Response-2000 for beams and Membrane-2000 for membranes. The program will be compared to these other programs as well as experimental evidence.

11-1 In-Plane Membrane Forces

Figure 11-1 compares the predictions of Shell-2000 and Membrane-2000 for shell element SE6 tested by Kirschner[12]. It can be seen that both programs give similar predictions, with Shell-2000 predicting a higher peak. This is due to this element being controlled by the crack check against shear on the crack. Crack spacing is calculated throughout the depth in Shell-2000 and only at the most critical depth for Membrane-2000. As such, Shell-2000 predicts a smaller average crack widths and, hence, a stronger response. Both predictions are good.

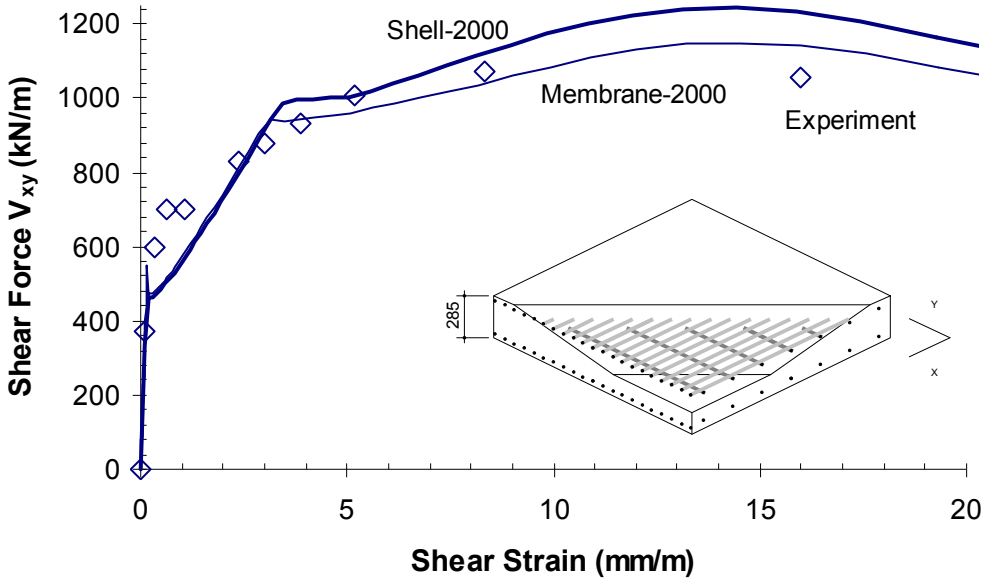

Figure 11 - 1: SE6 In plane shear strength

Kirschner also tested a series of similar panels to produce an interaction diagram of in-plane shear stress and flexure. Each element had 2.92 % total reinforcement in the X direction and 0.98 % in the Y direction, 40 MPa concrete and was 285 mm thick. Figure 11-2 shows the predictions of Shell-2000 compared to these tests. Note the inclusion of the pure shear strength predicted by Membrane-2000 as well as the prediction from Response-2000 prediction of the pure flexural strength. It can be seen that the predictions including strain hardening are good, but the predictions ignoring strain hardening are rather conservative for the cases with higher moment. A Response-2000 analysis with no strain hardening shows the same patterns as Shell-2000 does.

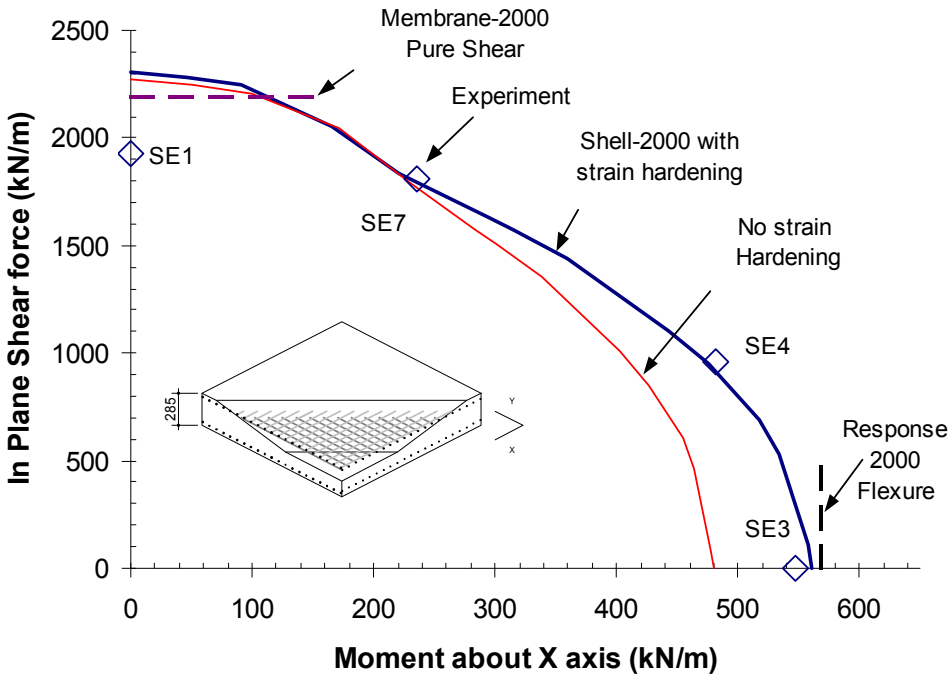

Figure 11 - 2: M-V_{xy} interaction diagram

For a more detailed look at one of these elements, the load deformation of element SE4 is compared to the predictions of Shell-2000 in figures 11-4 to 11-9. This element was loaded with 500 kNm/m of moment for every 1000 kN/m of in-plane shear. The pre-yield predictions are good, but Shell-2000 is underestimating the stiffness after

yield. Note in Figure 11-8 that Shell-2000 is predicting significant y direction curvature, but the tests measured virtually none. This and the over-prediction of twisting may be related.

Figure 11-4: SE4 V_{xy} - ε_x

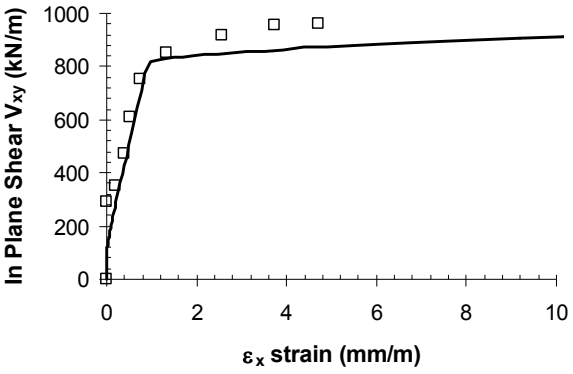

Figure 11-5: SE4 V_{xy} - ε_y

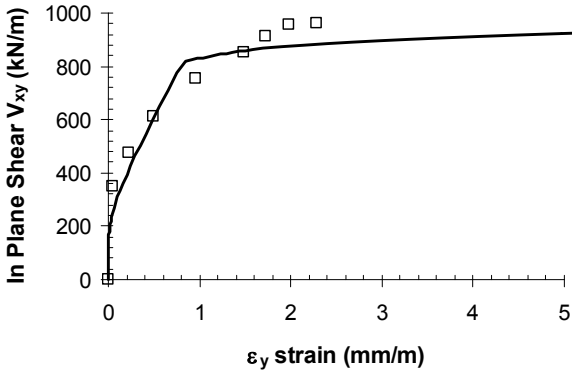

Figure 11-6: SE4 V_{xy} - γ_{xy}

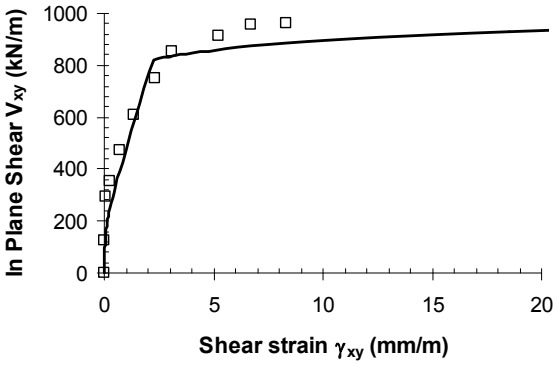

Figure 11-7: SE4 V_{xy} - ϕ_x

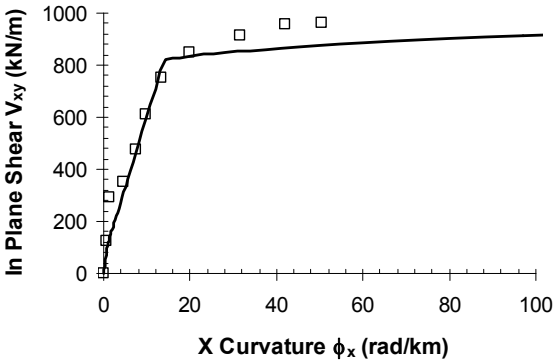

Figure 11-8: SE4 V_{xy} - ϕ_y

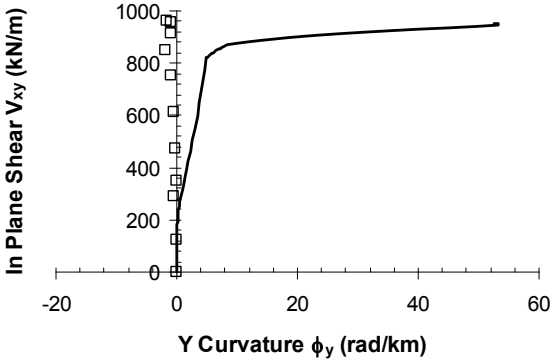

Figure 11-9: SE4 V_{xy} - ϕ_{xy}

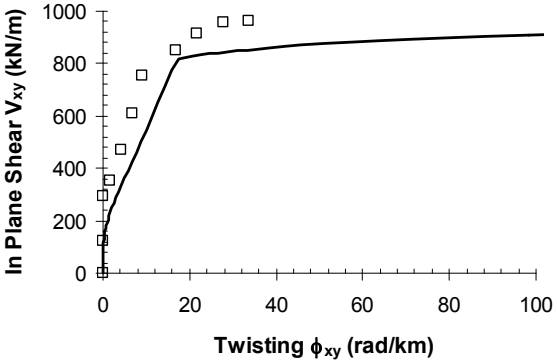

11-2 Out-of-Plane Shear

One of the advantages of Shell-2000 over earlier programs such as Shell-474[7] is that it explicitly deals with the out-of-plane shear stress distribution on the X and Y faces. Adebar tested a series of full size shell elements subjected to in-plane shear and out of plane shear[23]. These elements had 3.5% of reinforcement in both the X and Y directions and 0.08% of "stirrup" reinforcement in the Z direction. The results of these elements are shown in Figure 11-10 in the form of an interaction diagram. Figure 11-10 shows the

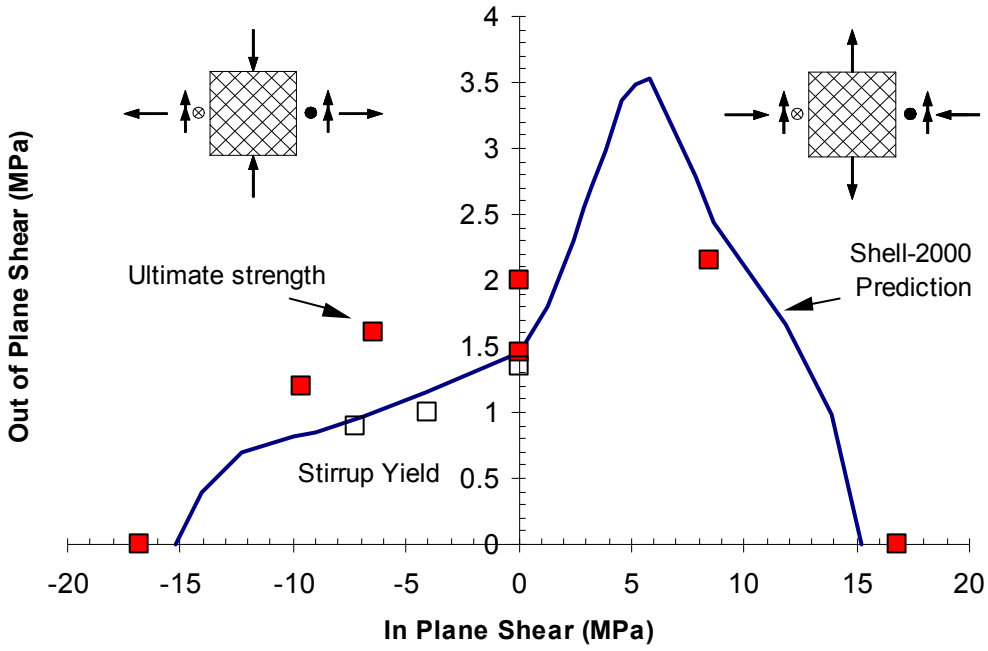

Figure 11-10 Adebar out of Plane Shear

predicted and measured effect of in-plane shear on the out of plane shear strength. Note that on the right side of the figure, the in-plane shear adds compression in the direction of the out-of-plane shear, increasing the strength beyond that of the zero in-plane shear case. The reverse is true for the left side of the diagram. The solid squares in the figure are the maximum loads resisted, but some of the elements were noted to have been restrained by the testing apparatus, partly explaining the degree of conservatism on the left side. For comparison, the out of plane shear stress at first yield of the stirrups is also shown.

As a final comparison of the out of plane shear abilities of Shell-2000, the predictions of Shell-2000 will be compared to Response-2000. A shell of reinforced concrete identical in the X and Y directions, similar to that tested above by Adebar, was entered into Shell-2000. A Response-2000 input file was made of the X direction of the shell element as well. Moment-shear interaction diagrams were then made with Shell-2000 of the shell element tested with moment and shear on the X face. Response-2000 was also used to calculate such an interaction diagram. Finally, an analysis was made of the shell element tested with the moment and shear applied at 45° to the reinforcement. As this element is isotropically reinforced, it may be expected that there would be no difference between these three results.

Figure 11-11 shows the result of these calculations. As the Response-2000 and X direction Shell-2000 analysis were modelling the same thing, it is satisfying that the same curves are produced from the two programs. Of more interest is that the analysis done on the element at 45° did not produce the same curve. The flexural strengths matched well, but the predicted shear strength is about 85 percent of the value predicted for the direct loading. This appears to be caused by the 45° case having to carry the shear over wider cracks. The failure of this element was controlled by shear on the crack.

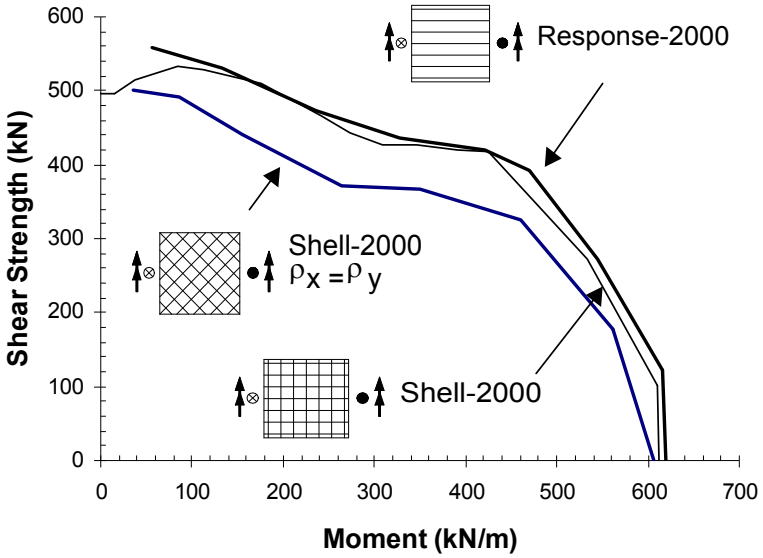

Figure 11-11 M-V interaction diagram

Chapter 12: Analysis guidelines and examples

This chapter provides guidelines on how to use the program Response-2000 to predict the behaviour of beams and columns as well as some examples.

12-1 Performing an analysis for beams with Response-2000

The key to performing analyses with a sectional analysis program is knowing at which section to perform the analysis. While it may seem a good idea to do the shear analysis for the location where there is maximum coincident shear and moment, this is generally not the best location at which to perform the analysis.

12-1-1 Point load on prismatic reinforced concrete beam on simple supports

This is perhaps the simplest experimental test on a beam that can be done. This problem is shown in Fig. 12-1. Assuming that there is no axial load, there are two ways for this beam to fail and therefore two calculations must be done to predict the failure strength. First the moment may become too large at midspan causing a flexural failure, and second the shear may exceed the shear capacity causing a shear failure.

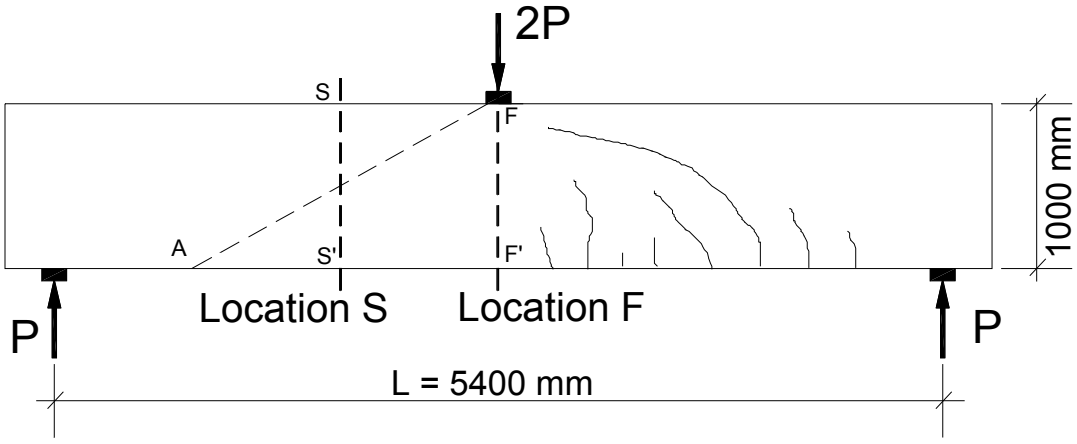

Figure 12-1 Sample Beam

To consider both these failure mechanisms, two Response-2000 analyses are required. The first, for flexure, is performed at location F in the drawing and is done ignoring the effects of shear. The second analysis, for shear, is performed at location S, a

distance approximately "d" away from the midspan. Whichever of these analyses corresponds to the lower strength of the beam, i.e. the lowest value of P in the figure, controls the failure and is the predicted failure mode.

It is recommended that the flexural analysis be performed without shear. This may seem to be inappropriate, as at the edge of the bearing plate for a test like this, the shear diagram indicates the full value of shear being present. It might seem wise to do the analysis at the maximum moment location with shear applied as well. This is a conservative assumption, but is not necessary. Directly under the load, the shear is not yet carried in a "sectional mode". That is, there will be significant transverse clamping near the load that will increase the effective local shear strength in this region. This non-sectional support mechanism means that shear can safely be ignored in the analysis for flexure in a case like this.

At the location used to check for shear failures, section S, it is important to include the correct values of the moment to shear ratio. A generally suggested distance from the load to the location S (distance SF or S'F' in the figure) is $0.5\ d_v \cot\theta$, where d_v is the flexural lever arm. In general the angle θ is not known until the analysis is completed and will vary over the depth of the beam, however. It is therefore suggested to assume that θ is about 30° for the sake of determining this distance. A line drawn at that angle is shown on the figure above as line A-F. This line crosses the mid-depth of the beam at a distance of about d_v from the edge of the bearing plate. Note that the line A-F is a reasonable choice largely as it is similar to the expected crack pattern as shown symmetrically on the right side. If the crack pattern was expected to be at an unusual angle, say due to high axial load, then the distance d_v may not be appropriate. Often details about the loading plate is not known so for most analyses it is recommended that the shear analysis be performed a distance d from the centre of the point load.

For the given example, then, the first analysis would be performed with an incremental M=1.0 and V=0 in the Response-2000 loads dialog box. That moment capacity would then generally be converted to an equivalent shear necessary to cause the

moment. Then an analysis with shear would be performed with M=1.8 kNm, V=1.0 kN if the value of d for this beam was 900 mm. Note that these ratios are unit dependent and would be M=5.91 ft.kips, V=1.0 kip in US units.

Note that while the shear failure is calculated to happen at location S, it will in fact happen with the opening of diagonal cracks as shown on the right of Fig.12-1. A consequence of this is that if there are stirrups that vary in spacing along the length of the beam, it is appropriate to calculate the average amount of stirrups within a band of length d in the beam centred on location S. For the beam above, the appropriate amount of stirrups to add to the Response-2000 file would be the average level of stirrups within a band stretching from 1.35 metres to 2.25 metres from the left support. Similarly, if the stirrup spacing is very high, say greater than 0.75 d, it may be necessary to assume a reduced effectiveness for the stirrups.

Consider also what would happen if the distance from the load to the support was less than two times the effective depth of the member. In that case, the line AF would not fit into the shear span, suggesting that a normal shear crack would also not fit. In cases like this, Response-2000 will be very conservative, as the behaviour will be that of a deep beam rather than that of a long beam. Chapter 7 explains how the use of the load-deflection option gives a simple way to account for this in Response-2000.

12-1-2 Analysis of large prestressed concrete girders with uniform load

Analysis of beams subjected to uniform loads, such as large prestressed concrete bridge girders under dead loads and lane loads, are analysed slightly differently than above. For such cases it isn't known a priori which location will be the most critical for shear. In such cases, an analysis will need to be made at many points along the length of the beam, say at the tenth points. The most critical location would then define the failure load and load factor at failure. There are two ways to calculate this load factor, which can be thought of as a safety factor. One is to assume that the calculated moments along the beam are fixed and that the shear can increase. The other is to assume that the moment and shear both increase proportionally. Each will produce a different safety

factor. Which to use will depend on confidence in the applied loads. If the calculated moment is effectively the highest that might realistically be seen, the safety factor associated with constant moment would give some idea of how close one is to a brittle shear failure at the given load level. The safety factor associated with a proportional increase in both moment and shear gives the safety against failure from an increase in total loads.

With pretensioned beams, one also needs to be concerned about the bond of the strands at the end of the beam. This is an area currently being researched, but a tentative proposal has been developed for Response-2000. An analysis should be performed at a location d/2 from the end of the beam (which assumes slip of strands and steep cracks). The moment and shear at that location should come from the statics of the beam loading and be increased proportionally. The maximum stress in the strand can be estimated as the stress resulting from 750 psi (5 MPa) of bond stress on the strand circumference along the strand from the end of the beam up to the inside edge of the bearing plate. This stress should be induced in the strands with an appropriate prestrain, and the stress-strain curve of the strands should be modified to provide a maximum at this level of stress. While this suggested procedure needs further study, it does give results in good agreement for the tests as shown in Chapter 10.

12-1-3 Column pushover analyses

Some seismic design procedures suggest that non-linear analyses be performed on columns to evaluate their ductility. Such "pushover" analyses are not difficult to perform with the help of Response-2000. As an example of such an analysis, an analysis will be performed on the piers of the Hanshin Expressway, which failed so spectacularly in Japan during the 1995 Kobe earthquake, See Figure 1-2. The cross section of these columns was circular, 3.1 metres (10 feet) in diameter. Outside of a 2.5 metre section near the ground that had more longitudinal reinforcement, the cross section is summarised by Fig. 12-2. The bars listed with a prefix of JD, say "JD16", mean a Japanese standard bar 16 mm in diameter. The area near the bottom of the columns that contained more reinforcement is ignored in this simple analysis.

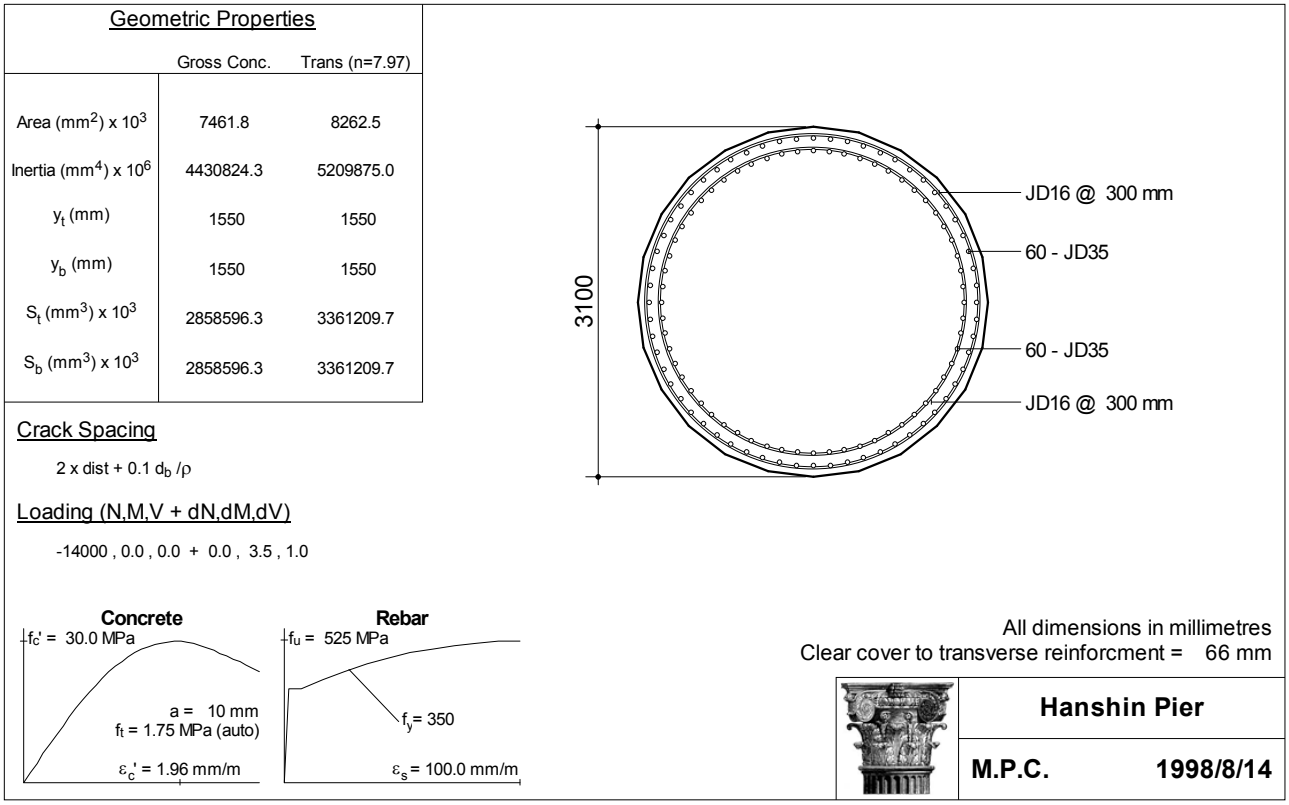

Figure 12-2 Hanshin Pier Response-2000 output

Using a simple dynamic analysis with a few assumptions, it was estimated that the 12 metre column would have an inflection point about 8 metres above from the ground. With this assumption and an assumed axial compression of 14,000 kN, Figure 12-3 was generated to represent the load-deflection pushover results for this column. The analysis took about one minute. Once calculated, effects of other assumptions of the location of

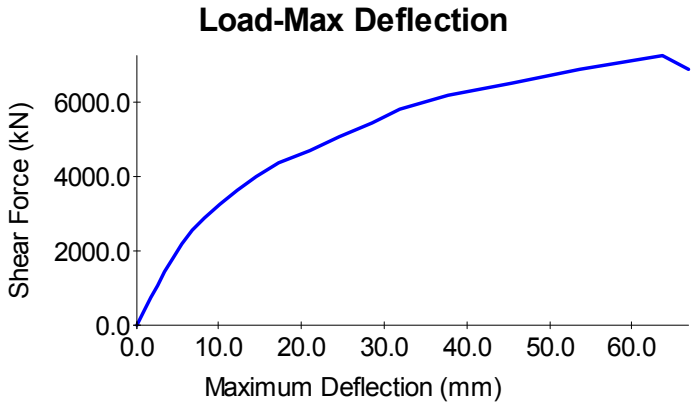

Figure 12-3: Load Deflection Curve, Hanshin Pier

the inflection point could be determined. While the load-deflection curve may look reasonably ductile, recall that the column is 12000 mm long, so a 60 mm deflection represents a drift ratio of only 0.5 %, which is certainly inadequate to survive a major earthquake.

The loading on the interaction diagram, shown in Fig. 12-4, touches the

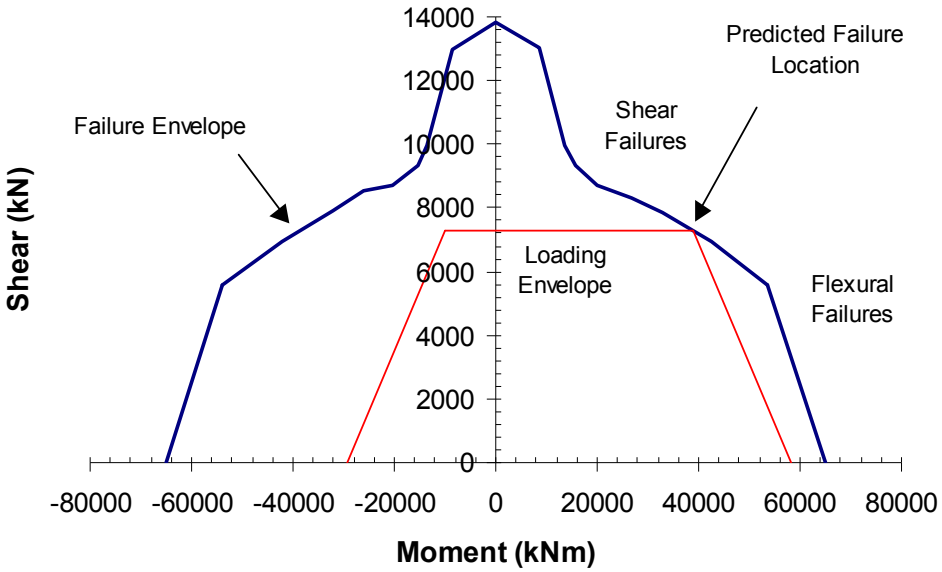

Figure 12-4: Interaction diagram for Hanshin Pier

failure envelope on the top indicating an undesirable shear failure. Note that this analysis ignored the extra longitudinal steel at the bottom of the column and hence the flexural capacity should in fact be higher. A column like this should be designed to fail in a ductile flexural mode rather than a brittle shear mode. While this extra steel near the bottom of the column would increase the flexural capacity, it would not affect the shear capacity significantly. As such, the extra steel in the very bottom of the column would have in fact made the column less safe rather than more.

Response-2000 can also predict the crack pattern for the column as shown in Fig. 12-5.

Figure 12-5: predicted cracks of Hanshin Pier

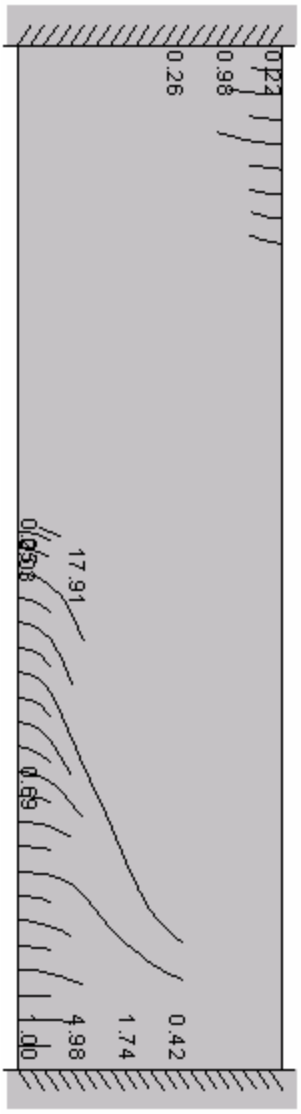

12-1-4 Predictions of size effect in shear

This thesis has included many examples that compare the predictions of Response-2000 to experimental tests. These last two examples compare the predictions of Response-2000 for members that would be difficult to test due to their size.

As noted in Chapter 10, structures have already been built that are up to 8 metres in depth, generally footings. While it would be very difficult to perform an experiment of that scale, Response-2000 has no difficulty predicting the behaviour of such members. The figure below shows the predicted shear strengths of large slab like structures subjected to uniformly distributed load. The vertical axis shows the predicted shear strength divided by the ACI code predicted shear strength as a percentage. It is predicted that slabs about 300 mm deep, such as the beams in Figure 10-9 of the last chapter, will be conservatively predicted, that is a percentage greater than 100. On the other hand, slabs 4 metres thick with, say, 0.5% of longitudinal reinforcement, are predicted to fail in shear at a shear stress less than 50% of the ACI code strength.

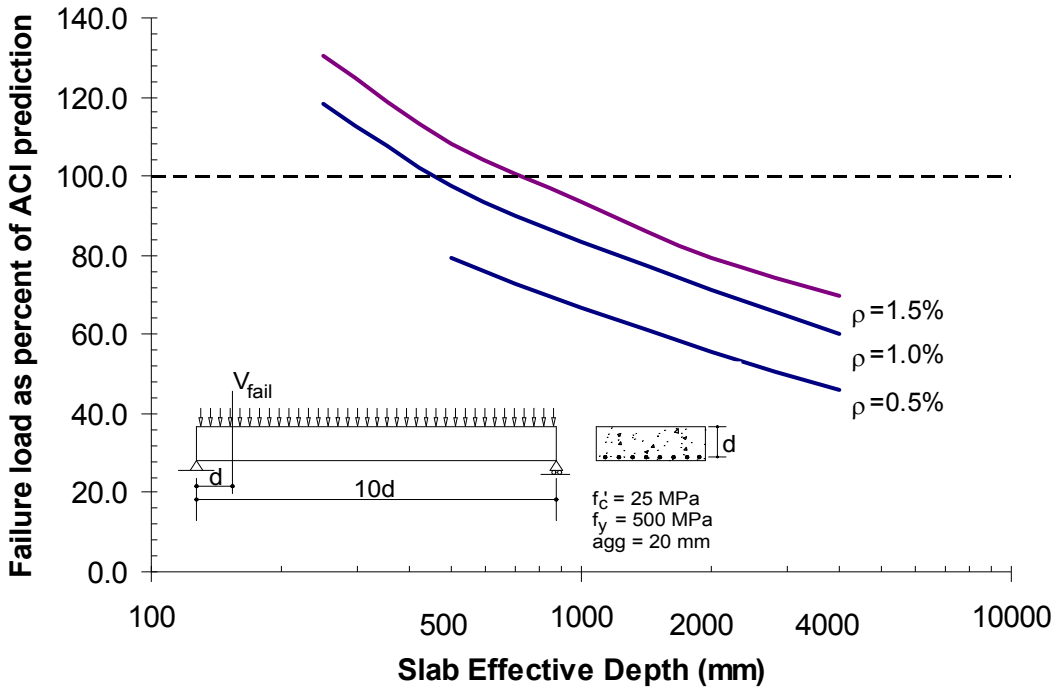

Figure 12-6 Predicted Size effect in shear for slabs

The next figure shows, for a similar slab with 0.5% of flexural reinforcement, and a total length of 6d, the predicted effect of adding the ACI code minimum value of stirrups, 0.35 MPa (50 psi). It can be seen that the predicted effect of adding this steel is dramatic. Response-2000 predicts that the addition of this light amount of reinforcement will mitigate the size effect and return the shear strength to something fairly close to that suggested by the ACI code expressions.

Note that the predicted strength of the slab without stirrups can be considered as V_c in the traditional expression that $V = V_c + V_s$. While the ACI code assumes that the value of these, in stress terms, does not vary with the depth of the member, Response-2000 can be seen to be predicting that V_c, the concrete contribution, decreases with increasing member depth, while V_s, the steel contribution increases as the members get larger. As such, Response-2000 predicts that the addition of this small amount of transverse reinforcement to a large slab can increase its strength by as much as a factor of four.

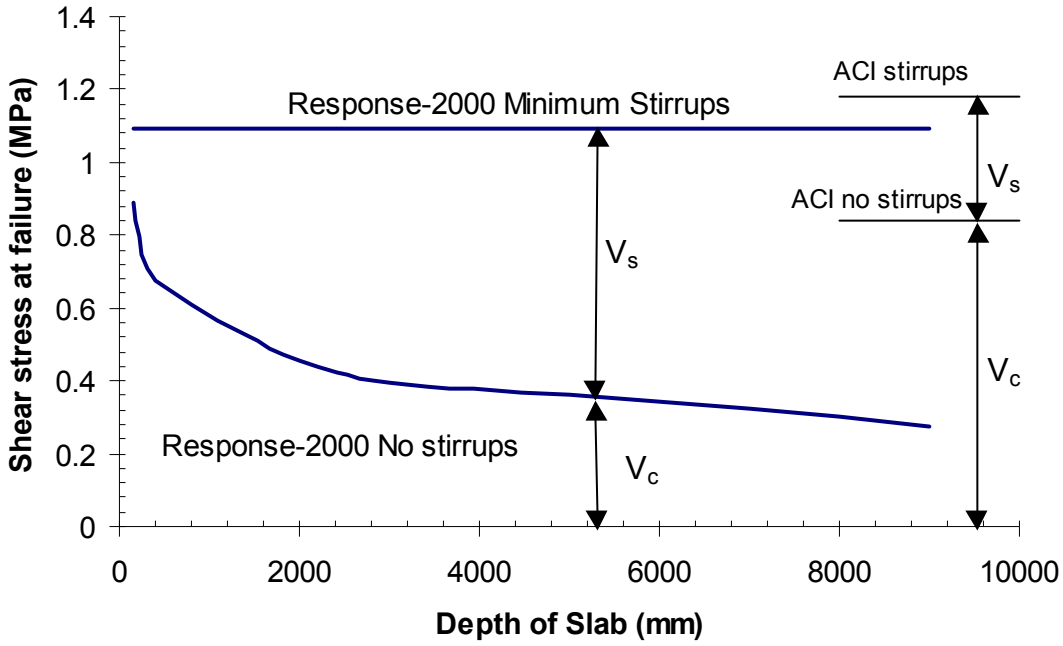

Figure 12-7 Predicted effect of adding minimum reinforcement

Chapter 13: Concluding Remarks

The analysis of reinforced concrete structures can take many forms, but a familiar one to most engineers is that of sectional analysis. This form of analysis considers the entire cross section of the beam, column, or shell in terms of its response to shear forces, axial forces, and moments. While there are many sectional analysis programs in existence that consider moment and axial loads, few exist that account for the more poorly understood case of coincident shear and moment. This thesis explains the background and theory underpinning a series of four easy to use programs that allow non-linear sectional analysis of reinforced concrete plates, beams, shells and blocks to arbitrary loading including significant shear.

The programs presented in this thesis are: Membrane-2000 for plates with in-plane stresses, Response-2000 for beams subjected to shear moment and axial load, Triax-2000 for arbitrary three dimensional blocks of concrete, and Shell-2000 for shells subjected to in-plane and out-of-plane forces. Each of the programs is available from the World Wide Web at the following addresses:

http://www.ecf.utoronto.ca/~bentz/m2k.htm	Membrane-2000
http://www.ecf.utoronto.ca/~bentz/r2k.htm	Response-2000
http://www.ecf.utoronto.ca/~bentz/t2k.htm	Triax-2000
http://www.ecf.utoronto.ca/~bentz/s2k.htm	Shell-2000

Each program is based on the Modified Compression Field Theory (MCFT) in two and three dimensions. This thesis provides an explicit description of the MCFT including a chapter on the so-called “crack check” that is critical in implementing the model. A new method is explained for dealing with the crack check against flexure as well as a new technique to calculate the shear on the crack components in three dimensions.

New constitutive relations were derived for use with the MCFT in the programs. A new relationship is proposed for the cracking strength of a large volume of concrete that better models higher strength concrete that was found to be over predicted by the

traditional equations proposed for use with the MCFT. A new tension stiffening relationship is proposed that explains some of the differences between existing published tensions stiffening relationships. This new tension stiffening relationship is shown to allow much better modelling of behaviour than the previous state of the art methods.

Central to Response-2000 and Shell-2000 is the longitudinal stiffness method. This new technique allows explicit calculation of the shear stress profile over the depth of a member. An extension of the previous state of the art, it solves a number of numerical problems that became clear in extension of the older methods to a higher precision analysis. The new methods allow the programs to run 5-10 times faster than they did using the previous state of the art while also being more numerically stable.

Each computer program is verified against a series of experiments. Two new experiments on large shear elements were also performed for this thesis to examine the effects of very high strength concrete. These comparisons highlighted some problems with the MCFT for high strain states and high strength concrete. For such cases, it appears to be inappropriate to allow steel to strain harden on average in MCFT predictions. Additionally, it appears that the MCFT predictions are poorer for higher strength concrete.

Response-2000 is demonstrated to provide a very good prediction of experimental behaviour when compared to a database of 534 beams tested in shear. These include prestressed and reinforced sections, very large footing-like sections, sections made with very high strength concrete and elements with unusual geometry. All are predicted well. The results indicate that Response-2000 can predict the failure shear with an average experimental over predicted shear strength ratio of 1.05 with a coefficient of variation of 12%. This compares favourably to the ACI code prediction ratios that have an average of 1.20 and a coefficient of variation of 32%. The ACI code is shown to be very conservative for beams subjected to axial tension, and very unconservative for beams that are large and lightly reinforced. Response-2000 predicts that the traditional terms of V_c and V_s are not constants in terms of stress for large lightly reinforced beams. Very thick slabs with no transverse steel are predicted to fail at a shear that is only 40% of the predicted shear strength of the ACI code. The addition of minimum stirrups is predicted

to increase the strength by up to a factor of four, bringing the strength close to that predicted by the ACI code.

With computers being as fast as they are today, a typical Response-2000 analysis taking less than 10 seconds on an inexpensive 1999-vintage computer for example, it seems reasonable to suggest that the time may have come to allow engineers to use experimentally verified tools more integrally in the design and analysis of structures. It is suggested that the code could be changed to directly allow the use of numerical tools that meet a number of requirements. These requirements would be that the tools:

1) satisfy the requirements of equilibrium,
2) satisfy the requirements of compatibility,
3) are based on experimentally verified stress-strain relations,
4) have been verified against a large set of data (preferably a prescribed set).

Such tools would then be able to be used by engineers on any analysis problem, including those that are poorly predicted today. It is suggested that the programs in this thesis represent a good start towards meeting these goals.

Chapter 14: Areas of Future Work

While the four programs presented in this thesis are seen as being a good start on the provision of a widely available set of non-linear sectional analysis tools, there are a number of things that can be done to improve them. Some of these are summarised here:

- Include confinement effects
- Improve treatment of crack check for brittle reinforcement
- Improve stability for analyses subjected to high shear and low moment
- Incorporate cyclic behaviour modelling
- Usability improvements
- Support hollow cross sections in the graphical displays of Response-2000
- Allow users to apply biaxial moments in Response-2000
- Support effects of transverse clamping stresses for low a/d ratios
- More numerical verification of programs
- Fix any undocumented features (bugs)
- Improve modelling for high strength concrete
- Further develop the MCFT relationships to answer questions about strain hardening
- Improve equations used for shear on the crack for high strength concrete
- Test program for beams constructed with lightweight concrete
- Further verify proposed tension stiffening relationships
- Use the calculated value of bond in Response-2000 and Shell-2000 to affect behaviour.
- Develop frame analysis or shell analysis programs based on Response-2000 and Shell-2000.
- Determine if dowel action is an important in predicting behaviour
- Determine if energy of fracture is important in predicting behaviour

References

1 Ritter, W., *Die Bauweise Hennebique* (Construction Techniques of Hennebique), Schweizerische Bauzeitung, Zürich, Feb. 1899.

2 Mörsch, E., *Der Eisenbetonbau* (Reinforced Concrete Construction), Verlag von Konrad Witwer, Stuttgart, Germany, 1922, 460 pp.

3 ASCE-ACI Committee 445, "Recent Approaches to Shear Design of Structural Concrete." ASCE, Journal of Structural Engineering, Vol. 124, No. 12, 1998, pp. 1375-1417.

4 Vecchio, F.J. and Collins, M.P. "The Modified Compression Field Theory for Reinforced Concrete Elements Subjected to Shear." ACI Journal, Vol. 83, No. 2, 1986, pp. 219-231.

5 Collins, M.P. and Mitchell, D. *Prestressed Concrete Structures*. Prentice Hall, Englewood Cliffs, 1991, 766 pp.

6 Vecchio, F.J. and Collins, M.P. "Predicting the Response of Reinforced Concrete Beams Subjected to Shear Using Modified Compression Field Theory." ACI Structural Journal, Vol. 85, No. 3, 1988, pp. 258-268.

7 Collins, M.P., Adebar, P.E. and Kirschner, U. "SHELL474 - A Computer Program to Determine the Sectional Resistance of Concrete Structures in Accordance with CSA Standard S474-M89." Canadian Standards Association, Rexdale, Canada, 1989, 32 pp. plus appendices.

8 Vecchio, F.J. "Nonlinear Finite Element Analysis of Reinforced Concrete Membranes." ACI Structural Journal, Vol. 86, No. 1, 1989, pp. 26-35.

9 Fulop, A.L., "Deformation-Controlled Procedure for Nonlinear Analysis of Reinforced Concrete Frames", M.A.Sc. Thesis, University of Toronto, 1992.

10 Vecchio, F.J. and Selby, R.G. "Toward Compression-Field Analysis of Reinforced Concrete Solids." Journal of Structural Engineering, ASCE, Vol. 117, No. 6, 1991, pp. 1740-1758.

10 Polak, M.A. and Vecchio, F.J. "Reinforced Concrete Shell Elements Subjected to Bending and Membrane Loads," ACI Structural Journal, Vol. 91, No. 3, May-June 1994 pp 261-268.

11 Vecchio, F.J. and Collins, M.P., "Response of Reinforced Concrete to In-Plane Shear and Normal Stresses", *Publication No. 82-03*, Department of Civil Engineering, University of Toronto, Mar 1982, 332 pp.

12 Kirschner, U. and Collins, M.P., "Investigating the Behaviour of Reinforced Concrete Shell Elements", *Publication No 86-09*, Department of Civil Engineering, University of Toronto, Sept 1986, 209 pp.

13 Mitchell, D. and Collins, M.P., "Diagonal Compression Field Theory - A Rational Model for Structural Concrete in Pure Torsion", *Journal of American Concrete Institute*, Vol. 71, August 1974, pp. 396-408.

14 Collins, M.P. "Towards a Rational Theory for RC Members in Shear," Journal of the Structural Division, ASCE, Vol. 104, 1978, pp. 649-666.

15 Vecchio, F.J. and Collins, M.P. "The Response of Reinforced Concrete to In-Plane Shear and Normal Stresses." *Publication No. 82-03*, Department of Civil Engineering, University of Toronto, 1982, 332 pp.

16 Collins, M.P. and Mitchell, D. *Prestressed Concrete Basics*. Canadian Prestressed Concrete Institute, 1987.
17 Zhang, L-X, and Hsu, T.T.C., "Behavior and Analysis of 100 MPa Concrete Membrane Elements," Journal of Structural Engineering, ASCE, Vol 124 No. 1, 1998, pp 24-34.
18 Hsu, T.T.C, and Zhang, L-X., "Nonlinear Analysis of Membrane Elements by Fixed-Angle Softened-Truss Model." ACI Structural Journal, Vol. 94, No. 5, Sept-Oct 1997. pp 483-492.
19 Kaufmann, W., and Marti, P. "Structural Concrete: Cracked Membrane Model." Journal of Structural Engineering, ASCE, Vol 124, No. 12, pp. 1467-1475.
20 Porasz, A. "An Investigation of the Stress-Strain Characteristics of High Strength Concrete in Shear", M.A.Sc. Thesis, University of Toronto, 1989.
21 Walraven, J.C., "Fundamental Analysis of Aggregate Interlock," Journal of the Structural Division, ASCE, Vol. 107 No. ST11, Nov. 1981 pp. 2245-2270.
22 Kirschner, U. and Collins, M.P. "Investigating the Behaviour of Reinforced Concrete Shell Elements." *Publication No. 86-9*, Department of Civil Engineering, University of Toronto, Sept., 1986, 209 pp.
23 Adebar, P.E. and Collins, M.P. "Shear Design of Concrete Offshore Structures." ACI Structural Journal, Vol. 91, No. 3, 1994, pp. 324-335.
24 Selby, R.G., "Three-dimensional Constitutive Relations for Reinforced Concrete," Ph.D. thesis, Department of Civil Engineering, University of Toronto, 1993, 195 pp.
25 Krpan, P., "The Behaviour of Open, Thin-Walled, Restrained, Reinforced Concrete Members in Torsion," Ph.D. thesis, Department of Civil Engineering, University of Toronto, 1974.
26 Hsu, T.T.C., "Stresses and Crack Angles in Concrete Membrane Elements," Journal of Structural Engineering, ASCE, Vol. 124, No. 12, December 1998, pp. 1476-1484.
27: Collins, M.P. "Procedures for Calculating the Shear Response of Reinforced Concrete Elements: A Discussion," Journal of Structural Engineering, Vol. 124, No. 123, December 1998, pp. 1485-1488.
28 Bhide, S.B. and Collins, M.P. "Influence of Axial Tension on the Shear Capacity of Reinforced Concrete Members." ACI Structural Journal, Vol. 86, No. 5, 1989, pp. 570-581.
29 Belarbi, A, and Hsu, T.T.C, "Constitutive Laws of Reinforced Concrete in Biaxial Tension-Compression", *Research Report UHCEE 91-2*, Department of Civil and Environmental Engineering, University of Houston, Houston, Texas. 155 pp.
30 Pang, X., and Hsu, T.T.C, "Constitutive Laws for Reinforced Concrete in Shear", *Research Report UHCEE 92-1,* Department of Civil and Environmental Engineering, University of Houston, Houston Texas.
31 Zhang, L.-X, "Constitutive Laws of Reinforced Concrete Membrane Elements with High Strength Concrete", *PhD Thesis*, University of Houston, August 1995.
32 Vecchio, F.J., Collins, M.P., and Aspiotis, J. "High-Strength Concrete Elements Subjected to Shear," ACI Structural Journal, Vol 91, No. 4, 1994, pp. 423-433.
33 Kuchma, D. "The Influence of T-Headed Bars on the Strength and Ductility of Reinforced Concrete Walls." Ph.D. thesis, University of Toronto, 1997.
34 Tamai, S. Shima, H., Izumo, J. and Okamura, H., "Average Stress-Strain Relationship in Post Yield Range of Steel Bar in Concrete." Concrete Library of JSCE, No. 11,

June 1988, p. 117-129. (Translation from Proceedings of JSCE, No. 378/V-6, Feb 1987).
35 Taylor, H.P.J., "Investigation of Forces Carried across Cracks in Reinforced Concrete Beams by Interlock of Aggregate," TRA 42.447, Cement and Concrete Association, London, 1970, 22 pp.
36 Jourawski, D. J., "Sur la résistnce d'un corps prismatique …," Annales des Ponts et Chauseés, Mémoires et Documents, 3rd Series, Vol. 12, Part 2, 1856, pp. 328-351.
37 Collins, M.P. "Reinforced Concrete in Combined Shear and Flexure," *Proceedings of the Mark W. Huggins Symposium*, University of Toronto Press, 1978
38 Felber, A.J., "RESPONSE: A Program to Determine the Load-Deformation Response of Reinforced Concrete Sections", M.A.Sc. thesis, Department of Civil Engineering, University of Toronto, 1990, 148 pp.
39 AASHTO LRFD Bridge Design Specifications and Commentary, "First Ed., American Association of State Highway Transportation Officials, Washington, 1994, 1901 pp.
40 Angelakos, D., "The Influence of Concrete Strength and Longitudinal Reinforcement Ratio on the Shear Strength of Large-Size Reinforced Concrete Beams with and without Transverse Reinforcement," M.A.Sc. Thesis, Department of Civil Engineering, University of Toronto, 1999, 181 pp
41 Taylor, H.P.J, "Shear Strength of Large Beams," Journal of the Structural Division, ASCE, Vol98. No. ST11, Nov 1972, pp. 2473-2489.
42. Shioya, T., Iguro, M., Nojiri, Y., Akiyama, H., and Okada, T., Shear Strength of Large Reinforced Concrete Beams. Fracture Mechanics: Application to Concrete, SP-118, American Concrete Institute, Detroit, 1989, 309 pp.
43. Shioya, T. Shear Properties of Large Reinforced Concrete Member. Special Report of Institute of Technology, Shimizu Corporation, No. 25, 1989, 198 pp.
44 Kani, G.N.J., "How Safe are Our Large Concrete Beams?", ACI Journal , V. 64, No. 3, March 1967, pp. 128-142.
45 Kani, M.W., Huggins, M.W, Wittkopp, R.R., *Kani on Shear in Reinforced Concrete*, Univerity of Toronto Press, Toronto, 1979, 225 pp.
46 Moody, K.G., Viest I.M., Elstner, R.C., Hognestad, E. "Shear Strength of Reinforced Concrete Beams, Part-1-Tests of Simple Beams," Journal of the American Concrete Institute, V 26. No 4, Nov. 1954, pp. 317–333.
47 Khalifa, J.U., and Collins, M.P., "Circular Reinforced Concrete Membrs Subjected to Shear," *Publication No. 81-08*, Department of Civil Engineering, Univesity of Toronto, Dec 1981, 103 pp.
48 MacGregor, J.G., "Strength and Behavior of Prestressed Concrete Beams with Web Reinforcement," Ph.D. thesis, University of Illinois at Urbana Champaign, 1960, 295 pp.
49 Benzoni, G. Priestley, M.J.N., Seible, F. "Seismic Shear Strength of Columns with interlocking Spiral Reinforcement", Presented to World Conference on Earthquake Engineering, January 2000, Auckland New Zealand.

50 Alvarez M. “Einfluss des Verbundverhaltens auf das Verformungsvermögen von Stahlbeton (Influence of Bond Behaviour on the Deformation Capacity of Structural Concrete)”, Ph.D. Dissertation, Swiss Federal Institute of Technology (ETH), Zurich, July 1998. Dissertation No. 12719, Available as IBK-Report Nr. 236.
51 Popovics, S., “A Numericasl Approach to the Complete Stress-Strain Curve of Concrete,” Cement and Concrete Research, Vol. 3, No. 5, May 1973, pp. 483-599.
52 Canadian Standards Association CAN CSA A23.3 “Building Code for Concrete Buildings”, CSA Rexdale, Ontario, 1984.
53 Ho, G. “Nonlinear Analysis of Reinforced Concrete Beams Subjected to Shear Moment and Axial Loads.” M.A.Sc. thesis, Department of Civil Engineering, University of Toronto, 1994, 221 pp.
54 Podgorniak-Stanik, B. “The influence of Concrete Strength, Distribution of Longitudinal Reinforcement, Amount of Transverse Reinforcement and Member Size on Shear Strength of Reinforced Concrete Members.” M.A.Sc. thesis, Department of Civil Engineering, University of Toronto, 1998.
55 Ghannoum, W.M., “Size effect on Shear Strength of Reinforced Concree Beams,” M.Eng. Thesis, Department of Civil Engineering and Applied Mechanics, McGill University, 1998, 115 pp.
56 Adebar, P.E., and Collins, M.P., “Shear Strength of Members without Transverse Reinforcement, “Canadian Journal of Civil Engineering, Vol. 23, No. 1, Feb. 1996, pp. 30-41.
57 Collins, M.P., Mitchell, D. and MacGregor, J.G. “Structural Design Considerations for High Strength Concrete,” Concrete International, May 1993, pp. 27-34.
58 Elzanaty, A.H., Nilson , A.H., and Slate F.O., “Shear Capacity of Prestresed Concrete Beams Using High-Sytrength Concrete,” ACI Structural Journal, Vol. 83, No. 3, May-June 1986, pp. 359-368.
59 Rabbat, B., “A Variable Angle Space Truss Model for Structural Concrete Beams,” Ph.D. Thesis, Department of Civil Engineering, University of Toronto, 1974, 236 pp.
60 Makwana, M.D., “The Effectiveness of Stirrups of Different Shapes in Laterally loaded Reinforced Concrete Columns,” M.Eng. Thesis, University of Canterbury, Christchurch, New Zealand 1977, 114 pp.
61 Aregawi, M., “An Experimental Investigation of Circular Reinforced Concrete Beams in Shear,” M.A.Sc. Thesis, Department of Civil Engineering, University of Toronto, 1974, 86 pp.
62 Kuzmanovic, S, “An Investigation of the Shear Design of a Reinforced Concrete Box Structure,” M.A.Sc Thesis, Department of Civil Engineering, University of Toronto, 1998, 126 pp.
63 Kawano, H., Watanabe, H., “Shear Strength of Reinforced Concrete Columns – Effect of Specimen Size and Load Reversal.” *Proceedings of the Second Italy-Japan Workshop on Seismic Design and Retrofit of Bridges*, Feb 1997, Rome Italy.
64 Yoon, Y.S., Cook, W.D., and Mitchell, D., “Minimum Shear Reinforcement in Normal, Medium, and High-Strength Concrete Beams,” ACI Structural Journal, Vol. 93, No. 5, Sept.-Oct. 1996, pp. 576-584.
65 Haddadin, M.J., Hong, S.T. and Mattock, A.H., “Stirrup Effectiveness in Reinforced Concrete Beams with Axial Force,” Journal of the Structural Division, Proceedings ASCE, V.97, No. ST9, Sept. 1971, pp. 2277-2297.

66 Pasley, G.P., Gogoi, S., Darwin, D. and McCabe, S.L., "Shear Strength of Continuous Lightly Reinforced T-Beams," SM Report No. 26, University of Kansas, Dec. 1990, 151 pp.
67 Palaskas, M.N. and Darwin, D., "Shear Strength of Lightly Reinforced T-Beams," SM Report No. 3, University of Kansas Center for research, Lawrence, Kansas, September 1980, 198 pp.
68 Ozcebe, G., Ersoy, U. Tankut, T., "An Evaluation on the Minimum Shear Reinforcement Requirements For Higher Strength Concrete", ACI Structural Journal Vol. 96, No. 3, May-June 1999.
69 Levi, F. Marro, P. "Shear Tests up to Failure of Beams made with Normal and High Strength Concrete" (summary), CEB Bulletin 193, Lausanne, Switzerland, Dec. 1989.
70 Roller, J.J., and Russell, H.G., "Shear Strength of High-Strength Concrete Beams with Web Reinforcement," ACI Structural Journal, V. 87, No. 2, Mar-Apr. 1990, pp. 191-198.
71 Arbesman, B., Conte, D.F., "The Design and Testing to Failure of a Prestressed Concrete Beam Loaded in Flexure and Shear," B.A.Sc. thesis, Department of Civil Engineering, University of Toronto, 1973, 176 pp.
72 Arbesman, B., "The Effects of Stirrup Cover and Amount of Reinforcement on Shear Capacity of Reinforced Concrete Beams," M.Eng. Thesis, Department of Civil Engineering, University of Toronto, 1975.
73 Kong, P.Y.L. and Rangan, B.V., "Shear Strength of High-Performance Concrete Beams", ACI Structural Journal, Vol. 95, No. 6, Nov-Dec 1998, pp. 677-688
74 Rangan, B.V., "Web Crushing Strength of Reinforced and Prestressed Concrete Beams" ACI Structural Journal, V.88, No1, Jan-Feb 1991 pp. 12-16.
75 Shahawy, M.A., Batchelor, B., "Shear Behavior of Full-Scale Prestressed Concrete Girders: Comparison Between AASHTO Specifications and LRFD Code", PCI Journal Vol. 41, No. 3, May-June 1996 pp 48-62.
76 Collins, M.P., "Shear Behavior ..." Discussion, PCI Journal Vol 42, No. 3, May-June 1997, pp. 72-81.
77 Seracino, R. "Towards Improving Nonlinear Analysis of Reinforced Concrete Shells," M.A.Sc. thesis, Department of Civil Engineering, University of Toronto, 1995, 177 pp.
78 Timoshenko S.P., Gere J.M., *Mechanics of Materials*, D.Van Nostrand, 1971, 541 pp.
79 ACI Committee 318, "Building Code Requirements for Reinforced Concrete (ACI 318-99) and Commentary ACI 318 R-99," American Concrete Institute, Detroit, 1999, 369 pp.
80 Gupta, P.R.G., "Behaviour of Reinforced Concrete Elements subjected to High Compression and Shear," Ph.D. Thesis, Department of Civil Engineering, University of Toronto, 1998.

Appendix A: Program Manuals

Appendix B: Detailed Zurich Data

Appendix C: Experimental Verification Tables for Response-2000